Optimal sizing of passive components in power converters using discrete methods

Timothé Delaforge

Communauté
UNIVERSITÉ Grenoble Alpes

THÈSE

Pour obtenir le grade de

DOCTEUR DE L'UNIVERSITÉ GRENOBLE ALPES

Spécialité : **Génie Electrique**

Arrêté ministériel : 7 août 2006

Présentée par

Timothé / DELAFORGE

Thèse dirigée par **Jean-Luc SCHANEN**

préparée au sein du **Laboratoire de Génie Electrique de Grenoble (G2Elab) et de Schneider Electric ITB**
dans **l'École Doctorale EEATS**

Dimensionnement optimal des composants passifs en électronique de puissance, utilisation de méthodes discrètes

Thèse soutenue publiquement le **05/02/2016**,
devant le jury composé de :

Mr, Michel, HECQUET
Professeur des universités Centrale Lille, Président
Mr, Eric, LABOURE
Professeur des universités Centrale Supelec, Rapporteur
Mr, Charles, SULLIVAN
Professeur des universités University of Darthmouth, Rapporteur
Mr, Jean-Luc, SCHANEN
Professeur des universités Université Grenoble Alpes, Membre
Mr, Hervé, CHAZAL
Maitre de conférences Université Grenoble Alpes, Membre
Mr, Robert, PASTERCZYK
Docteur Ingénieur Schneider Electric, Membre
Mr, Jean-Louis, COULOMB
Professeur des universités Université Grenoble Alpes, Invité

REMERCIEMENTS

Une fois la thèse finie et la soutenance passée, le public peut enfin se rendre compte du travail accompli et le juger.

Ce qui ne transparaît pas dans ce manuscrit c'est que le travail a bien peu d'importance face à la vie vécue lors de ces trois années. C'est pourquoi je tiens à travers ces quelques lignes, remercier tous ceux qui ont fait de cette thèse une riche expérience et un bel instant de vie.

J'en oublierais sûrement. À tous ceux qui ne se retrouveront pas dans les lignes suivantes, merci ! Et pardonnez mon esprit souvent distrait. Toute ressemblance de noms n'est pas une erreur de ma part, juste un manque d'originalité des parents…

Je remercie d'abords ceux qui étaient là au début et qui ne sont plus. **Pépé Degu**, **Loïc**, **Patrice**, **René** et **Julia** ainsi que **Odette**.

Un énorme merci à ceux qui sont là et qui sont le premier soutien et la première raison de mon bonheur, ma famille, mes amours. **Maëlle**, Mémé **Jacotte**, mes parents **Nicole** et **Patrick**, mes frangins **Colas** et **Yvain**, les pièces rapportées **Charlène** et **Pauline** et la relève **Faustine** et **Emile**, mes cousines **Mélaine**, **Aurélie** et **Mathieu**, **Alexia**, **Carole**, **Manon**, mes cousins **Mathieu** et **Léa** et **Milan**, **Martin** et **Coline** et **Lila**, **Bastien**, **François**, papy **Robert** et mamy **Lucette**, mes tantes **Catherine**, **Corinne**, **Christine**, **Astrid**, et mes oncles **Jean-Robert**, **Marc**, **Gérard**, **Stéphane**.

Une grosse pensée également pour tous ceux qui assurent ma santé mentale depuis longtemps déjà, mais qui m'aident également à détruire ma santé physique, mes amis. **Augustin**, **Loan** et **Mickaël**, **Carole** et **Damien**, **Agnès** et **David**, **Margaux** et **Basile**, **Audrey**, **Jérémy**, **Léa**, **Alexandre**, **Léa** et **Quentin**, **Camille** et **Quentin**, **Cécile**, **Joseph**, **Célia**, **Violette** et **François**, **Véréna**, **Jean-Loup**, **Bénédicte**, **Fanny**, **François**, **Aurélien**, **Flora**, **Laurianne** et **Timothée**, **Andréa** et **Florian**, **Guillaume**, **Paul**, **Laure**, **Charles**, **Adrien**, **Maxime**, **Gaëlle**, **Vincent**, **Emeric**, **Fabrice**, **Grégory**, **Félix**, **Ophélie**, **Maël**, **Damien** et tous ceux que j'oublie !

Grand pensionnaire du labo merci à tous les grimpeurs qui bloqués de longues soirées en ma compagnie.

Une ligne pour mes monstres qui font partie intégrante de ma vie **Manita**, **Granito** et **Kaori**.

La thèse m'a également apportée bien plus que des collègues, de belles amitiés, **Corentin**, **Benoît** et **Guillaume**. Ainsi que leurs pièces rapportées. Cela vaut bien plus que les résultats.

Même s'ils ne jouissent pas de la même complicité, merci à tous mes autres collègues actuels qui accompagnent mes dures journées de labeur, **Jérémie**, **Olivier**, **Lucas**, **David**, **Mickaël**, **Grégory**, **El-Hadji, Alain et Alain**, **Olivier**, **Hakim** et tous les autres de Schneider Electric et du G2elab !

Merci à tous ceux qui comme moi à cet instant sont passés chez Schneider mais qui ne se sont pas arrêtés et qui sont maintenant épinglés sur le mur des disparus, **Mathieu**, **Dominique**,

Mirela, **Mélanie**, **Aurélien**, **Guillaume**, **Olivier**, **Vincent**, **Lucas**, **Romain**, **Sylvain**, **Vincent**, **Jean**, **Brice**, **Fouzia**, **Loubna**, **Henrique**, **Tamiris** et **Nizar**.

Merci à ceux qui ont favorisé ma nouvelle passion et qui m'accompagnent toujours dans mes aventures apicoles (ceux de mes aventures à picole ayant déjà été cités) **Jean-Philippe**, **René** et les autres de l'Abeille Dauphinoise.

Merci aussi à ceux qui font swinguer mes soirées.

Enfin et non des moindres, merci à tous ceux qui ont chapeauté ce travail, merci à **Laurent** de m'avoir orienté vers cette thèse.

Merci à **Jean-Louis** l'incroyable aide de l'ombre.

Merci à **Hervé** pour son apport et son aide immense, source d'inspiration et de discussions passionnantes indispensables. Il restera le premier pilier de mes travaux.

Merci à **Robert** qui fut l'autre pilier de cette thèse, pour son apprentissage du monde industriel et de ses rouages. Sa grande expérience et son approche inimitable de l'ensemble des problématiques. Aux échanges passés et à venir.

L'ordre n'a aucune importance, mon amour et mon amitié vont à tous,

« Je sers la science et c'est ma joie »

TABLE OF CONTENTS

General Introduction 9
Chapter I - Optimization 13
1.1 Introduction 14
1.2 Specifications 15
1.2.1 Introduction: 15
1.2.2 Scales: 15
1.2.3 Converter environment: 15
1.2.4 Magnetics: 16
1.2.5 Products for industrialized application: 16
1.2.6 Engineer tool: 16
1.2.7 Conclusion: 16
1.3 Algorithms 17
1.3.1 Introduction: 17
1.3.2 Pareto-Front 19
1.3.3 Constraints 20
1.3.4 Determinist Algorithms: 22
1.3.5 Stochastic algorithms 30
1.3.6 Conclusions 37
1.4 Strategies 39
1.4.1 Introduction: 39
1.4.2 Schneider Electric Experience: 40
1.4.3 Analytical Modeling: 42
1.4.4 Discrete Values and Libraries: 42
1.4.5 Industrial Project: 42
1.4.6 Conclusions: 43
1.5 GoT 44
1.6 Conclusions 45
1.7 References 47
2 CHAPTER II – Passive Components 48
2.1 Introduction 49
2.2 Choke Core 50

2.2.1 Introduction: 50
2.2.2 Magnetic basics: 50
2.2.3 Classical Macro Models based on Steinmetz: 51
2.2.4 The Loss Surface: 54
2.2.5 Innovations: **Error! Bookmark not defined.**
2.2.6 Conclusions: 69
2.3 Choke coil 71
2.3.1 Introduction: 71
2.3.2 Dowell: 71
2.3.3 A-Model: 80
2.3.4 Conclusions: 95
2.4 Capacitor 97
2.5 Component Definition 100
2.5.1 Introduction: 100
2.5.2 Free Toroid chokes: 101
2.5.3 Datasheet Toroid chokes: 101
2.5.4 Two cores Toroid chokes: 101
2.5.5 Conclusions 102
2.6 Conclusions 103
2.7 References 105
3 Chapter III - Filter Model 107
3.1 Introduction 108
3.2 Models connection using converter waveforms 109
3.2.1 Introduction: 109
3.2.2 Separation of models: 109
3.2.3 Events sampling: 110
3.2.4 Conclusions: 111
3.3 DC/AC converters 112
3.3.1 Introduction: 112
3.3.2 Inverter output/ Filter input: 112
3.3.3 Load waveforms: 115
3.3.4 Filter model: 118
3.3.5 Validations: 122

3.3.6 Conclusions: 126
3.4 AC/DC converters 126
3.5 DC/DC converters 127
3.5.1 Introduction: 127
3.5.2 Nominal Charging mode: 127
3.5.3 Floating Charging mode: 128
3.5.4 Nominal Discharging mode: 128
3.5.5 Minimal Voltage Discharging mode: 129
3.5.6 DC/DC filter modeling: 130
3.6 Coupled Filter 131
3.6.1 Introduction: 131
3.6.2 Event waveforms: 131
3.6.3 Interleaving: 132
3.6.1 Filter modeling: 132
3.7 Conclusions 137
3.8 References 138
4 Chapter IV - Optimal Sizing 139
4.1 Introduction 140
4.2 DC/AC Interleaved Converter 141
4.2.1 4 levels 125kVA inverter: 141
4.2.2 Replacing existing solution: 141
4.2.3 Single vs Parallel solution: 145
4.2.1 Optimal dimensions vs catalog sizes: 146
4.2.2 Best permeability: 147
4.2.3 Capacitor 147
4.2.4 Conclusions: 148
4.3 DC/AC Coupled Choke 149
4.3.1 3 levels inverter/PFC: 149
4.3.1 Prototype validations 153
4.3.2 Conclusions 157
4.4 DC/DC Coupled Solution 158
4.4.1 DC/DC reversible converter 158
4.4.2 Assembling investigation: 158

4.4.3 Best permeability: 159
4.4.4 Optimization results: 159
4.4.5 Prototype validation: 160
4.4.6 Conclusions: 164
4.5 Conclusions 165
5 General Conclusions 166
Appendix A 170
Appendix B 176
Appendix C 177
Résumé 185
Abstract 187

GENERAL INTRODUCTION

Innovation in its whole definition is a way for industrial groups to preserve and create value over competitors on the market. Mainly technologic, innovation is also of use, a new way of using a product or service to answer market or user requirements. This work is an innovation for component design in power electronic systems, both in tools and user customs.

Power electronic is subject to same research goals as any modern system, i.e. cost and time to market reduction, efficiency increase in the global energy save world concern and modularity of solution to answer maximum customer needs. The last decades have seen amounts of innovation in structure, component and computer methods. Solutions for a converter designer in power electronic are numerous and complexes. One can choose to use new semi-conductor technologies, e.g. SiC or GaN switches, leading to higher frequency reducing filtering need but creating new issues over regulation or high frequency effects in components. The choice could also be done on new multi-legs and multi-levels voltage topology balancing efficiency and cost between passive and active components. Facing the multitude of design solutions, power electronic converter development has become a real headache and actual process does not guarantee the achievement of the best and most competitive industrial product. Thus, the need of new tools to help designers in their choice is clearly identified.

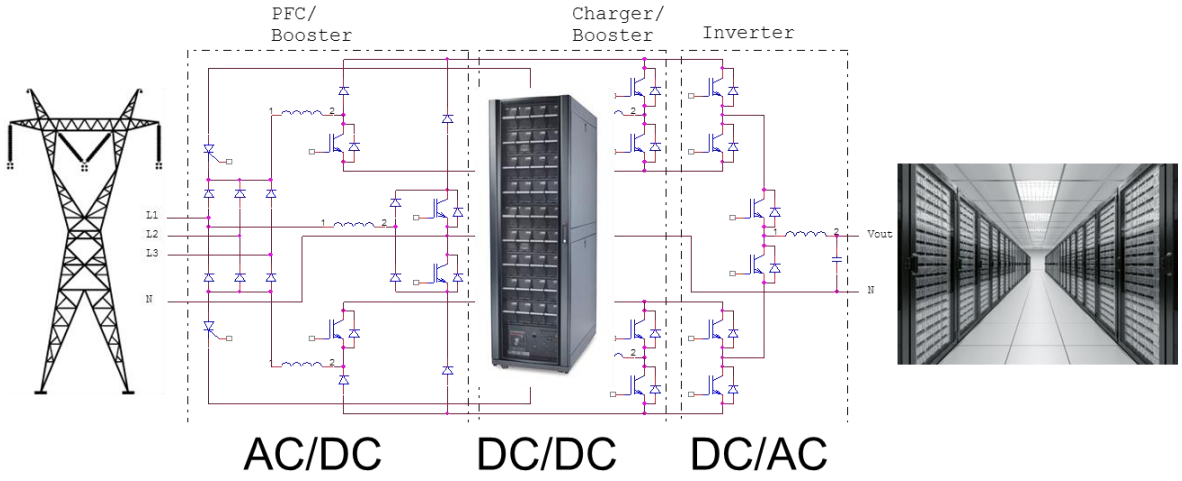

Figure 1: UPS topology example, connection between grid and data-center with battery storage

This work presents new processes to achieve passive component design in power electronics converter subject to high current density. It has been realized for Schneider Electric company and applied on uninterruptible power systems. Introduced in the 60s, to secure sensitive load from electricity hazards, UPS must deliver harmonic-free electricity when perturbations occur on the grid. The load is usually coupled to an alternative energy source, most of the time hydrocarbon one, which is slow to deliver its full capacity, up to several minutes. The goal of UPS is thus to guarantee the transition between grid and the second power source, implying energy storage up to megawatts, and transit it in few microseconds with total harmonic distortion reduction and perturbation cancellation. The UPS delivers energy during several minutes. Thus, storage is achieved with batteries. Converter topologies are fitted to this constraint, switching from alternative electricity to continuous current for battery and conversely, (Figure 1). UPS is a static converter; electric waves are changed without any motion of any component. In input several voltage potentials are connected alternatively to a

common point with a modulated time for this connection in order to produce a mean continuous value from a sinusoid at modulation frequency or reversely to switch from continuous to sinus in output. But switched waveforms contain harmonics whose must be filtered. The number of voltage potential available on the common point defines the converter capability to reduce harmonic content at high frequencies, reducing size of filter, (Figure 2). Capability to switch from one potential to another is done by semi-conductors. Increasing number of potential leads to increase number of semi-conductors, i.e. their cost and losses, but reduces the size of passive components. Study of two topologies of 500 kVA UPS is presented in (Figure 3). UPS topology is a balanced choice between passive and active components weight in price, efficiency, footprint, temperature, volume, etc. The designer faces a multi-topologies and linked multi-components problem with goals and constraints defined in so called specifications.

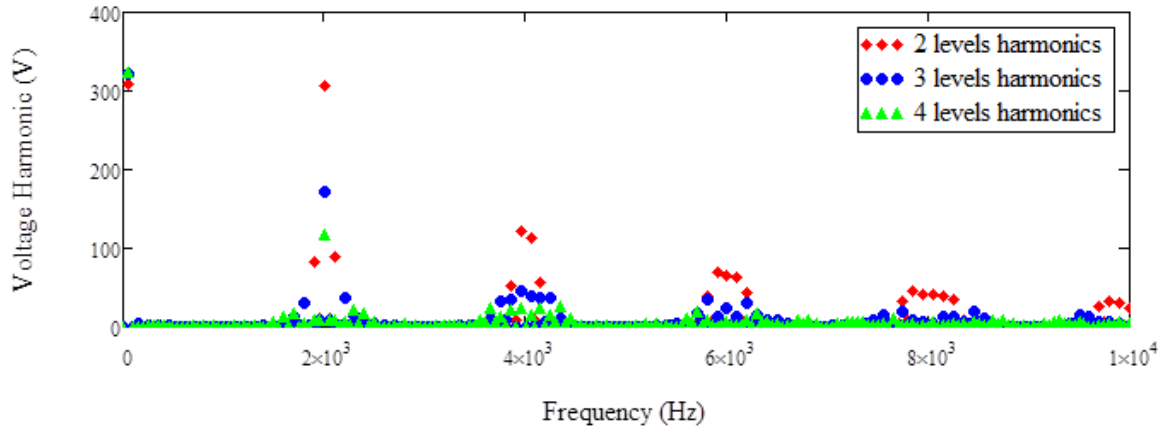

Figure 2: Harmonic spectrum for 3 UPS voltage levels

At the present time, the time to market for an UPS from definition of specifications to release on the market is several years. Any implementation of innovative technology increases dramatically this time because of prototyping and understanding of this innovation. Different points explain the time of new product development. As written previously, the large amount of possibilities to design an UPS and the choice of topology is a long process. The time of implementation of new topology in simulation tools and the accuracy of those tools don't make it possible to prototype directly a good and definitive solution. Several prototypes are required and upgrades of those prototypes. It takes many months between each prototype. For every prototype, long discussions with furnishers are needed about specifications and measurements requirement. Validation process are achieved on each component and then on their assembly. Optimization is also done by prototyping several solutions and choosing the best one, which is not the appropriate method. Finally, the prototype is validated regarding standards and not necessarily all working case the UPS will be faced to.

To answer these issues of picking the best solution fitting specifications in the lowest possible time, this work has associated mathematical simulation and optimization methods to the strong industrial knowledge of Schneider Electric in the field of power converters.

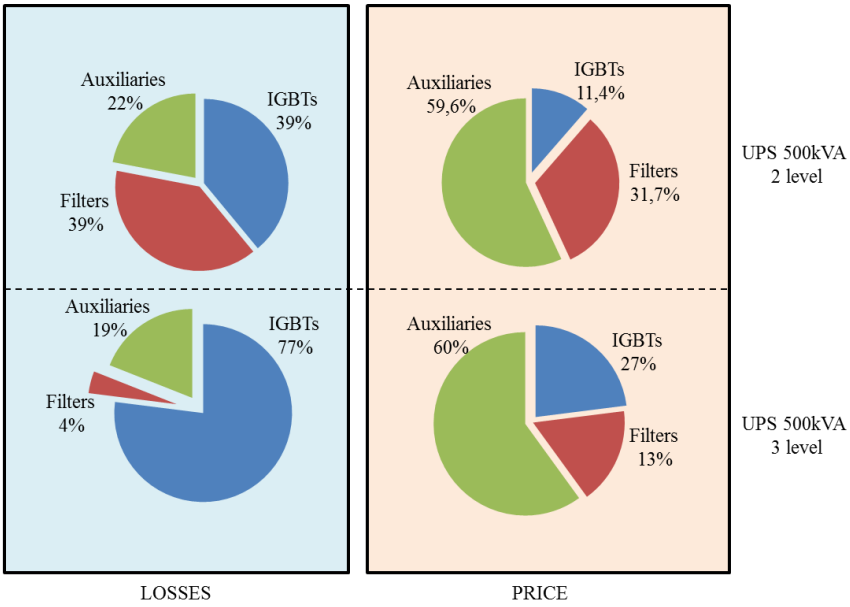

Figure 3: Comparison between 2 level UPS and 3 level UPS

A typical UPS operates in the range of hundreds of volts, 230 V ~ 800 V, high current, from a few amperes up to thousands 10 A ~ 3000 A, and delivers grid compatible electricity, so 50 Hz or 60 Hz sine wave, with 3 kHz to 25 kHz switching frequency. The emergence of new semi-conductor technologies, SiC or GaN, will lead to higher switching frequencies. This work is bound by these values.

In the first part of this manuscript, algorithm optimization is introduced and advantages of the method and its application to industrial design explained. Optimization strategies are presented, and the Schneider Electric knowledge on power converters leads to a specific choice among the different possibilities. Specifications for sizing of passive components are detailed. Algorithms are explained and illustrated on study cases, advantages and drawbacks in converter applications are highlighted. Finally, the optimization software is presented.

Optimization and strategy being defined, the second part of the manuscript develops the passive component modeling with optimization requirements impact on those models. Focus is on magnetics, for both their huge effect on the final converter efficiency and price but also of their high numbers of sizing parameters. Accurate models are presented and technologic innovations proposed. Validation of modeling is achieved with both simulation and measurements on prototypes.

The third part focuses on the converter definition and how component models are linked to simulate any topology of converter. All conversion used in UPS are presented AC/DC, DC/DC and DC/AC. New coupled filter solutions are also investigated.

Finally, the manuscript presents the applications of all developed simulation and optimization tools on industrial UPS projects. Three converters have benefited of this work, and validation is done by measurement and gains are demonstrated. Extension for active components is explained.

CHAPTER I - OPTIMIZATION

1.1 INTRODUCTION

Many projects in industry benefit from so-called optimized solutions. Most of the time several prototypes are realized based on the experience of the designer and the best of so many investigated solutions is selected. In the work of an expert designer, a local variation of parameters is achieved to find local optimum. However, this is not optimization in the mathematical world, and it does not make it possible to find the global optimum of the designed object addressing all constraints and goals.

The design of a component is the action of finding a set of the adjustable parameters in order to respect at minima the specifications, technical, geometrical and financial. The design of a component using an optimization process is to find the best set of parameters respecting the specifications but also providing the global optimum of goals. The choice of an appropriate set of parameters addressing a set of objectives is the definition of algorithmic optimization.

This approach of optimal sizing is now compulsory in industrial projects as explained in general introduction. In this PhD the optimal sizing of passive components in power converters is investigated. This design cannot be done regarding the component alone and manually. The converter topology and its electric waveforms, the standards applied to the whole structure, the other components, all have an influence on the global optimum of the solution for the converter. Thus, the number of possible solutions even in the simplest topology of converter is too great for a human mind to solve, or for a computer to test all possibilities. Taking the example of an inductor, general inputs are the coil, with the number of turns, the number of strands per turns, the strand diameter, material of the coil. The core can have different sizes also and different materials. Let's be generous and take only ten possible values of six inputs, we consider a real fast simulation of the inductor ~1 s. To verify all solutions will take a million seconds, more than eleven days. This cannot be used in the design of a whole converter. Thus optimization methods and algorithms are presented in this chapter to look on their impact on models and design strategies.

First the specifications that limited the project are defined to serve as main guideline in choice of algorithms or methods. Then the algorithms are presented in two families. Facing the multitude of existing algorithms only few are introduced but the aim is to familiarize the reader with possibilities and main ideas developed in optimization, in order to explain the choices we made and the other ways that could have been investigated. The selected strategy of sizing Schneider Electric components applying discrete methods and genetic algorithms is last presented. A fast review of the software integrated in sizing process concludes the chapter.

1.2 SPECIFICATIONS

1.2.1 Introduction:

The choice of an optimization algorithm has a huge impact on the model requirements and the optimization results. But in order to choose the fittest algorithm and the right strategy, it is essential to define the problem. Schneider Electric has a century long knowledge on power converter, and defined ideas of their needs. This paragraph introduces all the requirements established with Schneider and the boundaries of this PhD project.

1.2.2 Scales:

The optimization is achieved on passive component used in power converter implemented in UPS. The UPS is built from several power bricks, usually an AC/DC converter switching electricity from power grid to UPS, a DC/DC buck boost for batteries supply and finally a DC/AC inverter to deliver the power to the load. The model must be valid for the whole working scale of UPS. I.e.:

- Current: from 1 A to 1 kA
- Voltage: from 1 V to 1 kV
- Frequency: from 50 Hz to 50 kHz
- Component: from 1 mm to 1 m

So component models have to be coherent on the whole scale whatever the working power.

1.2.3 Converter environment:

Schneider Electric ITB is in charge of developing a new range of products, but also to upgrade old version of UPS or modify part of the UPS for customer special need. Thus, the modeling has to enable the optimization of the whole converter or only part of it with the rest of the structure unchanged. Every UPS has a different topology and power scale. Furthermore in the development of a product, several topologies are compared. So the optimization and the modeling must be flexible enough to consider all topologies without changing the model or the algorithms.

1.2.4 Magnetics:

With a wealth of experience in the design and manufacturing of power converters, Schneider Electric and G2Elab identified the magnetics as a key in the design of the whole UPS. The repartition of price and efficiency of the converter presented in general introduction, drive the focus on these components and the semi-conductors. Schneider Electric does not have huge leverage and possibilities on the manufacturing of the semi-conductors. They are treated as a library of components from suppliers' catalogs. Conversely, the magnetics have several adjustable parameters. Magnetics are not acquired on datasheets. This makes the magnetics particularly adapted to design by optimization approach. They will be widely investigated in this manuscript.

1.2.5 Products for industrialized application:

One of the major key requirements of this project is to reduce drastically the cost and the time of product development. I.e. this is not a pre-sizing process, but the optimization has to converge toward components directly implemented in industrialized converter. That means working on catalogs and supplier size of sub-components and library of materials. The optimization has to deal with discrete values, libraries and the model must be really accurate to give results close enough from final product behavior.

1.2.6 Engineer tool:

The optimization must be carried out by engineer accustomed to optimization but not expert in this domain. The optimization must be robust and without bug requiring expert analysis after each run. Users must be able to implement new material or component in library used in optimization. The deployment of models and algorithms must be easy and without high cost, multi-software platform is not recommended.

1.2.7 Conclusion:

This PhD has been achieved in strong collaboration with Schneider Electric ITB. The main goal was to apply scientific innovation and research on an industrial project. The specifications presented in this paragraph have been the guiding line of the work and research achieved during the PhD. Models, tools and optimizations are matching all the requirements established by Schneider and sometime exceed them.

1.3 ALGORITHMS

1.3.1 Introduction:

The choice of optimization algorithm according to specifications of the problem and goals of the optimization is as important as the model of the problem. Problems are distinct by their nature and their purpose. The choice of the algorithm matching the requirement implies the knowledge of these algorithms and their behavior, as well as the model behavior when used in these algorithms, since both cannot be decoupled. In this part some generalities on optimization methods are explained and few algorithms detailed. Among the multitude of techniques available for optimization it would be presumptuous to present all of them, so only relevant methods are explained.

Two approaches are distinct from each other by the origin of their outputs with the same specified inputs.

- The direct method uses directly the system to be optimized or its multi-physic accurate modeling. Simplest and faster this method uses real outputs.
- The indirect method takes its values form a surrogate model elaborate from the multi-physic modeling. It requires the elaboration of a new model but can be really useful when the system is too complex or the accurate model too expensive in time calculation.

Goals are to be clarified also. For each optimization problem, several optima can exist, local or global. In the case of amelioration, local optimum can be sufficient. But when searching the best solution, only the global optimum is satisfying. In other cases, the optimum can be dual, meaning that two objectives are in competition, in this case a tradeoff must be found. For each specification of the optimization goal, some algorithms are better fitted than other. Algorithms are usually classified into two families: if it is not based on any random mechanism, algorithm is classified *deterministic*. The convergence is determined by fixed mechanisms and will always converge to the same results for the same inputs. However, if random mechanisms are used, the algorithm is *stochastic*. The result will not necessarily be the same. The use of random method (e.g. Monte Carlo or Mutation in Genetic Algorithms) is supposed to widen the search domain and guaranteed the convergence to the global optimum, without trapping the optimization with knowledge of the user. New algorithms emerge to answer the need of coupling both methods; they are call *hybrid* and are a sequential use of stochastic and determinist algorithms.

Whatever the algorithm, it is classified by order:

- Method of 0^{th} order: only the outputs are used.
- Method of 1^{st} order: outputs and their derivatives are used.
- Method of 2^{nd} order: outputs, derivatives and second derivatives are used.

The appropriateness of the optimization method to the problem is an issue with no general solution.

In the following, algorithms are presented and tested on two problems.

1.3.1.1 Belledonne

The first problem is the Belledonne multi-optimum problem with the objective of minimizing (1).

$$f(y_1, y_2) = \left[1 - y_1^2\right]\cos(5.y_1) + \left[12 - y_2^2\right]\cos\left(\frac{4}{\sqrt{y_2} + 0.3}\right) \quad \text{with} \quad 0 \le y_1 \le 2 \quad \text{and} \quad 0 \le y_2 \le 2 \qquad (1)$$

This surface has one global minimum f(1.36864;0.01548), and 3 local minimums f(0.56434;0.01548), f(1.36864;0.86648) and f(0.56434;0.86648). It is really interesting for testing the capability of algorithms convergence toward local or global optimum. The surface from (1) is shown in (Figure 4), global optimum is highlighted in red and local optima in green.

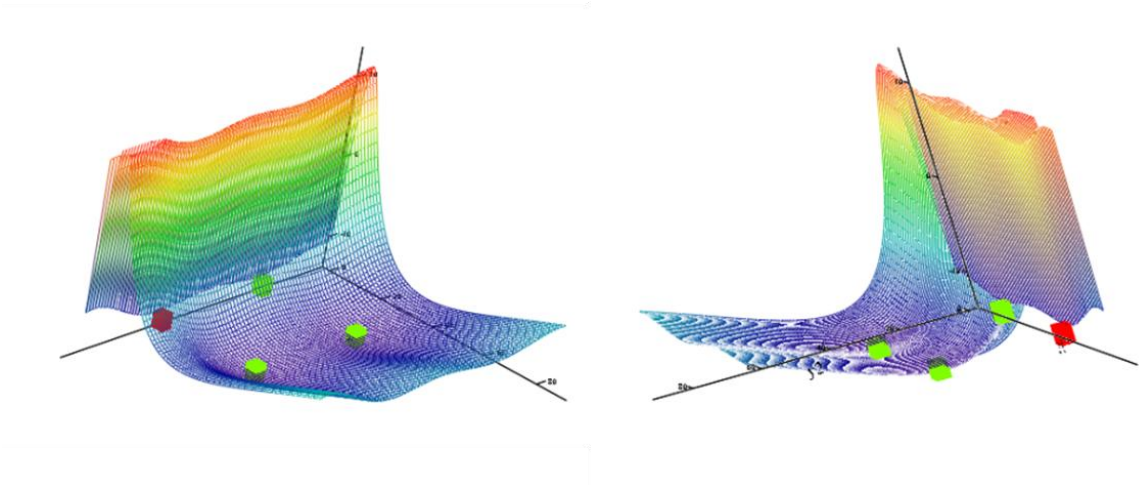

Figure 4: Belledonne problem surface with local optimum in green and global optimum in red

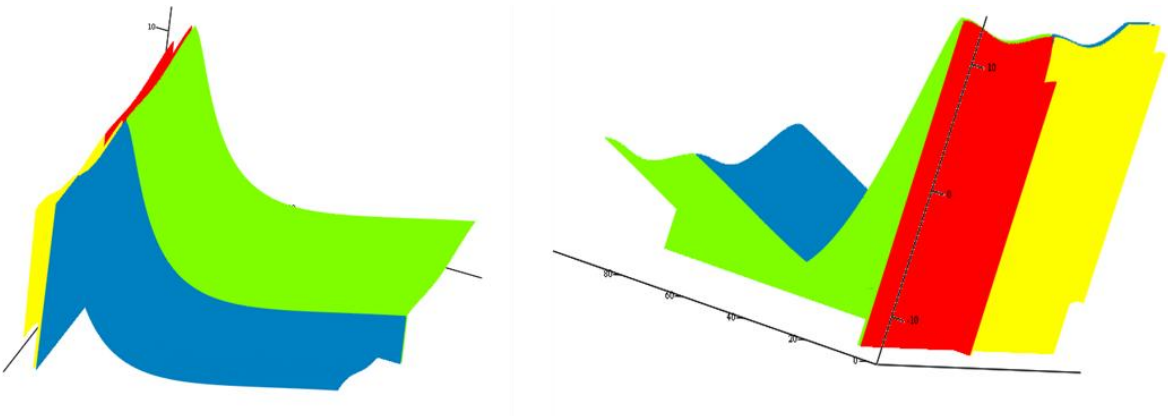

Figure 5: Belledonne surface, initial point convergence area

On the Belledonne case, the gradient algorithm convergence depends on the first set of parameters. Four quadrants can be found, for red, green and blue ones; the optimum will be one of the local optima. Only an initial set of parameters resulting in a value of (1) situated on the yellow area will converge toward the global optimum (Figure 5). The point of the surface chosen as initial point for optimization is situated at the intersection of the four areas.

1.3.1.2 Bi-sphere

The second problem is the Bi-sphere, multi-objectives of minimizing (2) and (3). Both optimums f1(1;0) and f2(0;1) cannot be reached at the same time; a compromise is compulsory. In multi-objectives problem, the goals are weighted to set a ranking. The choice here is to give same importance to both goals. The surfaces are illustrated in (Figure 6); optimums are highlighted in green.

$$f1(x_1, x_2) = (x_1 - 1)^2 + x_2^2 \quad (2)$$

$$f2(x_1, x_2) = (x_2 - 1)^2 + x_1^2 \quad (3)$$

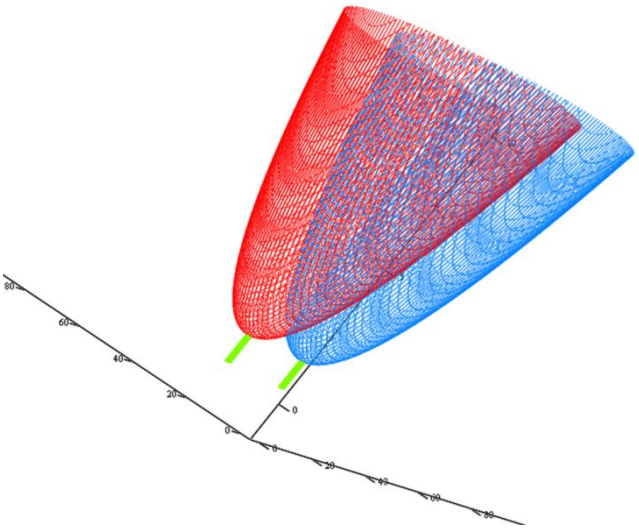

Figure 6: Bi-sphere surface with optimums in green

1.3.2 Pareto-Front

The optimal Pareto-front is an important tool for industrial designer. It allows selecting the best optimal solution regarding the tradeoff the designer want to make between several objectives. A Pareto-front can be built with many algorithms, determinist or stochastic. However, results and convergence have not the same relevance and easiness.

1.3.2.1 Single optimum algorithms

In presented algorithms only a few allow to find many optimums in a single run. The strategy for the others consists in several run with a fixed value of one of the objective. The value of the objective is fixed but all the other parameters and objective stay unchanged. It forces to repeat the optimization for several fixed values of the objective but also repeat the pattern for the other objectives.

This approach presents several drawbacks. For more than two objectives, the number of optimization can become important. With the risk that optimization may be not robust and with issues to converge, the Pareto-front becomes tricky to obtain. Another issue is the number of fixed points on the Pareto; for a smooth front this is not an issue, but for Pareto with several bindings, the number of values is essential to find good results (Figure 7).

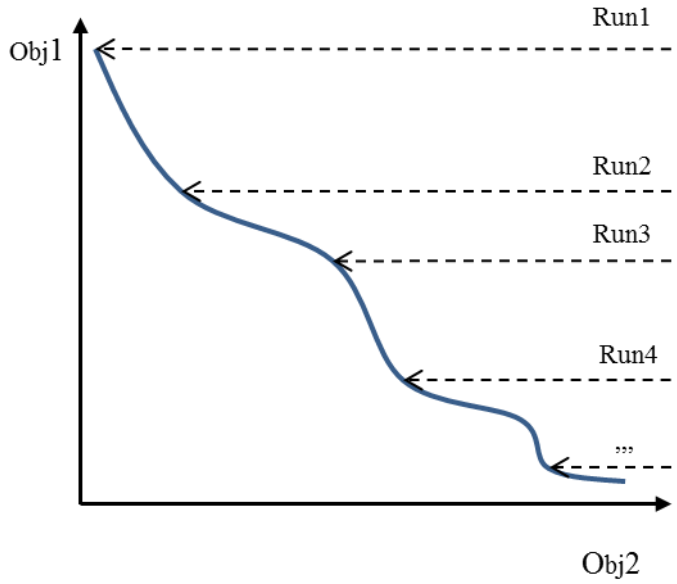

Figure 7: Pareto built from single optimum algorithm

1.3.2.2 Elitist Multi-Objective Evolutionary Algorithm

The EMOEA algorithms introduced in [1.3.5.3] and [1.3.5.4] are shaped to find optimal Pareto-fronts for multi-objectives problems. Unlike other algorithms, they require only a single run. The single run can be more expensive than several runs of other algorithm, but for numerous objectives or when Pareto-front is not smooth, they prevailed. Their mechanism of population selection on the front guarantees the search of the whole Pareto.

1.3.3 Constraints

Most of designs are realized with constraints from various origins, geometrical, electrical, financial etc. The constraints are an issue for the good convergence of the algorithms. Indeed they complicate the form of the domain of solution reducing the chance to find the optimum. But constraints also introduce a discontinuity in the problem, i.e. the model can be impossible to compute when constraints are not respected and thus the set of input creates an unfeasible

solution leading to the stop of the optimization. If the optimum is near the boundaries defined by the constraints the convergence can be dramatically slowed down because the refine of the solution will be more difficult. The main methods to deal with constraints are presented below.

1.3.3.1 Suppression of constraints

The best solution to prevent issues from a constraint is to suppress it. It relaxes the weight of optimization by diminishing the number of check and prevents the stop of convergence. The method is generally applied in the definition of inputs or in the model.

E.g. the definition of inputs $b_{inf}<x_1<b_{sup}$ and $c_{inf}<x_2<c_{sup}$ with the constraints $x_1<x_2$ can be rewrite replacing one of the input by another. $x_2 = x_1+x_3$ with $d_{inf}<x_3<d_{sup}$. Thus the constraint is suppressed.

This approach places the effort on the designer and liberates the optimization process. A careful attention has been paid to this in the model presented in chapter II.

1.3.3.2 Penalties

When the design does not allows the suppression of constraints, those ones can be integrated in the objectives function by the penalties method. This method adds a handicap on the set of inputs violating the constraints. Two approaches are possible.

The method of external penalties replaces the objective function by a summation of problems without constraints degrading the solutions violating the constraints: $\min f(x) + \sum_i \alpha_i . g(x)$. α is suite of scalar tending toward the infinite. Illustration is presented in (Figure 8) for objective function f with constraint that $x<1$.

The other method is the interior penalties. Instead of penalizing solution violating the constraints, the method penalizes the admissible solutions close to the constraints (Figure 9). This method is particularly fitted to problem where solution cannot be computed when constraints is not respected.

1.3.3.1 Lagrangian

The last solution for constraints is the Lagrangian function. The Lagrangian is a function that summarizes the dynamic of a system. In the case of optimization it unifies the objective function with the constraints of equality and inequality in a same function. The Lagrangian uses the same pattern than external penalties but with the multiplier are computed at each iteration.

$$L(x, f, \lambda) = f(x) + \sum_i (\lambda_i . g(x, f(x))) + \sum_j (\lambda_j . h(x)) \quad (4)$$

λi and λj are the Lagrange multiplier. Moreover, the Lagrangian does not impose the respect of constraints during the optimization, except at the end. So the convergence can be prevented when constraints must be satisfied at each computation of the objective function.

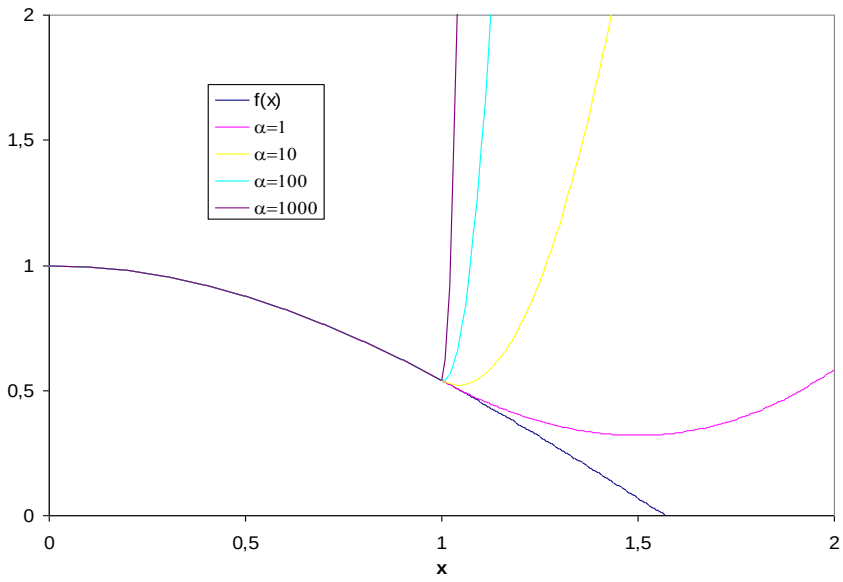

Figure 8: Method of external penalties to prevent solution x>1

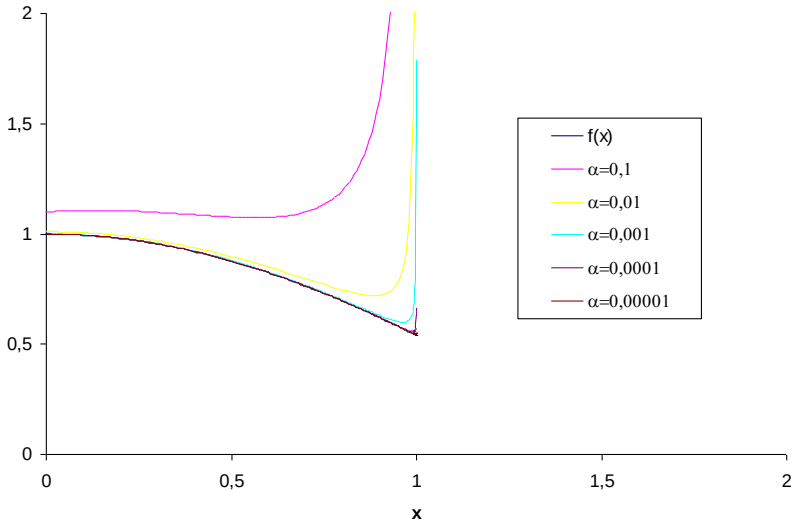

Figure 9: Method of interior penalties to prevent solution x>1

1.3.4 Deterministic Algorithms:

Deterministic algorithms search for the optimal solution with the fastest and most efficient convergence. This is also a drawback because the optimum is generally local and not global. They are fitted for large number of parameters and large number of goals and constraints.

1.3.4.1 Surface Mapping Method

The Surface Mapping Method (SMM) is widely used in optimization. It build surrogate model of the objective function to reduce the complexity of the problem and enhance the time of optimization. It is an indirect optimization; the surrogate model prevents direct communication between the algorithm and the initial model. The surrogate function can be computed at the beginning of the optimization and stay the same or it can be rebuilt locally at

each iteration [2]. With the local approach, at each iteration the surrogate function is more accurate than the previous one, derivative can be deduced from variation of the surrogates if the behavior is monotonous and finally preferred directions are computed. The SMM can be of 0^{th}, 1^{st} or 2^{nd} order regarding the approximation used. In the local approach three main methods are used in SMM and define strategy of optimization.

Sliding approach

The first map is constructed in a part defined by the user. This first map gives the preferred direction for convergence and the size of the map stay unchanged after. This information coupled with the previous maps lead to the next map. This is an iterative process, the optimum are locals because they rely on the first map (Figure 10).

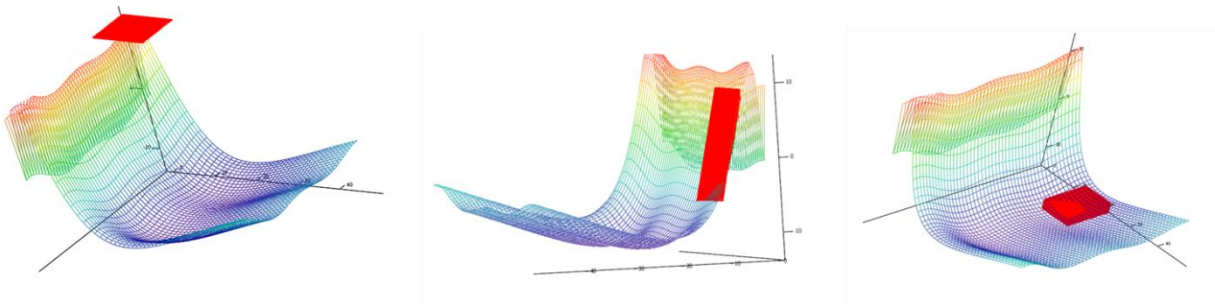

Figure 10: SMM sliding approach on Belledonne problem

Zoom approach

The previous strategy is local, only a slight part of the objective domain is searched. A better approach is to map the whole domain and zoom on the area giving the best convergence. The fastest process is to reduce consequently the map at each iteration, but this can lead to focus on a local optimum rather than the global optimum. To guarantee the convergence, a good balance must be found between speed (few zoom iterations) and precision (size of the zoomed map) (Figure 11).

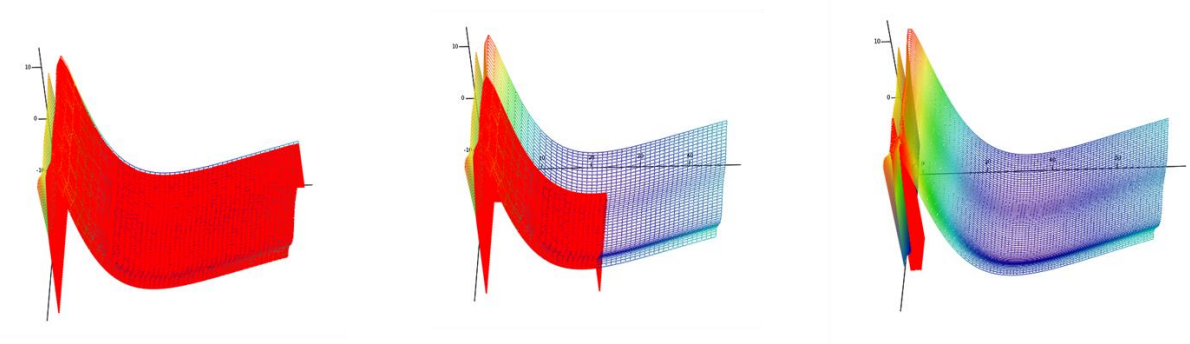

Figure 11: SMM zoom approach on Belledonne problem

Comprehensive approach

To guarantee the global optimum convergence, the SMM is used to model the variations of the whole domain. Each iteration, a polynomial function is surrogated to the objective

function to map it. Considering the limitation of modeling induced by polynomial function, the objective function is approached by piece map. The whole domain is divided in sub-domains; in each a map is computed. The continuity between sub-domains is not guaranteed (Figure 12).

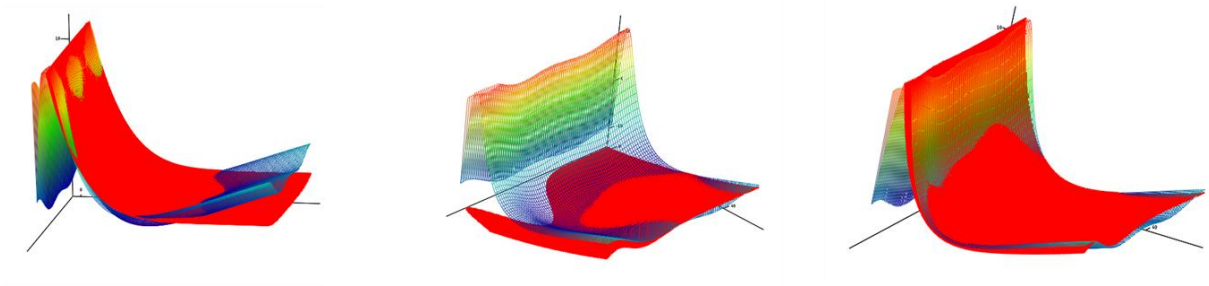

Figure 12: SMM comprehensive approach on Belledonne problem

The three approaches for SMM have not the same pattern; their use will depend on the problem. Sliding requires little iteration so it is fast but not accurate. This algorithm chained with a local search algorithm on the model proves efficient on complicated objective function. It is still a local optimum search.

The zoom SMM allows the search of the global optimum with a longer time of calculation. The convergence on the global optimum is not sure in every case.

The comprehensive approach increases the probability to find the global optimum by subdividing the domain. It is the most expensive of the three but makes it possible to compute accurate surrogate to the objective function.

However, SMM in general deals badly with constraints that prevent calculation. The maps are predefined and do not consider constraints. So if a model cannot be computed if the constraint is not respected the surrogate point is unfeasible. The choice of surrogate points is then difficult so the surrogate maps will be tougher to build.

1.3.4.2 The 0^{th} order

The direct search methods do not require derivatives. They only use direct value of the objective function. They can explore non continuous function and are not really sensitive to numerical noise.

1.3.4.2.1 The grid search

The grid search is the basest principle. Every input parameter is discretized between lower and upper bound. The whole combination of values of the k inputs parameters defines a k dimension grid mapping the objective function. The grid search consists in computing each node of the grid. The finest the grid is, the closest the solution is to global optimum. This method is expensive in computation time and increase dramatically with the number of parameters and the discretization of the grid. It is a determinist algorithm thus it delivers one optimum.

For the Belledonne case, the solution is close to the global optimum, only the accuracy of the grid will enhance the precision. But the algorithm is not trapped by local optimum. For the Bi-sphere, the algorithm always converges to the lowest point of the crossing of both spheres because goals have the same weight so crossing is the best tradeoff between both.

1.3.4.2.2 The simplex method

The simplex method is a local iterative optimization, with a spatial propagation form the previous point to the next, which means like many determinist algorithm, the initialization set of parameters will decide of the convergence toward a local or the global optimum. A *k* simplex is the generalization of a 2D triangle to a *k* dimension space. Its process is easy:

- Initialization
- Computation of the summit of the triangle
- Classification of summits regarding objective function
- Computation of new summits considering worst and best previous ones

Usually the summits are classified as Best point, Worst point *W* and *N* the second best point for convergence. The most known method is the Nelder and Mead [1] with the introduction of adjustable step. When a direction is favorable, biggest step are taken. Reversely, in the direction of the worst solution, steps are reduced. These notations are referred as *expansion* and *contraction* of the simplex. Relations to compute simplex are:

- Reflection $R = C + \alpha(C-W)$ $\alpha \sim 1$
- Expansion $E = C + \gamma(C-W)$ $\gamma > 1$
- Contraction to R $CR = C + \beta(C-W)$ $0 < \beta < 1$
- Contraction to W $CW = C - \beta(C-W)$ $0 < \beta < 1$

C represents the barycenter of the *k* best points of the previous simplex. The principle is shown in (Figure 13).

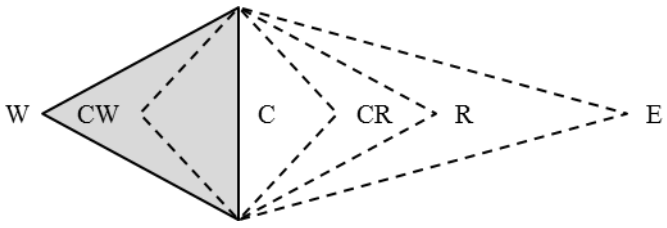

Figure 13: Simplex method

The simplex method is the most efficient of 0^{th} order approach. The mechanisms are easy and it does not require much time to converge toward the optimum. However the simplex needs many iterations to converge to the optimum when close of this one, because of the iterative reduction of the simplex. But coupled with another method, it can be really fast. Attention must be paid to the case of constrained optimization because a false value is imposed on the objective function when a constraint is violated. This trick to stay in the search domain leads to wrong information on the convergence of the algorithm.

On Belledonne problem, the simplex converged in 37 iterations. Its convergence is illustrated in (Figure 14). Only a local optimum is reached and the path followed by the algorithm is not the fastest one.

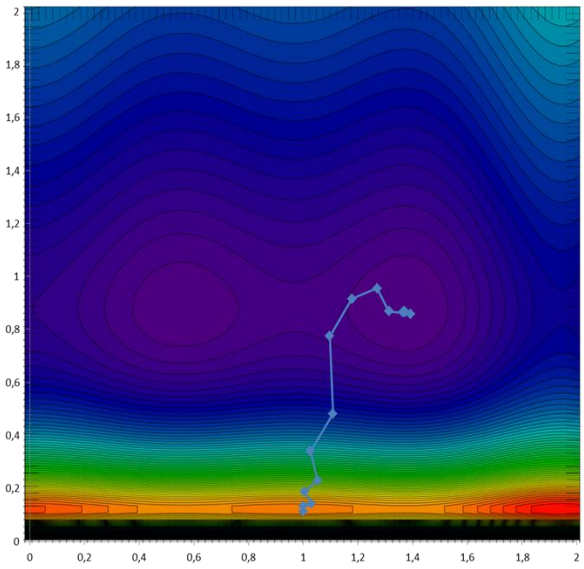

Figure 14: Simplex Nelder&Mead convergence for Belledonne problem

On the bi-sphere problem, the simplex converged in 32 iterations toward the minimum of mono-objective computed from *f1* and *f2*. The optimal point found by simplex is the exact balance between both objectives. It comes from weighting on goals. An unequal balancing would have leaded the algorithm toward one or the other goal.

1.3.4.3 The 1st order

The 1st order algorithm use first derivative of outputs according to inputs. This is the jacobian matrix build from gradient. It is an approach reducing the time to converge and the good direction taken between two iterations. Indeed, for a function *f* of C^1 category (differentiable with continuous derivative), the gradient of this function at the point x is the direction of the greatest increase of *f*. So it gives the best direction to search for reduction or increase of the function.

1.3.4.3.1 The Steepest slope

The Steepest Slope Method is one of the easiest gradient methods. The gradient giving the greatest increase, to minimize *f*, a step is taken in the opposite direction, which is the steepest slope. The direction for vector of inputs *x* is:

$$d(x) = -\nabla_x f \quad (5)$$

So, knowing vector of inputs x_i, the next set x_{i+1} is defined by:

$$x_{i+1} = x_i + \alpha . d(x_i) = x_i - \alpha . \nabla_{x_i} f \quad (6)$$

α defines the length of the step to x_{i+1}. A *line search* procedure based on residues is applied to find the best value of α (Appendix A). (Figure 15) illustrates on the search line that a best

value of α can be found to choose x_{i+1}. Indeed if α is not correctly set the next step contains part of the previous direction, which leads to lose time and efficiency. So for each set of inputs the gradient is used to find the best direction for the next step and a line search procedure is used to choose the length of the step. X_i is a vector of inputs, the gradient is unequal for each line of x_i meaning for each input parameter so is the value of α. The length is not necessarily the same for all input parameters

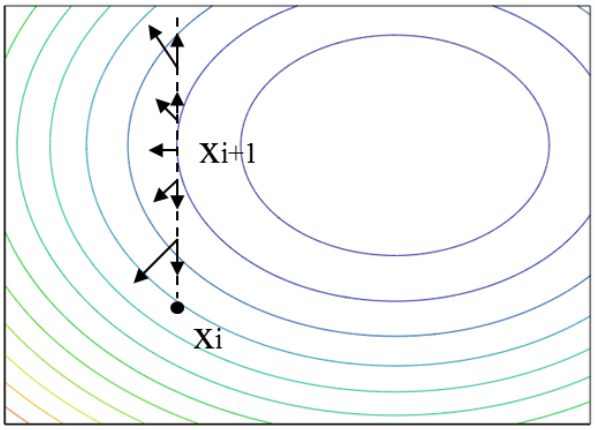

Figure 15: Steepest slope path from one point to the next

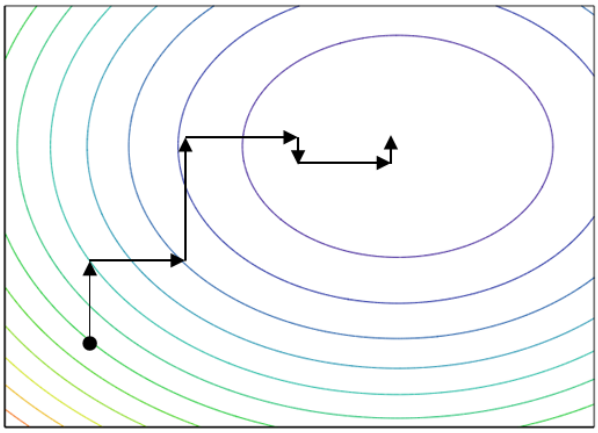

Figure 16: Convergence of SSM

The steepest slope method is known for slow convergence because the same direction can be taken many times (Figure 16). This default is corrected by the conjugate gradient method using the hessian. However, the SSM is easy enough to understand gradient convergence mechanisms.

1.3.4.4 The 2nd order

To correct the drawback of not taking into account the variation of the objective function, the 2nd order method use the hessian, the second derivative of the function considering local variations of the function.

1.3.4.4.1 The Conjugate Gradient

The purpose of the CG method is to keep the SSM principles and speed up the convergence. In the SSM same axes of research can be taken many times. It would be faster to impose that each step must be orthogonal to all previous directions. So an A-orthogonal family of vector is built for direction search *d(x)*. I.e. each new direction *d* is orthogonal to all previous directions. To find new orthogonal directions the local variations of the objective function *f* are considered using the hessian matrix. The hessian matrix is used to ensure the A-orthogonality of each new direction so it is not necessary to store old search vectors. This is what makes CG an important algorithm.

CG proves really effective on Belledonne problem. It took 7 iterations to converge toward the global optimum. The starting point was the same as the simplex but CG started in the good direction (Figure 18). We change the initial point of the optimization near the global optimum, to force CG to depart in the other directions. It took only two iterations each time for CG to reach the other optimums and finally converge on the best of the 3 local optimums (Figure 17).

On the bi-sphere problem, CG is much more efficient and the same optimum as simplex is reached in one iteration only.

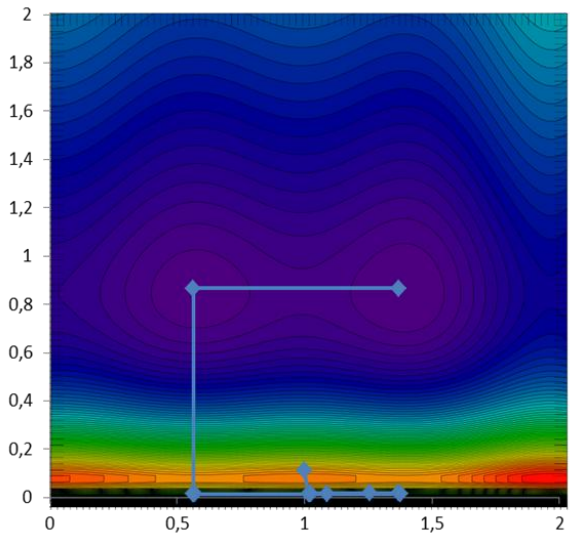

Figure 17: Convergence of CG algorithm on local optimums

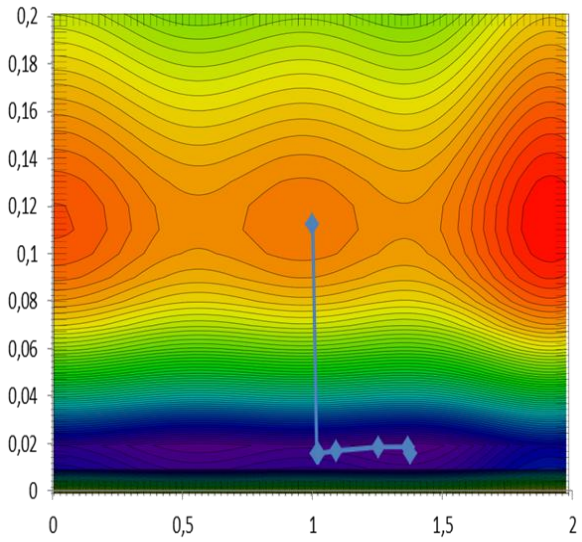

Figure 18: Zoom on Belledonne surface; Convergence of CG toward global optimum

1.3.4.4.2 The Quasi-Newton/ BFGS algorithm

The 2nd order algorithms like CG use the hessian matrix of a function, which is not always calculated analytically for speed up reason. The Quasi Newton method (QN) is based on the Newton approach to compute approximation of the second derivative of a function around a specified point. The development to second order of a function near x_0 is:

$$f(x_1) = f(x_0) + \nabla_{x_0} f^T.(x_1 - x_0) + \frac{1}{2}.(x_1 - x_0)^T.A.(x_1 - x_0) \quad \textbf{7}$$

So the purpose of the method is to find the value of x that minimizes the second order approximation.

$$\nabla_{x_1} f = 0 = \nabla_{x_0} f + A_{x_0}.(x_1 - x_0) \quad \textbf{8}$$

The next iteration point is easily deduced:

$$x_{i+1} = x_i - (A_{x_i})^{-1}.\nabla_{x_i} f \quad \textbf{9}$$

In this equation the inverse of the hessian matrix is needed, which lead to important calculation and time processing. A convergent iterative process is substituted to the inversion of the hessian by computing approximation of the inverse at each iteration. They are the QN approaches. The pattern of CG method is reused.

$$x_{i+1} = x_i - \alpha_i.S_i.\nabla_{x_i} f \quad \textbf{10}$$

α is still the minimum along the direction imposed by the opposite of S_i and the gradient (line search in an orthogonal base). S_i is the matrix approximation of the hessian A, built from the previous calculations, $S_{i+1} = S_i + C_i$. C_i is a correction matrix based on the condition of Newton. The best calculation of C_i matrix has been introduced by Broyden-Fletcher-Goldfarb-Shanno (BFGS method) [3]-[6].

The iterative and numeric approach of the hessian matrix impose the objective function to be continuous and with low level of numerical noise.

On the Belledonne problem, BFGS converged in 4 iterations towards the global optimum (Figure 19). However, unlike the CG, it took only 2 iterations to reach the good area, and the local search takes 2 iterations to refine the result.

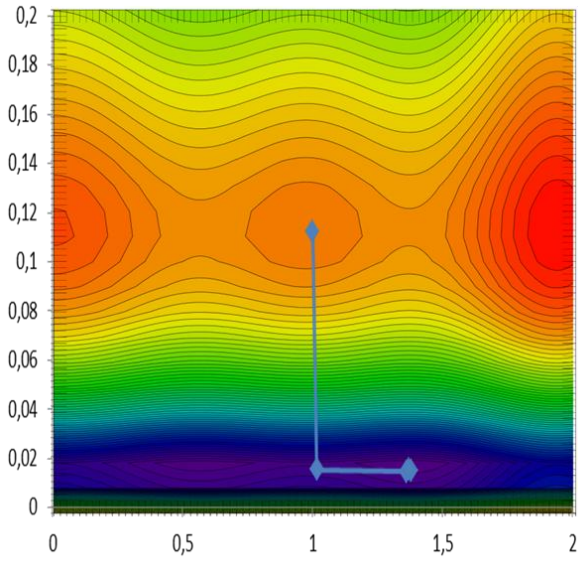

Figure 19: BFGS algorithm convergence on Belledonne surface

On the bi-sphere problem BFGS acts like CG.

1.3.4.4.3 The SQP

The Sequential Quadratic Programming method is based on the computation of the Lagrangian function. It is a nonlinear optimization innately taking into account constraints. This method is a strategy for finding the local maximum and minimum of a function subject to constraints. The purpose is to minimize this Lagrangian function, using a QN (Quasi Newton) approach to solve the quadratic problem of the second derivative minimization. The BFGS method is generally used sequentially until no better solution can be found.

The SQP algorithm is one of the best nonlinear constrained methods. However like the BFGS it is sensitive to numeric noise because of the local approximation of both gradient and hessian.

1.3.5 Stochastic algorithms

Unlike deterministic algorithms, stochastic algorithms are based on random approach. Two launches of the algorithm from the same starting point won't follow the same path. They are generally used for problem with discrete parameters or when several local optimums exist to find the global optimum. Stochastic approach are often based on observation of mechanisms of the nature, ant population, energy evolution of a cooling mass in fusion (simulated

annealing), or Darwin evolution theory. The genetic algorithms are of this last family. This manuscript focuses on the genetic algorithm because they are widely used in our optimizations.

1.3.5.1 The Genetic Algorithm (GA)

The GA is based on the genetic analysis of the human nature. The most performing individuals of a population have higher probabilities for their genetic material to be used in the next generation. Then every new generation must be better than the previous one. The creation of new individuals is achieved by elitism, combination of the best individuals but also by random mutation of the genes. This approach is easily translated to optimization.

An individual is a set of adjustable parameters. To match genetic, parameters are generally described as binary string of 0 and 1. A population is made from several individuals. Each individual is noted according to its performing in satisfying the objective function. The optimization finds the best individuals by amelioration of a fixed population at every step.

1.3.5.1.1 Selection

During each successive generation, a proportion of the existing population is selected to breed a new generation. The creation of a new generation of population is done using three operations. The elitism consists as keeping the n better individuals to carry over to the next generation, unaltered. It guarantees that the solution quality obtained by the GA will not decrease from one generation to the next. The tournament is the random selection of two individuals and only the better one is keep as a parent for the next generation individuals. This process is repeated until enough parents are selected to brew next generation. The roulette wheel selection or fitness proportionate selection is used to illustrate the performing proportion of an individual compared with the performing of the population. A wheel is created with segment for every individual. The segment size is proportional to the individual performing. Then a random selection is made similar to how the roulette wheel is rotated. Thus, best individuals have higher chance to be picked up but not necessarily.

Once the parents are selected, a new generation is created by their crossover.

1.3.5.1.2 Crossover

The one-point crossover, both parents binary strings are cut at the same length, and then the second parts of the data are swapped between them to create children.

The two-point crossover, both parents binary strings are cut two times at the same length and the middle parts are swapped.

The cut and slice crossover, both parents binary strings are cut at unequal length and swapped. This results in the change of size for children.

The uniform crossover uses a fixed ration of genes of the parents to be swapped.

The genes of parents and children match one input parameter. The crossover between a temperature input and an electric input would be incoherent.

1.3.5.1.3 Mutation

The mutation is an operation that changes gene values randomly. Its role is crucial in the convergence of a genetic algorithm because with selection and elitism the genetic algorithm tends towards a homogenization of the population. Mutation creates brand new individual and brings new area of research. Where selection and crossover lead to converge to accurate solutions, mutation extends the search to the whole domain. Several processes of mutation are used. The bit mutation is the flip of a random gene from 0 to 1 or inversely. Flip bit changes the genes value of the whole string. Many other mutation operators exist and are not listed here.

GA uses partial random set of adjustable parameters which guarantee a better exploration of the solution domain with simultaneous points of convergence. The chance of finding the global optimum is huge and new unanticipated solution can be found.

On Belledonne problem, GA reaches the global optimum in 42 generations of 50 individuals. Only the global optimum is delivered by the algorithm.

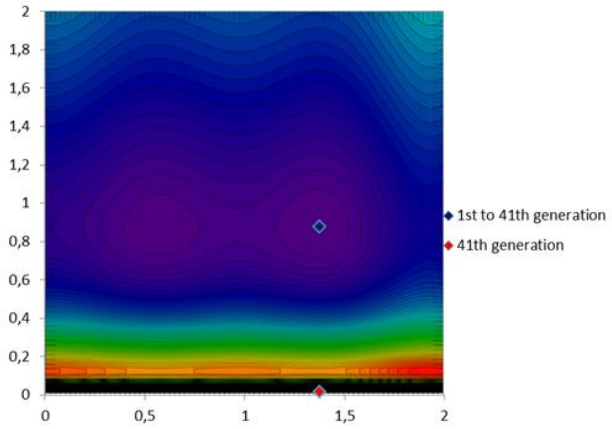

Figure 20: GA convergence on Belledonne problem

1.3.5.2 The Niching

GA is suitable for locating the optimum of unimodal functions as it converges to a single solution of the search space. Industrial optimization problems often lead to multimodal domains and so require the identification of multiple optimums, either global or local. For this purpose niching methods extend simple GA's by promoting the formation of stable subpopulations in the neighborhood of optimal solutions, the niches. Several niching methods exist [7].

1.3.5.2.1 The Fitness Sharing (FS)

The fitness is a representation of the performance of an individual. The purpose of the FS is to reduce the density of populated regions. It lowers each niche's individual fitness by an amount of the number of similar individuals in the niche population. For an element *i*, who shares a fitness f_i with m_i individuals the new fitness is:

$$f_{n_i} = \frac{f_i}{m_i} \quad (11)$$

The goal is to reduce the attraction of equivalent individuals and highlight unique individual. Actually, the more elements are sharing the same fitness, the more the equivalent fitness of those individuals will be reduced and thus also their chance to be selected for brewing new generation.

The niche count m_i is done by summing a sharing function over all the members of a generation population.

$$m_i = \sum_j sh(d_{ij}) \quad (12)$$

Where *dij* represents the distance between *i* and *j* and *sh* the sharing function that measures the similarity between two elements. It returns one if the elements are identical and zero if their distance is higher than a threshold dissimilarity, the niche radius.

$$sh\left(d_{ij}\right) = \begin{cases} 1 & \text{if } d < \alpha \\ 0 & \text{otherwise} \end{cases} \quad (13)$$

Sharing tends to encourage search in unexplored regions of the space and favors the formation of stable subpopulations. However setting threshold α requires the knowledge of the distance to the optimum which is not the case so setting the same α for all individuals can lead to privilege optimum rather than other.

1.3.5.2.2 Clearing

The clearing method is similar to fitness sharing, but instead of sharing the fitness with all individuals, only the least good individuals share fitness. So in a niche the best individuals' fitness is preserved and the others are reduced. As in the sharing method, individuals belong to the same niche (or subpopulation) if their distance in the search space is less than a dissimilarity threshold.

1.3.5.2.3 Crowding

Crowding method inserts new elements in the population by replacing similar individuals.

In standard crowding [9], an offspring replaces the most similar individual (in terms of genotypic comparison) taken from a randomly drawn subpopulation of size of a crowding factor from the global population.

In deterministic crowding [8], standard crowding is improved by introducing tournament competition between parents and children in a same niche when crowding with offspring.

The Restricted Tournament Selection [10] is a last improvement of the crowding method. RTS initially selects two elements from the population to undergo crossover and mutation. After recombination, a random sample of individuals is taken from the population as in standard crowding. Each offspring competes with the closest sample element. The winners are inserted in the population.

Conversely to all previous algorithms, Niching provides multi-optimum result (Figure 21). The optimums are less accurate than CG or BFGS, but all local optima plus the global optimum are found in 49 generations of 50 individuals.

On the bi-sphere problem, several optimums are given (Figure 22). The classic optimum provided by all previous algorithm plus other optima. These ones, not necessarily interesting, result only of the need for the algorithm to keep several niches along the optimization.

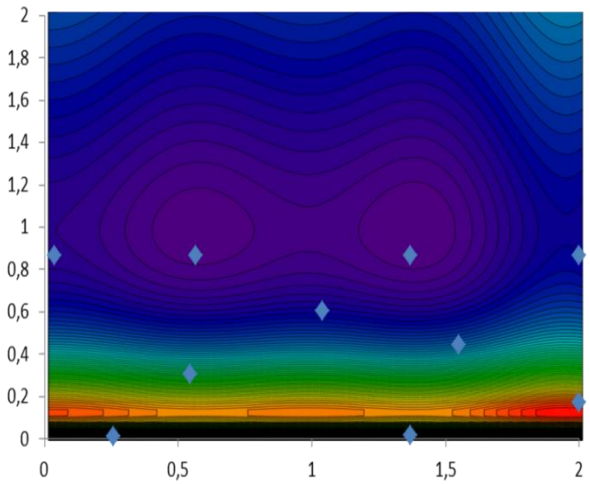

Figure 21: Niching solutions on Belledonne surface

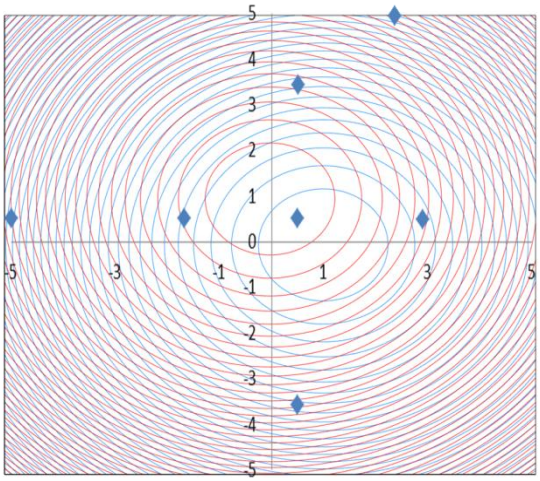

Figure 22: Niching solutions on Bi-sphere surface

1.3.5.3 Non Sorting Genetic Algorithm II

The NSGA-II [11] is an evolution of the NSGA [12] Elitist Multi-Objective Evolutionary Algorithm. As indicated by its name, this algorithm is part of the genetic algorithm build to find the Pareto-optimal front of a multi-objective problem in a single run. In the modern

application problem it is impossible to find a single optimal solution that optimizes all objectives. An algorithm that gives a large number of alternative solutions lying on the Pareto-optimal front is of great practical use for a designer in the industrial world.

NSGA has many faults: a high computational complexity of non-dominated sorting, a lack of elitism and the need for specifying a sharing parameter as in Niching fitness sharing. To address all these issues NSGA II was proposed and is now the most used multi-objectives algorithm.

First an initial population is created, then the population is sorted based on the non-domination. The goal is to sort all individuals in several Pareto-fronts, the 1st being the best and the nth the worst. In the NSGA approach all N individuals are compared with all N individuals for m objectives, mxN^3 calculation at max. The fast non-domination use in NSGA II is a process to reduce the number of computation to mxN^2 at max:

For each individual p in main population P :
- *Initialize Sp = [0]. This set would contain all the individuals that are being dominated by p.*
- *Initialize np = 0. This would be the number of individuals that dominate p.*
- *for each individual q in P*
  - *if p dominated q then add q to the set Sp i.e. Sp = Sp U {q}*
  - *else if q dominates p then increment the domination counter for p i.e. np = np + 1*
- *if np = 0 i.e. no individuals dominate p then p belongs to the first front; Set rank of individual p to one i.e prank = 1. Update the first front set by adding p to front one i.e F1 = F1 U {p}*

This is carried out for all the individuals in main population P.
- *Initialize the front counter to one. i = 1*

Following is carried out while the i^{th} front is nonempty i.e. Fi ≠ Ø
- *Q = Ø. The set for storing the individuals for $(i + 1)^{th}$ front.*
- *for each individual p in front Fi*
  - *for each individual q in Sp (Sp is the set of individuals dominated by p)*
    nq = nq-1, decrement the domination count for individual q.
    if nq = 0 then none of the individuals in the subsequent fronts would dominate q. Hence set $q_{rank} = i + 1$. Update the set Q with individual q i.e. Q = Q U {q}.
- *Increment the front counter by one.*
- *Now the set Q is the next front and hence Fi = Q.*

This algorithm is better than the original NSGA since it utilizes the information about the set that an individual dominate (Sp) and the number of individuals that dominate the individual (np). It is then faster and with less calculation to find all the fronts.

Then to get an estimate of the density of solutions surrounding a particular point in the population, the average distance is taken between the two points on either side of this point along each of the objectives.

Once all the individuals are sorted, the best individuals are taken, i.e. the individuals in the lowest ranked Pareto (the best Paretos) and with the higher density distance (isolated individuals, same principle as niche). Classical genetic tournament selection, crossover and mutation are done. Then the new population created with the best previous individuals (elitism) and the children is non-dominated sorted to create the next generation. Since all the previous and current best individuals are added in the population, elitism is ensured.

To sum up, a first population is created and sorted. Then each optimization iteration, the best individuals are used for genetic breeding. Fast non-domination sorting and density estimation

are used and a new population is selected from Pareto-front ranking and crowding comparison.

NSGA-II addresses multi-objective problems to find the optimal Pareto-front in a single run. It is often better than its competitors [13] [14] and [15].

1.3.5.4 Grid Multi-objectives Genetic Algorithm

Like NSGA II, GMGA is an algorithm to find the optimal Pareto-front of multi-objective problems. GMGA is perfect for industrial applications. It is based on the discretization of adjustable parameters to form a grid. Each parameter's grid step is chosen independently, for geometric parameter e.g. it could be really interesting to choose micrometers for wire or millimeters for magnetic core. This is also useful to set a grid step to one for library use, where each number represents a component or material.

The first step defines the grid setting bounds for the parameters and their grid step.

Then the first population is generated using the Latin Hypercube Sampling [16]. A LHS selects points on a grid in order to make certain that the n possible levels of parameters are tested one time (Figure 23). The points are uniformly distributed on the axes of the domain. It does not ensure the uniformity of resulting solution on the domain.

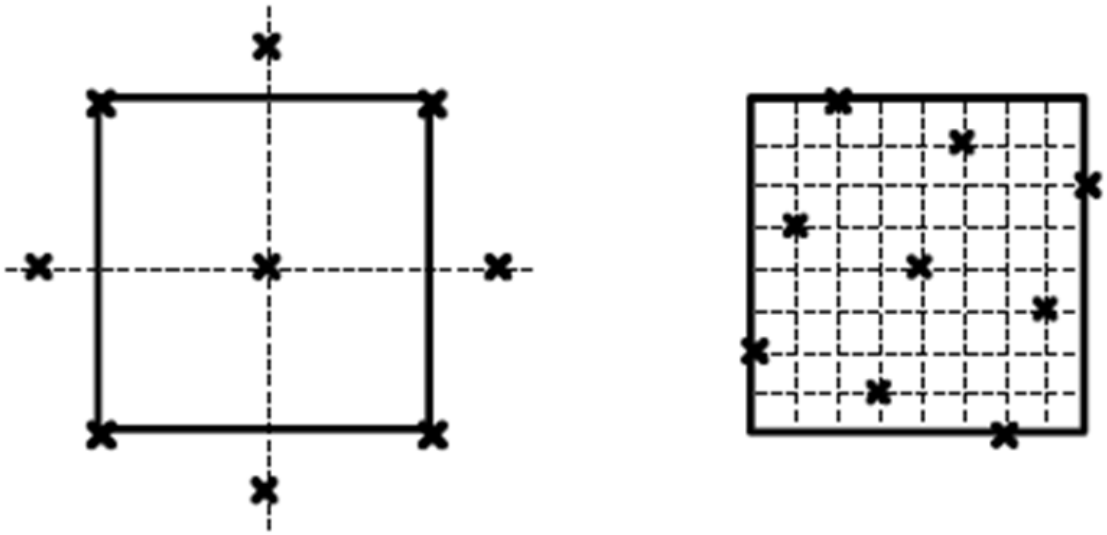

Figure 23: Grid selection, left standard sampling, right Hypercube Latin

For the next generation, the process is similar to NSGA II. Elitism is used to select the parents. Every point on the grid close to the best solution is explored. Then selection, crossover and mutation are used. The Pareto-front is improved using vicinity mutation.

The domination sorting is not the same as for NSGA II. Cells (i.e. the sizes of the grid step) are built for each parameter. Only one individual is authorized per cell. If the number of children after this sorting is higher than the required population, the cell size is increased. The best individual per cell is kept. The new population is built.

On Belledonne problem, for GMGA the goal is set inferior to -10 optimal solutions are returned (Figure 24). The optimums are distributed on grid points of the surface lower than 10.

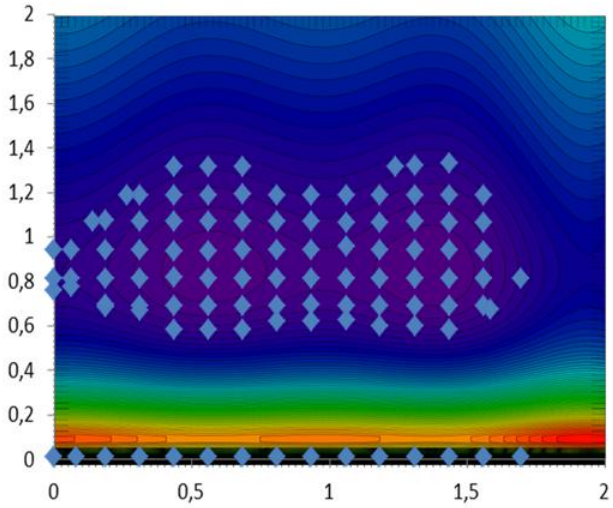

Figure 24: GMGA results on Belledonne surface

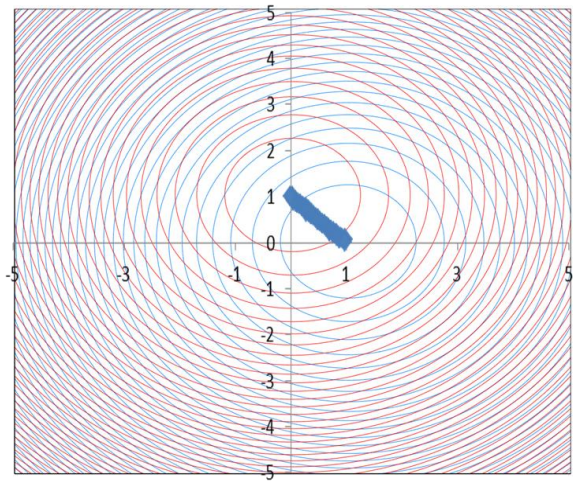

Figure 25: GMGA results on Bi-Sphere surface

On the Bi-sphere problem, GMGA gives all the optimums between both sphere minimums (Figure 25). This algorithm allows the perfect tradeoff between both goals unlike previous algorithms that gave only one. GMGA is particularly adapted for multi-objectives problem.

1.3.6 Conclusions

Two main families of algorithms have been presented. Determinist and stochastic most employed algorithms have been introduced in order to understand their mechanisms. The knowledge of algorithm convergence and capacities is essential to use them properly and in

the good application. Since many issues in optimization come from the wrong association of a model and an algorithm, this association is part of the strategy chosen for the optimization. The model can be imposed, but when no model exists it appears easier and better for convergence to build a model fitting algorithm capacities. This will be investigated in the following section.

1.4 STRATEGIES

1.4.1 Introduction:

The choice of algorithms for optimization cannot be done without according it to the strategy chosen for optimization. The strategy is the decision of which algorithm applied on which model for which purpose. Two main types of strategies can be separated, pre-sizing and sizing.

Pre-sizing is particularly fitted for heavy time computing model with lots of parameters and constraints. The complexity of the system to be sized compels to build a simplified modeling. Most of the time, this approach is associated to indirect methods. The goal is to find quickly an approximate optimized solution for the problem. However, the use of a surrogate model (e.g. linearized model), prevents directly obtaining a solution for industrialized production. Discrete values must be linearized. This approach is using determinist algorithms, what is better with lot of parameters. A second study is achieved after optimization around the optimal solution, e.g. discrete parameters are fixed to the closest discrete value from the continuous one. It can lead to the need for several prototypes. Furthermore, the use of determinist algorithm often leads to local optimum. Better solutions of pre-sizing are found using hybrid approach of coupling stochastic search of the domain and local focus with determinist algorithm. When searching discrete library of material e.g., strategy of linearization of this library are computed.

The pre-sizing context is then to be preferred with a large number of parameters and continuous problems with no library.

The sizing approach is really interesting in an industrial problem with library of components and discrete sizes of parameters. The optimal solution is then directly used for prototyping and reduces drastically the time to market of the product. However, discrete values and libraries prevent 1^{st} and 2^{nd} order determinist algorithms. Stochastic algorithms like genetic ones are fitted for this approach but the number of parameters, goals and constraints cannot be numerous because of the nature of those algorithms.

Sizing context is chosen for discrete problem with few parameters; it can be seen as a smart choosing method among too numerous market solutions.

More than these two definitions of approach, strategy of optimization also deals with the choice of modeling development platform. The sizing of a power converter is a multi-physics problem with many interactions. Nowadays, designers use multi-software: Finite Element Analysis for magnetic components or thermal simulation, circuit simulation for topology electric behavior, control software for regulation of the converter, etc. The emergence of multi-physic software like Comsol®, Moose® or Ansys® shows the need of this kind of approach.

The goal of optimization is important too. The approach is not the same if the purpose is to find an improved solution or to find the best possible solution or to provide Pareto-front solutions for designer help.

There are as many strategies as problems. The specifications defined by Schneider Electric and their manufacturer experience have influenced the strategy of this project presented in this paragraph.

1.4.2 Schneider Electric Experience:

Power converters are multi-physic and multi-interaction objects. Their multi-physic simulation is extremely complex and heavy time consuming, without simplifications. A strong aspect of this PhD is that several assumptions and problem reductions have been done based on Schneider Electric experience. Focus to be done on a given physical phenomenon, strong or weak interaction in the converter and industrial context are highlighted based on this experience.

1.4.2.1 Components

Power converters are built with passive components (resistance, capacitor and magnetics) and active components, mainly semi-conductors. For passive components, capacitors and resistors are picked from catalogs and don't benefit from adjustable parameters other than their electric value R,C. Magnetics for high power converters on the other hand are not available as catalog products. They are entirely designed by Schneider Electric. So the number of their adjustable parameters and their impact on efficiency and cost of the whole converter make them the principal case of study for optimization. Regarding efficiency and cost, the other focus must be on semi-conductors. However, the amount of leverage on semi-conductor manufacturing is low for Schneider Electric, semi-conductors are treated as library components, and only their modeling must be accurate because their losses are important and the optimization must find a good balance between filter and semi-conductors. I.e. the increase of legs and voltage level decrease the need of filter but increase the need of actives components. Thus for an optimal solution of efficiency increase losses must be correctly calculated for chokes and semiconductors.

1.4.2.2 Strong and weak Interactions

What makes the simulation of a power converter tricky is the multi-interaction between components' behavior and regulation. E.g. for an inverter, the DC source is switched between voltage levels in order to deliver an equivalent mean sinus voltage at the output. To do it, switch cells are assembled regarding the multi-leg multi-level topology and are controlled at high frequencies ~kHz to connect alternatively to a common point the DC voltage potentials with a modulated time for this connection in order to produce a mean sinus value at 50 Hz or 60 Hz. Switched waveforms contain harmonics thus passive RLC components are added to filter the HF harmonics. The HF switching command of the semi-conductors is done regarding the output waveforms. However, the filter components are not linear; their values L

and C depend on the level of current they are subject to, so they impact the high frequency current and voltage at each switch and consequently the low frequency required waveforms. Output waveforms must be sampled with frequency higher than HF switches and time of connection of semi-conductors readapted to guarantee output values. This is an iterative process with lots of sampling points and multi-component simultaneous simulation.

Schneider Electric experience reveals that some interactions can be ignored when looking at components separately and others cannot. The design must be achieved regarding electrical waveforms of the converter and not using the conventional filter approach with RLC values and simple cut-off frequency or attenuation requirement filter template.

The LF waveforms must be guaranteed at any time because they are the aim of UPS. This is the role of the regulation of the converter. LF waveforms represent a strong interaction inside the converter; they cannot be abided. To design the components of the converter, **we assume that regulation will be correctly done to insure LF waveforms**. However, the **HF waveforms are weak interactions** between components, they can be studied separately. Indeed, the good sizing of filter components with perfect regulation providing LF waveforms will guarantee that HF spectrum slight changes caused by HF modulation of switches with real regulation, will not impact the design.

This is a strong assumption validated by Schneider Electric experience. It allows designing converter directly in steady state, without regulation iterations. It reduces consequently the time of calculation. Another strong advantage of this approach is that passive components can be optimized without active components if needed. Whatever the semi-conductors, the voltage at the output of the inverter can be defined from the number of voltage level and the number of legs and the switching frequency. Constraints must be added to the optimization of passive components to prevent malfunctioning of active components, e.g. maximum current. Illustration of these assumptions and validations are presented in chapter three.

1.4.2.3 Sampling

In the power converter, LF and HF effects must be studied. Local maximum of HF waveforms are reached at each switching event. Experience shows that considering only these moments for simulation without regarding non-linear evolution of value between two switches is accurate enough. Note those maxima are computed considering non linearity of components. The sampling is consequently reduced.

This assumption is stronger with higher frequencies and magnetic powder core. When using FeSi steel transformer, non-linear evolution between two switches impacts the core losses calculation. So this assumption must be verified depending on the materials.

Schneider Electric experience makes it possible to simulate and size separately the passive components. The simulation time is drastically reduced and waveforms approach allows a flexibility of modeling.

1.4.3 Analytical Modeling:

Several demands from Schneider lead to develop an analytical model. One major goal of the PhD is to focus on magnetics but current models do not match required accuracy or are not fitted for power inductors. Thus new models are developed and implemented. The easiest way is building our own analytical code to implemented easily new models or improvements. Secondly, an analytical model is most of the time faster than Finite Element Analysis or other numerical methods. For optimization process the computation time is dominant. Finally, the resulting optimization software built in the PhD has to be deployed for every designer. Once again an analytical model is easier to spread than a multi-software platform with its cost and its support.

1.4.4 Discrete Values and Libraries:

One main goal of this project is to deliver optimized industrial products for market. In the industry, all values are discrete; the sizes of the components are imposed by supplier capability, e.g. magnetic powder core sizes are limited by press force, strand diameters for coils are defined by AWG table or other ones but are imposed. When designing inductors, many different magnetic materials must be investigated. Their physical parameters depend on the material (Fe powder, steel sheet, amorphous alloys). No universal model for magnetics exists; they must be handled as a library of parameters. The caps and the semi-conductors are also treated as libraries.

So the optimization must work with discrete values and libraries. Strategies to build a linear and differentiable model could be found in order to use 1^{st} and 2^{nd} order algorithms for fast computation. However, genetic algorithms are perfect for working with discrete values. The possibility of analytical modeling with considering previous assumptions [1.4.2] enables the conception of a very fast simulation model. The number of adjustable parameters for converter optimization does not exceed few dozens. Thus, genetic algorithm use coupled with fast modeling seems the easier strategy for our optimization. Furthermore the convergence toward best solution is more likely.

1.4.5 Industrial Project:

The genetic algorithm delivers only one optimum [1.3.5.1], but the R&D engineers face in project development many tradeoffs between price, volume, weight, efficiency or footprint. The optimization presents a bigger interest if it provides decision tools to help engineers in their choice. The elitist multi-objective evolutionary algorithm [1.3.5.3] and [1.3.5.4] are coded for finding Pareto-front tradeoff between multi-objectives. Pareto front can be found

using several convergences of determinist or genetic algorithms but it proves less efficient [1.3.2].

1.4.6 Conclusions:

The strategy has been chosen to match project requirements and many others could be found for other projects. However, generalities presented previously can be applied in design strategy choice for industrial designers.

Schneider Electric experience simplified the modeling by introducing assumption of strong and weak interaction between components and commands. This aspect is characteristic to power converters. The reduction of time computation makes it possible to consider more expensive algorithm like GA or EMOEA.

The industrial context makes discrete values and library management a mandatory requirement. Once again GA, Niching or EMOEA are particularly adapted to it. The use of discrete parameters rather than linearize the model simplifies modeling.

The models developed in this PhD are fitted to EMOEA algorithms; they are fast and accurate, dealing with discrete parameters and using libraries. The models are built to allow separate optimization of component or to be connected for global converter optimization. Optimizations are achieved to find Pareto tradeoff between multi-objectives and not local optimum.

1.5 GoT

The platform used in this project is Genuine Optimization Tool developed by Professor Jean-Louis Coulomb in G2ELab [17]. The platform is a java toolbox for:

- Software connection for external calculation (Document, Tabulator, Java, Python, Matlab, etc.)
- Parameter and function definition of a problem
- Screening
- Optimization i.e. definition of mono-objective or multi-objective problem
- Algorithms (possibility of building algorithm from elementary brick like mutation, elitism, etc.)
- Analysis (robustness, sensibility, plotting).

GOT is based on a grid discretization of parameters and function, particularly fitted to our strategy of optimization. The possibility of testing quickly new models with software connection is advantageous. Toolbox to deal with libraries defined in tabulator or text files is implemented.

GOT disposes of a user friendly interface in order to help with:

- Continuous or discrete parameters definition
- Mono or Multi objectives
- Problem unconstraint or with constraint
- Experience mapping
- Optimization direct or indirect
- Algorithms determinist or stochastic
- Post processing
- Software external calculation

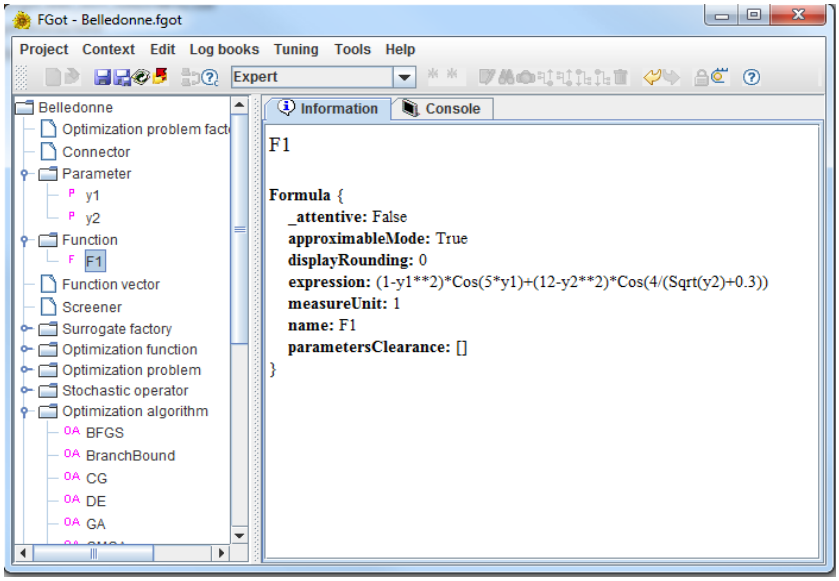

Figure 26: FGoT interface

1.6 CONCLUSIONS

The goal of this PhD is to deliver models and optimization tools for power converter optimal sizing. Many strategies and possibilities exist and selection has been done. The specificity of this project is the industrial impact of Schneider Electric. Innovation and research are applied to the industrial world. This chapter comes first to explain how the specifications by Schneider Electric shaped the strategy of the project and the modeling that derives from it.

The most interesting part of the scientific research is when it is associated to an industrial innovation. Schneider Electric has always designed its converter, but never using optimization methods. The gains they want to reach with this project have been established as specifications discussion. The specifications are explained and classified in order to feel their impact on the optimization and which boundaries they impose to the project.

Converter design is nothing new, but optimization changes dramatically the usual approach designers have. The innovation is the introduction of optimization algorithm in the sizing process. Many algorithms have been proposed in the literature. It would be impossible to present all of them. However it is essential to understand the major mechanisms to use them properly in the design of power converter. They are presented here in this chapter, because no models satisfied Schneider Electric requirements. The experience of optimization acquired previously shows that it is much easier to build a model fitting algorithm requirement rather than adapting the whole optimization strategy and algorithm to a fixed model. Two main families of algorithms are presented and few algorithms are detailed in both of them. Some algorithms are not adapted to the goals fixed by specifications, e.g. discrete values and libraries management, 1^{st} order and 2^{nd} order algorithms are thus dismissed. Another goal of the project is to deliver a decision tool to designers, EMOEA providing optimal Pareto-front answer this issue. They also manage discrete value and libraries. One issue is that model associated to these algorithms must be fast or computation time will increase hugely. One other is that experience shows these algorithms work well only with few numbers of parameters and objective functions.

Schneider Electric and G2Elab experiences fixe these issues. Indeed, simplifications of modeling and validated assumptions are presented based on several year of converter manufacturing experience. Thus, we have on one hand EMOEA algorithms that seem perfectly adapted to specifications and on the other hand a capacity of building models that fit these algorithms requirements. The strategy that ensues from it is obvious.

Several optimization softwares were tested. GOT has been chosen for its programming based on grid discretization of parameters and functions, which is close to the industrial design world that deals only with discrete values. Moreover, GOT is a java library of optimization tools dedicated to research and really flexible in the context of developing new approaches. Unlike commercial software, GOT can be used to develop designer own methods of optimization and implementation of innovating method is easy.

In this chapter specifications and strategies of the PhD project are presented. Models presented in chapter two have been shaped to answer all requirements established in this

chapter. Chapter three is the application of association strategy of algorithms presented here and models from chapter two. The validation of this strategy is done in chapter four with industrial product applications.

1.7 REFERENCES

[1] Nelder J.A., Mead R., "A simplex method for function minimization". Comput. J. 7, pp 308–313, 1965

[2] Vivier S., "Stratégies d'optimisation par la Méthode des Plans d'Expériences et Applications aux dispositifs électrotechniques modélisés par Eléments Finis". Ph.D dissertation, USTL - EC Lille, defended on 11/07/2002.

[3] Broyden C. G., "The Convergence of a Class of Double-rank Minimization Algorithms". Journal of the Institute of Mathematics and Its Applications, vol. 6, pp 76-90, 1970

[4] Fletcher R., "A New Approach to Variable Metric Algorithms". Computer Journal, vol. 13, pp 317-322, 1970

[5] Goldfarb D., "A Family of Variable Metric Updates Derived by Variational Means". Mathematics of Computation, vol. 24, pp 23-26, 1970

[6] Shanno D. F., "Conditioning of Quasi-Newton Methods for Function Minimization". Mathematics of Computation, vol. 24, pp 647-656, 1970

[7] Sareni B and Krahenbuhl L., "Fitness Sharing and Niching Methods Revisited". IEEE transaction on evolutionary computation, vol. 2, no. 3, September 1998

[8] Mahfoud S. W., "Niching methods for genetic algorithms". Ph.D.dissertation, Univ. of Illinois, Urbana-Champaign, 1995

[9] DeJong K. A., "An analysis of the behavior of a class of genetic adaptive systems". Ph.D. dissertation, Univ. of Michigan, Ann Arbor, 1975

[10] Harik G., "Finding multimodal solutions using restricted tournament selection". In Proc. 6th Int. Conf. Genetic Algorithms, L. J. Eshelman, Ed. San Mateo, CA: Morgan Kaufmann, pp. 24–31, 1995

[11] Kalyanmoy Deb, Samir Agrawal, Amrit Pratap, and T Meyarivan, "A Fast Elitist Non-Dominated Sorting Genetic Algorithm for Multi-Objective Optimization: NSGA-II". KanGAL Report no 200001

[12] Srinivas, N. and Deb, K., "Multi-Objective function optimization using non-dominated sorting genetic algorithms". IEEE transaction on evolutionary computation, vol. 2, no. 3, pp 221–248, 1995

[13] Zitzler. E, Laumanns M. and Thiele L., "SPEA2: improving the Strength Pareto Evolutionary Algorithm", TIK-Report 103, May 2001

[14] Knowles, J. and Corne, D., "The Pareto archived evolution strategy: A new baseline algorithm for multiobjective optimisation". Proceedings of the 1999 Congress on Evolutionary Computation, Piscatway: New Jersey: IEEE Service Center, pp 98–105, 1999

[15] Rudolph, G., "Evolutionary search under partially ordered sets". Technical Report No. CI-67/99, Dortmund: Department of Computer Science/LS11, University of Dortmund, Germany, 1999

[16] Kent R. Davey, "Latin Hypercube Sampling and Pattern Search in Magnetic Field Optimization Problems". IEEE Transactions on Magnetics, vol. 44, issue 6, pp 974-977, June 2008

[17] http://forge-mage.g2elab.grenoble-inp.fr/project/got

2 CHAPTER II – PASSIVE COMPONENTS

2.1 INTRODUCTION

Power converter modern design focus on efficiency increase and cost reduction of product development. Semi-conductors usually benefit of the most privileged attention for their losses and thermal issues. However, Schneider Electric experience has highlighted the weight of magnetics in efficiency and cost for UPS but also in terms of constraints for electric design. Moreover, in our optimization process, IGBT are treated as library whereas magnetics present lots of adjustable geometric and material parameters. The optimization process is suitable for inductors because both core and coil sizing could not be separated and are in competition for the optimal design of the other.

Chapter one introduced the algorithms and the strategy for optimization. The need for fast calculation comes from genetic algorithm use. Indeed, by their mechanism these algorithms calculate lots of possible sets of input parameters. GA and Elitist Multi-Objective Evolutionary Algorithm have the capacity to deal with few constraints, goals and only dozens of inputs. Considerations of these issues have been done in the capacitor and magnetic modeling. This strategy of adjusting model with algorithm requirement is a strong choice of this PhD and proved efficient in time of development and in term of optimization good convergence and robustness.

According to this strategy, the models of passive component presented in the second chapter are developed to be fast and using discrete values of both geometric parameters and materials. Accuracy of models is a major requirement from the choice of direct component sizing, meaning solutions found by optimization must be close enough to real components to decrease the need for prototyping thus development time and cost reduction. The trickiest part is to build a model that is complex but not complicated. I.e. the model must be accurate to provide enough information to the algorithm for good convergence but it must not become too complicated and thus speeding down the convergence and losing the algorithm.

Magnetics are widely investigated in this chapter in term of pertinent modeling and component definition with regard to the rest of the converter. The magnetics are presented in two parts, first the magnetic core and then the coil. The core is magnetic material so magnetic models from Steinmetz basic to new proposition are studied. Compatibility with discrete optimization and strategy of material modeling for library implementation are considered. The core like the coil is subject to high-frequencies effects, models must take into account the HF modeling. The coil is modeled as a frequency variable resistance. Already known model are implemented but technologic innovation leads to computation of brand new conductive material modeling. The capacitors are presented but they are less important in efficiency increase and optimization leverage. The caps do not have many adjustable parameters other than their electrical value. They are treated as linearization of a library. Finally, discussion is done on component definition. I.e. how the magnetics geometry is defined, which parameters are taken as inputs and the impact on optimization.

2.2 CHOKE CORE

2.2.1 Introduction:

Magnetic material is the most complex system to simulate in passive components. Under electric excitations the material has a non-linear hysteresis behavior impacted by material magnetic background. Moreover in power converters the magnetic is under low frequency and High Frequency stimulations; thus both static and dynamic phenomena have to be simulated. In filtering applications many different materials are used, from silicon-iron steel sheets to iron powder alloy through amorphous or nanocrystalline thin ribbons. The literature on models of magnetic material behavior is significant [18]-[24] and involves both physical and pragmatic means to model phenomena from microscopic to macroscopic scales. It results that none is able to predict theoretically the hysteresis behavior.

Thus models based on measurements must be implemented to compensate information not accessible theoretically. Facing the multitude of material behaviors, a modeling globalizing main characteristics is searched to prevent a multi-model implementation. Furthermore, in the discrete optimization resulting in specifications directly good for supplier we want to achieve, a general model based on suppliers' datasheets would be preferred.

2.2.2 Magnetic basics:

Magnetic materials are as numerous as they differ from each other in matter behavior. Numbers of books deal with it. So only a fast and exhaustive presentation is done here. The purpose is to understand the basics of magnetic material behavior and to present what they have in common we can assimilate in a model.

At the nanoscale, from hundreds of angstroms (10^{-10}m) to thousands, the material is an agglomeration of isotropic magnetized oriented domains. They are the Weiss domains, they come from material fabrication. Crystalline properties, methods of structures tailored by magnetic processing or other recrystallization annealing methods can impact the orientation of the domains and their numbers. Between the homogenous magnetic oriented Weiss domain, Bloch walls are thin areas where the magnetization changes directions (Figure 27). So at the macroscale the magnetization of a magnetic material is seen as the mean value of the magnetization over the Weiss domains.

When the material is subject to an outside magnetic field, energy is given to magnetization domains that try to align with this magnetic field. Many phenomena occur, e.g. at low magnetic field the domains with the same magnetizations that the external fields are preferred and walls move creating flux density variation. Then for higher field, near saturation, the magnetization rotations create the flux variation. Inside the material imperfection exist, carbide, nitride, etc. which act as anchors for walls. These phenomena of magnetization variation and wall movement are viscous flow so with the general idea that it depends on flux variation and its velocity [25]. Both flux density and its time variation are the main parameters.

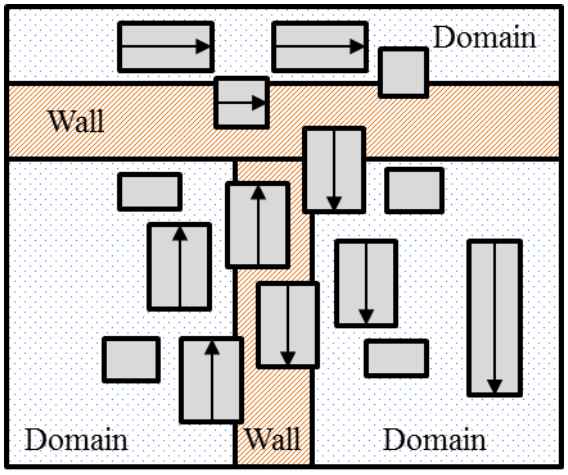

Figure 27 : Weiss oriented domain and Bloch wall

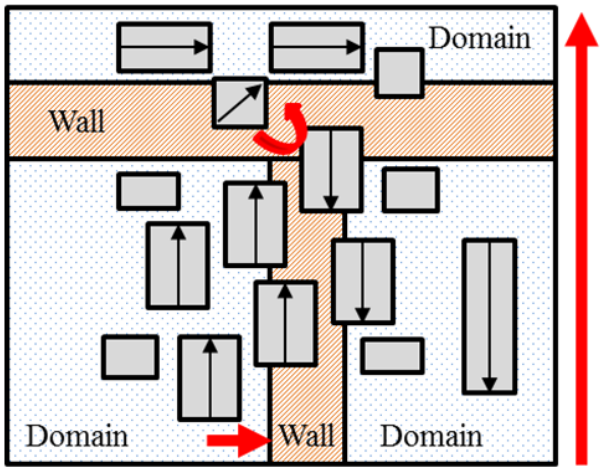

Figure 28 : Walls movement and reorientation under external field excitation

In the literature the losses are divided in three contributions. The quasi-static losses do not rely on the flux density variation; only really low frequency effects ~1 Hz. Then for higher frequency excitation the hysteresis is larger and losses more important caused by eddy currents. Finally the measured losses are generally larger than both previous contributions so exceed losses are added and can be explained by real microscopic dissipative magnetization processes [25].

These phenomena being analytically different at the microscopic scale for the several considered materials, global assumption are done at the macroscopic scale and presented in the following sections.

2.2.3 Classical Macro Models based on Steinmetz:

The computation of magnetic losses is essential for converter efficiency evaluation and optimization minimization goal. The most used macroscopic behavior law for magnetics is Steinmetz formula [23]. This proposition is based on measures achieved by Steinmetz with

sinus excitations. The dependency on flux density variation is integrated with the consideration of the frequency as an extension of [23].

$$P_v = k.f^{\alpha}.B^{\beta} \quad (14)$$

The frequency is directly associated to converter switch HF and k, α and β coefficients are empirical. Steinmetz approach is still use as reference since 1892, (Figure 29) shows the datasheet provided in every magnetic manufacturer catalogs, Steinmetz equation from sinus induction excitation. Generalization of this formula for other waveforms has been proposed.

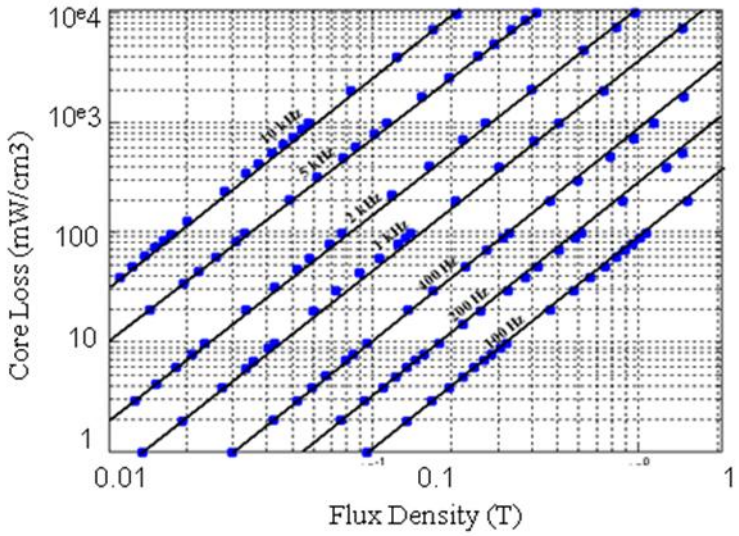

Figure 29 : CoreLoss curves from suppliers' datasheets

The modified steinmetz equation, MSE [28], the generalized steinmetz equation, GSE [29] and improved GSE, iGSE [30] have been proposed to consider that hysteresis losses depend on flux density variation speed dB/dt and not directly on the frequency to implement complex waveforms.

MSE has the formula:

$$P_v = k.fe^{\alpha-1}.B^{\beta}.f \quad (15)$$

The flux density variation is integrated in an equivalent frequency f_e calculate from the equality between flux variation rms value and sinus at f_e for a peak to peak flux ΔB.

$$fe = \frac{2}{\Delta B^2.\pi^2}.\int_0^T \left(\frac{dB}{dt}\right)^2.dt \quad (16)$$

One disadvantage of this formulation is that, although the dependence of loss on dB/dt is included, MSE implicitly assumes loss proportional to f^2, while at the same time assuming loss proportional to f^{α} leading to anomalies in loss prediction.

GSE overcomes this issue by suppressing the dependency on f, and associating loss with flux density and its variation:

$$P_v = \frac{1}{T}.\int_0^T k_1.\left(\left|\frac{dB}{dt}\right|\right)^{\alpha}.B(t)^{\beta-\alpha}.dt \qquad k_1 = \frac{k}{(2.\pi 2^{\alpha-1}.\int((|\cos(\theta\phi)|^{\alpha}.(|\sin(\theta i)|)^{\beta-\alpha})^{\beta-\alpha}.d\theta} \qquad \textbf{17}$$

The k_1 coefficient is deduced for consistence with Steinmetz equation in sinus case. So losses depend on flux density and its variation at every moment. Real waveforms are normally addressed. However this model is instantaneous; the magnetization historical of the material is not taken into account, and dynamics are the same for minor and major loops in case of converter waveforms. For material with large hysteresis major and minor loops, the error is consequent.

IGSE is an upgrade of GSE by replacing instantaneous value of flux density by its peak to peak value ΔB. The total loss for complex waveforms is computed from the summation of all minor loops:

$$P_v = \sum_i \left[(P_v)_i . \frac{T_i}{T} \right] \qquad \textbf{18}$$

This method is particularly fit to be used with constructors' datasheet and power converter waveforms. But two main source of error can be identified.

First experience shows these models deal badly with large frequency spectrum waveforms and with addition of LF modulation. It can easily be seen with command of converter by voltage, a same impulse at same frequency so same flux ripple and variation speed but with unequal LF polarization will not be addressed by iGSE because the formulation will stay the same. More complex phenomena cannot be addressed with this approach, relaxation or dynamic evolving with polarization of the material (Figure 30). The other error comes from datasheet [2.2.4.5].

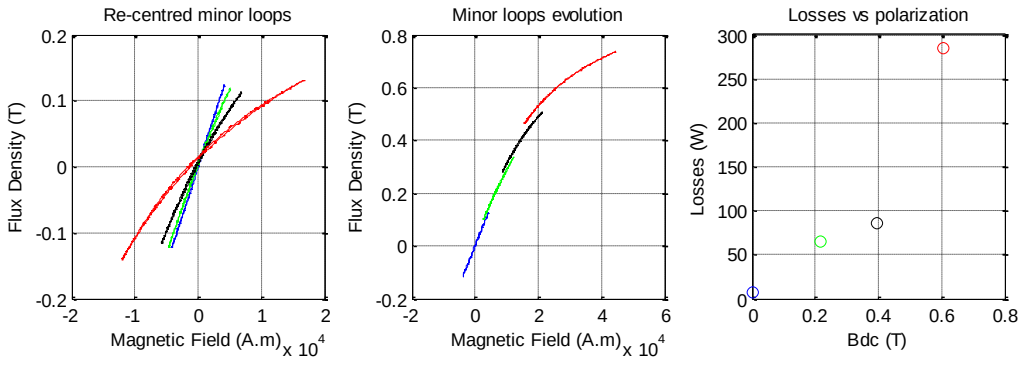

Figure 30 : Measurements, evolution of minor loops losses for same ΔB with several B_{dc} polarizations done on toroid FeSiAl alloy core @ 3 kHz

New improvements are still being proposed, like i^{2}GSE [31], and the last proposition is the addition of dynamic of material measurements. Yet several lacks are still present in Steinmetz approach so another approach is studied in next section.

2.2.4 The Loss Surface:

New models are evolving toward model already existing like the Loss Surface model [19] to address dynamic non-linear effects but also the quasi static contribution not considered in several models based on Steinmetz approach. The LS is a macroscale dynamic hysteresis modeling based on series of measurements, both static and dynamic. Its purpose is to rebuild the whole hysteresis of a magnetic material whatever the waveform and its harmonic spectrum. First developed for SiFe steel sheet, it has been extended to nanocrystalline material [32] and is presented for magnetic powder core later in this paragraph. It requires for the moment more measurements than Steinmetz. But the excitations are compatible with power electronic environment because excitations are square voltage waveform which is an advantage.

2.2.4.1 Static Model

To address quasi static contribution in hysteresis behavior of magnetic material, several static models are presented in literature. Like Jiles-Atherton [33] with optimization process for coefficient approximation. Another well-known model is Preisach [34] developed from bipolar magnetic switch with rectangular behavior. It often requires lots of measurements. The Raleigh model is basically achieved on small centered excitation. Most of static models have in common the decomposition between reversible part (the ability of the domains to take back their initial position) and the irreversible part (when deformation of the walls and domains prevent material to be in its initial magnetization state).

The static model of the LS is based on the same principle that Jiles-Atherton, without coefficients approximation. It represents the static magnetization built from reversible and irreversible contribution, $M = M_{rev} + M_{irr}$. The model takes the flux density B as input. So the reversible part is associated to the anhysteretic curve of the material $H_{anh}(B)$. The irreversible magnetic field is computed from an easy algorithm presented in (Appendix B).

This static model requires two measurements, the anhysteretic curve and a LF hysteresis ~1Hz from lower saturation to upper saturation (Figure 31).

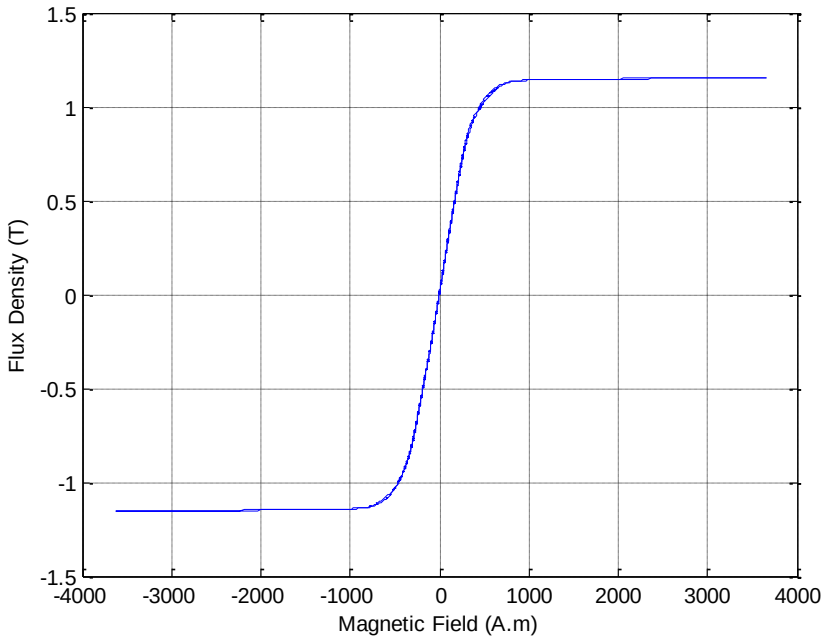

Figure 31 : Measurements, static hysteresis @1Hz for nanocrystallin μ=1700

2.2.4.2 Dynamic Model

The real improvement achieve by the LS compare with other dynamic model is the dynamic part. The idea is to create a behavior map of the material which can be used in any situation to retrace the path created by an external excitation. This approach is less mathematical and physical but more based on experience. It also includes in a same measure both classical dynamic hysteresis and exceeding dynamic part.

The 3D magnetization table is built from measurement. The flux density is the input of the model and like presented in other modeling, the hysteresis depends on the flux variation also. The model gives *H(B(t), dB(t)/dt)* (Figure 32). Note that static model consider historic of the material whereas dynamic part is not impacted by it. Measurement of magnetic field regarding *B* and *dB/dt* is done in order to simplify the mathematical computation of the map. B is imposed to be triangular excitation, thus *dB/dt* is rectangular (Figure 32). We have a whole evolution of *H(B(t))* at *dB/dt* fixed. The excitation is done from $-B_{sat}$ to $+B_{sat}$ so the map is for the whole functioning area of the material. The measures are generally with noise and 3D interpolation of the map in an algorithm is heavy time consuming. So the map is represented by polynomials (Figure 33). The polynomial *H(dB/dt)* is bijective but not the *coeff(B)* so the model cannot be inverted. However in power converter the commands generally impose the voltage, e.g. inverter, so *B(t)* is the perfect input. The resulting hysteresis for a filter choke made in nanocrystallin Kmu 1700 placed at the output of a 2 level inverter is illustrated in (Figure 34).

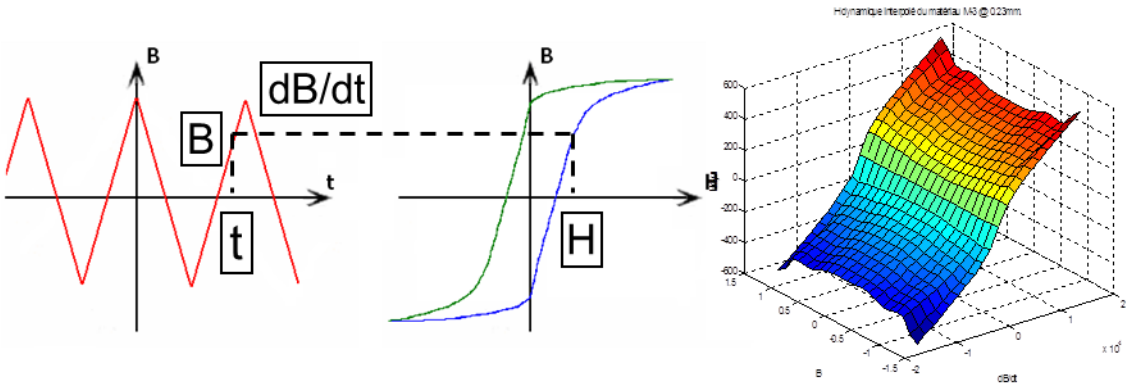

Figure 32 : Behavior dynamic map for FeSi steel sheet M3 - 0.23 mm

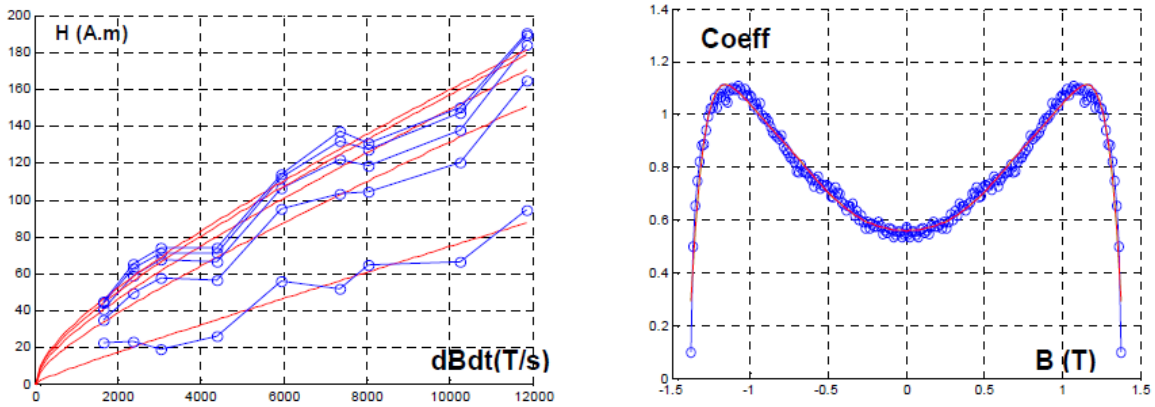

Figure 33 : Polynomial fitting of the LS dynamic map, left several dB/dt excitations, right corresponding evolution

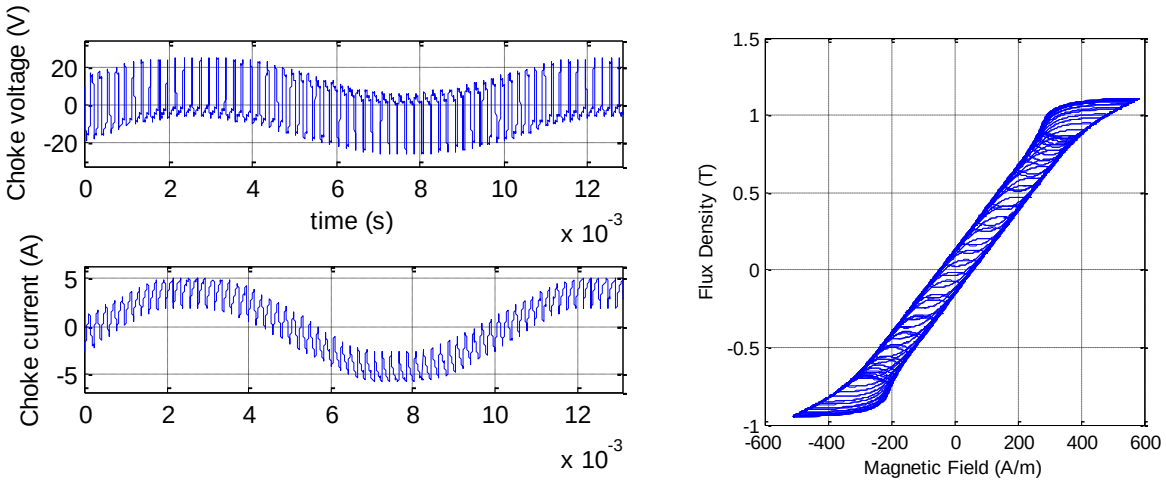

Figure 34 : Measurements, choke filter of nanocrystallin Kmu1700 waveforms and resulting dynamic hysteresis

2.2.4.3 Extension to Powder Core

What makes the LS model really interesting in our application is the fact it is built from measurements. So in the idea of developing a homogenous library of magnetic material for optimization, the LS map seems globalizable. Same measurement can be achieved on all materials and mathematical implementation stays the same.

But the Fe alloy powder cores with low permeability from 10 up to 100 have an oversized magnetic field for easy measurement. Several challenges must be answer before adapting the LS to powder core. First, coercive magnetic field for Fe powder core are around dozens of A/m but saturation field are greater than hundreds of kA/m. So acquisition material must be precise enough to sample signal from very different scales. Although Schneider Electric owns top quality equipment, the dynamic of the measure leads to an inaccurate result (Figure 35), the noise is as large as the coercive field thus no difference can be found between 2 kHz and 6 kHz. Another effect is the time laps between voltage measure (B) and current measure (H) [35]. Coercive field of low permeability powder core is so thin than a slight delay between the two acquisitions leads to important error on resulting hysteresis.

Even if all these issues where addressed, for all material the impact of the shaping of the final piece on losses must be investigated. Indeed, nanocrystallin and steel sheet are manufactured as sheets. The final inductor is made by assembling those sheets and put them in the required form. If it is done without changing the internal structure of the material (e.g. mechanical stress, cutting) the characterization of non-assembled sheet is still valid for the final piece. But for powder core, the final piece is pressed. And the shape as a huge impact on the material behavior [2.2.4.7], thus a LS map must be built for all size of cores. The measurement campaign will be too important even for Schneider Electric, without talking about integration of new material every year.

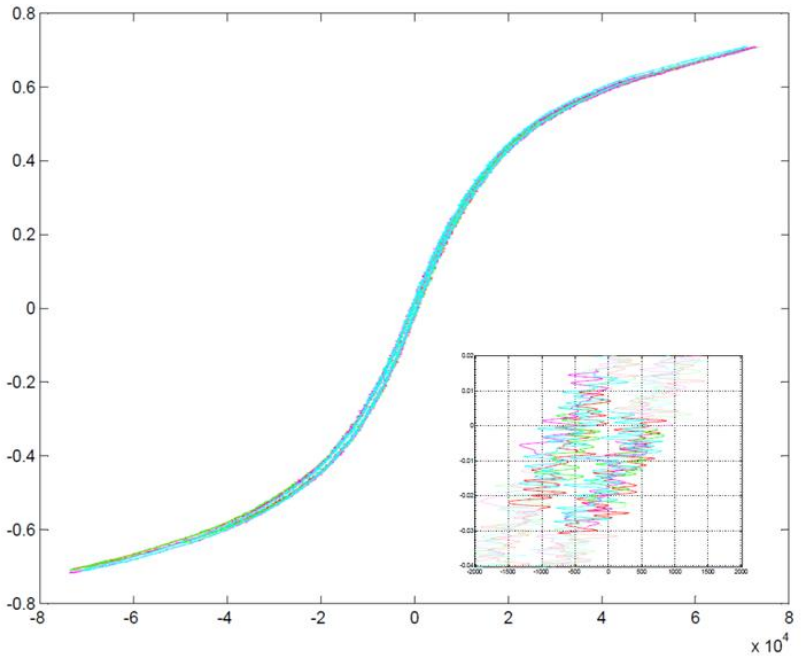

Figure 35 : Hysteresis for FeSiAl powder core μ = 26, measurement noise @ 2 kHz, 4 kHz and 6 kHz

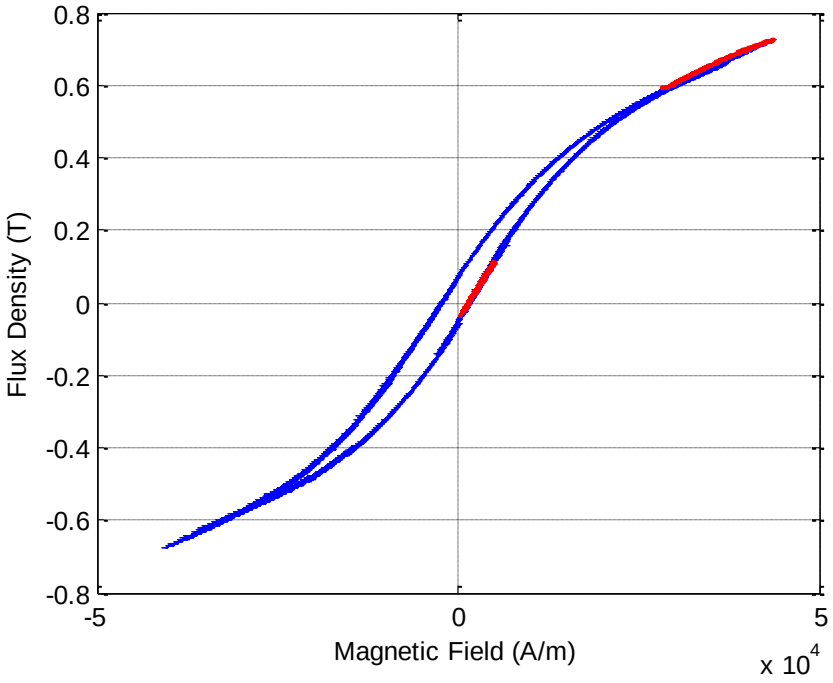

Figure 36 : Dynamic hysteresis for FeSiAl powder, RL load with 12 kHz MLI

In conclusion the LS model needs several changes to fit with powder core. However as presented in following paragraphs, such a complex model with measures issues is not necessary accurate for Fe alloy. Hysteresis models are difficult to implement for powder. Measurements and polynomials approximation generate too much cost and time. This spending is not justified by the obtained result. These models are based on the construction of the dynamic hysteresis of the material yet the thickness of the hysteresis for powder core and all the incertitude brought by measurements do not guarantee better losses computation than other models (Figure 36). Two minor loops are highlighted in red, the thinness of the loops do not guarantee good computation of losses unlike nanocrystallin hysteresis from (Figure 34).

Moreover, the main idea of this PhD is to be able to optimize passive component with suppliers 'datasheets. And suppliers will not comply to provide such difficult and expensive measurements.

2.2.4.4 Loss Map Model

Magnetic material suppliers provide datasheet with losses curves ideal for Steinmetz approach but not enough for non-linear evolution of dynamic losses with polarization effect (Figure 30). On more the necessity of a dynamic hysteresis model is proved useless (Figure 36) for thin hysteresis materials. So a model based on behavioral mapping of the material like the LS but deriving from Steinmetz approach is proposed.

In power converters the HF magnetic losses come from voltage square forms most of the time. Thus they depend on induction ripple, induction time derivative and induction polarization. Measurements of HF minor loops with a DC polarization are easier to achieve on large powder cores than saturation major loops. Hysteresis loops being small (Figure 37) the accuracy of measurements can be set far better than large dynamic phenomena (Figure 36). Moreover, the suppliers provide measurements of permeability versus magnetic field polarization (Figure 47). So the suppliers already perform these measures needed in our proposed approach of LossMap and could easily insert them in their datasheets on Schneider Electric request.

Indeed the permeability is measured from flux density minor loops excited around the polarization point from a DC magnetic field. Achieving these measurements at several frequencies like provided without polarization (Figure 42) nowadays, a map is built giving losses from induction ripple and induction polarization (Figure 38) at several frequencies. The map is fitted using polynomials which coefficients rely on induction derivative value as the LS model. Finally we have the losses depending on induction decomposition between each change of induction time derivative assuming linear evolution of induction we could approximate by easy formula:

$$P_V(dt, Bpeak, Bpol) = f_1(Bpol).\left(\frac{1}{dt}\right)^{f_2(Bpol)}.B_{peak}^{\,f_3(Bpol)} \qquad \textbf{19}$$

or adapting proposed iGSE, NSE or other formulas to fit the maps.

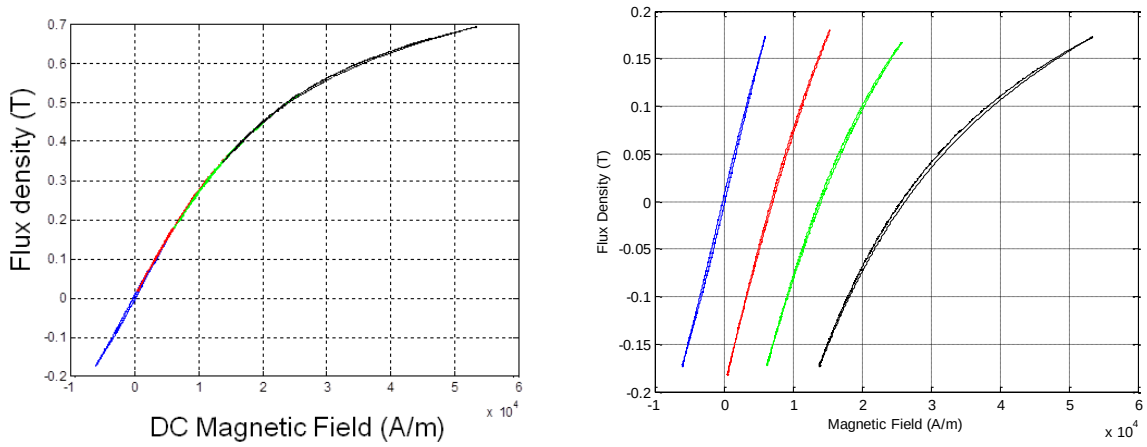

Figure 37 : re-centred 3kHz minor loops @ several polarization for FeSiAl powder core

For converter waveform, the induction is deduced from choke voltage and broken down into its different parts. The losses are then computed.

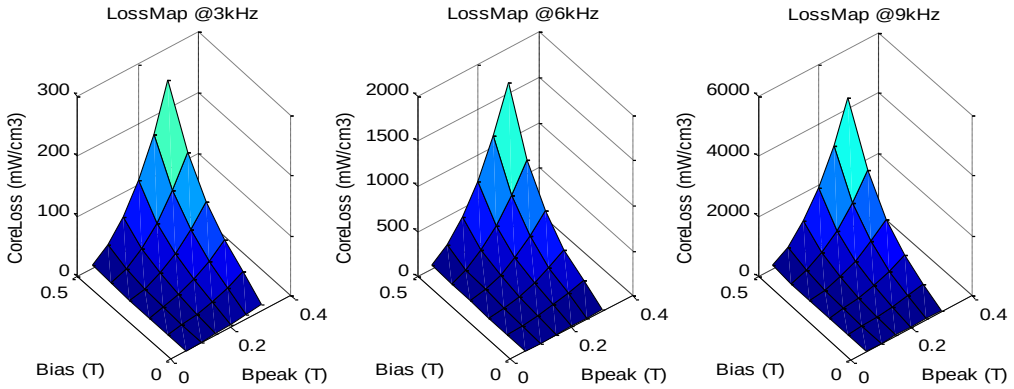

Figure 38 : LossMap for FeSiAl µ=26 powder core @ several frequencies

The losses estimated are compared with losses calculated from real waveforms (Figure 39) and give better approximation than classical model, (Table 1). However, the noisy signals used to integrate dynamic hysteresis losses also bring incertitude on losses computation. Yet the model gives an accurate simulation of *B* and *H* real waveforms (Figure 40) so losses computation from LossMap must be close to real losses. Validations should be achieved later using a calorimeter.

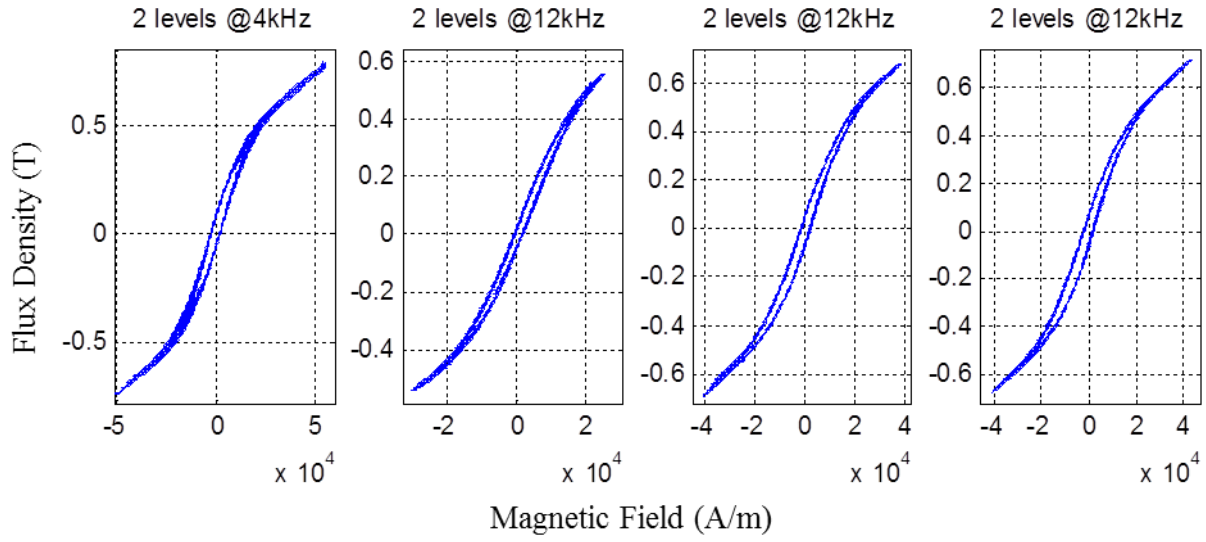

Figure 39 : Dynamic hysteresis for 2 level inverter choke filter with FeSiAl µ26 alloy material

Table 1 : Losses comparison from Error! Reference source not found.

	RL load, @4 kHz	RL load, @12 kHz	RL load, @12 kHz	RL load, @12 kHz
Hysteresis losses (kW)	30,54	24,32	39,4	47,72
Datasheet losses (kW)	6,08	10,85	6,3	7,08
LossMap losses (kW)	29,12	22,61	38,24	50,12

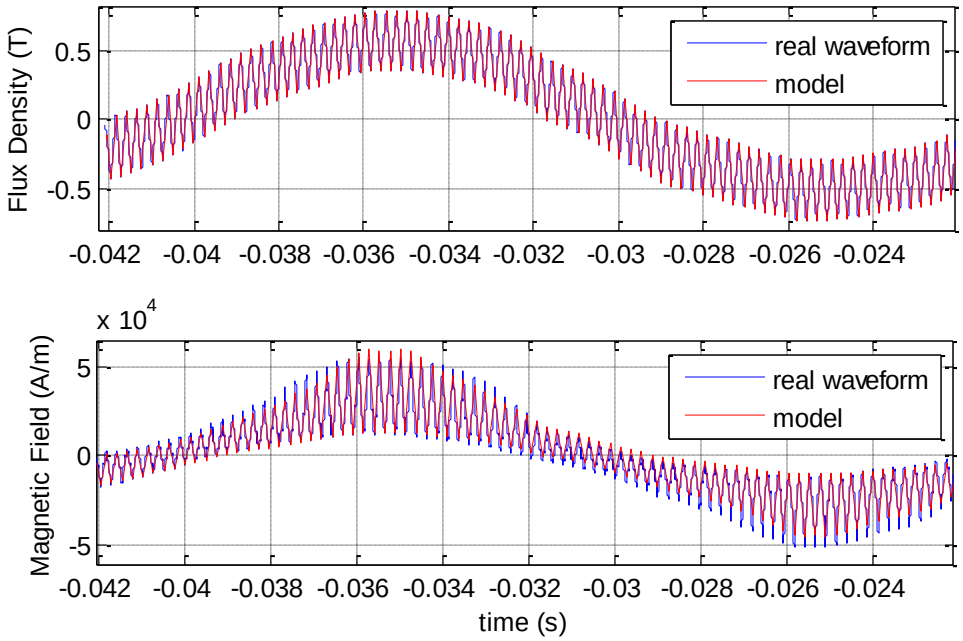

Figure 40: Real waveforms and model simulation

This model accurate enough to compare different materials losses could easily be built from new datasheets. However these values are not yet implemented by suppliers.

Thus when evolution of losses with DC bias are not provided by suppliers, we use the arc length of the anhysteretic curve for approximation. I.e. with the increase of the bias field, the length of the minor hysteresis loops will also increase for a same peak to peak induction excitation (Figure 37). The evolution of the loop orientation is close to the anhysteretic curve's one. So the arc length of the curve is computed for the 0 bias flux density excitation provided by suppliers and also for the loop with bias. Then the difference between both length is used to computed losses of the minor loop with bias from the minor loop without bias. The dynamic phenomena are not represented by this approach yet for powder core it is enough for tendencies approximation (Figure 41).

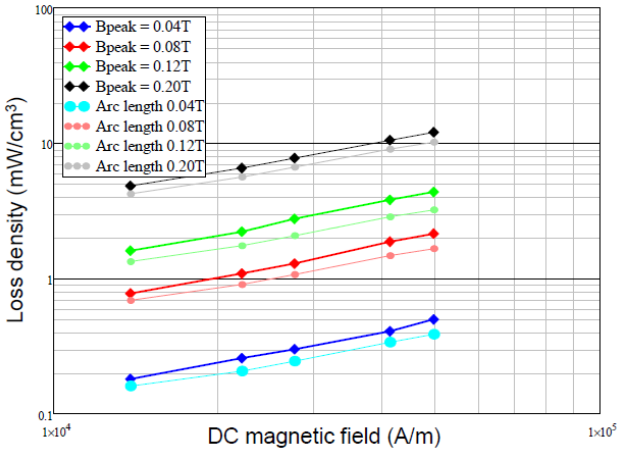

Figure 41: Arc length approximation of hysteresis minor loop losses for FeSiAl alloy @12kHz

2.2.4.5 Datasheet

The datasheet use is a key point in this PhD. Indeed, manufacturers propose new materials each year and new manufacturers are considered. For meaningful optimization, the magnetic material library must be up to date with all materials. A campaign of measurements cannot be done on every magnetics and every size any time a new material is proposed. Better data can be measured but after selection by the algorithms. Thus the use of datasheet is inescapable.

But there is still a doubt what is behind material datasheet curves (Figure 29). Manufacturers are most often using logarithmic scale, which makes the losses for a fixed frequency looking linear. The error is quickly rising enlarging the core losses measured range. Also there is not simple dependency of losses in the function of some power of frequency as per Steinmetz law, errors become flagrant between LF 50-60 Hz and high switching frequencies up to 300 kHz (Figure 42).

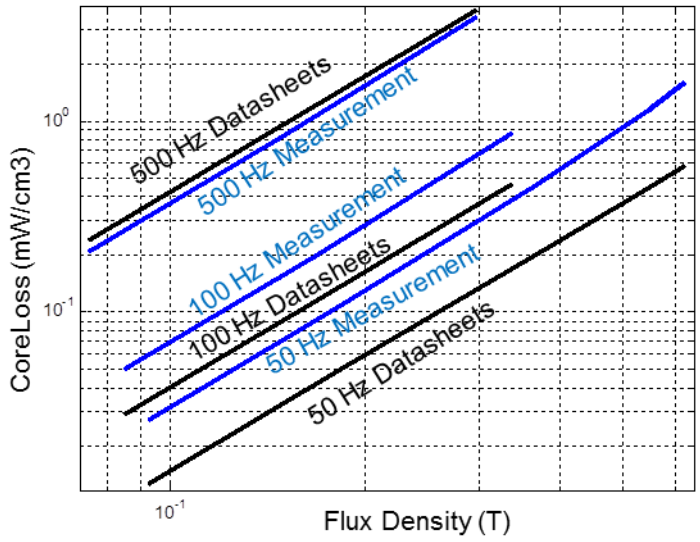

Figure 42 : Datasheet vs measurement, error @ LF

So it is important to be conscious what measurements have been really done to build presented curves. Supplier confess to apply only one measurement at 50 kHz / 0.1 Tp, widely held as reference in powder cores industry, to extrapolate this single result on all presented curves.

Fortunately measurements are generally done for at least 2 points per one frequency line and that for all shown frequencies, supposing linear excursion in the log induction scale. Errors however can become flagrant estimated by approximation calculated on only these two available points far from measurement boundary.

There are many other factors acting once again as potential source of wrong interpretation expanding the manufacturers' datasheets to losses calculation in the core. Each one could be a part of separate chapter but place restriction guide to summary:

Whatever the precision of curves given we do not know how many samples were tested and if the results reflect some typical average value or include the max and min margins. Knowing that losses can generally vary from batch-to-batch with the ratio of +/- 8 % it is necessary to consider mean vs maximum values of the indicated power dissipation in the produced batch of cores.

The next source of error is the size of core used for losses measurement vs varied cores dimensions available in the catalogs or computed by the optimization. For easier measurements by regular power bridges generally only small cores are suitable for characterization, often the toroid core of OD (outer diameter) ~1inch. But the same data are used whatever the application, in medium and high power converters the large cores are up to OD 7inch. The recipe of powder is kept the same for all size, however the force of pressing is not distributed equally in the core thus magnetization internal loops won't be the same for 1 inch core or 7 inch core (Figure 43).

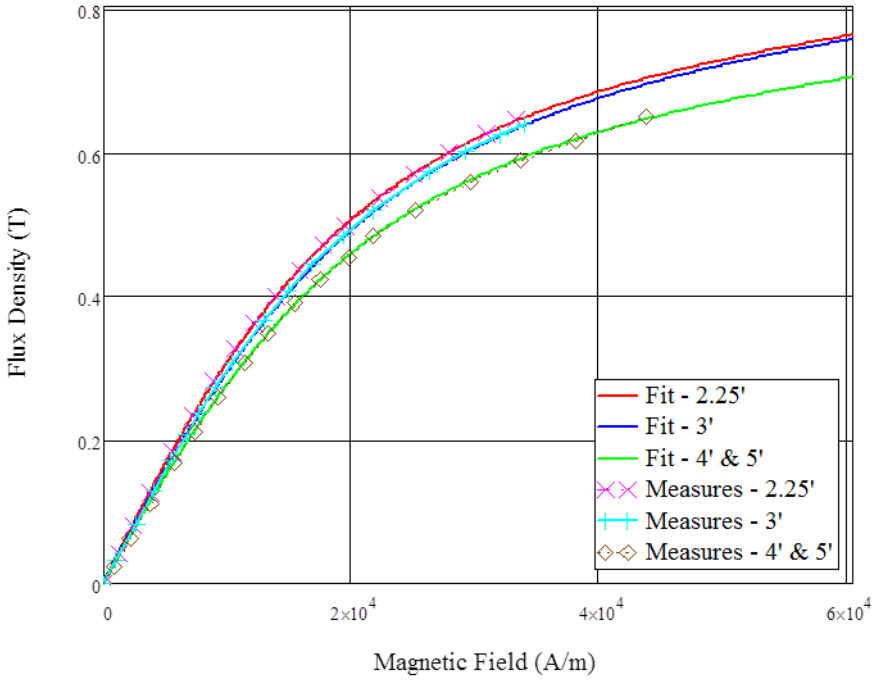

Figure 43 : Size impact on B(H) curve for FeSiAl powder from 2.25 inchs to 5 inchs

Finally, losses are very dependent on the temperature, but usually there is no even an indication at what temperature samples under test where exposed. So no indication to the customer how he can modify the given curves depends on his application from ambient to the working temp point. Fortunately losses are generally decreasing with temp (to the detriment of perm and saturation loosing), but many materials present their sudden increasing from 100° - 120° / 140°.

So both datasheet and proposed formulas are source of errors. Exact value of loss for material is never given. Thus a real complicated and accurate model giving errors less than few % is irrelevant. For optimization and prototyping, a good modeling allowing weighting of difference between materials is the most important for optimization.

2.2.4.6 Magnetic Considerations from Sinus Datasheet

Datasheet measures are from sinus flux density excitation. However in power converter most waveforms are square. Two effects allow neglecting this aspect. First, sinus flux density hysteresis loops cause more losses than squares (Figure 44). So losses will be a little overestimate. Secondly, for low loss powder material, the difference between waveforms is not quantifiable (Table 2). So sinus measurements are alright for losses estimation, not regarding other aspect.

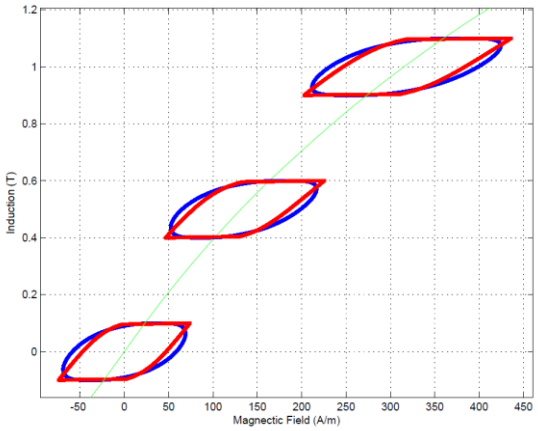

Figure 44 : sinus vs square flux density excitation

Table 2 : sinus vs triangle flux density excitation

	Bpeak = 0,09T 50 Hz	Bpeak = 0,075T 500 Hz	Bpeak = 0,08T 1 kHz	Bpeak = 0,077T 2 kHz	Bpeak = 0,073T 3 kHz
Sinus Losses (W)	1,78	13,56	30,88	60,56	80,93
Triangle Losses (W)	1,84	13,75	30,32	61,63	83,1

The real issue with sinus datasheet is that all flux density excitation are done without DC bias. Yet as presented before in power converter LF modulation are added to HF switches. LF fundamental component is biasing magnetic material moving the minor hysteresis loops to different areas on the *B-H* domain (Figure 30) and (Figure 37). These could lead to important errors for prediction of material behavior for complexes waveforms with both HF and LF pulses.

In power electronic systems, most of the chokes are subject to PWM voltages, a complex waveform. A common mistake when working with PWM signals is due to the idea of modification of the Steinmetz equation. Indeed, the manufacturer data giving the losses for a magnitude of the induction and its frequency, people associate the switching frequency of the semiconductors to the induction on the magnetic core to predict losses. Because the losses depend on *B* but also *dB/dt*, as shown previously, the calculation of an equivalent frequency depending on *dB/dt* of the minor hysteresis loop should be consider for each half pulse, this is highlight in (Figure 45). This mechanism is addressed in IGSE [2.2.3].

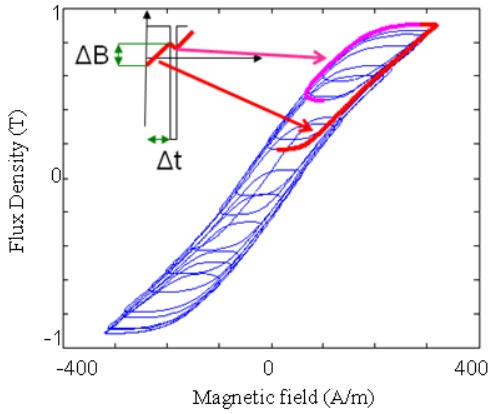

Figure 45 : Evolution of *dB/dt* impact on dynamic minor loops for PWM voltage

2.2.4.7 Geometric Consideration

With powder material process by pressing, we could imagine any form of core. In power converters, inductor toroid form prevailed. The solution is not the easiest one to wind but has many advantages. With low permeability material, air-gap are no longer required, thus a one bloc piece is a better choice for noise reduction and fringing flux prevention on coil losses. Square, rectangular or oblong forms are still used but toroid overmatches them. The repartition of flux in toroid is linear even with unbalanced coil (Figure 46). It is not the case for other forms that have flux density high concentration in corners. This effect could result in saturation of the magnetic material in bad design case. Yet even with good design those areas are lot more stressed and lead to local temperature rise and so higher losses. The toroid shape is extended to its coil that prevents side effect of current density distribution in wires increasing the toroid interest.

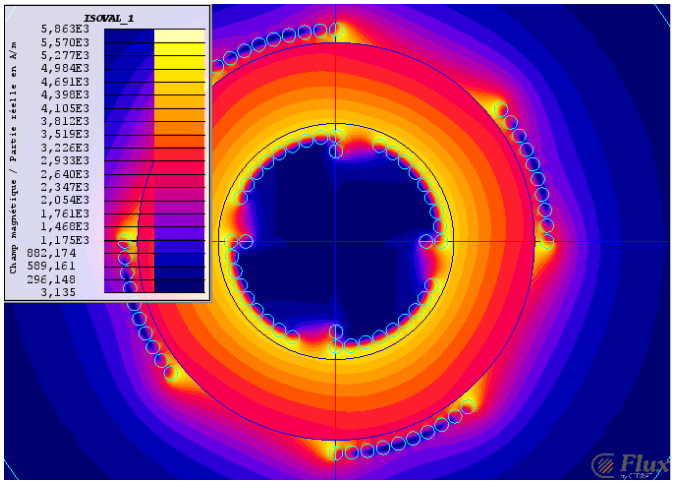

Figure 46 : Toroid flux distribution with unbalanced coil, Flux2D simulation

Despite their superiority toroids have a drawback that must be addressed when sizing. Appling the Ampere law on round geometry, one will easily see that flux density and magnetic field distribution is reversely proportional to the radius.

$$H(r) = \frac{Nturns.\sum_{Nturns} I}{2.\pi.\pi} \quad \textbf{20}$$

So the inner area of the toroid will has higher flux density than outer area. Designers size the core using a magnetic mean path from integration of Ampere law. But in optimal design the core will be reduced as much as possible so saturation of the inner part can happen without seeing it on mean path calculation. It is essential to compute the inner radius flux density value in model to guarantee good design.

2.2.4.8 Electrical behavior

The core model must deliver electrical behavior of the choke. I.e. the modulated square waveform voltage generally applied on choke in power converter creates current ripple linked to the magnetic material behavior. This effect is correlated to hysteresis behavior of the material. The most common formula for choke is:

$$U_L(t) = L(t).\frac{dI_L(t)}{dt} \quad \textbf{21}$$

So the ripple current is linked to the imposed voltage by the inductance value L. the inductance value is done by:

$$L(t) = \mu_0.\mu_r(t).\frac{Nturns^2.Section}{lm} \quad \textbf{22}$$

The inductance depends on the geometric parameters Section of the core, lm mean magnetic path length of the core and Nturns the number of coil turns. The magnetic behavior of the material is translated by the permeability μ_r. For the consideration of a linear material the permeability is fixed to its initial value leading to a fixed value of ripple current. For power converters, modulation imposes LF variation and thus permeability evolution. Indeed the permeability is linked to flux density and magnetic field so to the hysteresis of the material.

$$\mu_r(t) = \frac{B(t)}{\mu_0.H(t)} \quad \textbf{23}$$

Dynamics of magnetic materials have an influence on permeability evolution. However for low losses powder material some simplest modeling can be achieved and is more efficient. The previous models are based on measurement, and, as we explained, are difficult for low

permeability powder. Secondly, regarding real hysteresis e.g. AC/DC inverter (Figure 36), the thinness of the loops make accurate measurements quite impossible; the acquisition error is as large as the minor loops. So it would be difficult to validate a hysteresis model. But based on LS static model, some assumption can be done. The LS supposes that anhysteretic curve gives the main orientation to the minor loops. The dynamic part is added and can deform slightly the minor loop but once again for powder with thin loops the change is negligible compared with anhysteretic direction. For electrical behavior we search the direction of the loop and not the size because losses are already computed. So measurements show anhysteretic is enough. The power of powder is that datasheet provided by material supplier gives the information.

The anhysteretic is generally built by reducing the energy stored by the material around a polarization with decreasing wave, to make difference between first magnetization curve and anhysteretic. For powder material the main hysteresis is so thin that difference is insignificant. Moreover, the energy and the residual magnetic field when polarizing with addition of small impulsion are inexistent. So the suppliers give the evolution of permeability versus polarization magnetic field (Figure 47). The anhysteretic is directly deduced from this curve. Whatever the magnitude of the flux density imposed by the supplier, experience shows that there is small impact on the curve (Figure 48). Only large flux density excitation will change the curve.

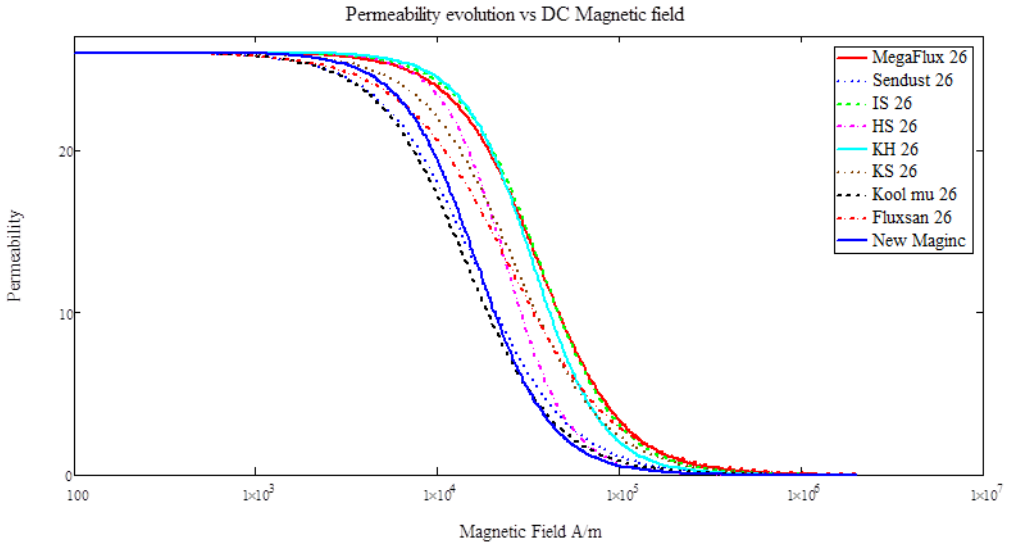

Figure 47 : Evolution of incremental permeability vs DC magnetic field

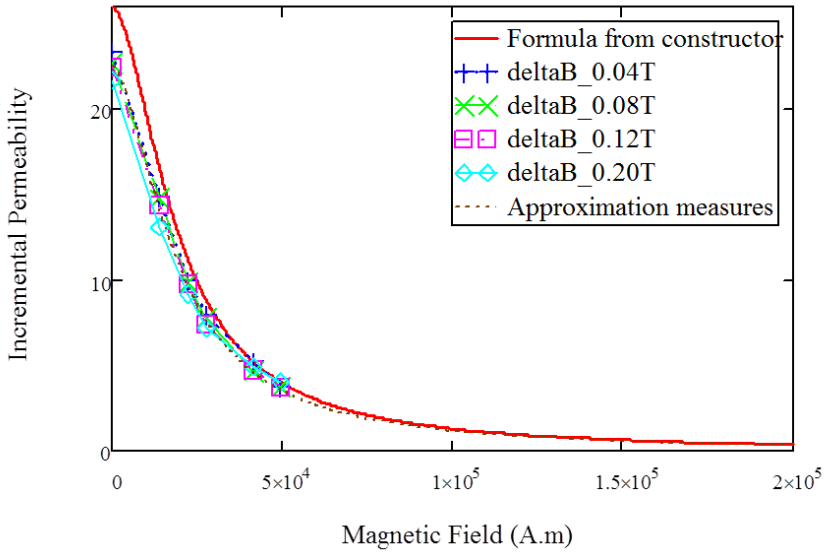

Figure 48 : Impact of flux density excitation on permeability measurement

The anhysteretic curve is computed as a reversible polynomial formula that addresses initial permeability, curve bend and saturation (Figure 49).

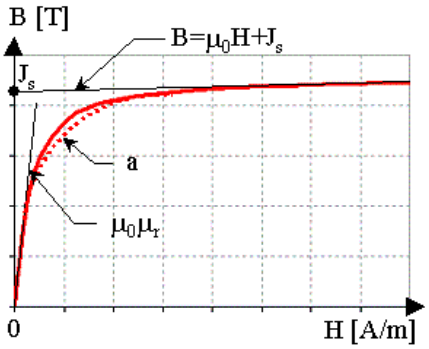

Figure 49 : Anhysteretic curve formula, dotted for different value of a

$$B(H) = \mu_0.H + b.\frac{\mu_0.H.\frac{\mu_r - 1}{b} + 1 - \sqrt{(\mu_0.H.\frac{\mu_r - 1}{b} + 1)^2 - 4.(\mu_0.H.\frac{\mu_r - 1}{b}).(1-a)}}{2.(1-a)} \quad \textbf{24}$$

$$H(B) = \frac{-\mu_0.\left[B.(\frac{\mu_r - 1}{a-1} - 2) - b.\frac{\mu_r}{(a-1)}\right] + \sqrt{\left[\mu_0.\left[B.(\frac{\mu_r - 1}{a-1} - 2) - b.\frac{\mu_r}{(a-1)}\right]\right]^2 - 4.B.\left[\mu_0^2.(\frac{\mu_r - 1}{1-a} + 1)\right].(B + \frac{b}{a-1})}}{2.\mu_0^2.(\frac{\mu_r - 1}{1-a} + 1)} \quad \textbf{25}$$

The coefficients *a*, *b* and μ_r are the same for both formulas. The *a* coefficient represents the bending of the curve, the *b* coefficient the magnetization saturation level and μ_r the initial permeability.

In case of voltage command for power converters, the flux density B is computed from choke voltage, the magnetic field calculated from formula then real current considering hysteresis bend is deduced. In case of current command the reverse is possible. These formulas are used successfully to predict inductance evolution vs DC current (Chapter III) or power converter current (Figure 40).

2.2.4.9 Conclusions

The efforts that must be spend on steel modeling or other high losses materials do not extend to powder core. The time and the cost of developing hysteresis dynamic model for powder material are too highs and unnecessary because the result is not assured to be accurate. The hysteresis thinness and the important field dynamic from 1A/m up to 200kA/m prevent accurate measurement. Yet all modern and precise models are based on measurements. An accurate model based on poor quality measurement and variability of same powder regarding manufacturer treatment or weather could be less pertinent than simplest models. Moreover, the fabrication process of powder core compels to build a model for every size and forms. The numbers of measurements and the high frequency of new material implementation are too great to be admissible.

Whatever, powder hysteresis mechanisms allow simplifications useful to build a model based on supplier datasheets. The integration of material in a homogenous library is fast and easy and new materials can be added without measurement. This approach is accurate enough in the optimization context to separate solutions and converge toward the best material and its best use.

2.2.5 Conclusions:

The magnetic material is one of the most complex components to model. In this PhD their modeling has been driven by their implementation as a library for optimization.

In power converter the choke are subject to complex waveforms, square ones most of the time, in addition with LF modulation. Then it is essential for the model to report the magnetization effects related to the waveforms. A dynamic model is compulsory. In the process of building a homogenous library for easy implementation, a behavioral model is the fittest approach. Based on measurements and polynomial approximation, models such as LS are applicable to all kind of material because they do not require microscale mechanisms modeling of the material. Developed first for FeSi steel sheet the LS model has proved efficient for nanocrystallin also. However, the extension of the LS for powder core is difficult because of the measurement. Powder core being the most use magnetic material at Schneider Electric ITB, the development of a specific model rather than spending too much effort on a global modeling is pertinent. Considerations on powder processing hazard, size effect and powder thin hysteresis mechanisms, demonstrate that dynamic hysteresis modeling will not necessarily be accurate. The error of measure acquisition being sometime same scale than hysteresis width, accurate measure proves difficult. Moreover, for frequent implementation of

new material and cost spare, model must be based on suppliers' datasheet and not on measurements. Thus a validated model is developed for losses approximation and electrical behavior specific to powder material.

2.3 CHOKE COIL

2.3.1 Introduction:

For high power choke, now using low losses powder core, the losses and heat increase come mainly from conductors. The use of algorithm optimization methods, especially genetic algorithm for the ability to switch between material library and discrete value of parameters prevents FEM simulations that are heavy time consuming and not suitable for optimization without surface mapping procedure that reduce their accuracy. So for analytical models, two approaches are developed here.

Common approach is based on the homogenization of a stack of conductors in an equivalent area. The definition of equivalent geometric and electric parameters is done differently regarding the methods. The most known are equivalent complex permeability [36] and Dowell [37] approaches. G2Elab has a strong experience and feedback using Dowell for power conductors, so this method has been investigated and automated in the PhD. Application, validation and good results are explained and shown. Its implementation in an optimization is fast and easy.

However, like said before, optimization leads to optimal solution but not technology breakthrough. The proposition of new windings has reached the limits of Dowell or other homogenization method for modeling. Thus a brand new method for conductive area modeling is introduced in this work and several upgrades investigated. Based on the solution of magnetic potential from Maxwell equations the model allows modeling of real geometry of stacking.

2.3.2 Dowell:

2.3.2.1 Introduction

The homogenization method presented here has been first proposed by Dowell [38]. It is based on the observation that in a stack of conductors, magnetic field isovalues at low and medium frequencies behave linearly as in a sheet (Figure 50). Thus, transformation parameters between the stack of the conductors and an equivalent conductive sheet can be found. Several ways to achieve it can be chosen; our particular approach is presented below.

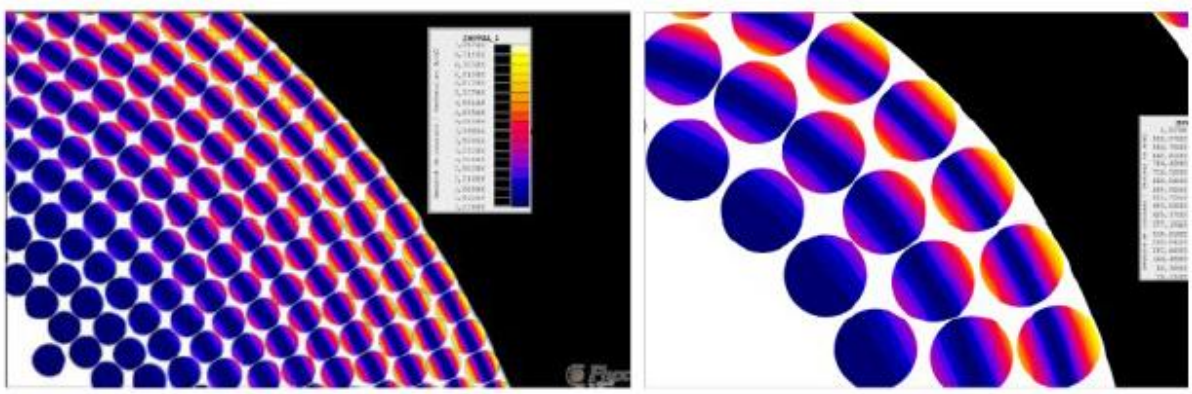

Figure 50 : linear magnetic field in round conductors

2.3.2.2 From conductors to sheet

The idea of the homogenization is to transform several conductors with same properties and submit to same magnetic field into an equivalent sheet. The steps are presented from litz wire which is the smallest conductor for this approach to the final sheet. Other geometries like solid round conductors or square or flat ones follow the same approach starting at different steps of the process.

The Litz wire is a fragmented conductor in many insulated strands whose small diameter allows reducing the skin effect. Likewise, the strands are twisted to ensure the uniformity of the current distribution in the conductor and reduce proximity effect. This makes it possible to model those wires into equivalent sheet. Effectively, one strand alternates between low magnitude magnetic field zone and high ones, we can then considerate the fact that each strand participate punctually in a Dowell sheet. Attention must be paid to the importance of the twisting length, because the assumption is valid if the total twist of a strand is achieved.

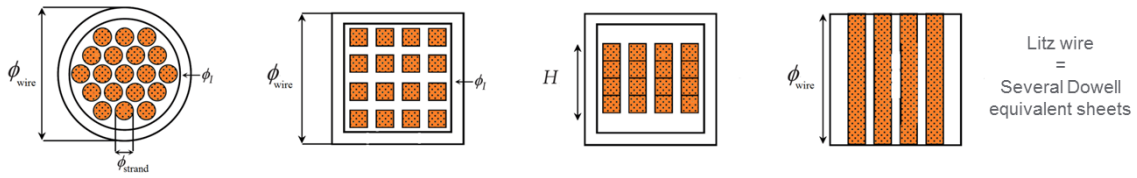

Figure 51 : From Litz wire to equivalent sheets

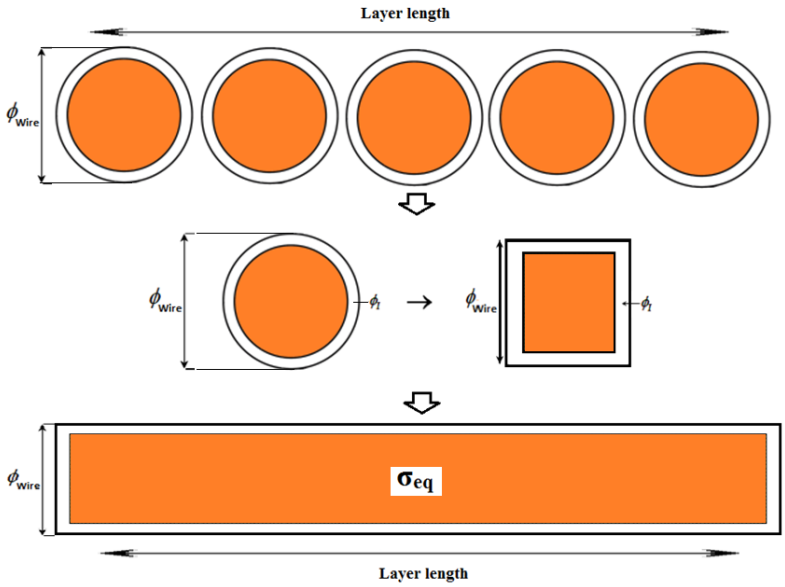

Figure 52 : From round conductor layer to equivalent layer

A common mistake is to say that litz wires reduce the proximity effect in the winding. However, the twisting of the strands only prevents proximity effect in the wire between strands, not between the several wires of the winding. This aspect is a reason to assume that every Litz strand operate the same task. The method to homogenize Litz wire is presented on

(Figure 51) then (Figure 52), it has been proposed in [39]. To sweep from round shape to rectangular one, the strands are transformed into equivalent square conductors, and then they are all equally positioned on the wire surface. Many methods have been proposed to achieve the homogenization: keep the same conductor surface or keep the same layer length or some else. The choice is to be done addressing LF resistance, skin and proximity effect and homogenization effect. We decide here to preserve the same conductor surface, the same layer length and also the diameter of the whole wire as the larger of the sheet. The equivalent conductivity is then calculated by adjusting the height of the sheet to keep the same DC resistance of the winding. The choose of the height as the adjustment parameter is logical because its variation will not interfere with the HF phenomenon, then the total evolution curve of the resistance versus the frequency will only change its offset with the height. The diameter of the wire is preserved to guarantee the sizes implied in the proximity effects and the length of the layer is kept to do not alter the magnetic field magnitude at each side of the layer. Every round wire can be transform following the same procedure. Thus, the eddy-current effects can be calculated for an equivalent conductive sheet. This approach implies that the magnetic field is parallel and invariant along the layer. It is valid for the axial conductors for which magnetic field is orthoradial. For radial conductors also called transition ones, the losses could be obtained by the average power dissipated by the internal and external axial conductors on which they depend. However, a better modeling is achievable using the previous method; it has been first presented in [40]. The dissipated power is calculated on an infinitesimal sheet. Once unwound, the layer verifies the same properties as before, the same formulas can be used adapting the equivalent sheet parameters regarding the axe of transition conductors. An example is presented for a toroid shape; (Figure 53) shows the homogenization for axial coil part and the approach for radial coil part.

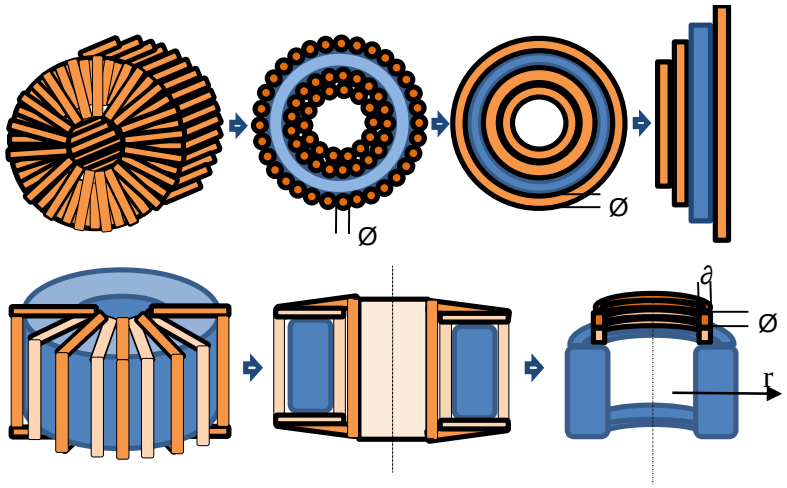

Figure 53 : Toroid coil into Dowell equivalent layers

Both algorithms to wind a toroid coil and divide it in Dowell's sheets are presented in annexes.

2.3.2.3 Resolution of Maxwell Equation for sheet

The benefit of this analytical modeling is to evaluate separately proximity effect and skin-depth effect as function of choke geometry and wires characteristics. Moreover, power losses are evaluated using continuous and differentiable equations that are able to be implemented in any optimized design procedure. The study of a conductor sheet is achieved in 1D; the border effects are insignificant in toroid applications cases. Toroid being the major geometry used the choice is coherent. The magnetic field is depending only on the distance from the origin. The axes and magnitudes are presented on (Figure 54). The Maxwell equations are:

$$\mathrm{rot}(E) = \frac{-dB}{dt} \quad (26)$$

$$\mathrm{rot}(H) = J \quad (27)$$

$$J = \sigma.E \quad (28)$$

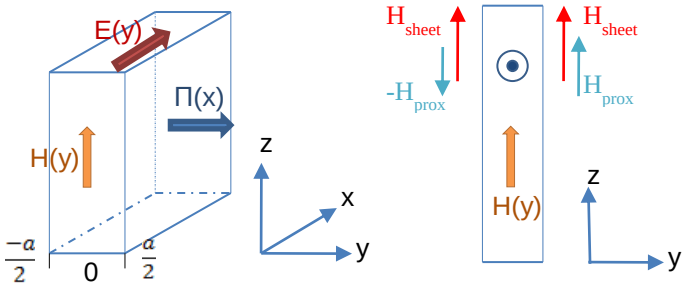

Figure 54 : Dowell sheet notations

The modeling is done for a sheet of thickness a, and for a magnetic field along the y axe. Then, Maxwell equation leads to consider the diffusion equation:

$$\Delta H = -i.\sigma.\sigma.\omega_0.H \quad (29)$$

The solution to this equation has the form:

$$H(y) = A.e^{(1+i).\frac{y}{\delta}} + B.e^{-(1+i).\frac{y}{\delta}} \quad (30)$$

The approach by layer, allows dividing the total magnetic field in two contributions, the field generated by the sheet Hsheet and the field created by the other neighboring ones, so called Hprox. See on (Figure 54). Expressing field in a/2 and –a/2 gives the constants A and B considering the both contributions. Thus, we have the magnetic field in the sheet:

$$H(y) = \frac{e^{(1+i).\frac{y}{\delta}} + e^{-(1+i).\frac{y}{\delta}}}{e^{(1+i).\frac{a}{2\delta}} + e^{-(1+i).\frac{a}{2\delta}}}.H_{sheet} + \frac{e^{(1+i).\frac{y}{\delta}} - e^{-(1+i).\frac{y}{\delta}}}{e^{(1+i).\frac{a}{2\delta}} - e^{-(1+i).\frac{a}{2\delta}}}.H_{prox} \quad (31)$$

The energy through a surface is given by Poynting vector:

$$\Pi(y) = \frac{1}{2}.E(y).\overline{H(y)} \quad \textbf{32}$$

$$E(y) = \int -i.\mu_0.\omega.H(y).dy \quad \textbf{33}$$

For a total winding, losses of all layers are summed. The radial part is integrated along radius r.

2.3.2.4 Coil resistance

The purpose of the PhD is to optimize the coil to maximize converter efficiency in terms of losses, price and other goals. Then, we must supply in the algorithm a way to compare various windings between them. Assuming a unitary current in conductors we have, thanks to (32), the equivalent resistance of the coil for any k harmonic of the current flowing through it.

$$R_{sheet} = \frac{L_{sheet}}{I_{rms}^2} = \frac{h.l}{n.\sigma.\sigma}.\left[\frac{sh(\frac{a}{\delta}) + \sin(\frac{a}{\delta})}{ch(\frac{a}{\delta}) - \cos(\frac{a}{\delta})}.H_{sheet}^2 + \frac{sh(\frac{a}{\delta}) - \sin(\frac{a}{\delta})}{ch(\frac{a}{\delta}) + \cos(\frac{a}{\delta})}.\left[\frac{n^2 - 1}{3}.H_{sheet}^2 + n^2.H_{prox}^2\right]\right] \quad \textbf{34}$$

Thus, whatever the environment is, the comparison between various windings can be achieved by the comparison between their resistances for both LF and HF harmonics.

Two major eddy current phenomena are influencing the resistance of the coil, the skin effect and the proximity effect. The first one is depending on the diameter of the wire and can be dramatically reduced using litz wire. The second one relies on the number of wires put together and their proximity. So both effects are in competition, because choosing a small diameter to prevent skin effect will lead to a higher number of conductors and then to more proximity effects. The evolution of the resistance of a winding versus the frequency is a useful tool to understand the both effects. (Figure 55) shows the typical curve where three domains are discriminated. At LF, no effect deteriorates the conductors' behavior, so the resistance value is constant and depends on the material, the temperature and the length and section of wires. Then, in the range of kHz, a transient phase happens when proximity effect first then skin effect, unbalance the magnetic field repartition in the coil. The whole conductivity surface is now longer entirely used, consequently, the resistance increases. The last area interesting in our applications is the range from few kHz to hundred kHz when the reduction of useful surface is decreasing constantly in logarithm scale. At higher frequency, the resistance will re-increase dramatically, because of the resonance of the capacity between wires. However, this effect occurs generally for MHz which frequency is out of our operating frequency.

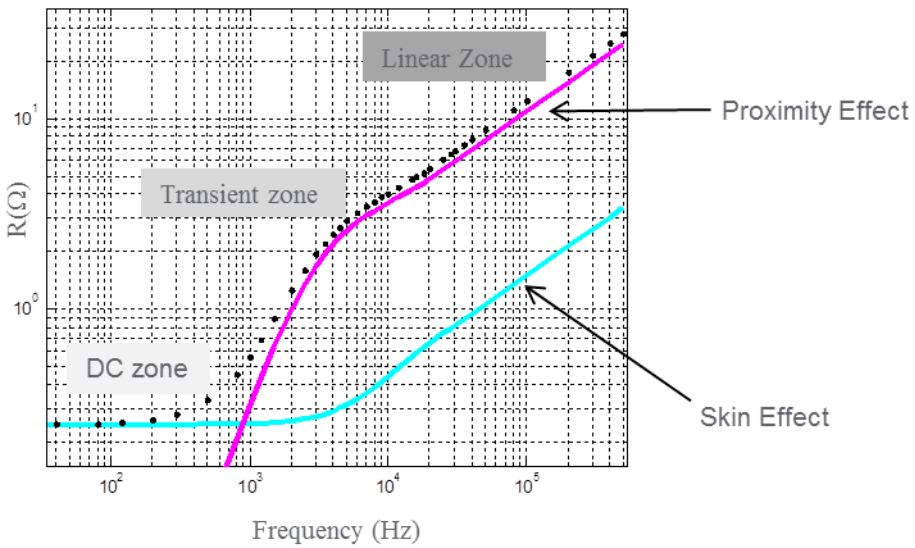

Figure 55 : Evolution of coil resistance vs frequency, skin and proximity effects

The shape of the curve can be explained dividing skin and proximity effects. The final resistance value is reminded in dotted line on (Figure 55). In high power electronic application several layers of conductors are generally needed to support current density without critical temperature rise. Thus, on these curves representing a three layers winding, the proximity effects are dominating. The skin effect can't be considerate as the only factor of sizing.

The (Figure 56) shows the previous analyzed coil, realized with two different wires assuming the same DC resistance, on a non-magnetic toroid core. The magenta curve represent a 116 turns 4mm copper wire winding, the cyan curve represent a 116 turns winded with copper wire of 16 strands of 1mm. The impact of frequency takes higher frequencies to occur in small wires as common thought with skin effect. However, the occupancy rate is poor and results in more layers to wind the coil. So, the proximity effects are higher for high frequencies. Thus, depending on the frequencies spectrum of the current flowing in the conductors, one coil is better than the other. We see here that any time the core will change and thus the current spectrum the coil must fit..

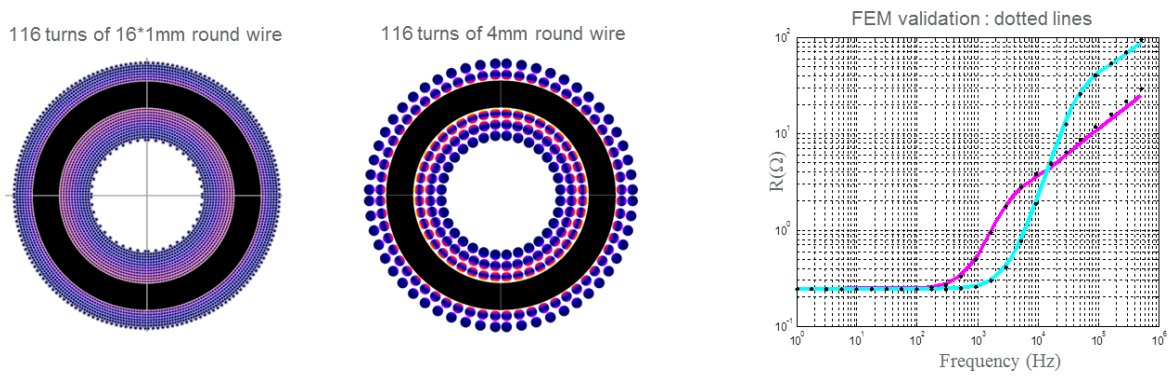

Figure 56 : Comparison of two coil using Ø1mm and Ø4mm, validation with FEM

With PWM waveforms, the spectrum presents LF harmonics with HF harmonics of the switching frequency. Thus coil resistance is interesting only in few part of the frequency range and thus optimization is really interesting to help finding the best coil in these areas.

Meanwhile, the resistance is not the only parameter to take into account; the price of litz wire will be more expansive than large solid round wire and the occupancy rate being poor, the footprint of the device will be less advantageous than large wire. The price will also be more expansive for smaller conductors and for their winding by a manufacturer. Considering all this parameters, the optimization process becomes inevitable to reach the better design taking into account the coil environment.

2.3.2.5 Validations

The Dowell approach proves accurate enough for our toroid coil. The validation is achieved comparing simulated frequency evolution of the coil resistance with FEM and prototypes. If the resistance is correctly computed and the HF current also is, the losses of windings will be accurately close from reality.

The first validation is done comparing both previous analyzed coils with FEM simulation from Flux2D®, (Figure 56).

The second validation is achieved on two windings. They are wound on wood cores to prevent effect of core on measurements with an Agilent 4294A impedance analyzer. The simulation is in 1D while the measurement is done on 3D coils. The first is 117 turns of 100x0.1 mm copper litz wires (Figure 57). The second coil is realized with 400 turns of 1.6 mm copper solid round wires (Figure 58). The first conclusion is that even simulated in 1D, coil resistance illustrates the 3D behavior, particularly because of the toroid shape. The second one is that both Litz and solid conductors are well modeled. Note that even with a bulky coil, meaning magnetic field is not straight and sheet neither, the simulation is still correct. The consideration of radial part is essential. However, resonance of windings is not modeled with Dowell approach.

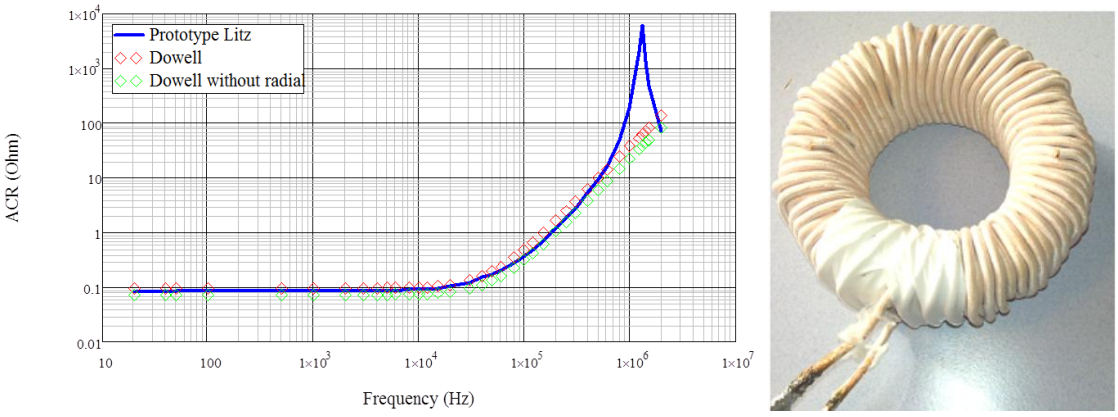

Figure 57 : Coil model validation for Litz wires

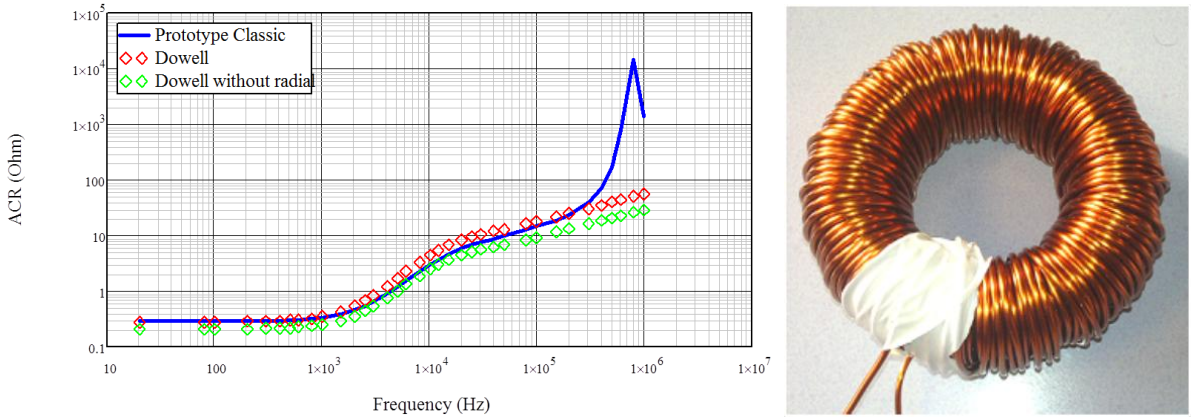

Figure 58 : Coil model validation for solid round wires

The last test is the measurement of several prototypes of a same power choke implemented in an inverter. Both LF and HF resistances were given by supplier. The results are compared in (Table 3).

Table 3

Manufacturer1 a		Manufacturer1 b		Manufacturer 2 a		Manufacturer 2 b		Simulation	
Lo	Ro/Rac	Lo	Ro/Rac	Lo	Ro/Rac	Lo	Ro/Rac	Lo	Ro/Rac
164.98 µH	2.14 mΩ/37,5mΩ	164.14 µH	2.58 mΩ/40,3 mΩ	170.72 µH	2,34 mΩ/39,8mΩ	171.3 µH	2,36 mΩ/40mΩ	172,4 µH	2,3 mΩ/39,3 mΩ

2.3.2.6 Limitations

Dowell works perfectly with our power toroid choke and is accurate enough for optimization requirement. However, toroids are not the only form used. Square and oblong core forms are still implemented in Schneider converters, meaning coil with sides unlike toroid ring coil. The side effect in coil is dramatic on current density distribution and thus equivalent resistance (Figure 59). Proximity effect depletes inner and central layer.

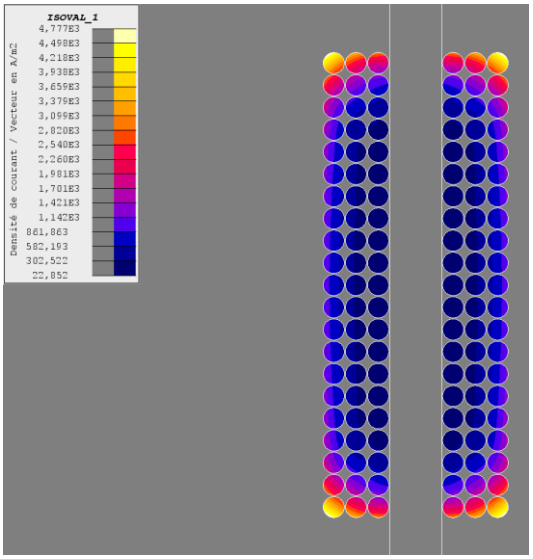

Figure 59 : Side effects in vertical stack of conductors

Another shortcoming of Dowell, rarely happening in power choke, is the irregular filling of layer of wires. Effectively, homogenization approach supposes a well repartition and full conductive area. (Figure 60) illustrates that empty layer of wires are far from straight magnetic field approximation done for Dowell and lead to important error.

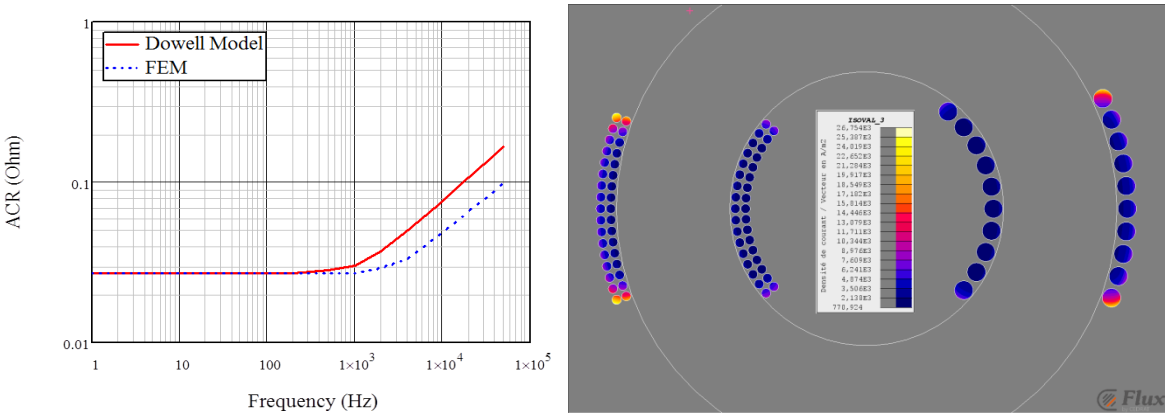

Figure 60 : Empty layer effects

To control equivalent permeability of a transformer or a choke, designers use air-gap in the magnetic core. The air-gap acts as a source of magnetic field on conductors and thus enhanced proximity effect in that area (Figure 61). This effect is important because most of the time the air-gap is surrounded by the coil and increase of losses in this area leads to critic temperature increase. Sadly, Dowell approach is unable to simulate the air-gap magnetic field.

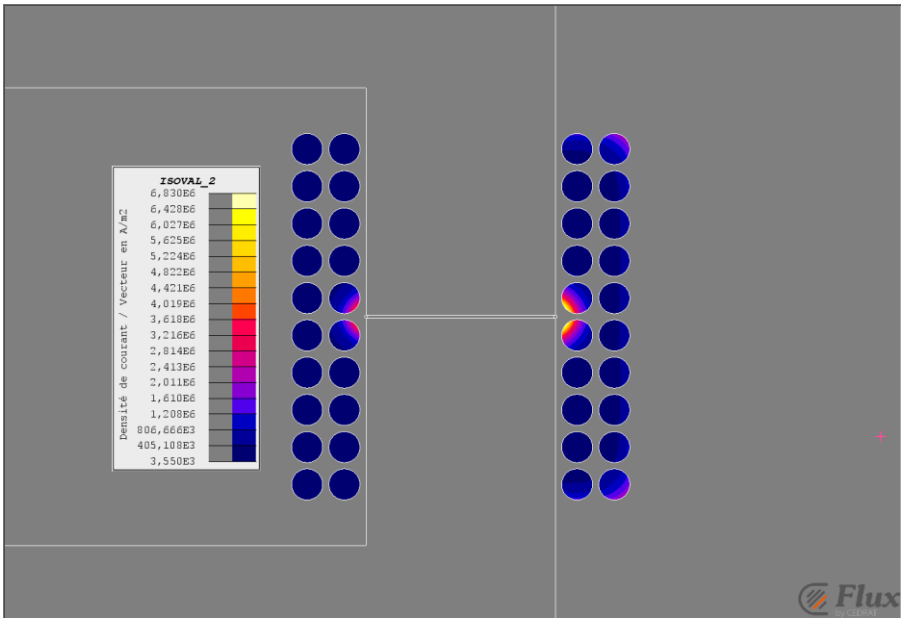

Figure 61 : Air-gap fringing flux effect on windings

Last, new geometries of conductors are proposed in [2.3.3.1] that Dowell approach does not address.

2.3.2.7 Conclusions

Schneider Electric applications use more and more toroid choke and transformer, both for core and coil advantages. The simplification brought by toroid coil makes it possible to use a 1D model for simulation without noticeable error. Dowell homogenization method is presented and applied to power choke coil. It shows accurate results enough for optimization requirement.

However, for other shapes of coil or conductors, or for air-gap consideration Dowell proves limited. In order to achieve technology improvement using optimization a different model is needed.

2.3.3 A-Model:

2.3.3.1 Introduction

In power devices, e.g. transformers, electromechanical actuators and magnetic sensors, where materials exhibit both magnetic permeability and electrical resistivity and undergo the diffusion of the magnetic field, finite element method and integral methods – that include boundary element method, are commonly employed for numerical simulations. When geometric data are changed by the algorithm, the mesh has to be redefined that involve larger running time for FEM method. Both of these methods rely on the idea of approximate function to describe the solution on the mesh elements. For example, quadratic polynomial function is widely used to approximate the solution on the mesh entity in FEM codes when IM codes mainly consider uniform function over the element. It results that for large ratio of skin-depth to size, the meshes have to be refined to ensure accuracy. The re-meshing of the

whole domain and the associated running time is the main issue to use these methods in optimized design process.

To address the problem, three ways are pointed out by the state of art review and two consider the approximate function on the mesh entity as the starting point. One way is to increase the polynomial order of the shape function. But how is the number of unknowns on a mesh element is balanced by the number of elements? And what about the running time? The second way is to define the shape function from the formal solution of a physical problem. For example, in FEM, shell elements could be used to solve problem where skin-depth to size ratio is very large. Shape function is so defined by the formal solution of the diffusion equation for semi-infinite situation. Another way to avoid re-meshing of the whole domain is to use homogenization techniques. These techniques are very helpful in case of large pattern but lack of accuracy when periodicity is gone.

For all of these methods, computational time dedicated to the iterative process is pulled down when optimization strategies as surface mapping and experimental design procedure are used but accuracy is then counterbalanced.

The main objective is then to model the losses in power electronics devices to improve the optimization design process, e.g. power inductors and cables. It follows that we consider the computation of the magnetic vector potential field distribution on the cross-section of a bundle of parallel conductors. As a caricatured picture of numerical methods, we focus on the idea of Integral Method where the approximate function on the element is based on a formal solution of the Laplace - Helmholtz equations: the projection of the magnetic vector potential onto basis functions - Fourier basis truncated to N^{th} order term for cylindrical situation. It follows that mesh is then defined by circular elements carried by the geometry. It results that no mesh is finally required! The formal solutions of the Helmholtz and Laplace equation are reminded. . The chosen numerical method is then detailed. It allows computing the magnetic vector potential for a bundle of multiple conductors. It differs from the integral-equation method widely used in Integral Method codes. To conclude, the bifilar line problem is chosen to validate our approach and to compete other methods in terms of accuracy and computation time. This approach was first investigated in [51].

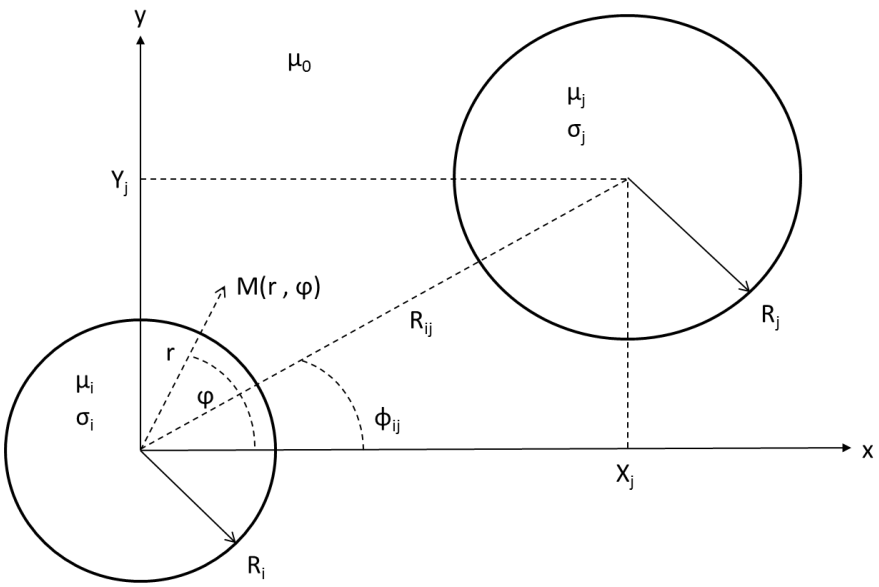

Figure 62 : Cylindrical conductors, notations

2.3.3.2 Single conductor solution

In this part the solutions of Laplace and Helmholtz equations are presented for a single round conductor in term of time harmonic expressions. Other useful mathematical formulas for one conductor are introduced before extending the approach to several conductors in section [2.3.3.3].

2.3.3.2.1 Solution of the Helmholtz equation

We consider an infinitely extended cylindrical conductor of radius r_i, described by its cross-section, perpendicular to the z-axis of a cylindrical polar coordinate system (r,φ) as depicted in (Figure 62). The current density $\vec{j}$ through the conductor is driven by an electric field due to the electrical source and magneto-motive electrical field related to Eddy current density as:

$$\vec{E} = -\overrightarrow{\text{grad}}V - \partial\vec{A}/\partial t \qquad \textbf{35}$$

$\vec{E}$ is so given by Ohm's law $\vec{j} = \sigma_i \vec{E}$ where σ_i, the conductivity is uniform.

In the cross section of the conductor, magnetic vector potential is given by the Helmholtz equation written in time-harmonic form as follows:

$$\Delta\vec{A} + k^2\vec{A} = -\mu_i\sigma_i\overrightarrow{grad}V \qquad \textbf{36}$$

Where $k = \frac{(1-i)}{\delta}$ with $\delta = \sqrt{2/\mu_i\sigma_i\omega}$ at the angular frequency ω. $\vec{E}$ and $\vec{A}$ are along the z-axis and rely only on scalar values $E_z(r,\varphi)$ and $A_z(r,\varphi)$. The general solution of (36) found in literature [41] and [43] and expressed in Fourier series expansion is:

$$A_z(r,\varphi) = \sum_{n=-\infty}^{+\infty} J_n(kr)\gamma_n e^{in\varphi} \quad \textbf{37}$$

Where J_n are the Bessel function of the first kind of order n. The Bessel functions of the second kind diverge at the origin and are ignored. Because of the relation between Bessel function of positive and negative order $J_{-n}(kr) = (-1)^n J_n(kr)$, magnetic potential (37) is rewritten according to:

$$A_z(r,\varphi) = \frac{-gradV}{i\omega} + \gamma_0 J_0(kr) + \sum_{n=1}^{+\infty} J_n(kr)(\gamma_n e^{in\varphi} + \gamma_{-n} e^{-in\varphi}) \quad \textbf{38}$$

where the particular solution $-\overrightarrow{gradV}/i\omega$ is added to the general solution of (36). The total current I_i flowing through the conductor's section is given by Ampere's law. The integral of the magnetic field at $r = R_i$ involves $\overrightarrow{H_\varphi} = -1/\mu_i \cdot (\partial A_z/\partial r) \cdot \overrightarrow{u_\varphi}$. Consequently, only the zero order term of (38) is related to the total current I_i:

$$\left[-\frac{1}{\mu_i}\frac{d}{dr}(\gamma_0 J_0(kr)) \right]_{r=R_i} = \frac{k}{\mu_i}\gamma_0 J_1(kR_i) = \frac{I_i}{2\pi R_i} \quad \textbf{39}$$

Moreover, the expansion of exponential in cosines and sinus gives:

$$\gamma_n e^{in\varphi} + \gamma_{-n} e^{-in\varphi} = (\gamma_n + \gamma_{-n})\cos(n\varphi) + i(\gamma_n - \gamma_{-n})\sin(n\varphi) = p_n \cos(n\varphi) + q_n \sin(n\varphi) \quad \textbf{40}$$

With p_n and q_n complex harmonic coefficients depending on external magnetic field solicitation. Due to the infinitely extended situation, the current I_i is not well defined by the voltage across the conductor and we choose it to have a null potential vector magnetic at $r = R_i$., (36) is then expressed as:

$$A_z(r,\varphi) = \frac{\mu_i I_i}{2\pi k r_i}\frac{J_0(kr) - J_0(kR_i)}{J_1(kR_i)} + \sum_{n=1}^{+\infty} J_n(kr)(p_n \cos(n\varphi) + q_n \sin(n\varphi)) \quad \textbf{41}$$

With p_n and q_n complex harmonic coefficients depending on external magnetic field solicitation. It could be noticed that the left term of (41) involves the current flowing in the conductor and is related to the skin effect. The sum on the right depends on the time-harmonic coefficients that describe the effect of external sources on the conductor and is related to the proximity effects.

2.3.3.2.2 Solution of Laplace equation

Outside the conductor, in nonconductive area e.g. the air, the magnetic potential is relying on a Laplace equation $\Delta\vec{A} = 0$ and solved using Fourier series expansion:

$$A_z(r,\varphi) = a_0 + \alpha_0 \ln(\frac{C}{r}) + \sum_{n=1}^{+\infty} r^n (a_n \cos(n\varphi) + b_n \sin(n\varphi)) + \sum_{n=1}^{+\infty} r^{-n} (\alpha_n \cos(n\varphi) + \beta_n \sin(n\varphi)) \quad \textbf{42}$$

As previously mentioned, Ampere's law implies that zero order term is related to the total current I_i. Additionally, to guarantee the continuity of magnetic potential at $r = R_i$, (42) is written as:

$$A_z(r,\varphi) = -\frac{\mu_i I_i}{2\pi} \ln(\frac{r}{R_i}) + \sum_{n=1}^{+\infty} r^n (a_n \cos(n\varphi) + b_n \sin(n\varphi)) + \sum_{n=1}^{+\infty} r^{-n} (\alpha_n \cos(n\varphi) + \beta_n \sin(n\varphi)) \quad \textbf{43}$$

2.3.3.2.3 Reflection and Transmission coefficients

According to the n-order potential term previously detailed in (42) and (43), 6 coefficients have to be defined, but the continuity equations is used to reduce to 2 the number of unknowns. So-called reflection coefficient Re_n and transmission one Tr_n are then introduced. Using $\vec{B} = \overrightarrow{rot}\vec{A}$ and the boundary conditions for the normal component of flux density $\overrightarrow{B_r}$ and the tangential component of the magnetic field $\overrightarrow{H_\varphi}$ at $r = R_i$ we have for cosines coefficients :

$$\begin{aligned} a_n R_i^n + \alpha_n R_i^{-n} &= p_n J_n(kR_i) \\ a_n R_i^n - \alpha_n R_i^{-n} &= p_n \frac{\mu_0}{\mu_i} \left[\frac{kR_i}{n} J_{n-1}(kR_i) - J_n(kR_i) \right] \end{aligned} \quad \textbf{44}$$

The same expressions are valid for sinus coefficients. It results:

$$\mathrm{Re}_n = \frac{\alpha_n}{a_n} = \frac{\beta_n}{b_n} = R_i^{2n} \left[\frac{2n}{kR_i} \frac{J_n(kR_i)}{J_{n-1}(kR_i)} - 1 \right] \quad \textbf{45}$$

$$Tr_n = \frac{p_n}{a_n} = \frac{q_n}{b_n} = R_i^n \frac{2n}{kR_i J_{n-1}(kR_i)} \quad \textbf{46}$$

Note that for $n = 1$ the reflection coefficient is equivalent to the polarizability of a cylindrical conductor in a uniform magnetic field perpendicular to its axe. The Polarizability could be then used by homogenization techniques to estimate the equivalent complex permeability of infinitely extended conductor pattern. It could be highlight that if a_n and b_n are solved, then all other coefficients may be deduced and if required, magnetic potential could be estimated over the whole domain but focus is only made on the power losses estimation. .

2.3.3.2.4 Solution of Poynting Vector

The main purpose of solving the magnetic potential is to simulate conductors at any frequency to improve the efficiency of an electromagnetic system. Thus the Poynting vector is calculate through the conductor surface to deduce active and reactive power:

$$P_i = -\oint_{Cyl} \vec{E} \wedge \overrightarrow{\overline{H}} \overrightarrow{ds} = L \int_0^{2\pi} E_z \cdot \overline{H_\varphi} R_i d\varphi \quad \textbf{47}$$

We deduce the power per length unit:

$$\frac{P_i}{L} = V\bar{I} + \omega\sum_{n=1}^{+\infty} n\frac{a_n\overline{\alpha_n} - \overline{a_n}\alpha_n + b_n\overline{\beta_n} - \overline{b_n}\beta_n}{2i} + \dots$$
$$+ i\omega I\bar{I}\ln(R_i) + i\omega\sum_{n=1}^{+\infty} n\left(R_i^{2n}\frac{a_n\overline{a_n} + \overline{b_n}b_n}{2} - R_i^{-2n}\frac{\alpha_n\overline{\alpha_n} + \overline{\beta_n}\beta_n}{2}\right) \quad \textbf{48}$$

The first line of (48), real, is the active power. The first term exists even with the absence of an external field if a current flows through the conductor. The second one exists even without current if the conductor is submitted to an external filed. The second line of (48) is pure imaginary so the reactive power. It depends on the temporal variation of stocked energy. If this energy increase it is that the flux come into the conductor, it is summed positively (a_n,b_n) the inverse is linked to α_n β_n coefficients.

2.3.3.3 Several conductors solution

The general Laplace and Helmholtz equations have been solved in a polar coordinate system related to the conductor *i* and inside and outside of the conductor. The magnetic potential solution depends on time-harmonic coefficients that we have to solve. Because the approximate solution - Fourier series - is solution of the differential equations (36) and (37) to solve, integral-equation is no more required. It follows that the difficulties associated to the integration process between very close elements are avoided. We have now to detail the method that we chose for solving the whole set of coefficients. It implies to write matrices relation to solve the coefficient set elated to the element *i*. The whole system of equations is then skillfully deduced.

2.3.3.3.1 Change of coordinates system

To compute harmonic coefficients of one conductor, the external field applied to this conductor must be calculated. If the external field comes from another conductor, the link between them is presented below.

The first sum of (43) increases with *r*, whereas the second sum and the logarithm term decrease with *r*. So we can assume that in a polar coordinate of a conductor *i*, the increasing part is the one decreasing in the polar coordinate of a conductor *j* and reversely. So the first harmonic increasing summation of (43) is written in a global Cartesian system for each n order, see (Figure 62):

$$r^n(a_n\cos(n\varphi) + b_n\sin(n\varphi)) = a_n\,\mathrm{Re}\left[(re^{i\varphi})^n\right] + b_n\,\mathrm{Im}\left[(re^{i\varphi})^n\right] =_n \mathrm{Re}\left[(x+iy)^n\right] + b_n\,\mathrm{Im}\left[(x+iy)^n\right] \quad \textbf{49}$$

Using the Newton binomial development and noting that real terms are the even and imaginary terms are odd sums we deduced:

$$r^n(a_n\cos(n\varphi)+b_n\sin(n\varphi))=a_n\sum_{k=0}^{n/2}\left[\frac{(-1)^k n!}{(2k)!(n-2k)!}x^{n-2k}y^{2k}\right]+b_n\sum_{k=0}^{n/2}\left[\frac{(-1)^k n!}{(2k+1)!(n-2k-1)!}x^{n-2k-1}y^{2k+1}\right] \quad \textbf{50}$$

Now if we use Maclaurin expansion or the Taylor expansion of an expression A(x,y) at a point of coordinate (X,Y), we get:

$$A(x+X,y+Y)=A(X,Y)+\ldots$$
$$+\sum_{n=1}^{+\infty}\left[\frac{1}{n!}\frac{d^n}{dx^n}A\sum_{k=0}^{n/2}\left[\frac{(-1)^k n!}{(2k)!(n-2k)!}x^{n-2k}y^{2k}\right]+\frac{1}{n!}\frac{d^{n-1}}{dx^{n-1}}\frac{d}{dy}A\sum_{k=0}^{n/2}\left[\frac{(-1)^k n!}{(2k+1)!(n-2k-1)!}x^{n-2k-1}y^{2k+1}\right]\right] \quad \textbf{51}$$

Replacing the expression A of (51) by the negative summation and logarithm, we get by similarity with (50) in a point depleted from current near the *i* conductor coordinate center:

$$a_{i_n}=\frac{1}{n!}\frac{d^n}{dx^n}A=\frac{(-1)^n}{n}\frac{1}{R_{ij}^n}\cos(n\Phi_{ij})I_j+\sum_{m=1}^{+\infty}(-1)^n\frac{m}{m+n}\frac{(m+n)!}{m!n!}\frac{1}{R_{ij}^{m+n}}\left[\alpha_{j_n}\cos((m+n)\Phi_{ij})+\beta_{j_n}\sin((m+n)\Phi_{ij})\right] \textbf{52}$$

$$b_{i_n}=\frac{1}{n!}\frac{d^{n-1}}{dx^{n-1}}\frac{d}{dy}A=\frac{(-1)^n}{n}\frac{1}{R_{ij}^n}\sin(n\Phi_{ij})I_j+\sum_{m=1}^{+\infty}(-1)^n\frac{m}{m+n}\frac{(m+n)!}{m!n!}\frac{1}{R_{ij}^{m+n}}\left[\alpha_{j_n}\sin((m+n)\Phi_{ij})-\beta_{j_n}\cos((m+n)\Phi_{ij})\right] \textbf{53}$$

So the increasing summation coefficients a and b of (43) for a conductor *i* can be expressed using the coefficients α and β of the decreasing part of (43) for a conductor *j*. R_{ij} and Φ_{ij} are the polar coordinates of the center of *i* in the polar coordinates of *j*. Equations (52) and (53) can be written for the a and b coefficients of *j* from the α and β coefficients of *i*. Both conductors' expressions of magnetic potential are linked in a general Cartesian system. Note that the development order of *i* and *j* can be unequal m≠n, which can be useful when two conductors are of different size, precision can be set higher for larger size.

2.3.3.3.2 Solution of harmonic coefficients

In order to solve the harmonic coefficients, we denote by [a,b] the vertically concatenated vector of coefficients a_n and b_n, truncated to the Nth order. In the same way, [α,β] and [p,q] denote the concatenated 2N size vectors of coefficients α_n, β_n and p_n, q_n respectively. Likewise, the so-called reflection and transmission coefficients are transformed to 2N*2N (N for cosines and N for sinus) diagonal matrices [Re] and [Tr] where diagonal elements are given by (45) and (46).

So for one conductor (52) and (53) can be addressed by a single matrix equation:

$$[a,b]_i=[M_{ij}]\cdot I_j+[C_{ij}]\cdot[\alpha,\beta]_j \quad \textbf{54}$$

The $[M_{ij}]$ matrix is a 2N vector whereas $[C_{ij}]$ is a 2N*2M matrix, Nth order for *i* [a,b] and Mth order for *j* [α,β]. The magnetic potential vector is cumulative so (54) will also contain the addition of $[M_{ik}]$, $[C_{ik}]$ and $[\alpha,\beta]_k$ for any other *k* conductor. Using (45), (54) is developed as:

$$[a,b]_i = [M_{ij}]\cdot I_j + [C_{ij}]\cdot[\mathrm{Re}]_j \cdot [a,b]_j \qquad 55$$

The equation (55) is written for the *j* conductor and any other *k* conductor. We then have a matrix system

$$\begin{bmatrix} [a,b]_i \\ [a,b]_j \\ \dots \end{bmatrix} = \begin{bmatrix} 0 & [M_{ij}] & \dots \\ [M_{ji}] & 0 & \dots \\ \dots & \dots & 0 \end{bmatrix} \cdot \begin{bmatrix} [I_i] \\ [I_j] \\ \dots \end{bmatrix} + \begin{bmatrix} 0 & [C_{ij}]\cdot[\mathrm{Re}]_j & \dots \\ [C_{ji}]\cdot[\mathrm{Re}]_i & 0 & \dots \\ \dots & \dots & 0 \end{bmatrix} \cdot \begin{bmatrix} [a,b]_i \\ [a,b]_j \\ \dots \end{bmatrix} \qquad 56$$

Finally we can see that once the geometries of conductors and their physic properties (μ,σ,f,ω) fixed, the magnetic potential can be solved with only one matrix inversion and multiplication:

$$\begin{bmatrix} [a,b]_i \\ [a,b]_j \\ \dots \end{bmatrix} = \begin{bmatrix} 1 & -[C_{ij}]\cdot[\mathrm{Re}]_j & \dots \\ -[C_{ji}]\cdot[\mathrm{Re}]_i & 1 & \dots \\ \dots & \dots & 1 \end{bmatrix}^{-1} \begin{bmatrix} 0 & [M_{ij}] & \dots \\ [M_{ji}] & 0 & \dots \\ \dots & \dots & 0 \end{bmatrix} \cdot \begin{bmatrix} [I_i] \\ [I_j] \\ \dots \end{bmatrix} \qquad 57$$

The harmonic coefficients [a,b] are solved regarding internal and external filed effects for all conductors. No simplifications are assumed and no mesh is used. The solution is then valid for any arrangement of round conductors. The couples [α,β] and [p,q] are found using [Re] and [Tr] for each conductors.

2.3.3.4 The bifilar line application

The aim is to calculate the magnetic potential of the bifilar example shown on (Figure 62) in order to validate the solutions presented in 85 and 82. As previously mentioned, Fourier's series are actually truncated and the matrixes are sized by N. The question that arises is therefore how to set the value of N. In order to validate our approach, a careful numerical study compares the solution obtained by Finite Element Method on a fine mesh to the one obtained by solving (57) and by deducing the magnetic potential values over the domain. The FEM method is applied using Flux© software. The geometry is described by radius ratio rr = R_j/R_i and the ratio between the distance center to center and radius dr = R_{ij}/R_i. The conductors are in copper $\sigma_i = \sigma_j = 5.777\text{x}10^7$ Sxm^{-1} and immersed in air. The system is studied from 1 Hz to 1 MHz, so the mesh is realized to guarantee 5 triangular elements for the skin depth length @1 MHz. The currents that flow through the conductors are chosen as I_i = 1A and I_j = 0A. Equation (48) is used to compare active power and reactive power between the model and FEM.

2.3.3.4.1 Ri = 4mm, dr =3 and rr = 1

The first example is the less challenging one because conductors are of same size with large gap, (Figure 63). The error between FEM and model is plotted on (Figure 63). With only one harmonic order the difference is less than 1% @1MHz and with third order we decrease it to a hundredth of %. For N = 3 the computation is done in 0.116815s for the whole data from 1Hz to 1MHz whereas FEM need several minutes.

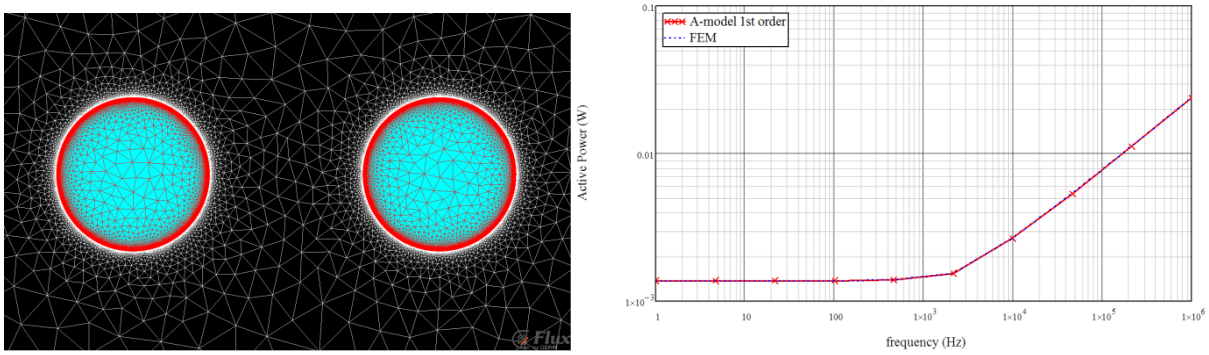

Figure 63 : 1st example of bifilar line, left zoom on geometry with infinite circular box, and right error between FEM and model vs frequency

2.3.3.4.2 Ri = 4 mm, dr = 2.01 and rr = 1

The second example is set with a tiny gap between conductors, (Figure 64). Two parameters are impacted by the number of harmonics, the distance between the two conductors coordinate centers and the ratio between coefficients [a,b]. So here the study is done for Ri = 4mm and Ri = 20mm in order to assess the impact of the distance between coordinates centers only. The impact of radius ratio between two conductors is assessed in next sub-section. The first observation is that the closeness of conductors leads to an higher number of harmonics for accuracy N>10 to drop under 1% of distance to FEM result and N>20 to drop under 0.01%. The ratio between conductors being the same, when Ri = 20 mm we clearly see the effect of distance between conductors centers. The number of harmonics has to go up to N = 30 to achieve same accuracy than case with Ri = 4mm and N = 20. However the model still computes results in 0.18s for N= 10.

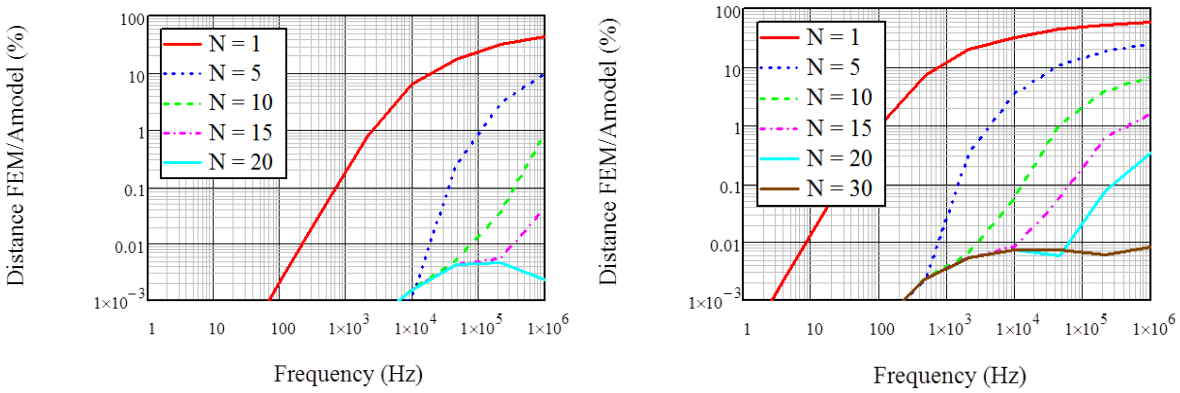

Figure 64 : 2nd example of bifilar line, left R = 4 mm, and right R= 20 mm

2.3.3.4.3 Ri = 4 mm, dr = 2.01, and rr = 5

The last case is the most complicated one. Two conductors are extremely close and with a large difference of sizes. A numerical limit occurs for the model. Indeed, the model even if analytically true, it still requires the inversion of a matrix (57) to compute harmonic coefficients. On (Figure 65) the number of harmonics required for good accuracy increases yet the model diverges. The matrix inversion is the only numerical calculation so it could be incriminated.

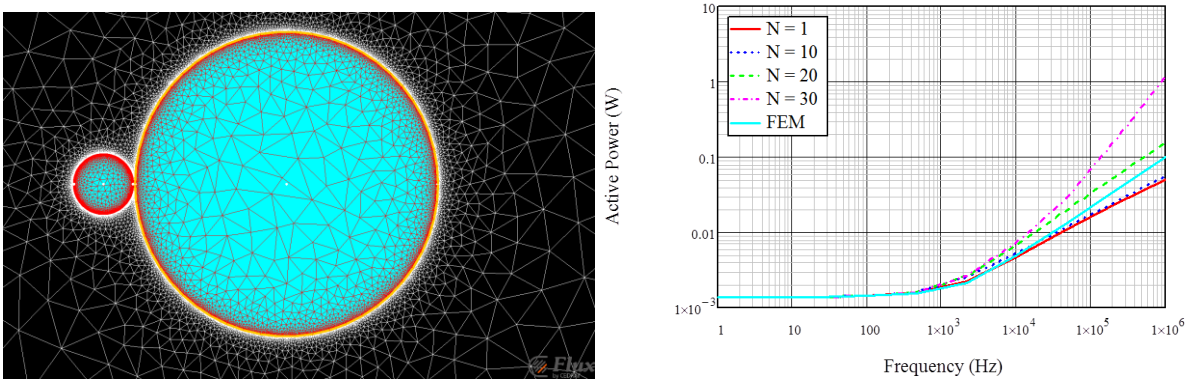

Figure 65 : 3rd example of bifilar line, left geometry, and right active power FEM and model vs Frequency

2.3.3.5 Conclusions

A-model is a new methodology to simulate electromagnetic system in time harmonic. It is based on the formal solution of the magnetic potential for round conductor. The mathematical solutions are clearly presented and explained. The method proposes a real fast and accurate alternative to time consuming FEM simulations. The solution is tested on 3 bifilar line cases with different properties and compared with accurate FEM simulation. The analytical solution proves to be true and it computation fast <0.2 s and accurate <0.01% of difference @1 MHz. However an issue is highlighted. The model differs from FEM in cases where a high number of harmonics is required but the mathematical solution is not in cause. The limitation comes from numerical implementation of the method. Study on matrix inversion should be conducted.

2.3.3.6 Extension to other round geometries

More than just upgrading round conductor 2D modeling, the A model has been designed to simulate new geometries of conductors. To prevent eddy current effects or limit them new technologies arise. E.g. bi-metal conductors, multi-layer conductor for corrosive environment, shield conductor or following proposed hollow conductors and flat edge wound coil. The A model is fully explained previously so mathematic formulas are not repeat here. However, the solution of (36) differs from solid round shape for new round technologies. Thus, the solutions in polar coordinates are expressed using classical Fourier expansion and notation from (Figure 66).

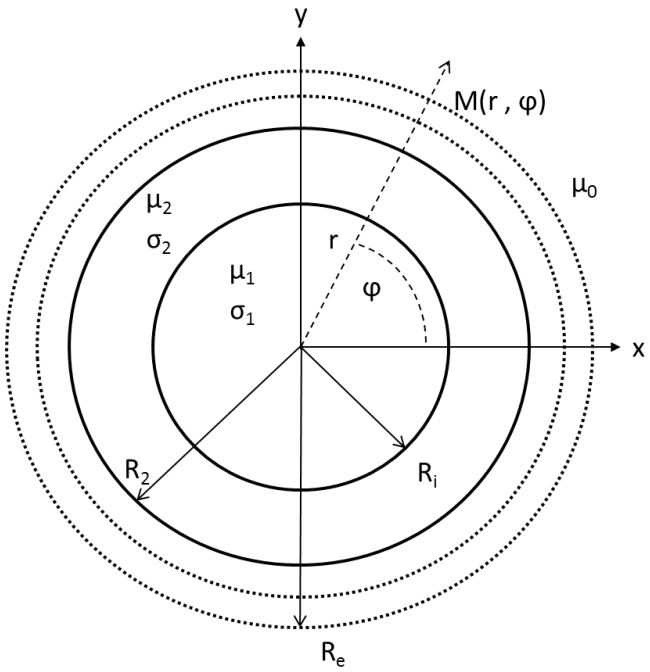

Figure 66 : Cylindrical notation for multilayer round conductor

First, the solution of Laplace equation being unchanged in the air around the conductor, the solution to write links between conductors stay exactly the same, the matrix solution (57) is still valid for harmonic coefficients solution. The only changes are the reflection and the several transmission coefficients at each surface interaction inside the conductor.

The strategy of resolution is not complicated. The different equations for the different environment inside the conductor are (41) for solid round conductive area without cavity inside, e.g. previous cases. Equation (43) for nonconductive area like air or insulation and finally (58) for conductive ring where second kind of Bessel function Y_n can exist:

$$A_z(r,\varphi) = \frac{-gradV}{i\omega} + \gamma_0 J_0(kr) + \eta_0 Y_0(kr) + \sum_{n=1}^{+\infty} J_n(kr)(\gamma_n e^{in\varphi} + \gamma_{-n} e^{-in\varphi}) + Y_n(kr)(\eta_n e^{in\varphi} + \eta_{-n} e^{-in\varphi}) \quad \textbf{58}$$

Then same approach as [2.3.3.2.3] is used to express reflection coefficient on the outer surface of the conductor and the transmission coefficients between layers of the conductor. The easiest way is to express a general transmission coefficient between external environment [a,b] and inner layer of the conductor as presented in (Appendix C) for hollow conductors and bi-metals ones.

The Ampere's law is used to solve coefficients of the 0^{th} order.

2.3.3.1 Innovations/Validation

Learning is made of repetitions, so optimization brings better coil for choke or transformer, but it does not create ways of preventing skin effect or proximity effect.

So a known proposed solution [45] is the use of bi-metal conductors. Indeed at HF, current is concentrated on external part of the conductor because of skin effect. Copper being better conductive than aluminum it is better for resistance reduction. But copper is double the price than aluminum and less flexible. So the proposition is to clad cheap aluminum for LF with copper that will support better HF.

Another proposition for high power choke ~1-3MW, is the use of hollow conductors. Skin effect depleting current from the inner part of the conductor at HF, this inner part can be removed to gain material and use it as cooling tube. This approach revealed some very interesting magnetic field distribution effects as presented next.

Finally, the last proposition is born from the consideration of current depleting layer far from the core because of proximity effect between layers. So building a conductor assuming part in every layer should prevent proximity effect. Flat conductors wound on the edge are introduced (Figure 67). It results in an equivalent 1D skin effect inside flat conductor.

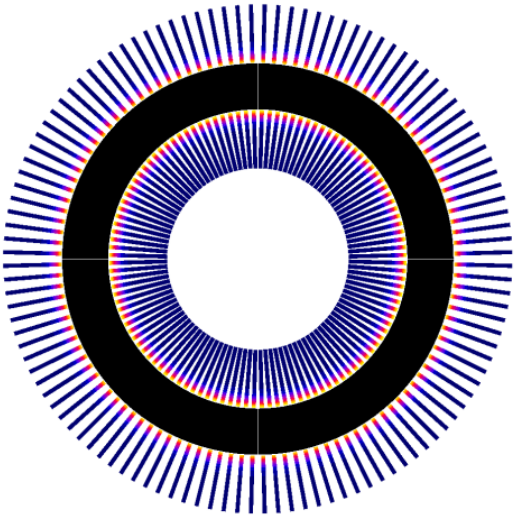

Figure 67 : Radial 2D cut view of toroid choke wound with flat conductors on the edge

All technologies are presented follow and A-model validated at the same time.

2.3.3.1.1 Stack of several conductors

A rectangular stack of 12 conductors is chosen to compare results from model with FEM simulation from Flux2D®. This stack is subject to both proximity effects of close conductors and border effects on the edge of the stack what is illustrated in (Figure 68). Conductors are large enough for skin effect to be important too. (Figure 69) presents the evolution of active power in the stack for all three geometries, from 1Hz to 500kHz. Once again some remarks can be made on the number of harmonics needed for accurate results. For solid round geometry refer to [2.3.3.4]. For Cu clad Al or hollow conductor, when the external ring is really thin, the number of harmonics is up to N=10 to 20 for less than 0.01% of difference with FEM. In tested cases, stack and following toroid coil [2.3.3.1.3], no numerical limitation has been encountered and the solution is still less than 1s even for numerous conductors. When frequency is several hundreds of kHz, the meshing for FEM simulation must be really tightened thus time computation and computer memory are putted to limits. This issue is

another advantage for A-model to be used because computation is much faster and only numerical matrix inversion could lead to error.

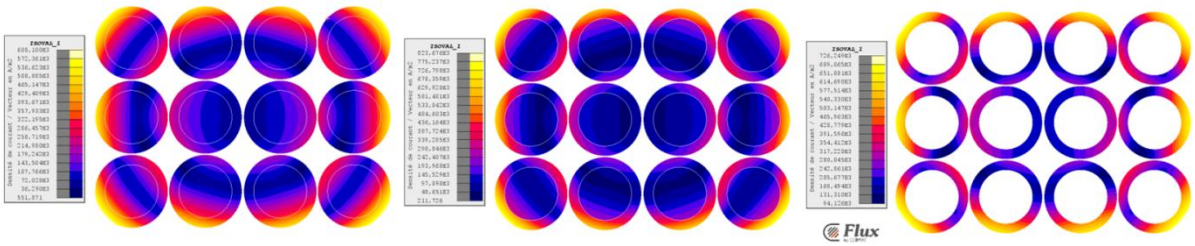

Figure 68 : Stack of 12 round conductors, left solid, middle Cu clad Al, right hollow

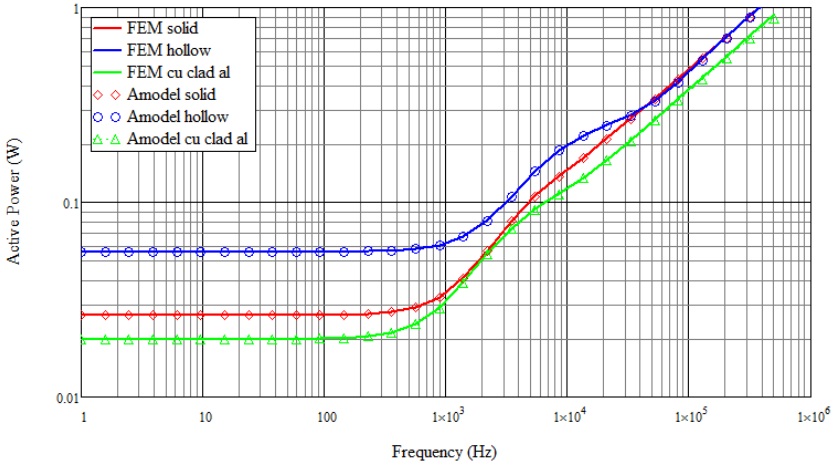

Figure 69 : Evolution of previous stacks active power vs frequency

2.3.3.1.2 Hollow wire behavior

Hollow conductors are less compact that other technologies and harder to produce. Yet, they offer direct liquid cooling solutions in the hollow. This solution is interesting when using high power transformer >1MW.

Further, their physical behavior is not conventional. (Figure 70) illustrates the current density distribution for solid round conductor and hollow conductor at 1 Hz, 5 kHz and 10 kHz. Bifilar line is studied. Same color scale is used. At 1 Hz current is slightly higher in hollow wire but not significant. At 5 kHz current is depleted from solid wire because of both skin effect and proximity effect. However, for hollow wire, the hollow acts as a trap for magnetic field and consequently linearize the current density. The same effect occurs at 10 kHz. Thus, where hollow could be seen as a lost material area, it behaves as a current density equalizer and the surface is better used than solid wire.

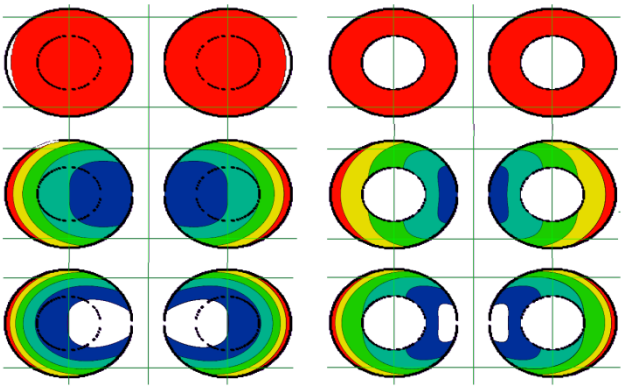

Figure 70 : Current density, left solid right hollow, @ 1Hz, 5kHz, 10kHz

2.3.3.1.3 Toroid Filter Choke Design by optimization

Extension of A-model can be used in optimized design process to find better solutions than standard solid conductor technologies.

The model will be actually used in a design process employing genetic optimization. Magnetic core section and number of turns are fixed in order to compare only winding technologies. The inputs parameters are:

- Strands Diameter Re
- Number of parallel strands per turns
- Strands inner diameter Ri
- Material Cu/Al
- Wire geometry

The outputs to be minimized are:

- Raw price of material
- Resistance of windings from 1 Hz to 500 kHz
- Overall external diameter of choke

(Figure 71) presents the Pareto of the resistance vs raw materials price on left, while right presents resistance vs external diameter. As can be remarked the hollow Al wires give better efficiency for lowest price. However, their use leads to the bulky design of the choke. Conversely, hollow Cu technology allows compact choke but with lowest efficiency. Copper clad aluminum wire offers a compromise between both other choices.

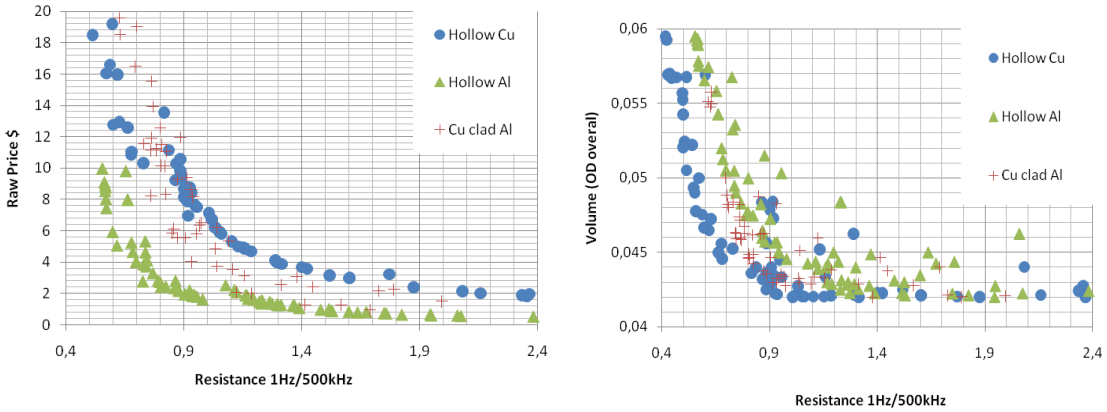

Figure 71 : Paretos for Cu clad Al and hollow coils

2.3.3.2 Air-gap

The possibility of modeling any stack of wire in any position with whatever geometry or physical and electrical properties is presented. So a lacks of Dowell that must be overcame is the implementation of air-gap effect. Consideration of air-gap acting as a conductor with equivalent current are presented in [44]. The same approach is used here. A single conductor is introduced in the place of the air-gap with the equivalent current. Note that this conductor is not allowed to have eddy currents or losses of any type.

$$I_{eq} = e_{air\_gap} \cdot \frac{B_{air\_gap}}{\mu_0} \cdot \left(1 - \frac{1}{\mu_{core}}\right) \quad 59$$

A-model result is compare with FEM and Dowell on (Figure 72). The divergence of air-gap magnetic field from equivalent conductor being shadowed by conductors' absorption, the approach proves working. Yet accuracy is not as good as for other previous cases. Two source of error could be corrected using following section, first the consideration of magnetic core [**Error! Reference source not found.**] and secondly to replace the air-gap with an equivalent rectangular conductor [**Error! Reference source not found.**] rather than a solid round one.

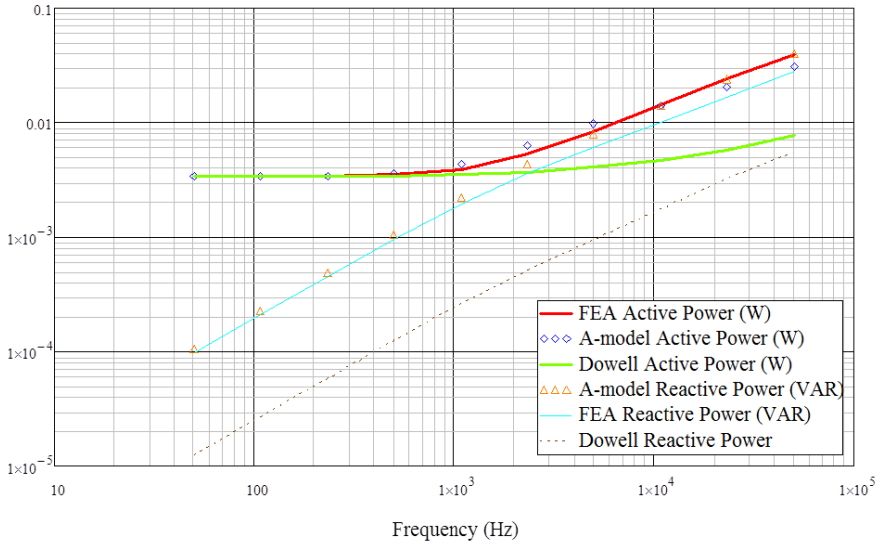

Figure 72 : Air gap simulation, A-model vs Dowell vs FEM

2.3.3.3 Conclusions

To address all possibility of coil geometry or physics a new semi-analytical method is presented. The A-model is based on the solutions of magnetic potential for Laplace and Helmholtz equations in a 2D space. Electromagnetic waves behavior is mimicked to solve harmonic coefficient of magnetic potential. The model is unrivaled at the time even by FEM in simulation time. The only calculation is the inversion of a square matrix. The matrix shows interesting properties, plus the addition of symmetries of the coil, perspectives are good to reduce drastically matrix inversion time. An investigation must be done on numerical divergence during the matrix inversion in some cases [2.3.3.4.3]. Modeling of square core and other shape are also considered.

2.3.4 Conclusions:

The chokes used by Schneider Electric deals with current up to hundreds of amperes. With the use of low loss cores like powder, nanocrystallin or amorphous, efficiency is mainly gain on coil. So their modeling is the most important one. A Dowell homogenization method is presented and applied to toroid coil. It proves accurate and fast, sufficient for optimization. However few cases like air-gap consideration or other geometries than toroid need another modeling. The A-model is introduced based on magnetic potential analytical solution. It allows the simulation of any geometry of coil or conductor for various physical properties.

The magnetic and electrical behavior of the coil is well modeled in this chapter and meets optimization and innovation requirements. But a thermal model has not been implemented yet and thermal issues are important in power converters. However, thermal considerations are quite difficult and not relevant. Indeed, the mechanical structure of the power converter

cannot be represented analytically thus the air flux is impossible to obtain correctly on the surface of the choke. Moreover, the convection coefficient is empirical so it would require a huge library to address all geometries of choke tested during optimization. But according our library approach this solution is retained for future thermal impact study on convergence.

2.4 CAPACITOR

In this PhD only filtering capacitors are used. The capacitors are employed to decrease ripples of a unidirectional voltage. In UPS they are used:

When a rectifier is used to supply the DC bus of a converter by a continuous voltage thus to limit ripples a capacitor is placed in parallel at the converter output. The low frequency of the rectified signal leads to the need for high value capacitor generally electrolytic ones.

At the input and the output of AC/DC and DC/AC converters the capacitors are placed in association with an inductance to limit voltage ripples from switches of semi-conductors. The capacitor is subject to high frequency and high density current. To guarantee its function the capacitor must have good frequency behavior with a low series resistance and inductance. Ceramic or wound plastic technologies are generally preferred. These last ones are mainly used in our optimized filter and will be investigated briefly.

The polymers present interesting properties for power electronic applications [46]. They offer high dielectric strength, low dissipation ratio and mainly excellent stability of the permittivity regarding frequency [47]. This allows considering a scalar value of capacity C on our frequency operating range. The most implemented material is the polypropylene.

In our case what is interesting is the value C of capacitor for filtering need and also the impedance of the capacitor to evaluate losses and harmonics spectrum for THD control on protected loads. The losses in capacitors have two main origins, the dielectric material and the ohm losses in metallic part of the capacitor [48]. Both cases can be modeled by a single series resistance the ESR [49]. The resulting model for our capacitor is illustrated in (Figure 73). The current and voltage in capacitor are studied in Fourier harmonic expansion as in coil modeling.

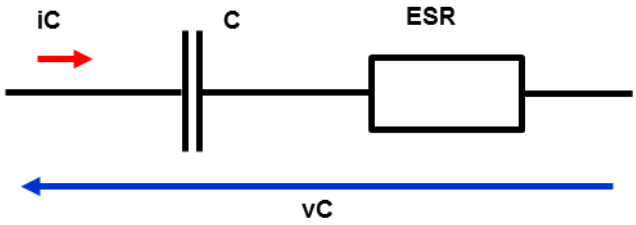

Figure 73: Series model of capacitor

The dielectric materials are characterized by their dissipation ratio tanδ which is the tangential angle of losses, the ratio between active power and reactive power. The losses in the dielectric are expressed by:

$$P_D = \tan\delta.Q = \frac{\tan\delta}{C.\omega}.I_{rms}^2 = R_D.I_{rms}^2 \quad \textbf{60}$$

Q represents the reactive power stocked in the capacity C. The dielectric losses are represented by a resistance R_D. this resistance is summed in series with the resistance of metallic part of the capacitor to form the Equivalent Series Resistances:

$$ESR = R_D + R_\Omega = \frac{\tan\delta}{C.\omega} + R_\Omega \quad \textbf{61}$$

The evolution of this ESR regarding the frequency is generally approximated by polynomials [50]. An inductive series component L could be added to simulate inductive behavior of capacitor but it occurs at frequencies higher than our operating frequency of several kHz maximum. The chosen model assumes that ESR and C value are invariant regarding voltage on capacitor verified in [49]. The resulting curve ESR(f) of the proposed model is illustrated on (Figure 74). The ESR will decrease with temperature rise (Figure 75) so with no thermal model yet implemented the losses will be a little over evaluated but are negligible compared to choke and semi-conductors ones.

The value of R_Ω and tanδ are provided by suppliers. In this PhD we decided to use Schneider Electric database of already implemented capacitor to approximate evolution of both parameters R_Ω and tanδ, price and maximum RMS current admissible in capacitor as functions of value C. so the only optimization parameter will be the value C.

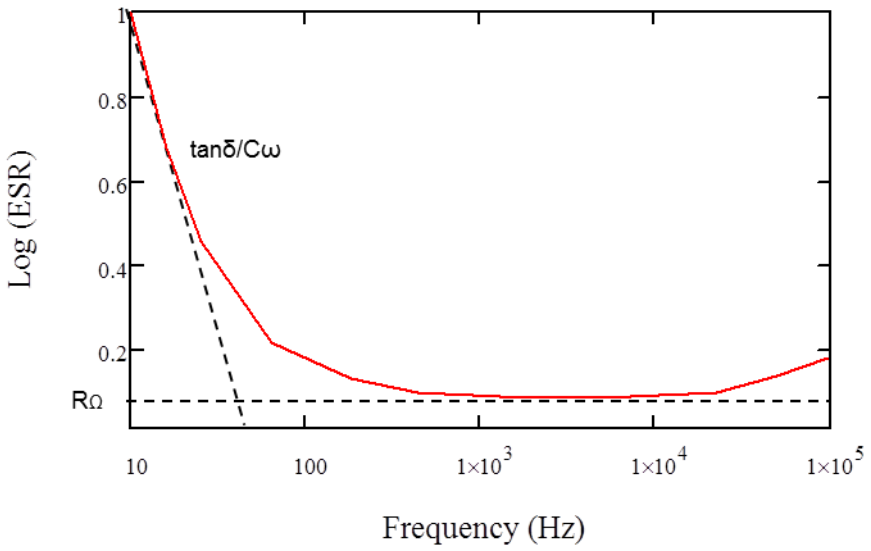

Figure 74: typical ESR(f) curve

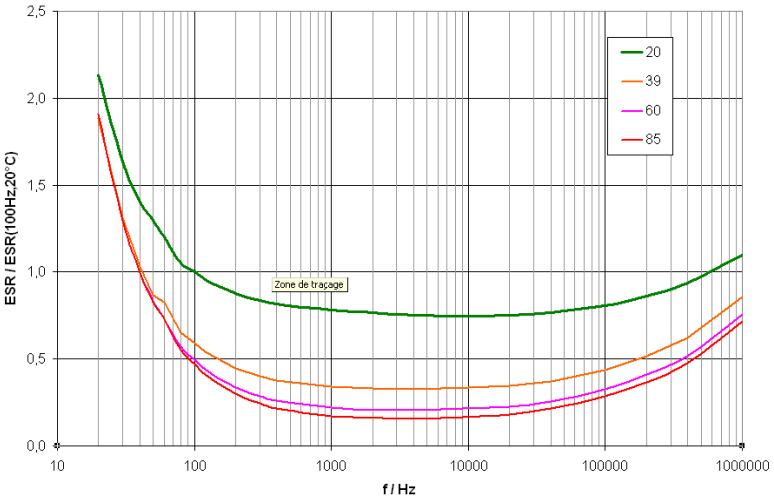

Figure 75: Evolution of ESR(f) versus temperature in polypropylene capacitor

2.5 COMPONENT DEFINITION

2.5.1 Introduction:

The design of passive components is based on efficiency and thermal study in the power converter environment. Both are computed from physical and electrical parameters but also from geometric parameters. The way designer defines the geometry of the component in an optimization process has a huge impact on convergence. In Chapter I, several ways to address constraints are presented and the best is to eliminate constraint by problem definition. So in this section we present an example that the specifications defined for purchase are not necessarily the ones used as input set of optimization.

The toroid form for chokes has been widely investigated during this PhD, so it is used as example along this section. The studied geometry is presented in (Figure 76). We can see that magnetic core is defined by inner diameter and outer one. The datasheet's constructors always provide these two parameters. Now if they are used as input parameters, OD can be smaller than ID. The core is then not realistic and computation is impossible. Depending on the algorithm and the optimization software, and the definition of constraint used to prevent this case the optimization convergence can be interrupted.

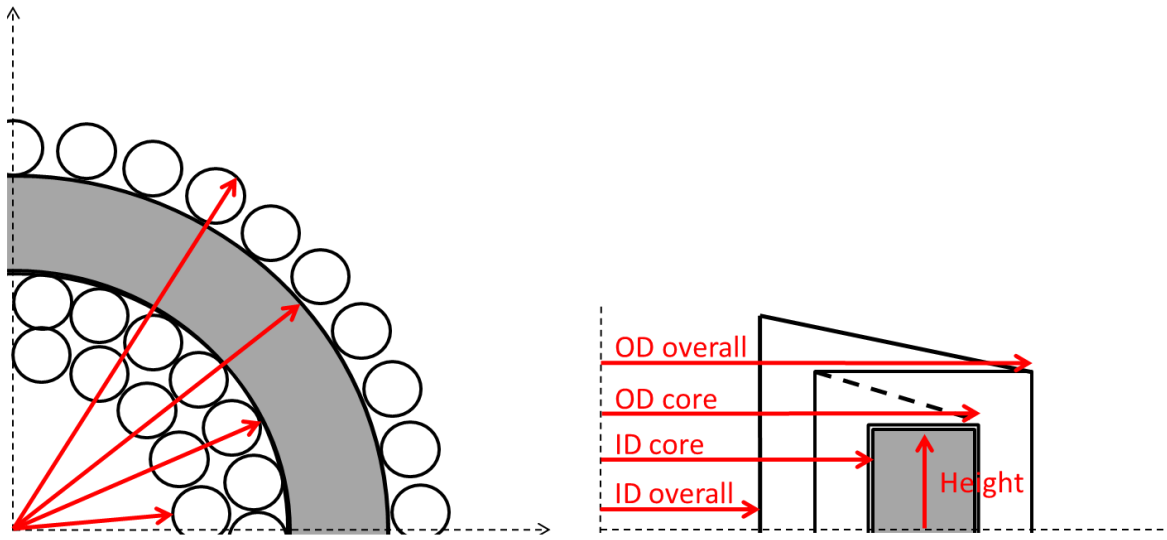

Figure 76 : Toroid geometry definition

A second drawback of this approach is highlighted when considering ID and the number of coil conductors. The number of conductors can be higher than the window available inside ID. Once again it can be solved using constraint. But this gives no information to the algorithm. When aiming to the reduction of price and volume the algorithm will always try to reduce the core and this case will always happen. By just discarding the non-feasible solution, the algorithm will try repeatedly to reduce the core size preventing convergence and losing time.

So in following sections ways to define component are proposed in order to help algorithm and guarantee good convergence of optimization.

2.5.2 Free Toroid chokes:

The geometry widely use in Schneider Electric is the toroid for magnetic and coil reasons described in [2.2.4.7]. The aim is to use a set of input parameters to define the geometry guaranteeing core and coil models are always valid. The toroid form main issue is that a diameter can be smaller than another. So the idea is to define the object from the smallest diameter to the larger one. The solution is presented based on (Figure 76) geometry. The overall ID is the first input parameter; it is convenient to use it as a parameter to set a lower limit for fabrication requirement without using a constraint. Then the number of turns, the number of parallel conductors and the wire diameter are set so resulting ID of the core is computed. The limb of the core is the adjustment parameter for the core thickness. This approach prevents the use of catalog size of core because both ID and OD are not used as input parameters but depend on others. The overall OD is also computed as a resultant of the input parameters. The second dimension, the height as no definition issue, classical HT parameter is used.

So in this case the set of geometric inputs is {ID_ov, Øconductor, Nturns, N//, Limb and HT}.

2.5.3 Datasheet Toroid chokes:

The previous geometric definition allows the best optimal geometry of toroid regarding the specifications because no constraints exist on core dimensions. However, magnetics suppliers have developed standard sizes of core available on datasheet. Custom sizes generally leads to create a new matrix and thus over cost. The following proposition is done to use standard size in a discrete optimization while keeping achievable solution. The core size ID and OD are fixed. The overall inner diameter is still an input. Thus an available space is defined between ID and ID overall, with the diameter of conductors, the number of possible wires is established. The number of wires in parallel defines the resulting number of turns. Once again the height is not a problem. Note that upper limit of ID overall must be set in order that at least one turn with the maximum of parallel conductor can be wound around the core.

The set of geometric inputs is {ID, OD, HT, $Ø_{conductor}$, N//}.

2.5.4 Two cores Toroid chokes:

A trickiest case occurs when assembling two magnetic cores together as presented in [**Error! Reference source not found.**]. The problem is still to define the object in order that for any set of inputs the model provides an existing solution. It is compulsory for good convergence. So in this case (Figure 77) for custom sizes there is no issue, the same pattern than [2.5.2] is followed. But at the present time, the larger size of OD for powder core is imposed by the manufacturers limited by their press machine. So once again to prevent the insertion of a new constraint, the effort is done on geometry definition. The application is presented below.

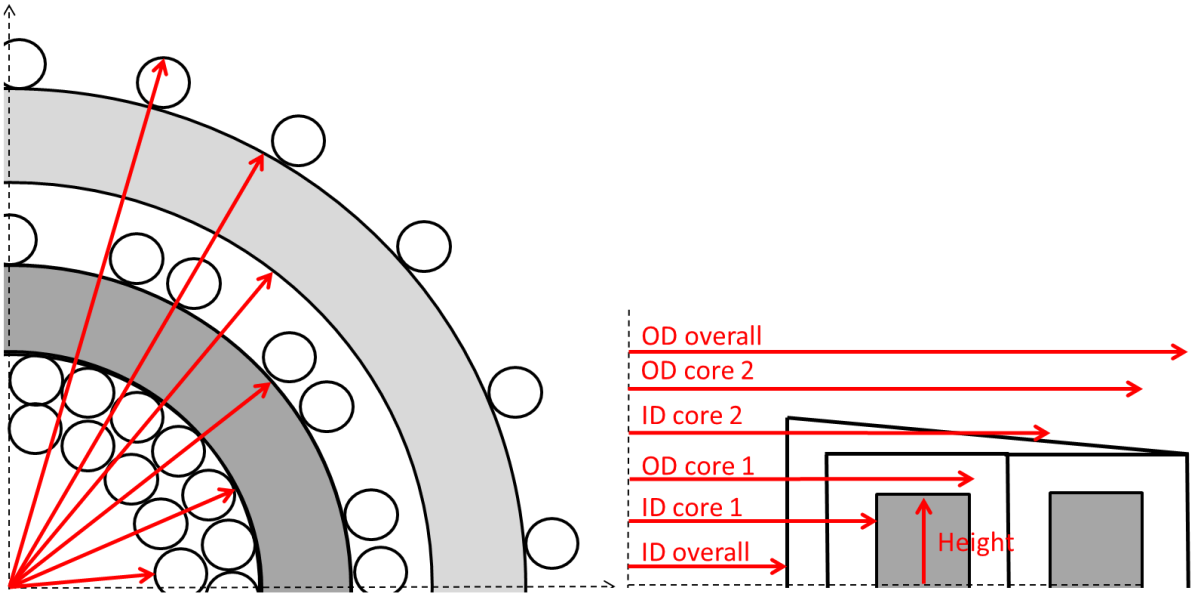

Figure 77 : Two toroid cores assembling

A parameter defines the length between ODcore2 and the IDcore1. This parameter as for limits the minimum acceptable IDcore2 and the minimum feasible ID overall. Then a weighted parameter is introduced to define the actual ID overall guaranteeing at least a turn of the maximum parallel wires of the maximum diameter inside the IDcore1. Then the number of possible turns around core1 is computed from the free available place and a second weighted parameter sets the number of turns for 1 and for 1 and 2. The third weighted parameter fixes the ODcore1.

2.5.5 Conclusions

The definition of geometrical parameters is critical for optimization convergence. In optimization process most limits can be set using constraints. However, models are generally calculated before constraints check and can lead to non-feasible cases. In these cases the convergence of the optimization is stop or lost. To prevent it solutions are proposed to use alternative input parameters for the optimization different from model inputs. Guaranteeing the good functioning of the model calculation this approach allows reducing the number of constraints and then the complexity of optimization.

This way to achieve modeling effort to define the problem reducing the optimization complexity can be spread for other definition, e.g. electrical or magnetic one.

2.6 CONCLUSIONS

In chapter 1 a strategy has been defined to realize optimization of passive components in power converters. The experience of Schneider Electric, the tender specifications and our analysis lead to the achievement of discrete optimization using libraries. More specifically grid multi-objectives algorithms are implemented to deliver Pareto tools to give Schneider teams a panel of choices.

The models presented in chapter II are built according this strategy and the requirements of grid genetic algorithms. The models must be fast because thousands of runs are used during convergence of optimization. They must be robust to guarantee same convergence for any run. And finally, the aim of this work is to achieve sizing of component and not pre-sizing. I.e. the models must be accurate enough for the solutions of optimization to be directly purchased from suppliers.

An important focus is done on magnetic materials. The model of magnetic core must deliver the losses but also the effective flux density and magnetic field to compute voltage and current on the choke considering saturation effects. A fast review is done on existing loss model principally based on Steinmetz assumptions. The LS model from G2Elab is used to build dynamic hysteresis of steel sheet [19] and nanocrystallin [32]. The idea of a behavioral model is seducing in the target of getting a unique model for all kind of magnetic materials. However, for cost and efficiency reasons the most employed material in Schneider Electric power converters is the pressed powder. Yet a dynamic hysteresis model proves inadequate for this technology because of both measurement issue and capability of model validation, i.e. thin hysteresis with huge band of magnetic field. Easier model like LossMap are proposed and simplification based on manufacturer's datasheets studied. This approach allows integrating without measurement the material inside a discrete library, gaining time and cost. It is sufficient for losses approximation and electrical simulation of the choke in the aim of optimization convergence.

The effort and cost spend on more complex and more accurate models are not justified in an optimization target. First the measures on powder core are difficult to realize and often with bad accuracy. Secondly, the variation of powder properties from supplier +/-8% and also from fabrication, e.g. size effects, prevent accurate model. Actually a model with less than a 1% error even considering good measurements, will be out of target if it has been achieved on a powder in the +8% pack and applied on a core in the -8% limit. A mean model will require several measurement campaigns on lots of cores which is not viable in industrial context.

In the second part of the chapter, coil modeling is presented. In efficiency increase aim, with low losses and low price magnetic cores, a great gain can be achieve on coils. The current being correctly simulated by the core model, the coil model must represent the coil AC resistance for a spectral analysis in the frequency band of the converter. The Dowell homogenization method is investigated and applied with correct results on toroid coil. However for other shape and considering air-gap or new wire technologies, this approach reaches its limits. Thus analytical solutions for magneto-harmonic study of the magnetic

potential are introduced. The validation is done for several geometries and successfully use in optimization context. Yet the resolutions of harmonic parameters for the analytical solution being numerically done, numerical issue are highlighted and should be overcome by investigation on matrix inversion methods.

Finally definition of problem especially for geometry of components is discussed. The issues of cases when model is not computable are presented. Solutions are proposed as example to prove the meaning of putting effort on problem definition to simplify optimization problem and guarantee convergence of the method.

Optimization methods and models of components being discussed in chapter one and two, the chapter three presents the modeling of the converter electrical environment considerations on passive component.

2.7 REFERENCES

[18] G.Bertotti, "General properties of power losses in soft ferromagnetic materials," IEEE Transactions on Magnetics, vol. 24, no. 1, pp. 621-630, 1988.

[19] T.Chevalier, A.Kedous-Lebouc, B.Cornut, C.Cester: "A new dynamic hysteresis model for electrical steel sheet"; Physica B: Condensed Matter 2000, vol. 275, No 1 – 3, pp. 4171 -4184

[20] J. Li, T. Abdallah, C.R.Sullivan: Improved calculation of core loss with nonsinusoidal waveforms", Conf. Record IEEE IAS Conf 36th IAS Annual Meet. 2001, pp. 2203 - 2210

[21] J.Muhlethaler, J.Biela, J.W.Kolar, A.Ecklebe, "Improved core loss calculation for magnetic components employed in power electronic systems," IEEE Transactions on Power Electronics, vol. 27, no. 2, 2012.

[22] J.Reinert, A.Brockmeyer and R.D.Doncker, "Calculation of losses in ferro- and ferromagnetic materials based on the modified Steinmetz equation," IEEE Transactions on Industry Applications, vol. 37, no. 4, pp. 1055-1061, July / August 2001.

[23] Ch. (Carl) Steinmetz : "Law of hysteresis"; Electrical Engineer magazine of American Institute of Electrical Engineering, 1892

[24] K. Venkatachalam, C. Sullivan, T. Abdallah, and H. Tacca, "Accurate prediction of ferrite core loss with nonsinusoidal waveforms using only Steinmetz parameters, " 8th IEEE Workshop on Computers in Power Electronics, COMPEL pp. 36-41, 2002.

[25] G. Bertotti, « Physical interpretation of eddy current losses in ferromagnetic materials. I Theoretical consideration », J. Appl. Phys. Vol. 57, N° 6, pp. 2210-2217, 1985.

[26] W.J. Carr, « Magnetic domain wall bowing in a perfect metallic crystal », Journal of Applied Physics, 47, 9, pp 4176-4181, 1976.

[27] H.J. Williams, W. Shockley, C. Kittel, « Studies of the Propagation Velocity of a erromagnetic Domain Boundary », Phys. Rev. 80(6), pp 1090, 1950.

[28] J.Reinert, A.Brockmeyer, R.W.DeDoncker,"Calculation of losses in ferro- and ferromagnetic materials based on the modified steinmetz equation", IEEE Trans. Ind. Appl., vol. 37, no. 4, pp. 1055–1061, Jul./Aug. 2001.

[29] Jieli Li, T. Abdallah, and C. R. Sullivan, "Improved calculation of core loss with nonsinusoidal waveforms", in Conference Record of the 2001 IEEE Industry Applications Conference. 36th IAS Annual Meeting, 2001, pp. 2203–2210.

[30] K. Venkatachalam, C. R. Sullivan, T. Abdallah, and H. Tacca , "Accurate prediction of ferrite core loss with nonsinusoidal waveforms using only Steinmetz parameters", in Proc. of IEEE Workshop on Computers in Power Electronics, pages 36–41, 2002.

[31] J.Muhlethaler, J. Biela, J.W. Kolar, A. Ecklebe, Improved core loss calculation for magnetic components employed in power electronic systems, IEEE,2012

[32] H.Chazal, "Caractérisations physicochimique et magnétique de rubans nanocristallins à haute perméabilité et étude de leur intégration en électronique de puissance", PhD dissertation UJF, defended on 16/12/2004 in Grenoble France.

[33] P.I.Koltermann_L.A.Righi_A Modified Jiles Method for Hysteresis computation Including Minor Loops

[34] G. Bertotti, V. Basso., Journal of Applied Physics, 73 (10), pp. 5827-5829, 1993.

[35] D.Hou, M. Mu, F.C.Lee, Q. Li, "New core loss measurement method with partial cancellation concept",pp 746-751, APEC 2014

[36] X. Nan and C.R.Sullivan, "An equivalent complexe permeability model for litz-wire winding", IEEE Industry Applications Society Annual Meeting, pp. 2229-2235, October 2005.

[37] T. Delaforge, H. Chazal and R Pasterzyk, "Optimization of windings in PFC boosts and PWM inverters to maximize converter efficiency", APEC 2014, FortWorth, USA.

[38] P. L. Dowell, "Effects of eddy currents in transformer windings," Proceedings IEE, vol.133, n°8, pp 1387-1394, August 1966.

[39] J.Schutz, "Methodologie de conception d'une alimentation a découpage", thèse INPG, 1992, France

[40] G.Lefevre, "Conception de convertisseurs statiques pour l'utilisation de la pile a combustible", PhD dissertation INPG, defended on 2004, France

[41] C. W. Trowbridge, K. J. Binns, P. J. Lawrenson, "The Analytical and Numerical Solution of Electric and Magnetic Fields", Edition Wiley, 1992

[42] A.E. Heins and S. Silver, "The edge conditions and filed representations theorems in the theory of electromagnetic diffraction", Proc. Cambridge Phil. Soc., t. 51, p.149, 1955

[43] N. Ida, JPA. Bastos, "Electromagnetics and calculation of fields", Edition Springer, 1997

[44] C.Larouci, "Conception et optimization de convertisseurs statiques pour l'électronique de puissance. Application aux structures à absorption sinusoïdale", PhD dissertation INPG, defended on 13/05/2003, Grenoble France

[45] C. Kamidaki and N. Guan, "Theoretical Analysis of AC Resistance of Coil Made by Copper Clad Aluminum Wires", PIERS Proceeding, Stockholm, 2013.
[46] B.P. Kang, " Temperature coefficient and capacitance retrace of polypropylene films capacitors". IEEE Transactions on Electrical Insulation, Vo1.EI-9, N°l, p.5-11, 1974.
[47] W. White and L.Galperin, "Material considerations for high frequency, high power capacitors". IEEE Transactions on Electrical Insulation, Vol.EI-20, No.1, p.66-69, Feb.1985.
[48] R. Price, " An analysis of the ESR of metal film condensers". Elettronica Oggi, No.lO, p.91-100, Oct. 1981.
[49] B. Seguin, "Les pertes dans les condensateurs bobines utilizes en electronique de puissance: mesure calorimetrique et modelisation", PhD dissertation of INPG, defended on 16 may 1997 in Grenoble, France.
[50] R.E. Lafferty, "Capacitor loss at radio frequencies". IEEE Transactions on Components, Hybrids, and Manufacturing Technology, Vo1.CHMT-15, No.4, 590-3, August 1992.
[51] A.Besri, "Analytical modeling and tools for optimization of high frequency planar transformers ", PhD dissertation of INPG, defended on 26 may 2011 in Grenoble, France.

3 CHAPTER III - FILTER MODEL

3.1 INTRODUCTION

The aim of the PhD is to size components in a fixed power structure but also the converter electrical parameters, e.g. switch frequency or DC bridge voltage. To achieve an optimal sizing of all the converter components and parameters, the converter environment must be described addressing all the requirements from optimization algorithms presented in chapter one as it has been done for passive component definition in chapter two.

I.e. the converter topology is fixed. Although it is an extraordinary and rich subject, the definition of a power structure to reach the optimal topology is not part of this work. The optimal topology will be selected after optimization on all proposed structures. This being done, the converter definition is easier because electrical behavior is known for the different working cases. The simulation of the topology, particularly the passive component solicitations cannot be done using classical software, e.g. PSIM, PSPICE SABER, SIMPLIS or Portunus, because these platforms are based on time simulation convergence and need the establishment of a steady state through an initial state simulation of the converter. Meaning this approach requires lots of calculation and time. The general idea introduced in previous G2Elab works [52] is to simulate analytically the converter electrical behavior using waveforms between component or part of the converter as inputs and outputs of black box component models. For a fixed topology and assuming criteria on good regulation of the power converter, LF electrical waveforms are generally the same. The global approach is presented in first section of the chapter then description of the converter environment is explained for DC/AC, AC/DC and DC/DC power filter in different sections. With emerging technologies, new components are implemented in Schneider Electric power converters thus extensions of previous modeling are introduced for coupled filter solutions.

Results for several power converters optimizations are presented in chapter four as a global validation of the models and methods presented along the PhD.

3.2 MODELS CONNECTION USING CONVERTER WAVEFORMS

3.2.1 Introduction:

The sizing of power converter in our research is achieved for fixed topologies. I.e. the steady states waveforms for the converter several functioning modes are defined. With some considerations; only the values of components and regulation will change their magnitudes. **A strong assumption done in this work is that regulation is addressed by constraints over filter behavior**. Thus the modeling of waveforms is considered valid otherwise the constraints are not respected and then the modeling and optimization null and void.

3.2.2 Separation of models:

The main advantage of considering good control of the converter thus the respect of topology electrical waveforms is the separation of the models of the converter parts. Indeed the waveforms are impacted by both topology and components. We assume all components being perfectly sized for the converter operational constraints; which is the goal of optimal sizing otherwise the solutions will be discarded. Then whatever the model of one part of the converter for losses price or other value, the waveforms at its terminals can be considered unchanged or impacted by only general parameters L, C or alike. E.g. the inverter and load being unchanged, the output voltage of the inverter and the voltage and current on the load are the same so the output filter between them can be optimized without considering switching cells.

The components are then considered as black boxes with inputs and outputs fixed. The model used for each component can be changed without changing the whole converter modeling. Regarding the objective of the optimization the level of complication inserted in the model can be update. I.e. for a fast survey of the converter behavior in optimization process the model can be set basic. Another advantage is that optimization can be done on only one component, useful when replacing an existing solution inside an already build UPS.

The last advantage of this approach is that the models of component are taking waveforms as inputs and outputs. They can be inserted in any converter topology (Figure 78) and (Figure 79), the model is exactly the same in both converter and in any part of the converter. They have been designed for this modularity and will make it possible to insert them in a new converter solution.

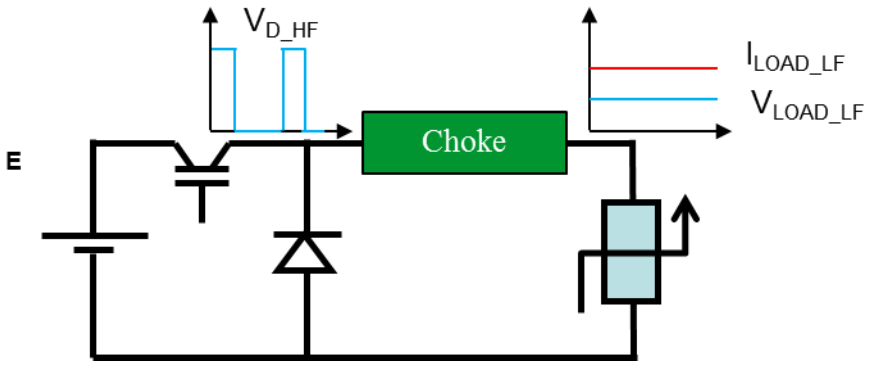

Figure 78: Buck converter with choke black box model

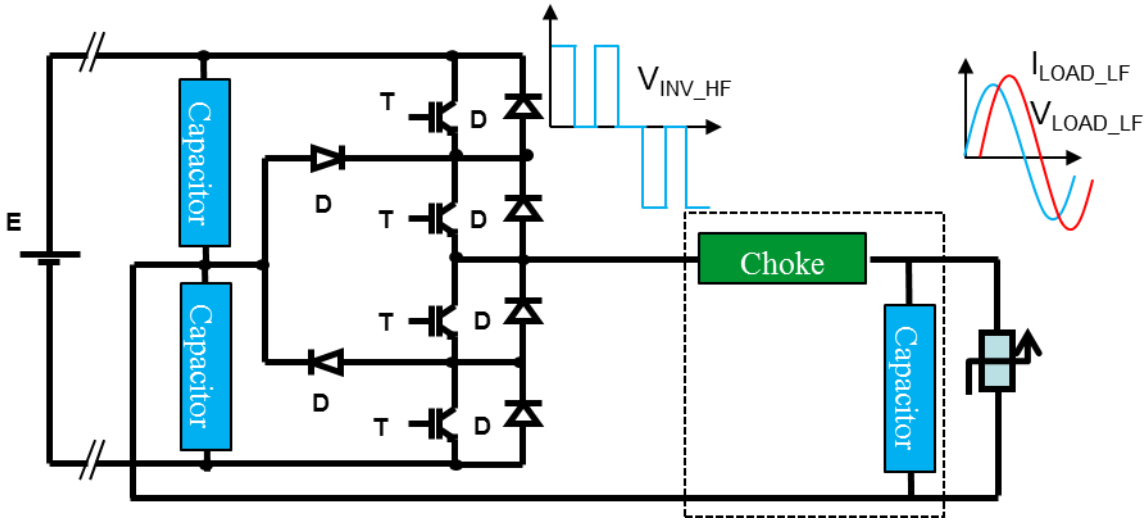

Figure 79: 3level NPC inverter with black box choke and capacitor

3.2.3 Events sampling:

Most of simulation software and control structure are time based. Meaning the signal is sampled in time discretization. A general approach applied in our work is to replace time sampling by event sampling. Indeed in power converters, all phenomena are linked to the fact that current is cut to sweep from alternative to continue and reversely. Maximum magnitudes of electrical and magnetic waveforms are reached at each switch of commutation cells. A time discretization must be done using a thin step sampling to guarantee a sample at peak value of waveform. Yet, when the topology of the converter is known and the switching frequency and its modulation also, all events switch can be deduced (Figure 80). Computing only these points inside the converter simulation is a huge gain in signal sample and so calculation. It insures the computation of peak values for all waveforms. The evolution between peak values can be nonlinear, but it will have no consequences on our modeling and optimization. For choke or capacitor, the nonlinear evolution of current and voltage between two switches will impact the dynamic losses. Yet no dynamic hysteresis model has been chosen for optimization only models based on peak value and equivalent time evolution which fit this approach. For coil losses using Fourier spectral analysis of the current, once again the impact

of curved current forms between two peaks is negligible. The same for voltage slight evolution. The difference will be reduced to nothing as the switching frequency will increase.

Note that this approach is not effective for converters where switches are imposed by waveforms (diode and Zero V/I switching).

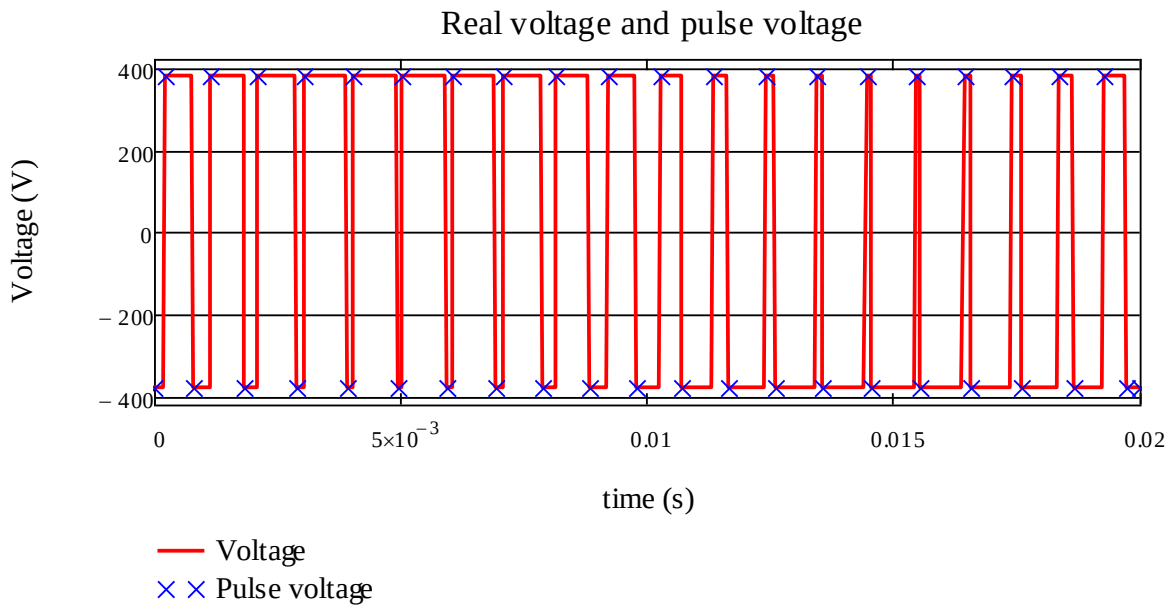

Figure 80: Real waveform vs event sampled one

3.2.4 Conclusions:

The approach to describe converter using waveform between models of component makes the description of converter modular and flexible. It allows integrating passive component modeling presented in chapter two in any topology as well as future semi-conductors models. Moreover the optimization of a single component is then possible for upgrading already existing solution without impacting the rest of the converter.

An event sampling is proposed to gain memory, time and accuracy on signal processing.

3.3 DC/AC CONVERTERS

3.3.1 Introduction:

The DC/AC inverter is used at the output of the UPS to adapt DC power from battery storage to the AC load. It the most constrained converter of the UPS because it is subject to many working case and must guarantee good quality of power for the load. The gain achieved using optimal sizing is generally greater for inverters.

In DC/AC and AC/DC converter, low frequency modulation 50Hz~60Hz is added to high frequency switching. Yet in [53] it is demonstrated that if the ratio between LF and HF is higher than 10, the consideration of LF and HF effects can be separated. It has been experimentally validated in [54]. These assumptions verified for filter in our work are useful for considering HF from inverter and LF from load.

The modeling of output filter for inverter is presented addressing connection between model using waveforms and event sampling introduced previously. All working cases are explained and considered for optimization constraints. Filter behavior, goals and norms are highlighted. Then validations are performed on actual inverters in Schneider Electric UPS.

3.3.2 Inverter output/ Filter input:

To simulate the output filter of an inverter the waveforms are used. Whatever the topology to connect the DC bus to the filter, the output voltage of the converter will be the same. The steady state is established, the control working without closed loop of current. The DC bus is at is full capacity (batteries charged); the power is only delivered to the load.

Multi-level and multi-legs topologies are used in Schneider Electric converters. The number of voltage level of the inverter refers to the number of voltage potentials imposed to the output filter (Figure 81). The switching frequency is defined as the inverse of the period of the commuted voltage between the switch cell and the filter and not as the instantaneous or mean frequency of semi-conductor switch. Indeed the increase of voltage levels distribute the charge of switching on the several switch cells and do not multiply the switch frequency. This is the principal difference between topologies of inverter. It validates the approach of waveforms because the DC bus and the voltage linked to the common point (the choke) stay the same. The multi-leg refers to the number of identical inverter switch topology connected in parallel to support the power distribution. The current in each leg must be controlled and balanced but is easily achieved. The legs can be interleaved, meaning the modulation is delayed between legs to create an equivalent higher frequency at the output of the filter. The filter can be on each leg however it is better to mutualize it between all legs to benefits of the equivalent higher frequency then reduction of the required filtering need. The interleaving also reduces drastically the current ripple inside the capacitor both filter and DC bus.

The most common control to modulate the HF voltage switches is the PWM. It produces an equivalent sinus signal of the modulation LF frequency with several component of HF.

(Figure 81) illustrates output voltage of inverter for 2, 3 and 4 levels. The switching frequency is intently low to see the waveforms.

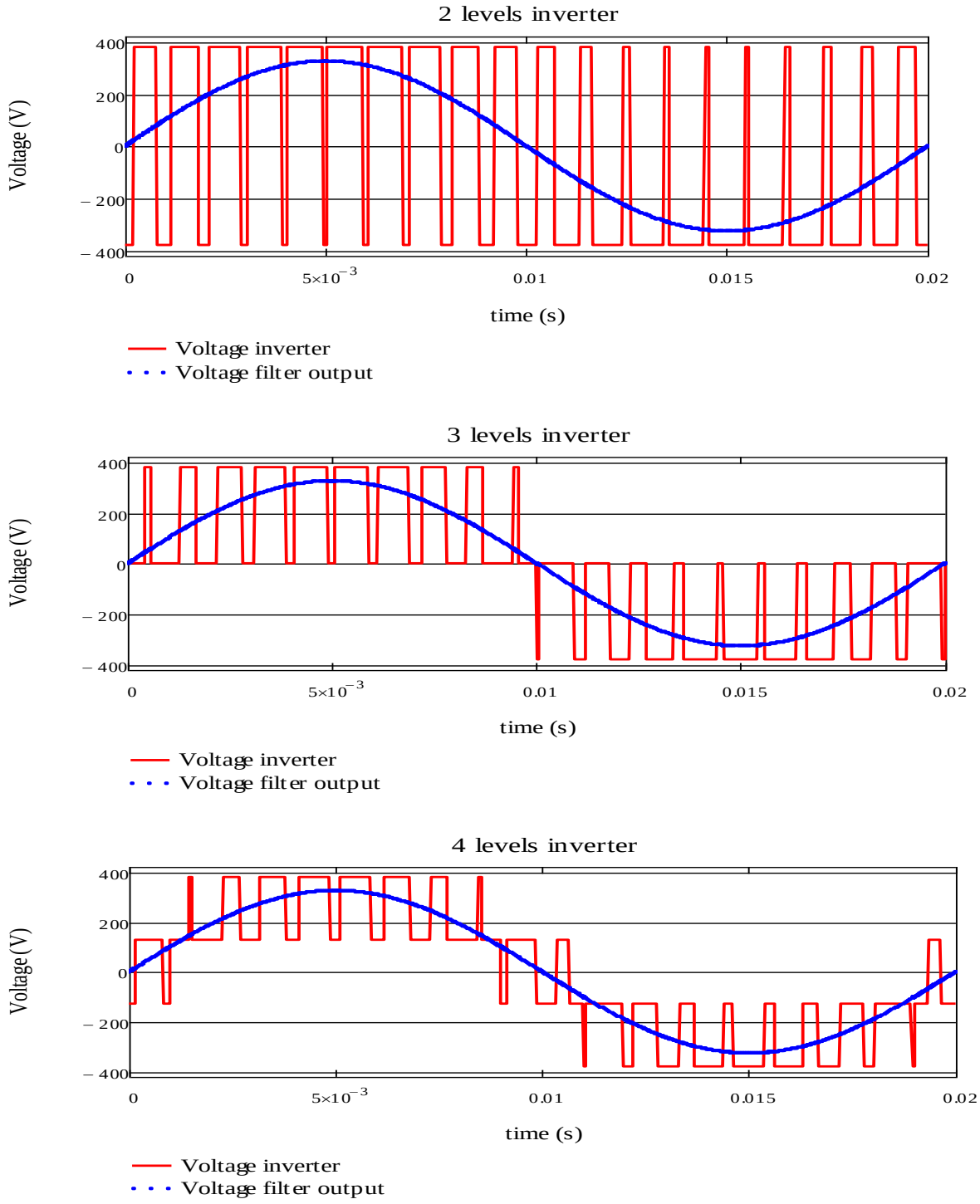

Figure 81: Inverter output multi-level voltage and desired load voltage

The surface of square voltage impulse gives an idea of the voltage spectrum. The increase of voltage level reduces the need of filtering as presented in general introduction.

The output voltage of the inverter can be simulated generically whatever the number of voltage level. The system tries to follow the reference sinus voltage required at the output of

the filter (400V phase to phase or 480V in USA, 50Hz or 60Hz USA). The evolution of each switching cell is controlled by a variable duty cycle defined by the intersection between the reference and triangular carriers at the HF switching frequency. In [55] a single duty cycle is proposed, built from a fictive reference. The duty cycle is defined as the mean value on the switching period of the commuted voltage. With no control error this voltage is equal to the RMS value of output voltage. The filter modifies the magnitude and the phase of the ratio in order to keep the output voltage equal to the reference. Yet here the proposition is to suppose a perfect command not impacted by the filter to prevent loops of calculation and so loss of time. The resulting ratio is illustrated for several levels on (Figure 82) with the equation (62):

$$\alpha(t) = \frac{Nlevels - 1}{2} . \frac{Vout_{eff} . \sqrt{2}}{V_{DC} / 2} . \sin(\omega . t) + A \qquad \textbf{62}$$

With Nlevels the number of voltage levels, $V_{out,eff}$ the RMS value of output phase voltage and V_{DC} the DC bus voltage. The constant A is used to set the initial value of ratio 0.5 for even levels and 0 for odd ones. Note that the definition of the ratio does not refer to any topology, only converter standard values. Each level will have the potential:

$$Ve = \frac{V_{DC}}{2.Nlevels - 2} \qquad \textbf{63}$$

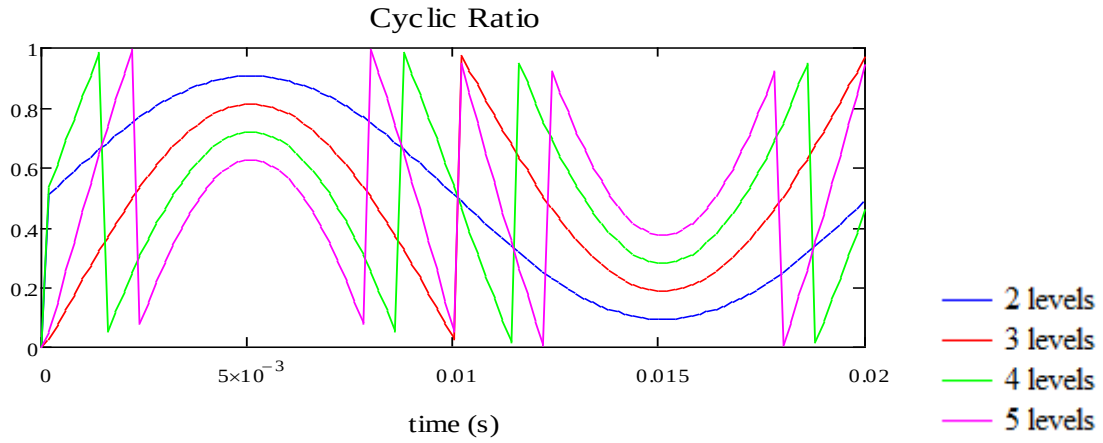

Figure 82: Time evolution of equivalent cyclic ratio for several voltage levels

Although the command will change with load and filter impact, e.g. nonlinear load, the control will be assumed equivalent as for RL load. The idea is to keep a correct approximation of the inverter output. Only when threshold of current is reached the command will drastically change to limit RMS current to the threshold value. E.g. for overload or short-circuit. In this case the duty cycle is fixed to a defined value as for DC/DC converter. This value is set to guarantee the required output voltage. A real short-circuit is not frequent, generally it is equivalent to deliver a small DC voltage for a resistance. For even level converters only the middle voltage is used to deliver the potential (Figure 83) and for odd level converters the first level is used (Figure 84). Note that for even levels the ratio is close

to 0.5 and thus the maximum ripples possible, so short-circuit and current limitation modes will be particularly disadvantageous.

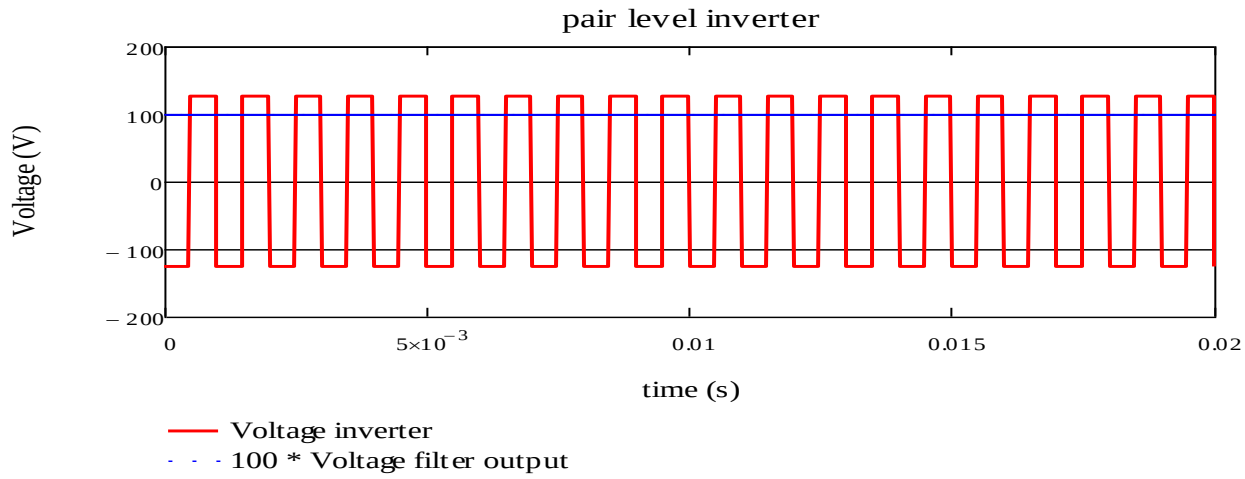

Figure 83: even inverter short circuit mode

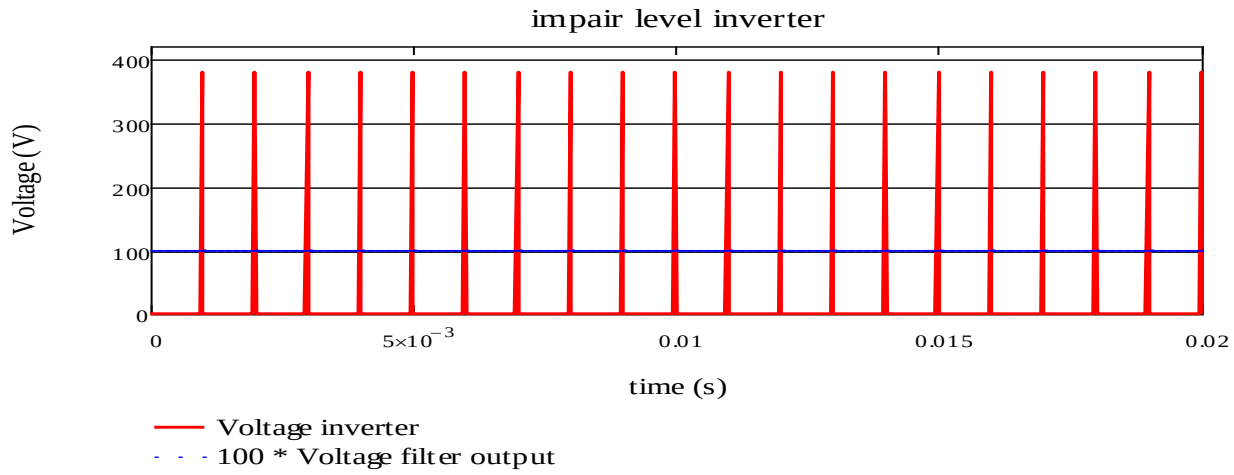

Figure 84: odd inverter short circuit mode

3.3.3 Load waveforms:

The other input for the filter is the load connected after the filter for which the filter is designed to deliver perturbation and harmonic free waveforms. Several cases are presented.

3.3.3.1 The RL load

The RL load is the most classical load for which the UPS will be used. The current and the voltage delivered to the load are sinus and with a THDU up to 3% maximum. The phase shift between voltage and current is imposed by the inductive part of the load (Figure 85).

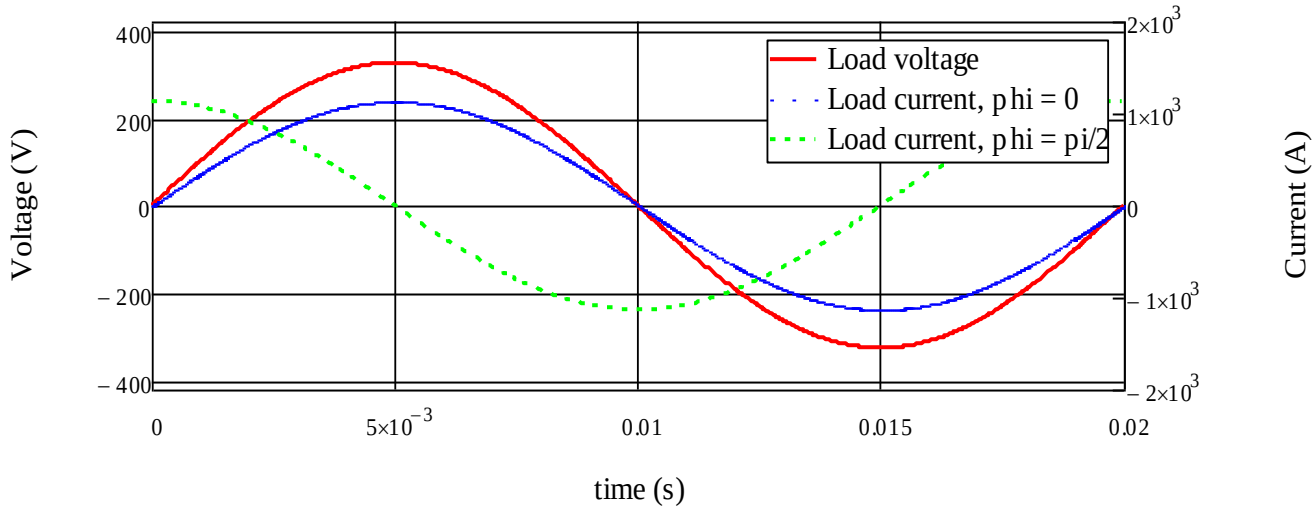

Figure 85: RL load waveforms

3.3.3.2 The nonlinear load

UPS are widely installed in datacenters and so work on RCD load. Meaning the inverter delivers power on Diode Bridge (Figure 86). The current is established only when the inverter filter output voltage V is higher than the capacitor DC voltage U. so in a short time the same RMS value of current than a RL load must be delivered. It leads to non-sinus voltage and current at the output of the filter (Figure 87).

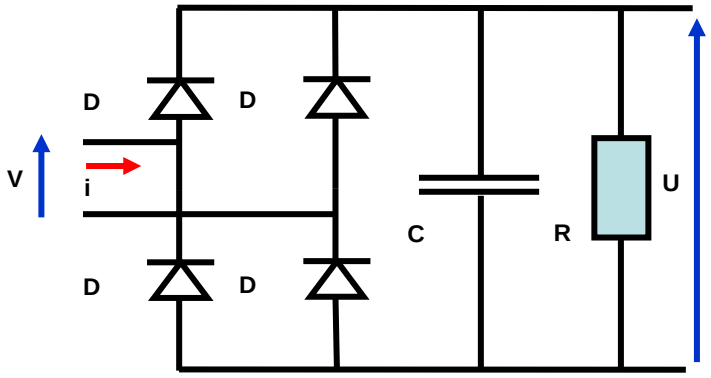

Figure 86: RCD load, Graëtz bridge

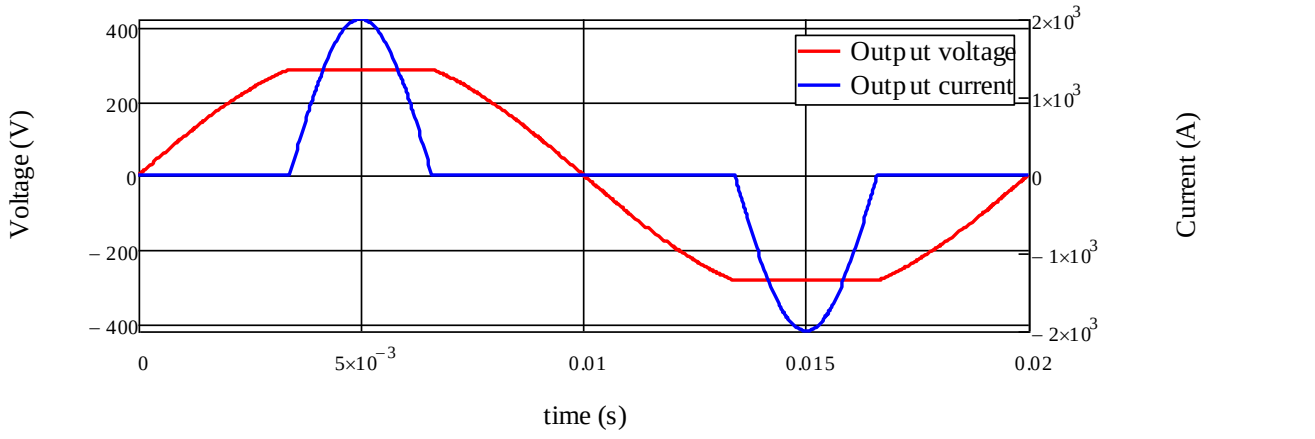

Figure 87: RCD simulated voltage V and current i from (Figure 86)

We speak here of non-sinus waveforms so it is important to remind the definition of the RMS value of a harmonic signal:

$$Y_{eff} = \sqrt{\sum_{n=1}^{\infty} Y_n^2} \quad \textbf{64}$$

The total harmonic distortion of a signal is given by CEI dictionary definition:

$$THD\% = 100.\frac{\sqrt{\sum_{n=2}^{\infty} Y_n^2}}{\sqrt{\sum_{n=1}^{\infty} Y_n^2}} \quad \textbf{65}$$

The global distortion of a signal (CIGREE definition):

$$D\% = 100.\frac{\sqrt{\sum_{n=2}^{\infty} Y_n^2}}{Y_1} \quad \textbf{66}$$

3.3.3.3 Current limitation

The UPS must deliver power to the load even in particular cases. One really impacting the sizing of the inverter filter is the limitation of current. For a UPS two current thresholds are generally defined. When the load absorbs too much current and it reaches the first threshold, the control modifies the duty cycle to regulate the current around the threshold value. The voltage cannot be control to a perfect sinus anymore and drops (Figure 88). It results in a high DC current with around 0.5 duty cycle and thus large HF current ripple. This case is studied because it is for odd level inverter where short-circuit is not difficult to control, the worst case for filter sizing.

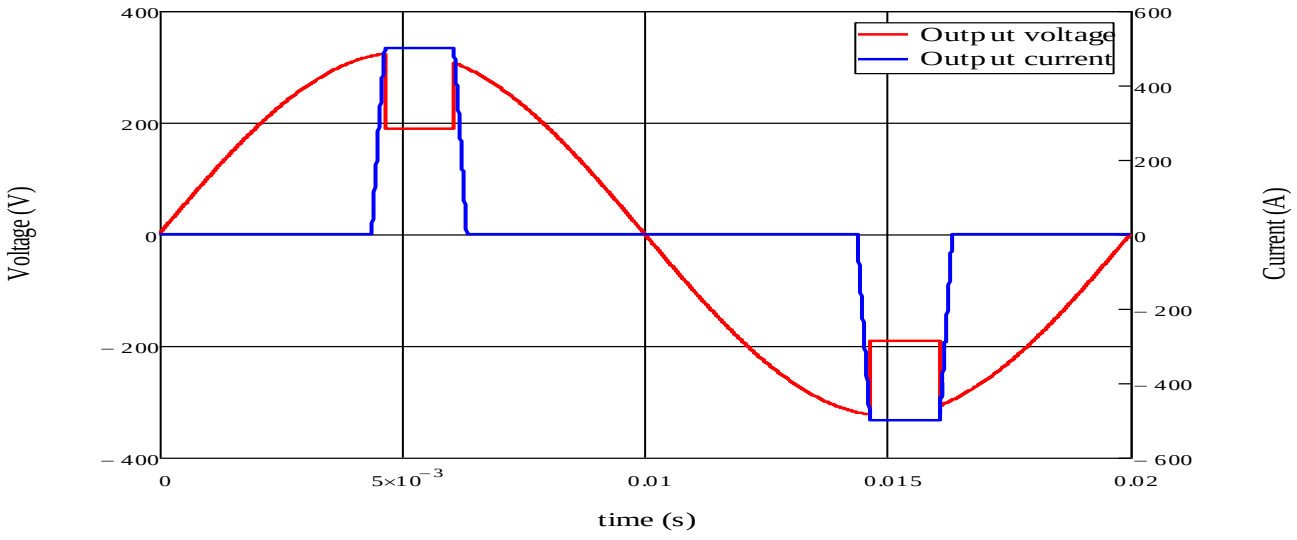

Figure 88 : Current limitation case

3.3.3.4 Short-circuit

The short circuit case has been defined previously. The current is limited to a defined threshold for which the UPS is design to work for only few minutes before shutting down. For odd level inverters the voltage delivered is low in harmonic content so HF ripple is ridiculous and do not impact the filter. However regarding the semi-conductors, classical control leads to work with the maximum current on the same switch cells during the short-circuit and can lead to huge temperature rise for the IGBTs. Alternative controls are proposed but are not part of this work. For even levels inverter the short-circuit mode will be the worst case for filter sizing.

3.3.4 Filter model:

The waveforms for DC/AC converters as inputs of the filter have been introduced. Thus in this section the models for the filter choke and capacitor is presented addressing component models from chapter two. The presentation is done for interleaved legs and groups, coupled topologies are introduced in [3.6]. The classical RC filter used at the output of the inverter is presented on (Figure 89). The choke and capacitor are of course made of one or more components in series or parallels.

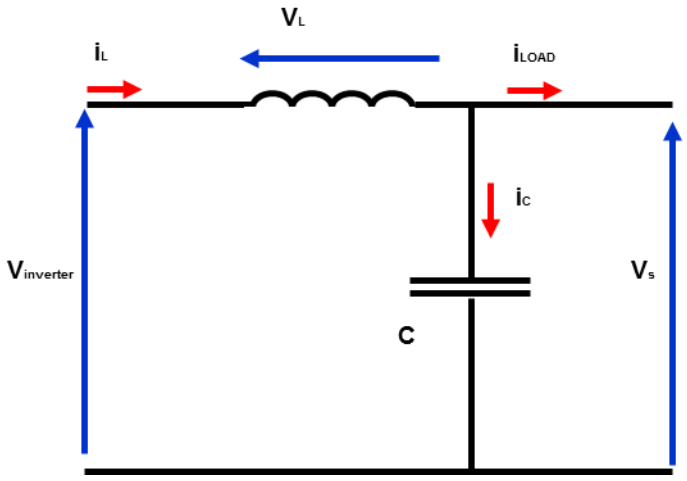

Figure 89 : Inverter output filter

3.3.4.1 Choke modeling

The filter is sized to deliver harmonic and perturbation free V_S and I_{LOAD}. So we assume that control will impose the LF current flowing through the inductance as:

$$I_L = I_{LOAD} + I_C = I_{RMS}.\sqrt{2}.\sin(\omega.t) + \frac{V_s.\sqrt{2}}{Z_C}.\sin(\omega.t + \frac{\pi}{2}) \quad (67)$$

We consider that this LF current is equivalent to the LF polarization magnetic field inside the core. The anhysteretic curve of the material gives then the LF flux density inside the core, which is close to reality (Chapter II):

$$H_{LF} = \frac{Nturns.I_L}{lm} \qquad \text{and} \qquad B_{LF} = B_{anhysteretic}(H_{LF})$$

On the other side of the filter, the assumption is done that inverter PWM control is achieved to deliver sinus V_S. The voltage drop caused by the saturation of choke is prevented by an optimization constraint. The resulting inverter output voltage is giving the HF voltage. The integration of V_L leads to the HF flux density ripple.

$$B_{HF} = \int \frac{V_L.\Delta t}{Nturns.Sec}$$

As presented in Chapter two and [3.2.3] the values are computed only for switch event and considered linear between two events. This is quite true for HF induction because only the sinus part of V_S brings non-linearity but it is negligible for a pulse time, even more for high frequency. The total induction in the magnetic core is finally the addition of both LF and HF contribution. The magnetic field is deduced from the anhysteretic curve. Indeed the HF flux density ripple creates magnetic field ripple occurring at the different levels of polarization. This total magnetic field even computed only at pulse events represents the saturation of the material and thus the real current in the choke. Only bending between pulses is not addressed but has no meaning in electrical simulation or chosen model for losses computation.

The flux density is used to compute losses from chosen model of Chapter two. The magnetic field gives the current i_L from which losses are computed in the coil and will serve as input for the capacitor model but also for current constraints on the converter. The magnetic field relying on the radius of the core, the maximum value is computed for the inner radius of the core to check on material saturation.

Prices are computed from material weight and price/kg given by suppliers. Electrical, magnetic and geometric values are found for the chokes. (Figure 91) summarized the process. In this process the interleaving of legs is addressed. Indeed the multi-leg topology can creates unbalanced currents on the several legs and must be checked. This unbalance can also come from choke core that supplier furnish with +/-8% of magnetic characteristics. For the first case the computation is easy, the I_{LOAD} is divided between legs using a weighting corresponding to the desired unbalancing that must be checked. In the second case when it comes from unequal inductance value the impedance of chokes are used. For this a convergence loop is used (Figure 90).

Finally the last value that is computed from choke simulation is the voltage drop. Indeed, a high value of inductance L reduces the current ripple but it also increase the equivalent impedance of the choke and thus the voltage drop occurring at its terminals. This drop must be limited in order to the DC bus voltage being sufficient to deliver V_S. The choke voltage drop is:

$$V_{drop}(t) = Z_{choke}.I_L(t) = I_L(t).\sqrt{R_{DC}^2 + (\omega.L_{choke}(t))^2} \qquad \textbf{68}$$

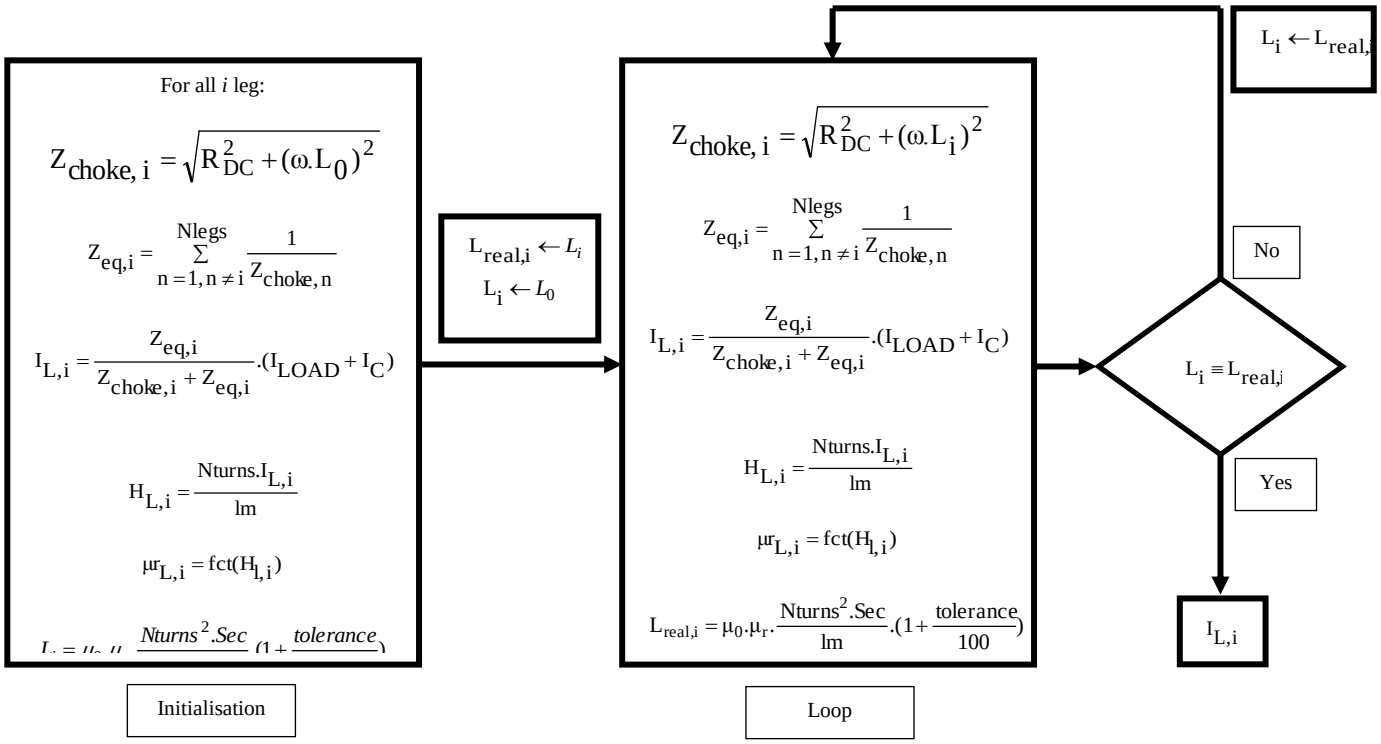

Figure 90 : Unbalanced leg LF current computation

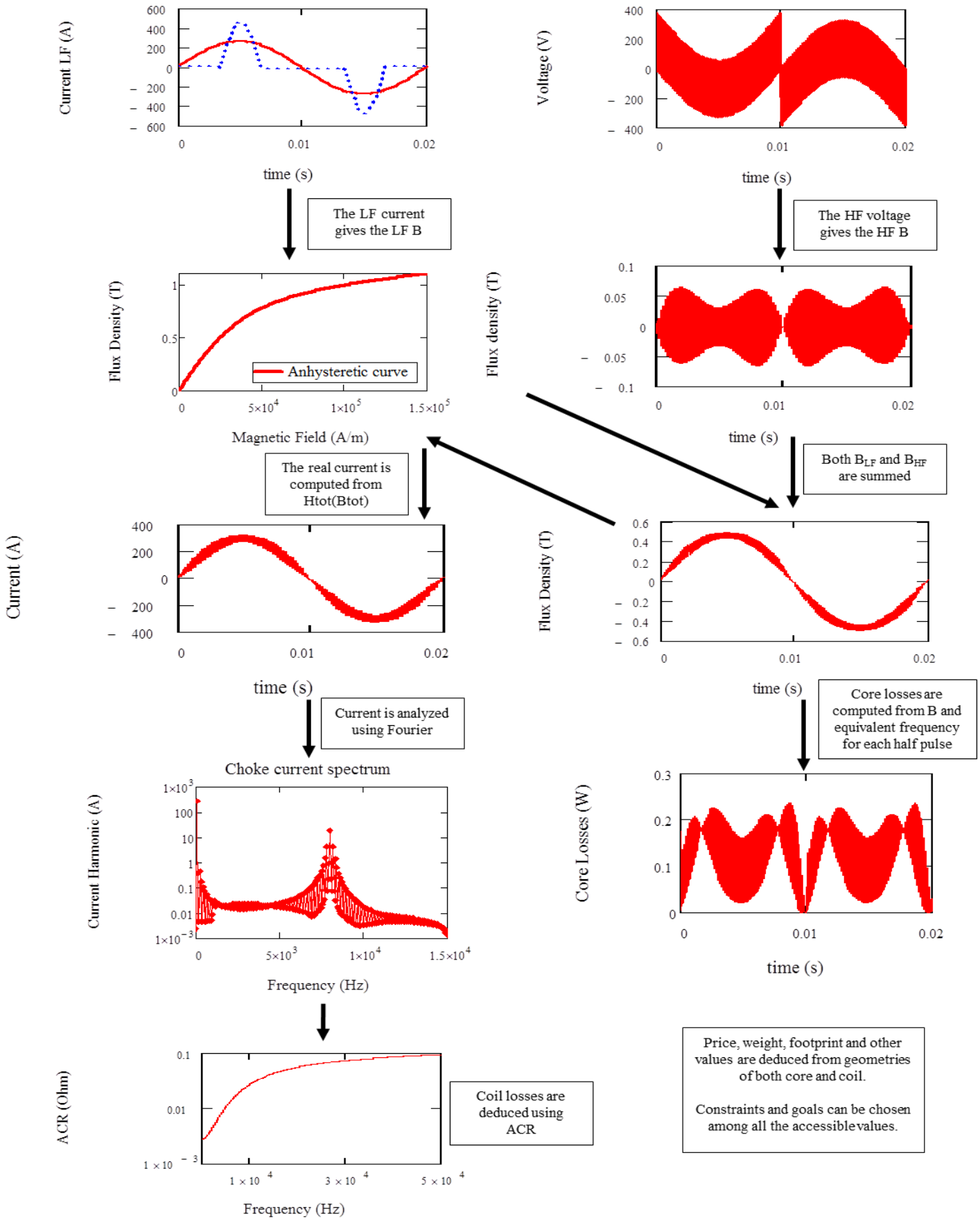

Figure 91 : Choke DC/AC modeling

3.3.4.2 Capacitor modeling

Most of the modeling effort is already done on the choke. So the LF current I_C in the capacitor is deduced from sinus V_S controlled on the load and LF capacitor impedance.

$$Ic_{LF} = \frac{V_s}{Z_c} = \frac{V_s}{\sqrt{esr^2 + \frac{1}{(\omega.C)^2}}} \quad \textbf{69}$$

Then for current's HF harmonics computed from choke magnetic behavior, a current divider is applied at each harmonic frequency. The AC impedance of both capacitor and load will impose repartition of harmonics and thus THD on the load and total current in capacitor.

$$Ic_{HF} = \frac{Z_{LOAD}(\omega)}{Z_{LOAD}(\omega) + Z_C(\omega)} . I_{L_{HF}} \quad \textbf{70}$$

The modeling of chapter two is used to compute losses from current spectrum and esr frequency evolution. The RMS current in the capacitor is compared with supplier limit indication and used as constraint to prevent capacitor damage.

3.3.5 Validations:

3.3.5.1 RL load

The validation is first achieved on a RL load. A 2 levels inverter is used and delivers a 50Hz sinus with few LF harmonic voltage with 12 kHz switching frequency @ 73kVA. The choke is a stack of 4 cores of 5 inches FeSiAl powder µ26 simulated from anhysteretic curve measured on 3 inches test core.

The first waveform input of the model is the inverter output voltage (Figure 92). The blue measured voltage is compared with pulse simulated voltage. Then the other input is the LF current absorbed by the load, approximated here with harmonic definition (Figure 93).

The HF flux densities from both measured and simulated voltage are compared on (Figure 94). Only a slight difference is visible. The total measured flux is compared with simulated one from LF and HF summed contributions (Figure 95). Here a slight error on modeling is observed. The error comes from both control not integrated in simulation and also LF hysteresis delay not considered using anhysteretic curve. The final simulated pulse current is compared with measured current on the choke (Figure 96). Both currents do not match perfectly but are really close. The saturation effect of the core is well simulated because measured ripple increase of the current near LF current peak is matching the simulated one. On minimum current value an error is noted between both curves. Indeed the simulation is symmetric whereas the control of the converter introduces a difference between positive and negative part.

In conclusion a slight error exists on simulated waveforms yet the forms and peak values are well represented. The ripples are close enough from real choke measurements to conclude that event sampled waveforms approach and choke electrical model are accurate for optimization.

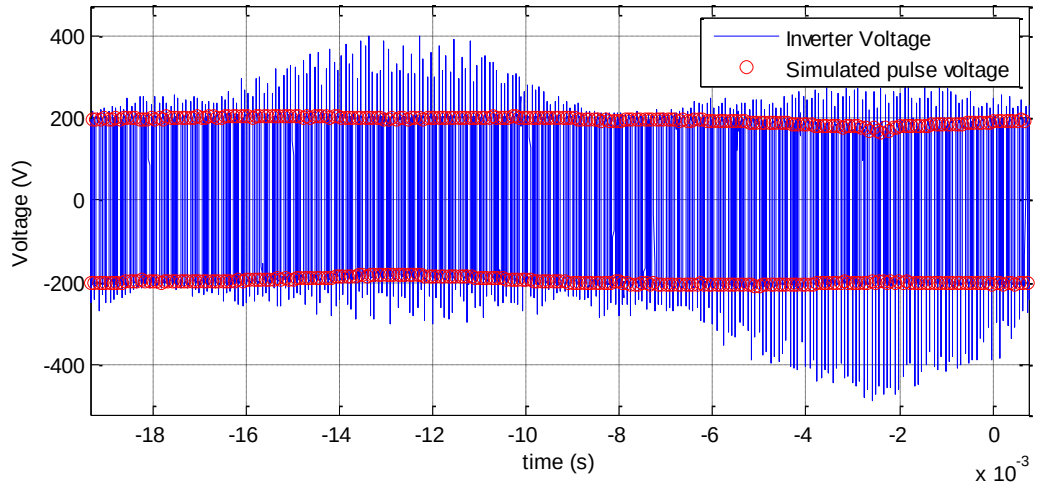

Figure 92 : Measured inverter voltage vs simulated pulse voltage

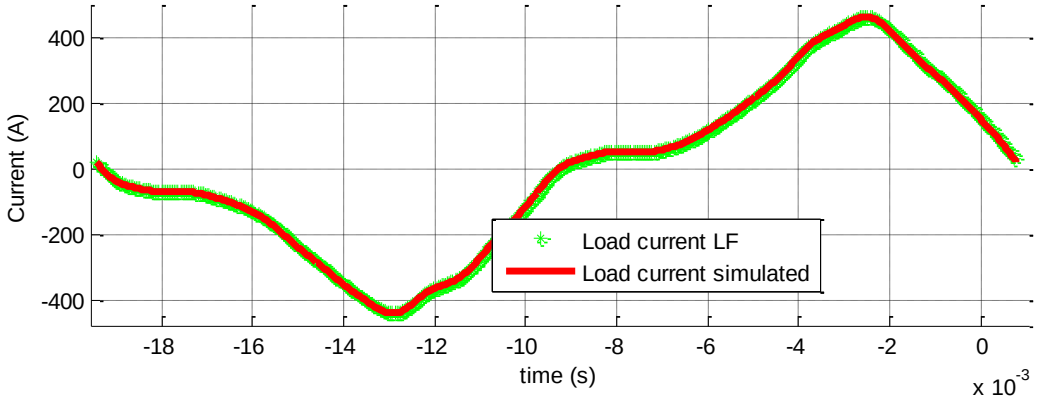

Figure 93 : Absorbed RL load current, LF harmonic build simulation

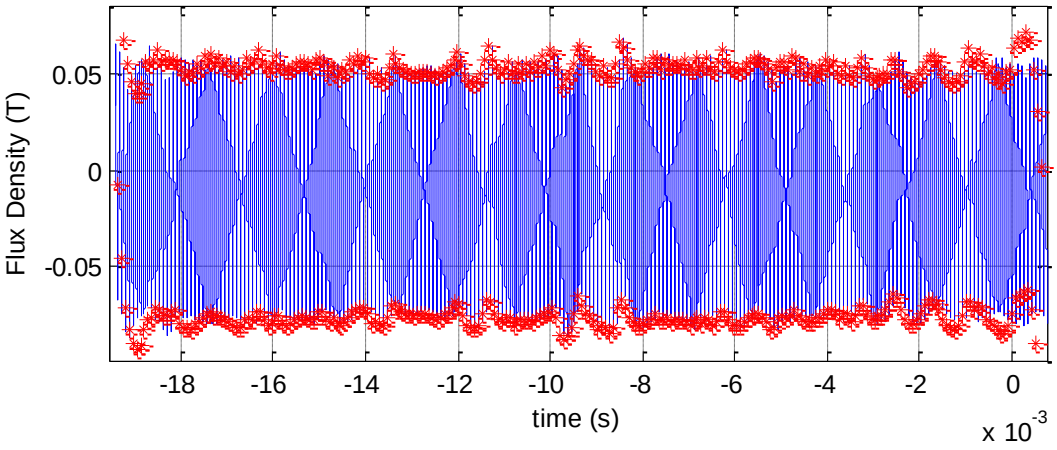

Figure 94 : Measured HF flux density (blue) vs simulated (red) from pulse voltage

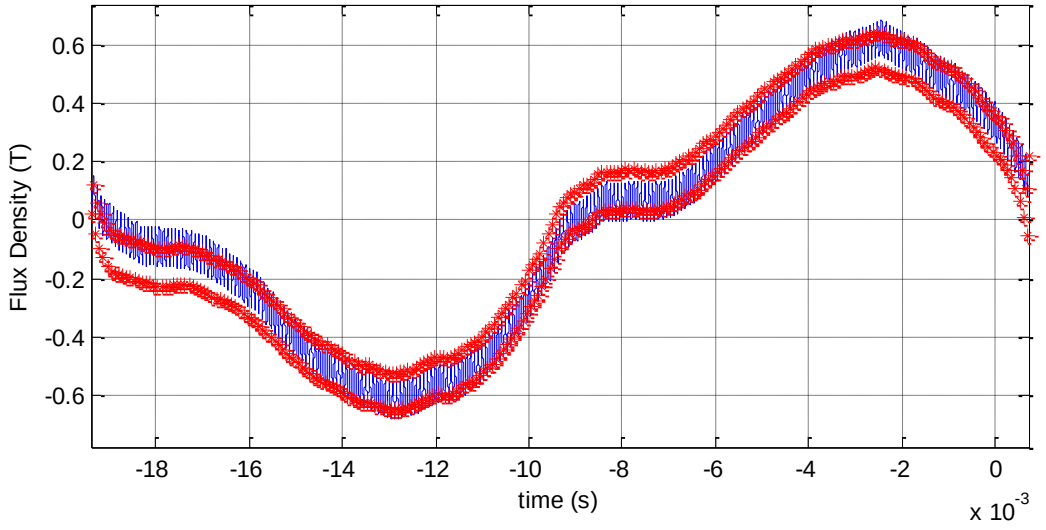

Figure 95 : Measured flux density (blue) vs simulated pulse one (red)

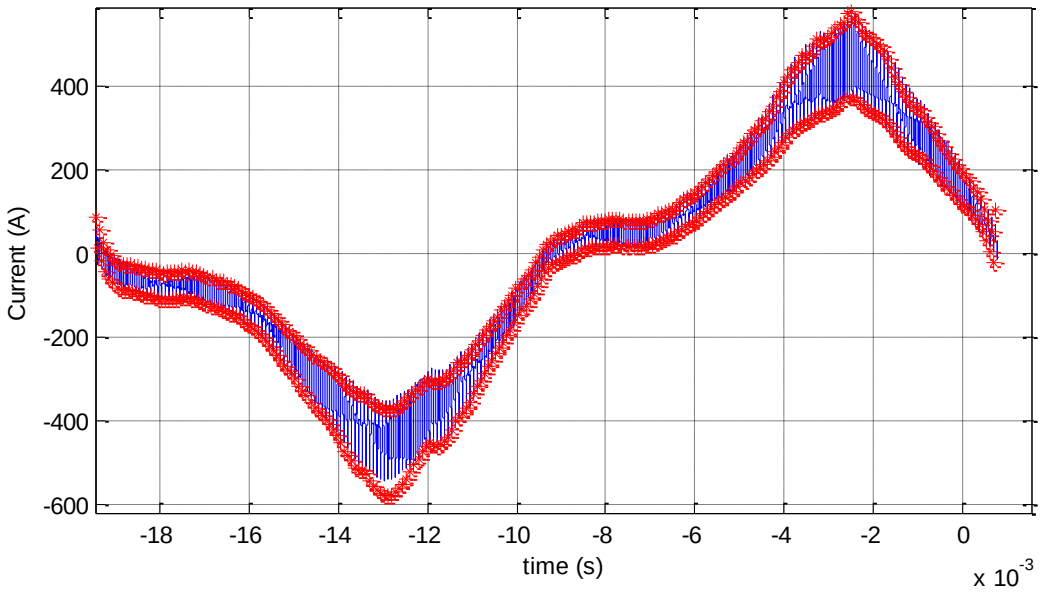

Figure 96 : Measured current (blue) vs simulated pulsed (red)

3.3.5.2 Nonlinear load

For the second validation a nonlinear load is replacing the previous RL load. The assumption of same inverter output voltage for both loads has been done [3.3.3.2]. It is validated here. On (Figure 97) three HF flux density ripples are compared. The blue is the measured one on choke. The pulse red flux comes from inverter voltage simulation with load waveform consideration. Finally the green flux density ripple is the simulated one from RL case. An error exists but is not important and comes from control loop.

The distorted LF current is illustrated on (Figure 98) and approximate once again with harmonic sum. The final current is plotted on (Figure 99). This time ripple at peak current is

still well simulated. However an error is observed on ripple for linear zones. The simulated HF flux density is larger than real one and results in a more important ripple but does not explain the difference because peak ripple is ok.

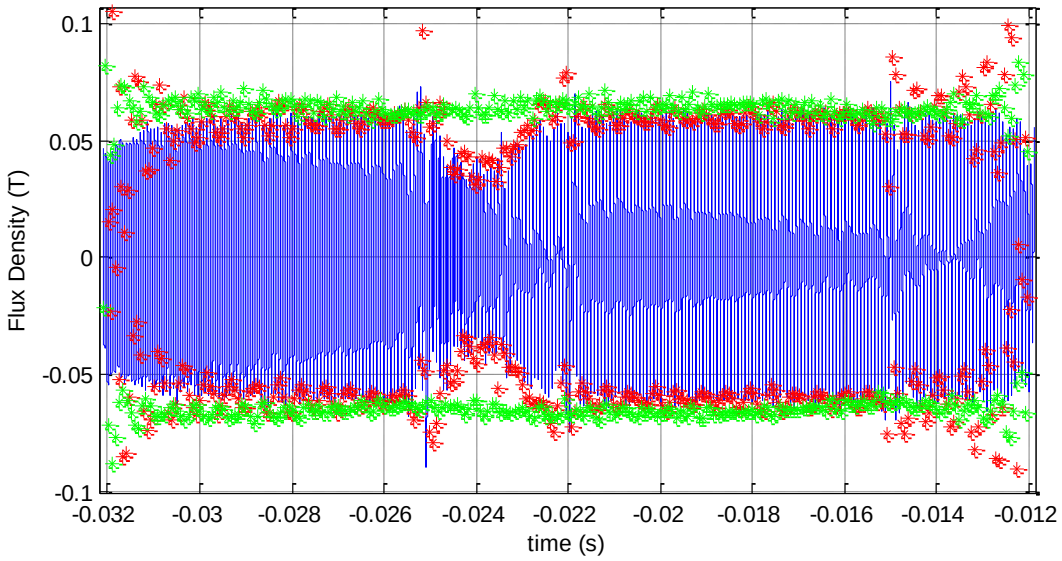

Figure 97 : HF flux density ripple. Blue measured, red nonlinear load simulated pulse one and green simulation from 3.3.5.1

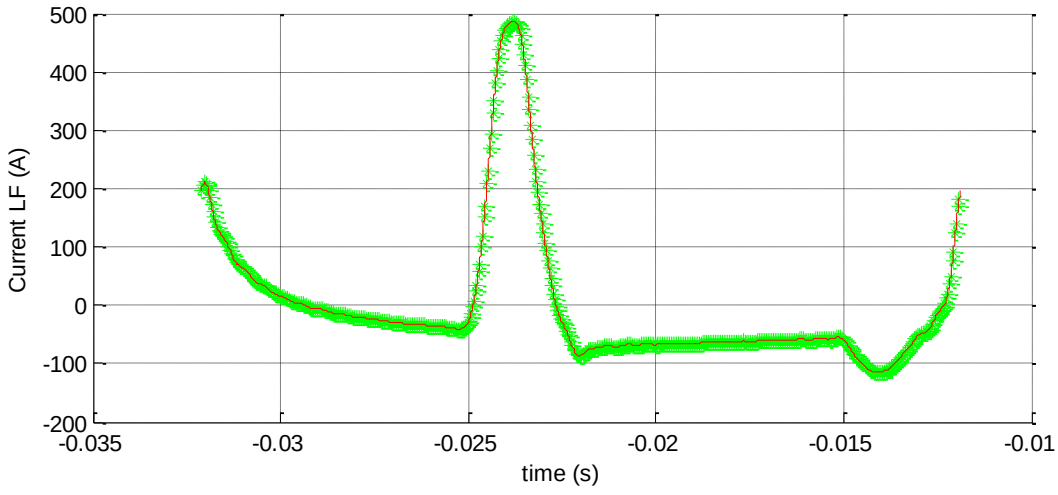

Figure 98: Nonlinear load LF current

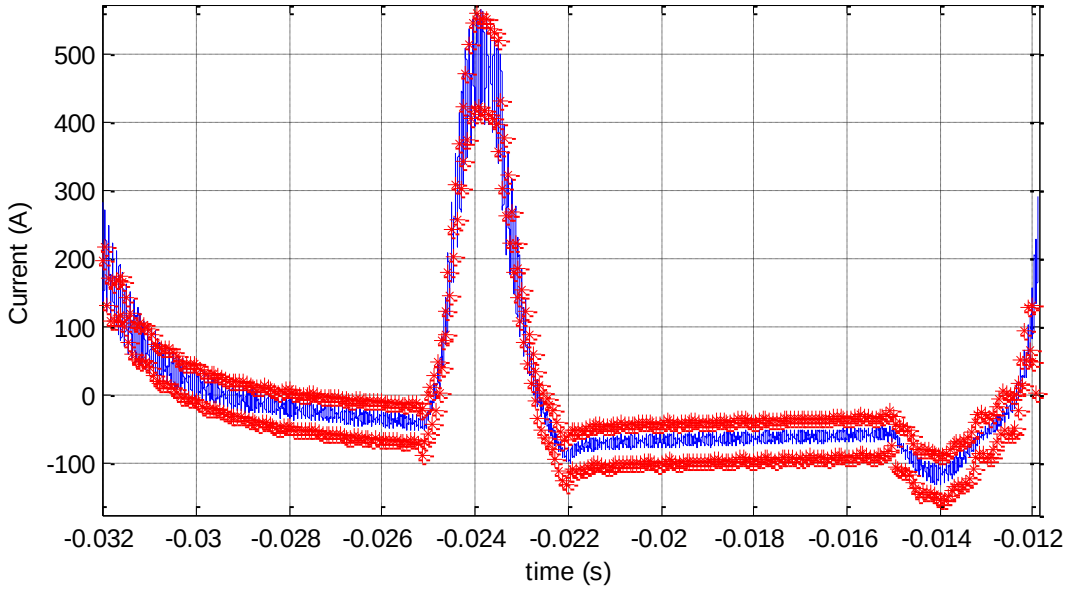

Figure 99: Choke current (blue) and simulated one (red)

3.3.6 Conclusions:

The modeling of output DC/AC inverter interleaved filter is presented in this section. An approach of communication using waveforms is used to model inputs on the filter as inverter voltage and load required LF voltage and current. Some assumption are done taking into account passive components behavior.

All electrical, magnetic and geometric parameters can then be deduced from converter model and component models from chapter two. Any value can be used in optimization as goal or constraint. Several applications are presented in chapter four.

3.4 AC/DC CONVERTERS

The AC/DC converter is the link between the grid and the UPS. Also called Power Factor Corrector, it works to eliminate harmonics created by the load. The topology is generally the same as the inverter, only the control differs. For price reason the AC/DC filtering choke is the same as for the inverter. The choke is submitted to less drastic cases than in inverter thus the design effort of passive components is done for the DC/AC. The PFC is not subject to short-circuit or worst case so the filter is checked only for THD%.

The approach is exactly the same as for [3.3] so not repeated here. The case being less constrained, it is often not used in optimization but only for validation with inverter choke.

3.5 DC/DC CONVERTERS

3.5.1 Introduction:

In the UPS the energy storage like in other power system is batteries. The batteries require a current DC level different from the power grid or the protected load. Thus the DC power is adapted from AC/DC to DC/AC converter using buck/boost DC/DC topologies. Topologies in UPS are reversible and used for both charge and discharge so a unique model is sufficient. The DC/DC converter is submitted to less drastic cases than DC/AC converter but must still be design for several cases. The chemical technology of batteries imposes special control of the converter with issues different from DC/AC. The battery chemical charging process has unequal characteristic time constants. The time constant associated with the charge transfer could be one minute or less, which is the actual chemical reaction taking place at the interface of the electrode with the electrolyte and this proceeds relatively quickly. Whereas the mass transport time constant, in which the materials transformed in the charge transfer process are moved on from the electrode surface, making way for further materials to reach the electrode to take part in the transformation process, can be as high as several hours or more in a large high capacity cell. This is one of the reasons why cells can deliver or accept very high ripple currents, but much lower continuous currents. (Another major factor is the heat dissipation involved). These phenomena are non-linear and apply to the discharging process as well as to charging. There is thus a limit to the charge acceptance rate of the cell. Suppliers give the charging rate xC and applied x ratio for the different charging phases.

3.5.2 Nominal Charging mode:

In buck/charging mode, power is taken from DC bus to supply batteries. The voltage is reduced to match battery capacity; currents are not large to respect charging rates. Transit state is not studied, in this mode highlighted in green on (Figure 100) the voltage is regulated to a charging value with decreasing current along the charge time. The sizing of the filter is done for maximum voltage and maximum current.

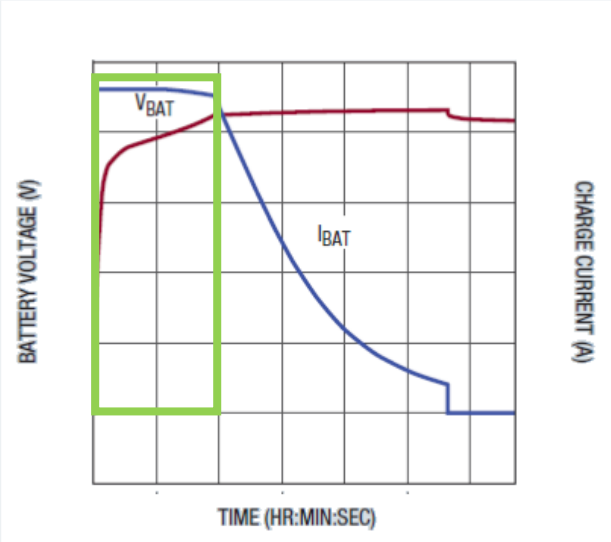

Figure 100: Typical battery curve, steady buck mode

3.5.3 Floating Charging mode:

At the end of battery charging, current is very low and control is not any longer done on voltage. The floating voltage point of the battery is reached; this mode is quick, few seconds so converter frequency is increased to limit current ripple and then RMS current inside the battery, imposed by charge capacity xC. The increase of frequency in this part is acceptable because it is short so losses rise in semi-conductor and passive component will not be dramatic neither the temperature rise.

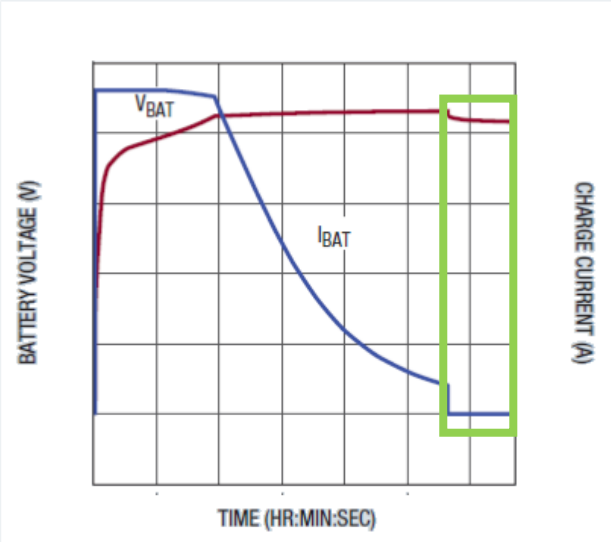

Figure 101: Typical battery curve, floating buck mode

3.5.4 Nominal Discharging mode:

In discharging mode the UPS must guarantee power to the secured load, so batteries must deliver large amount of power in really short time (seconds to minutes maximum). This mode

implies huge current tens to a hundred times higher than in charging mode. Where charging mode is checked for charging requirement xC, the discharge is studied for efficiency and limit current or thermal capability of the converter.

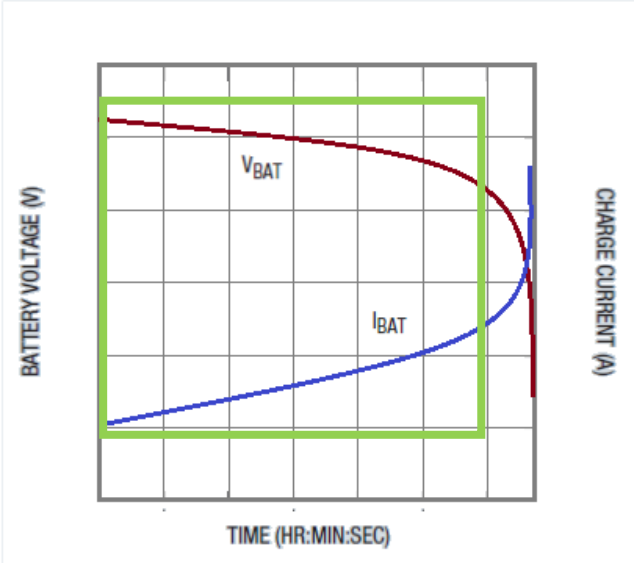

Figure 102: Typical battery curve, steady boost mode

3.5.5 Minimal Voltage Discharging mode:

At the end of the discharge the voltage available at the output of the batteries decrease rapidly with a resulting peak current absorbed. Then the batteries are disconnected to prevent deep discharge and damages. This mode is once again really short like end of charge but the high current involved is constraining for the converter design and must be checked.

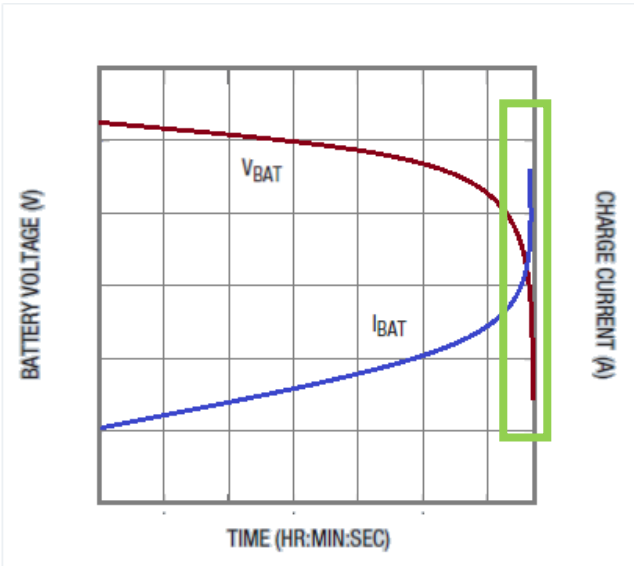

Figure 103: Typical battery curve, end of boost mode

3.5.6 DC/DC filter modeling:

The modeling for DC/DC passive components is the same in all cases. It is easier than DC/AC because the LF is a DC current and polarization. So same approach is used but only a HF period is necessary so the model is even faster.

The voltage on the choke is computed from duty cycle to switch between DC bus voltage and battery voltage. The battery current gives the LF polarization on choke material. HF flux density is deduced from voltage same as in [3.3.4]. Anhysteretic curve gives the LF equivalent flux density and total flux is deduced. Total magnetic field is computed from the same curve and real current is accessed. Same choke core and coil models are used to compute losses, price, weight and any other values.

The validation of this converter has been done but is not presented because it is even easier than [3.3.5] and redundant. Moreover validation is achieved in chapter four on coupled DC/DC filter.

3.6 COUPLED FILTER

3.6.1 Introduction:

In order to reduce the filter size many solutions are proposed. The multi-level converters allow reduction of harmonics of the output voltage and thus the need for filtering. To reduce the current and voltage ripple multi-legs interleaved topologies are introduced. However the interleaving decreases ripple on the capacitors but not in inductors so size is not reduced dramatically. New better solutions are found using coupling transformers between interleaved legs [56] to [58]. The coupling makes pulses on one leg seen by the other legs, thus the equivalent frequency on each leg is multiplied by the number of coupled legs. The HF harmonics are occurring at higher frequencies, reducing the size of the low pass filter. Even with the addition of new component for couplers, the gain is still huge.

Solutions of monolithic coupled choke are proposed in [58]. Yet better solutions are achieved using toroid and separated coupling transformers. The separation of components as a separation of function allows a better sizing of each one. Indeed in integrated solution the leakage flux of the choke is used as coupling effect between legs. Thus the choke must be degraded to increase the coupling. Optimizations are used to find the best compromise but still degrade the inductance part. The leakage flux is also a drawback for sensors because LEM used for acquisition are disrupted by this additional flux. Thus shielding is necessary and increase price of the solution. Another drawback of this approach is the fact that if the coupler saturates and breaks down the whole filter is down. Last but not the least, monolithic solution are with air-gap and noise in not acceptable; tested prototype >95dB for DC/DC coupled solution presented in chapter four. By separating component, even if the coupler is down the converter can still work as an interleaved one. Moreover, UPS are generally designed for several power points. The addition of new power block is facilitated by the physical separation because new chokes and couplers can easily be added where with monolithic solution a new one must be created. Works on monolithic approach are also driving toward separated transformer solutions [59]. Toroids are also preferred for already presented advantages (chapter II) and noise reduction with no air-gap.

The coupling modeling is different from previous presented solutions but still remained the same approach for DC and AC converters. The method is presented in next section. The filters are subject to same cases than before so waveforms at the terminals of the filter are not reminded; only choke and coupler behaviors are explained.

3.6.2 Event waveforms:

As presented in [3.2.3], a huge reduction of simulation time and increase in accuracy are possible using event sampling. Yet in coupled converter, events on each legs impact the other leg. So input waveforms on the filter are sampled at each switch event on one leg, value on other legs even unchanged are computed for these events (Figure 104).

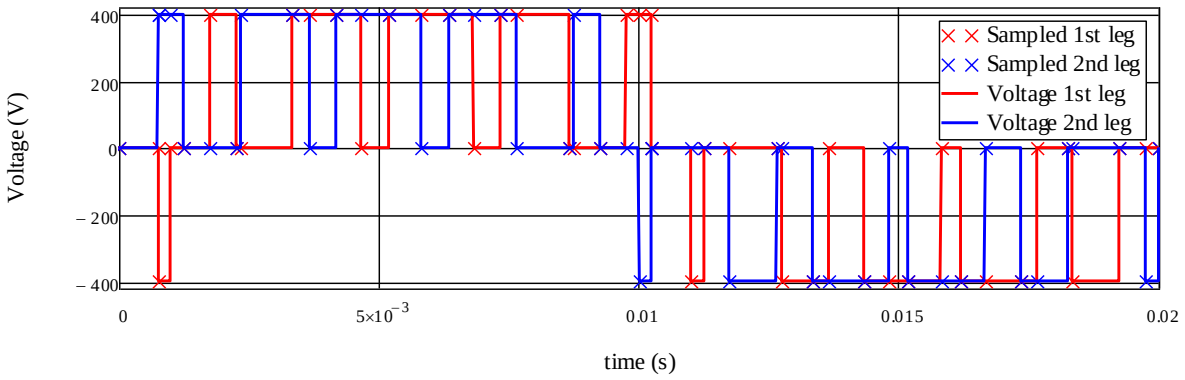

Figure 104 : Sampled signal for coupled solution

3.6.3 Interleaving:

The coupling between legs is an extension of the interleaving approach. I.e. to decrease dramatically the current ripple after the legs in multi-legs converter, commands on legs are shift. Indeed the multi-legs topologies allow the separated command of the legs. Then the commands are shift on an HF period (Figure 105). 0° meaning the fronts are the same and 360° that up front is a down front for the other leg. The legs are short-circuited at their end to form what we call a power block. The first observation for interleaving is that ripple current on legs is not reduced, whatever the shift the HF phenomena on the inductance are the same. But at the output of legs the ripple is dramatically reduce in case of good shift; ripples are in opposition so their summation results in a thin ripple (Figure 106). To decrease the ripple even more, blocks can be shift also. The interleaving of legs does not reduce the size of choke because current ripple on each legs and thus on semi-conductors stays the same but it creates a real diminution on the capacitor filter and thus its size.

3.6.1 Coupling:

Gain being achieved on capacitor using interleaving, coupling is used to decrease ripple on chokes. The input waveforms on the filter are unchanged compared to interleaved cases. Only event sampling is changed as presented [3.6.1]. The capacitor is placed as before at the output of the legs in order to benefit of the reduction of ripple. The size of the capacitor is then dramatically reduced because for several leg coupling and sometime groups of legs interleaved, the output of choke/coupler stage is ripple free. Several coupled filter topologies are investigated but only those that allow one transformer per leg, other are denied for too high number of transformers (Figure 107).

The shift between legs is generally of 180°/Number of legs but can be used as an optimization parameter to find the best delay between legs for ripple reduction. The couplers are inverse transformers with m ~-1, the ratio of coupling is defined by the ratio between choke turns and coupler primary or secondary turns. An ideal ratio can be found (Figure 108). Indeed the summed legs output current is unchanged by the ratio of coupling (Figure 108) but the ripple on the legs is. Increasing the ratio the ripple is reduced on legs, and then after a certain value of ratio the impact is unchanged, only the design of the coupler could lead the algorithms to choose a higher ratio to decrease induction on coupler.

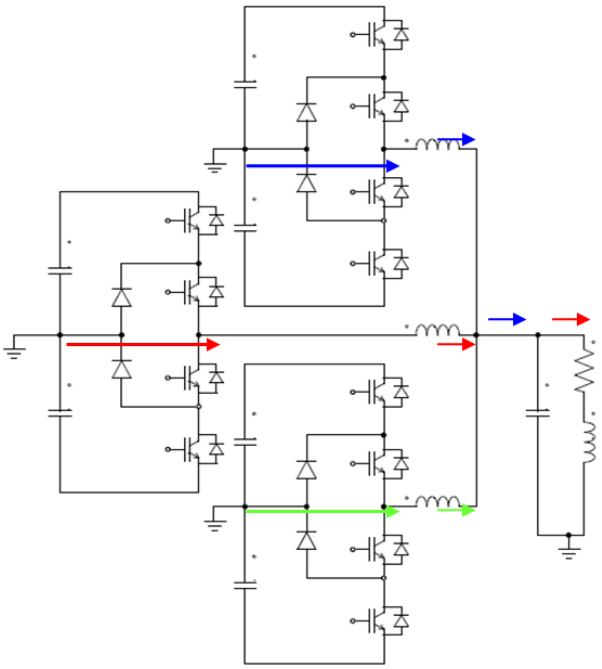

Figure 105: 3 legs 3 levels inverter with interleaved legs, inverter legs' voltages and all currents

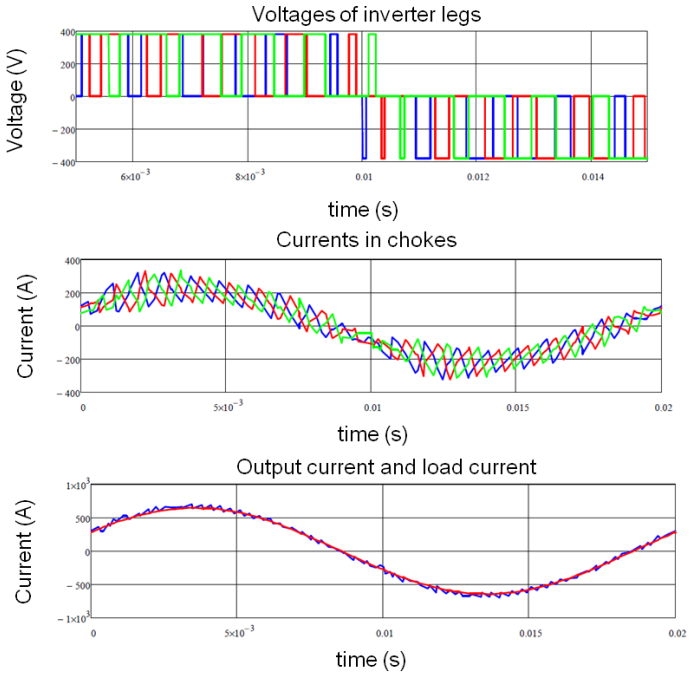

Figure 106: above voltage of previous inverter legs, middle currents on legs, below output and load currents

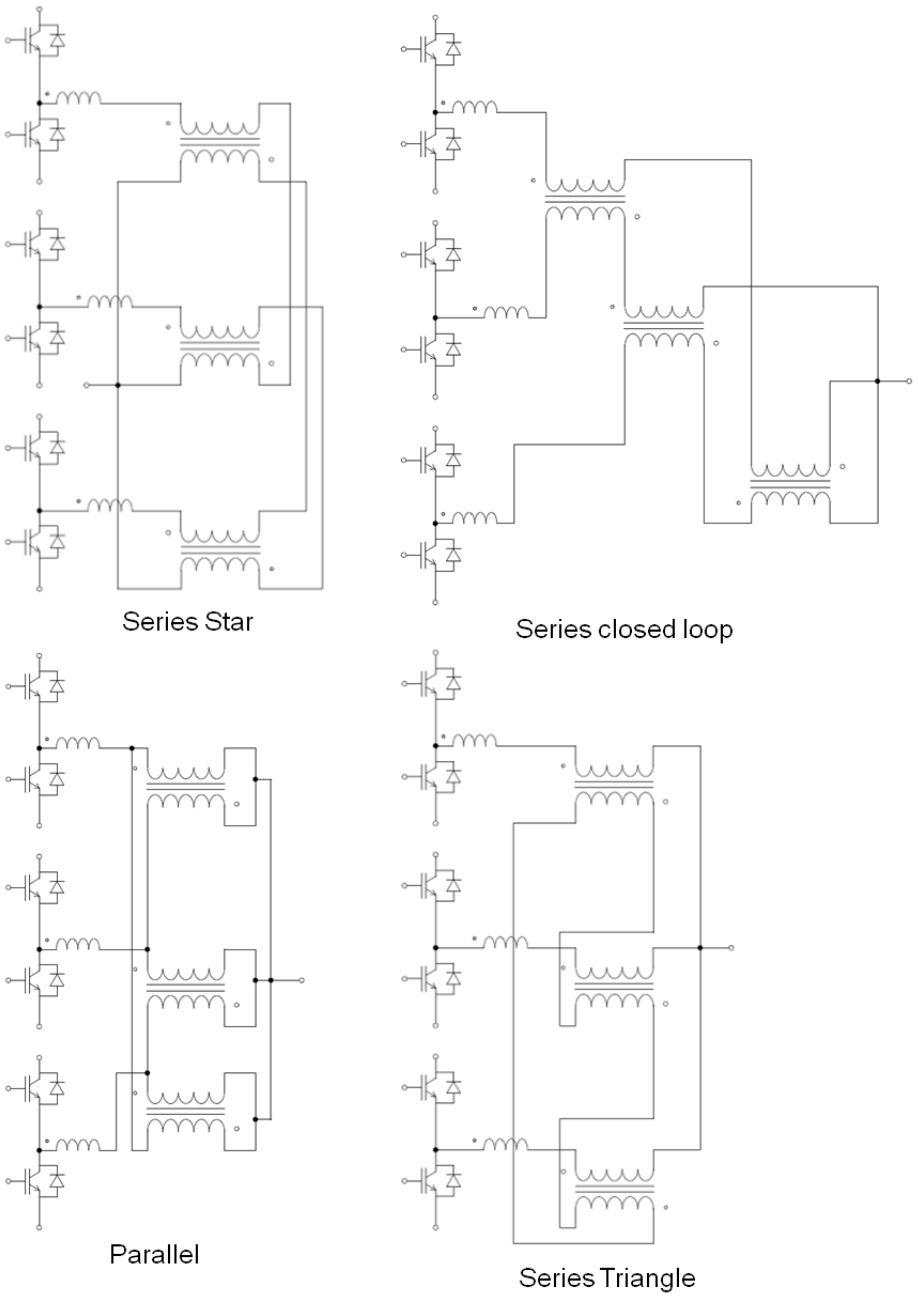

Figure 107 : Coupled multi-legs multi-groups filter

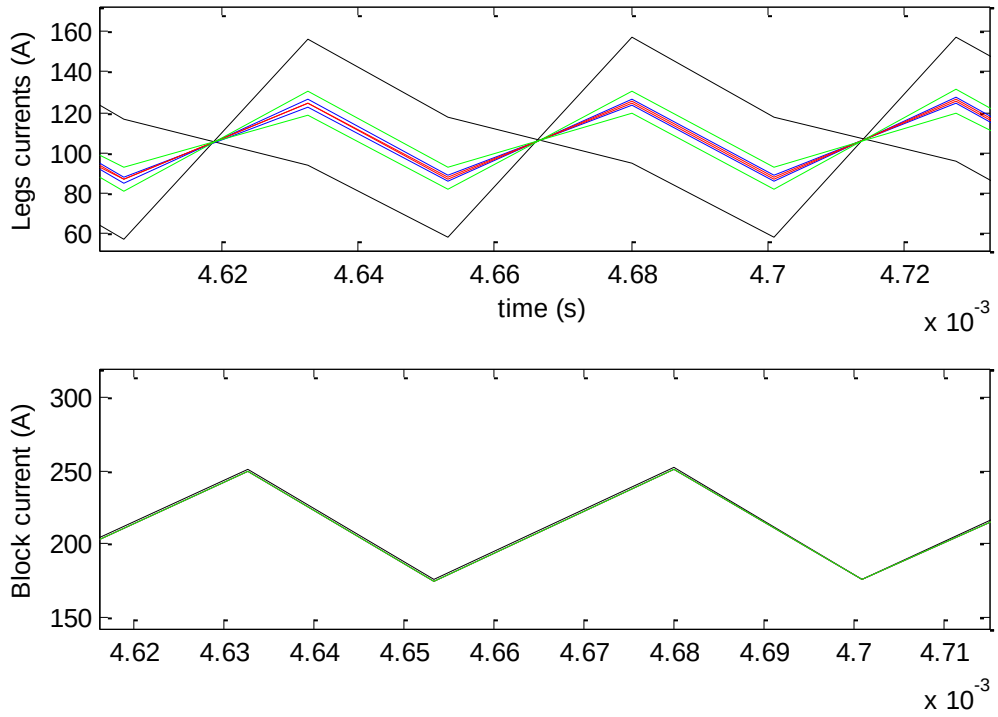

Figure 108: Current ripple for two coupled legs, above legs currents, below block current. Black ratio = 0.03, green ratio = 0.12, blue ratio = 0.25 and red ratio = 0.36

The inputs on the filter are still the converter voltages and the load LF current divided between the legs equally or considering unbalanced control or impedance of coils and core of inductance and coupler. The difference between classic choke leg and a coupled leg is that voltage distribution between choke and coupler is unknown because it depends on choke and coupler response to LF+HF behavior.

What we know is that current flowing through the choke coil and coupler coil is the same. So between each event on one leg *i* we can write:

$$V_{L,i} = L_i . \frac{\Delta I_i}{\Delta t} \quad (71)$$

$$V_{L,i} + V_{M,i} = V_S - V_{converter,i} \quad (72)$$

$$V_{M,i} = M . \frac{f(\Delta I_i, \Delta I_j)}{\Delta t} \quad (73)$$

With V_L the choke voltage, V_M the coupler voltage and L and M the value of inductance for choke and coupler between two events. For each leg we have 3 equations with 3 unknown V_L, V_M and ΔI. L and M are defined from the LF current and core curves. We then have the solution for ΔI regarding the topology simulated.

Once again a loop is necessary in this case. Indeed L and M value will change with the magnitude of current ripple. So the calculation is looped with L and M recalculated with I_{LF} and summation of ripple until convergence toward steady state. The loop loses time but is

compulsory for saturation consideration. Nevertheless it always runs in less than ten iterations.

The current ripple gives V_L and V_M on each leg then same pattern as for interleaved legs is used to find flux density from voltage then magnetic field and current, losses, price, etc.

Validations are presented in chapter IV for an optimized 2 legs chokes + coupler and a 6 legs DC/DC converter.

3.7 CONCLUSIONS

The approach chose in this PhD for the optimization is to use discrete parameters and libraries. Genetic algorithms fitted to this choice have been presented in chapter one. The component models introduced in chapter two are matching these algorithms requirement. Thus the converter topology modeling must also match the requirements of fast time model computation, robustness, and reduced inputs and outputs parameters.

An approach to modeling circuit behavior using waveforms between converter parts and components is explained. The steady state of the converter is then simulated without transition state behavior so there is no need for control loop convergence and thus there is a huge calculation time reduction. Event sampling is preferred to time sampling once again for time saving but also to guarantee maximum of waveforms and parameters computation.

The approach with waveforms communication makes it possible to switch model of component without changing the converter topology model. This is an advantage to test new model or complexity of model impact on optimization convergence. The assumption of accuracy leads to correct convergence whereas approximate linear model leading to errors can then be checked for exactly same converter and waveforms.

The waveforms modeling is presented for DC/AC, AC/DC and DC/DC interleaved filter. Many working cases are considered and impact on component and converter sizing highlighted. The approach is validated with few classic cases and other validations are brought in chapter four with optimization results.

New coupling solutions have been proposed in both academic and industrial laboratories. So modeling extensions for these technologies is presented in order to model output converter coupled filter for optimization. Successful implementation of optimized coupled solution is presented in chapter four with other optimization results on industrial cases.

3.8 REFERENCES

[52] Pasterczyk R., Guichon J.M., Schanen J.L. and Atienza E., "PWM inverter output filter cost-to-losses tradeoff and optimal design", IEEE Transactions on Industry applications, vol. 45, issue 2, pp. 887-897, 2009.

[53] L.K. Mestha, P.D. Evans, "Analysis of on-state losses in PWM inverters" IEE Proceedings on Electric Power Applications, vol.136, no.4, pp.189-195, July 1989.

[54] B. Masserant, T. Stuart, "Experimental verification of calculated IGBT losses in PFCs" IEEE Transactions on Aerospace and Electronic Systems, vol.32, no.3, pp.1154-1158, July 1996.

[55] C. Rizet, "Amelioration du rendement des ASI", PhD dissertation INPG, defended on 10/05/ 2011, France.

[56] B. Cougo, T.Friedli, D.O. Boillat, J.W. Kolar, "Comparative evaluation of individual and coupled inductor arrangements for input filters of PV inverter systems", CIPS 2012, Nuremberg.

[57] W.Wu, N.C. Lee and G. Schuellein, "Multi-phase buck converter design with two-phase coupled inductors", 2006.

[58] N. Bouhalli, "Etude et integration de convertisseurs multicellulaires paralleles entrelaces et magnetiquement couples", PhD dissertation INPT, defended on 2009 France

[59] S. Sanchez, "Contribution a la conception de coupleurs magnetiques robustes pour convertisseurs multicellulaires paralleles", PhD dissertation INPT, defended on 24/03/2015 France.

4 CHAPTER IV - OPTIMAL SIZING

4.1 INTRODUCTION

In previous chapters of this PhD dissertation, tools and methods have been proposed to realize optimal sizing of power converter. We focused on passive component for filtering need in UPS structures. In this last chapter, proposed innovations are applied on several industrial cases.

The presented optimizations are selected to highlight possibilities and results of the proposed approach of discrete sizing of choke and capacitor. Upgrade of already existing solution is first investigated in a highly constrained problem. Then this case is used to comment all possibilities that optimization could have bring if used in pre-development of the product and gains that could have been achieved. New Schneider Electric UPS has benefited of this work and solutions are presented for both interleaved and coupled solutions for DC/AC, AC/DC and DC/DC conversions. Yet in all applications real values of components, materials and sizes are not numbered for company privacy politic.

All the optimizations are done with the same implementation. A niching algorithm of 100 generations of 40 individuals is first used to explore the solution domain. Optimization experience showed niching algorithm being the most efficient stochastic algorithm to widen the search of optimal solution. Then 10 generations of Elitist Multi-Objective Evolutionary Algorithm GMGA of 500 individuals are used to build the Paretos tradeoff between objectives from points found by niching algorithm. The chaining of both algorithms is efficient most of the time on our problems. The niching is preferred to GA because of its better solutions but also because by its mechanism it keeps several niches and thus several point on the Paretos, facilitating the GMGA work. Only our experience guided those choices. E.g. niching is better with few individuals and lots of generation whereas GMGA build better Paretos with few generations but lots of individuals.

4.2 DC/AC INTERLEAVED CONVERTER

4.2.1 4 levels 125kVA inverter:

The first investigated topology of is a 120kVA 4 levels inverter (Figure 109) operating at 16 kHz switching frequency. The output filter is simulated with models from chapter II and filter approach from chapter III. For all presented optimizations IGBTs maximum current defines a constraint on the choke admissible ripple. Thresholds for peak current are also imposed by the control of the topology, i.e. if the current is higher to the threshold control limits its value to prevent converter damages even if the outputs are no longer guaranteed.

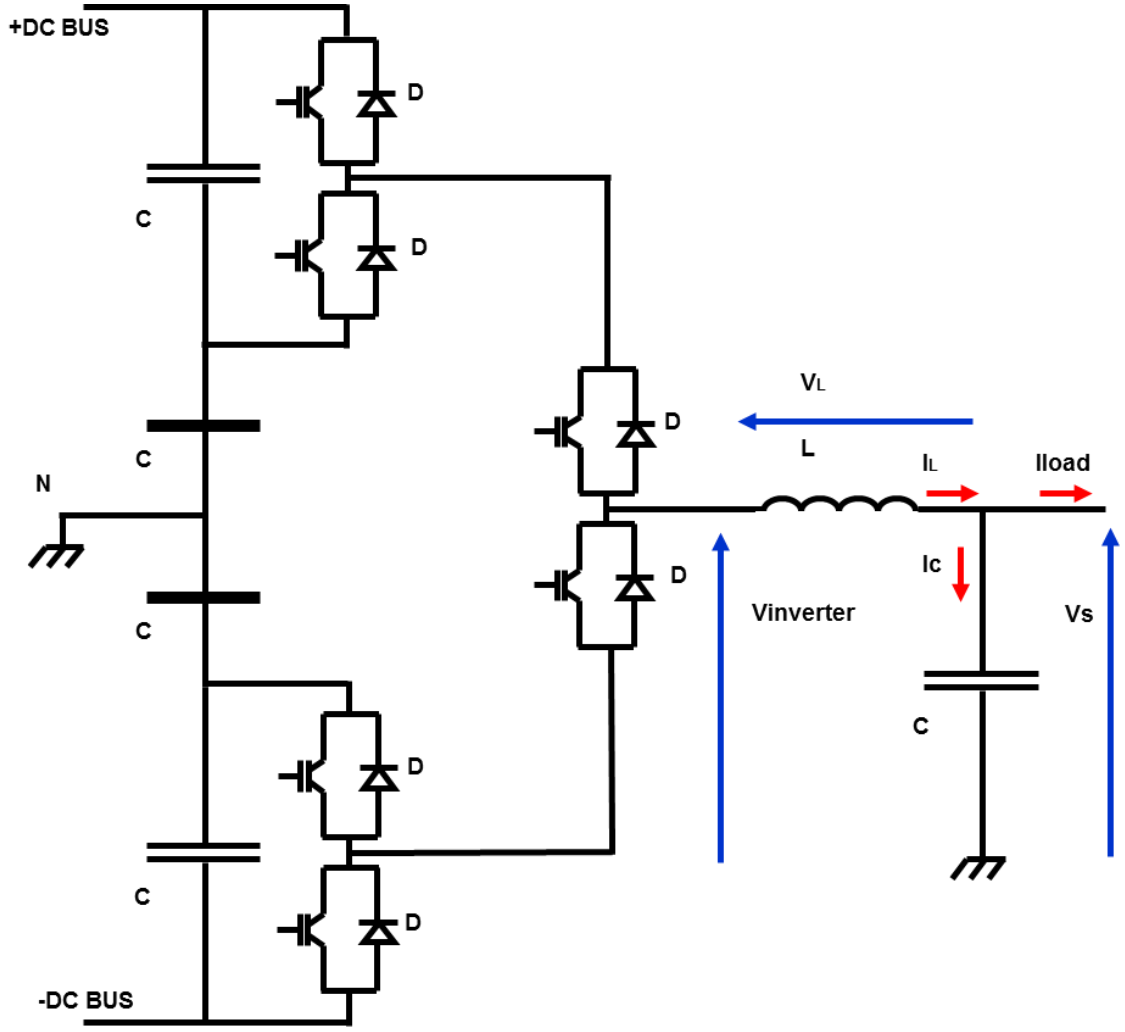

Figure 109: 4 levels inverter

4.2.2 Replacing existing solution:

The first request for proposed approach was to replace an already existing solution of the presented output filter. The capacitors are unchanged, only the choke must be replace because temperature rise was too high. The installed solution was two chokes in parallel with no interleaving. The place allowed inside the power block was fixed (Figure 110). So

optimization is constrained by geometrical dimensions, fixed capacitor and actual converter electrical limitations (i.e. output THD, maximum ripple current in capacitor).

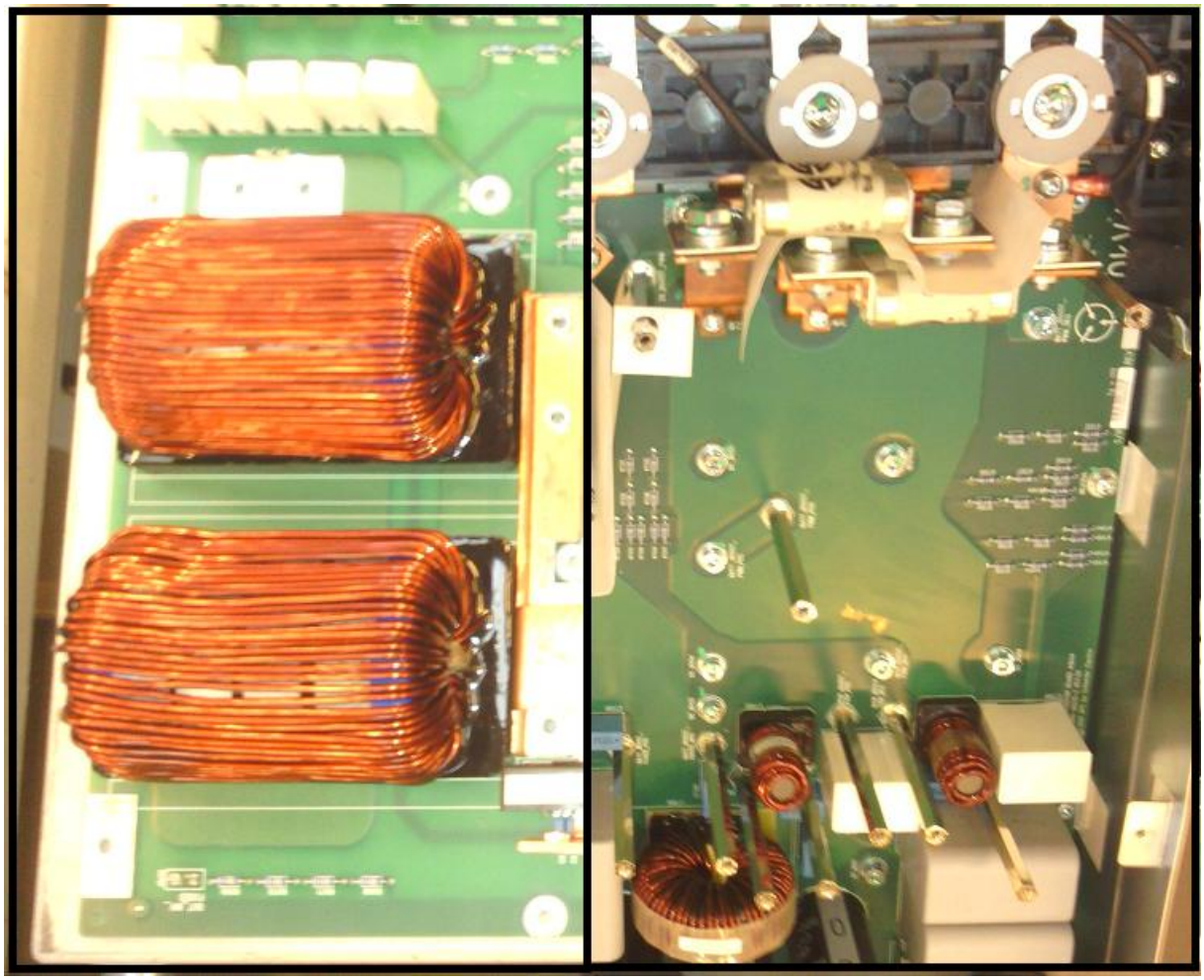

Figure 110: Chokes to be replace and place available in power block

4.2.2.1 Windings alone

The first analysis of the existing solution shows that 83% of choke losses comes from windings (Figure 111). On the choke picture, we can see that convection surface exist between air cooling and core because coil is spared enough. So temperature rise comes mainly from the coil with current density 4A/mm² for RL load up to 7.5A/mm² for non-linear load case. An optimization is achieved only on resizing the coil with fixed number of turns in order to not impact actual filter design.

The optimization results are shown on (Figure 112). The losses and price of raw material of the coil are expressed in percent of original coil version. The gain achieved on coil only is huge. A solution can be realized with only 20% of initial losses for 50% of the price (less material and less labor); it is presented on (Figure 113). The algorithm chose a larger wire – still using copper- with no strands in parallel. The current density is reduced to 3A/mm² for RL load and 5A/mm² for non-linear load. The larger size of wire induces higher skin effect,

but proximity effects are reduced so resistance of coil for current harmonic is almost same as old version for HF (Figure 114), and obviously better at LF.

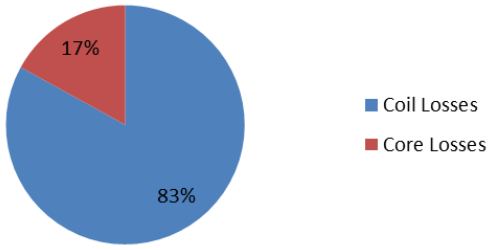

Figure 111: Choke losses repartition

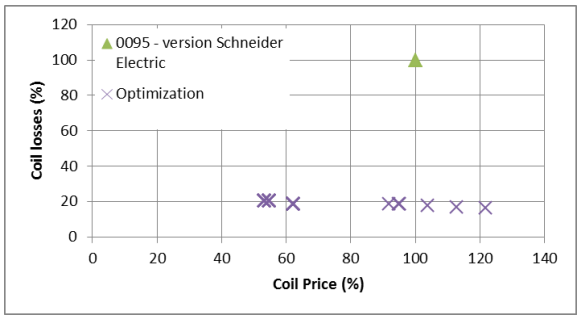

Figure 112: Coil optimization results in % of initial price and losses

Figure 113: New solution of coil

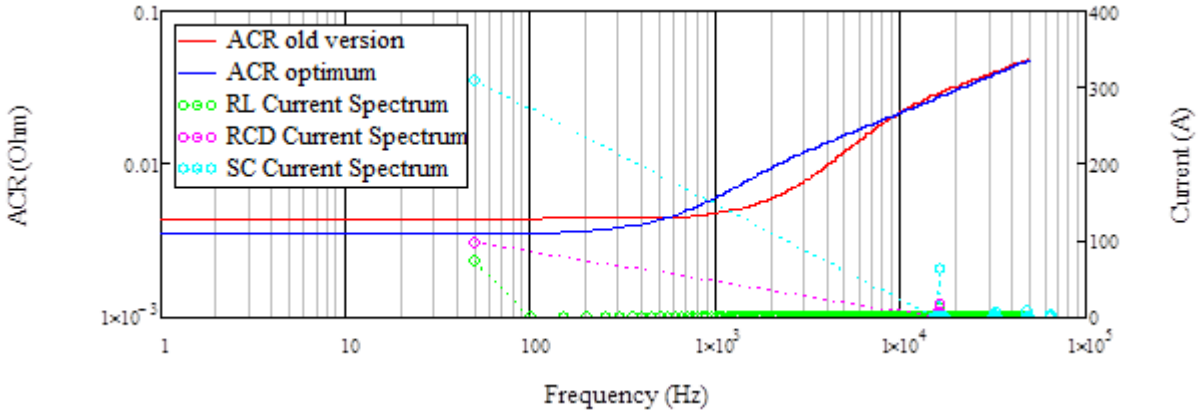

Figure 114: Evolution of AC Resistance for old and new version of coil. Illustration of Current Spectrum from 3 load cases

4.2.2.2 Upgrading power

The second request was to boost converter power up to 125kVA. The thresholds are a little higher but allowed space is still the same (Figure 110). So this time no solution could be found by changing only the coil, actual core had a too weak inductance value at high current especially with a crest factor of 2.5. This case was still an optimization under both electrical and geometrical constraints. The first optimization was done in several runs with each time a fixed material (Figure 115). The second optimization discrete material library is used for core material (Figure 116). The validation of material library is achieved because where first optimization required 7 runs, the second optimization is done in one run with only a new free parameter (material index) which didn't slow down the time of convergence. The library is 50 materials long but the algorithm has no issue picking the good ones. A new material we had not considered is highlighted by optimization (Material_35), which shows the interest of optimization, which may explore a wider space of solution that a human designer. Other validations of library are done later in this chapter.

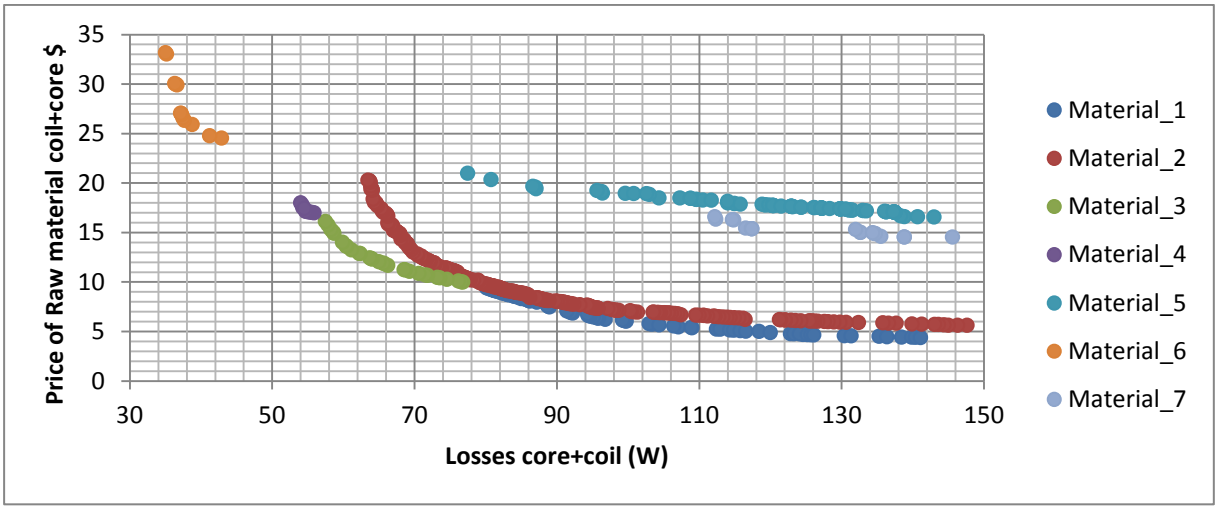

Figure 115: Pareto Losses vs Price, material by material

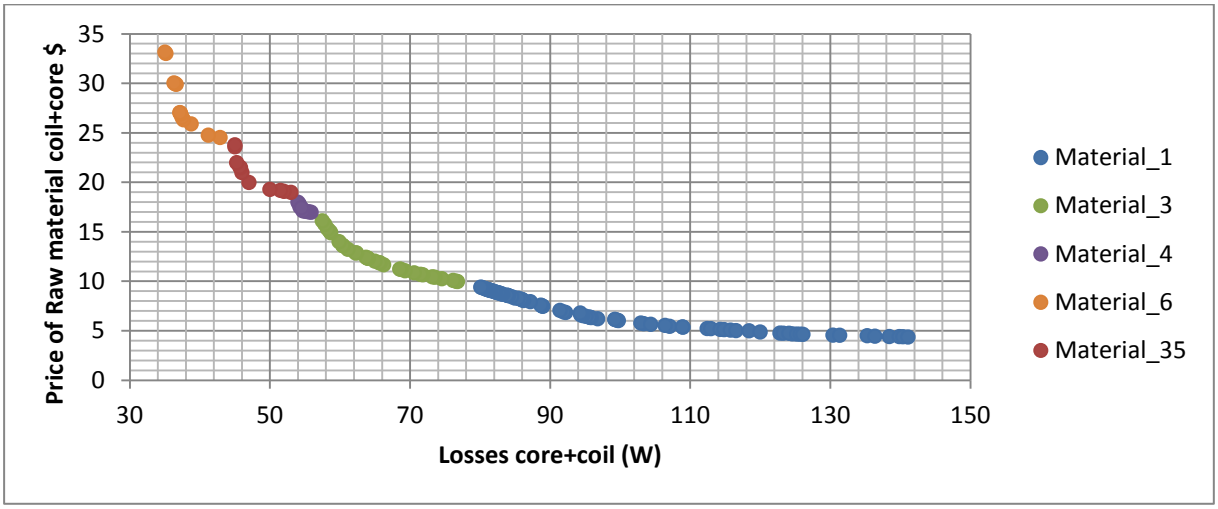

Figure 116: Pareto Losses vs Price, Material library

The following studies were not part of the design to be implemented in the UPS but present the possibilities of optimization if it has been used in pre-development of the product and not as resizing a geometrical constrained solution.

4.2.3 Single vs Parallel solution:

A general idea in Schneider Electric Innovation Team is that paralleling chokes is a loss of efficiency. To verify this principle, which was actually not applied in the old design, the optimization is performed on previous 4 levels inverter output filter (choke + capacitor) but this time without constraints on overall sizes, and considering both cases, one and two inductors.

The objectives are to reduce price and increase efficiency. The constraints are the THD on the RL and RCD loads limited to respectively 3% and 5%. The RMS current in the capacitor is limited to supplier maximum value for preventing damage and the voltage drop on the choke is also checked to guarantee voltage on the load. A minimal value of inductance is fixed by regulation team. The thermal is guaranteed by constraints on power density in choke and coil based on Schneider Electric experience. On (Figure 117) the superiority of one choke against two parallel chokes is shown. It would have been much better for project to choose the one choke solution rather the chosen one.

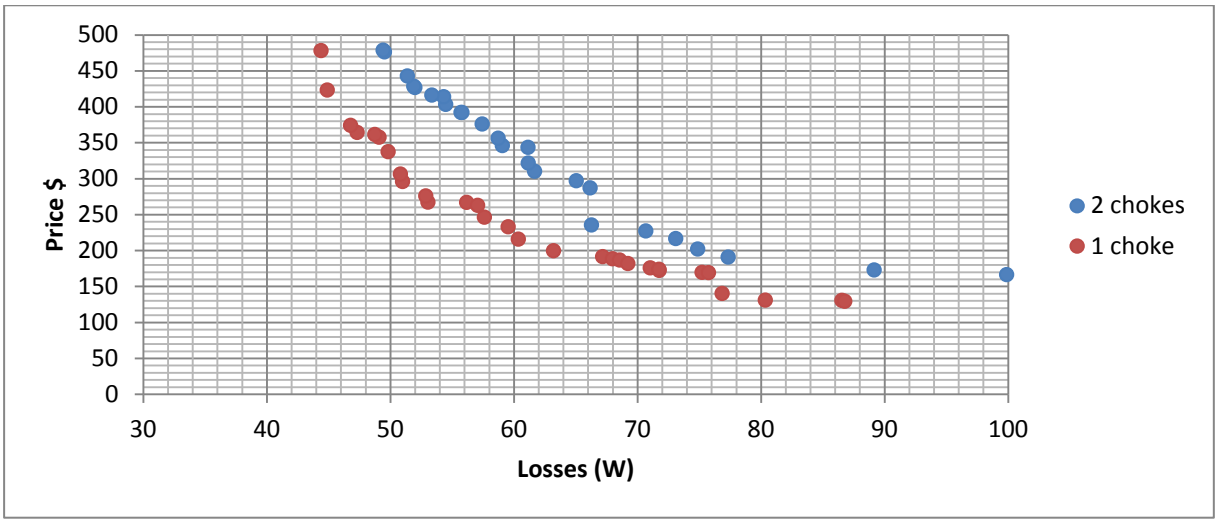

Figure 117: Single choke solution vs 2 parallel chokes solution

4.2.1 Optimal dimensions vs catalog sizes:

For conductors and magnetic cores the size are defined by catalogs. The choice to optimize sizes using catalog values as a library is done because for a new size of core, Schneider Electric should buy a new tooling for manufacturers to build the optimal size. This would lead to longer time to prototype and higher cost. Since the design assisted by optimization will spread in industry, the feedback could validate that prototyping is no longer necessary if the models used in optimization are accurate enough to provide designer with solution really close to reality. Moreover the price of the new tooling can be admissible if the gain achieve by optimal size is high enough compare to catalog size. Two optimizations are run with free size parameters and catalog size. The results are presented on (Figure 118). The gain achieved by optimal size varies between 20$ to 40$ depending on Pareto points at same losses. A tooling is of several thousand dollars so optimal sizes become really interesting for production of thousands of UPS but not for hundreds. This can vary depending on project.

Note that the Paretos are not smooth for two reasons. The first is that niching algorithm is used before GMGA for its capacity to explore solution domain then GMGA build the Paretos from resulting points. So niching solutions are returned by the optimizer even not on the Paretos. The second one is that this time price volume and losses are minimization objectives. So a smooth Pareto cannot be built because optimal tradeoff between two objectives is not necessary the best tradeoff for both other.

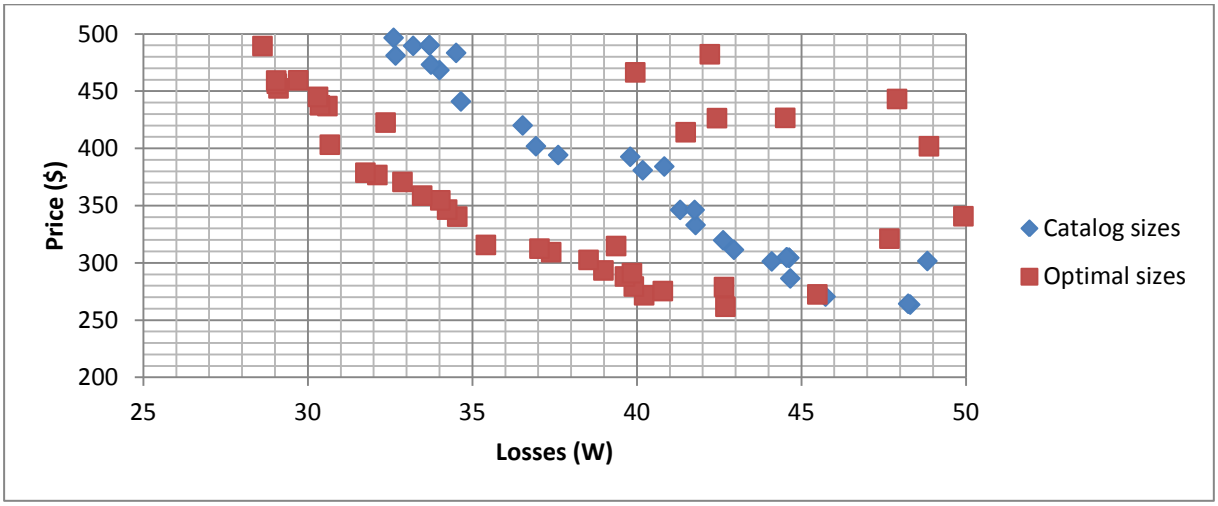

Figure 118: Catalog size optimization vs free size optimization

4.2.2 Best permeability:

Like the optimal size, few permeabilities are available on catalog. It can be interesting to investigate the gain we can get from optimal permeability. Two families of FeSiAl alloy and FeSi alloy are used to build two fictive materials. The losses and magnetic behavior coefficients are approximate by polynomials relying on permeability as input parameter same for price and density. The optimization is run for catalog material and then for optimal material. The results are presented on (Figure 119). A slight gain is achieved with free permeability for low losses part of the Pareto. The best permeability seems to vary between 60 and 70; this is verified by the Pareto for catalog µ60.

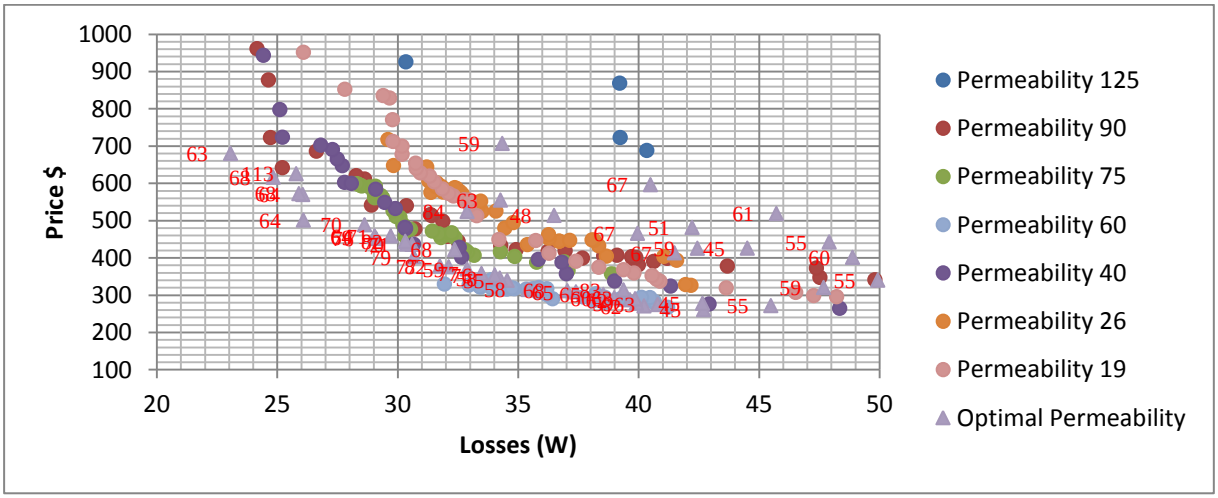

Figure 119: Pareto Losses vs price, permeability in labels

4.2.3 Capacitor

The design of the capacitor is not impacted by the several methods of choke design presented before because only the current ripple at the output of the choke changes its value for THD limitation on the load. For all solutions i.e. permeability or size analysis, the current ripple at the output of the chokes does not vary much. The constraints on maximum current on choke and limit on inductance minimum value imposed by control plus the reduction of ripple for

losses reduction all lead to same range of ripple on the caps. The losses for polypropylene capacitor are negligible compare to choke. Only the tradeoff between price and capacitor C value is researched by the algorithm.

The sizing of capacitor and choke can be achieved separately.

4.2.4 Conclusions:

In this project the design using optimization is applied with success on real constrained problem to replace existing choke solution. Discrete libraries of capacitor, magnetic material and catalog sizes are used. The implementation of libraries as input parameter in algorithm is validated lessening the time and runs to build Paretos.

Optimal sizes, permeability and parallelism are investigated and possible gains are highlighted. The optimization runs in few dozen minutes so its use required few times and efforts it would be a loss to not implement it in the design process.

4.3 DC/AC COUPLED CHOKE

4.3.1 3 levels inverter/PFC:

The second study case is a 3 levels NPC inverter of 125kVA with switching frequency 10.5 kHz (Figure 120) with two parallel converters of 62.5kVA. The existing proposition was a 2 coupled interleaved legs chokes. In a first time the gain of coupling over interleaving is presented, then optimization is achieved to investigate efficiency increase and price reduction gain compare with R&D solution. The inverter is optimized for all working cases presented in chapter III.

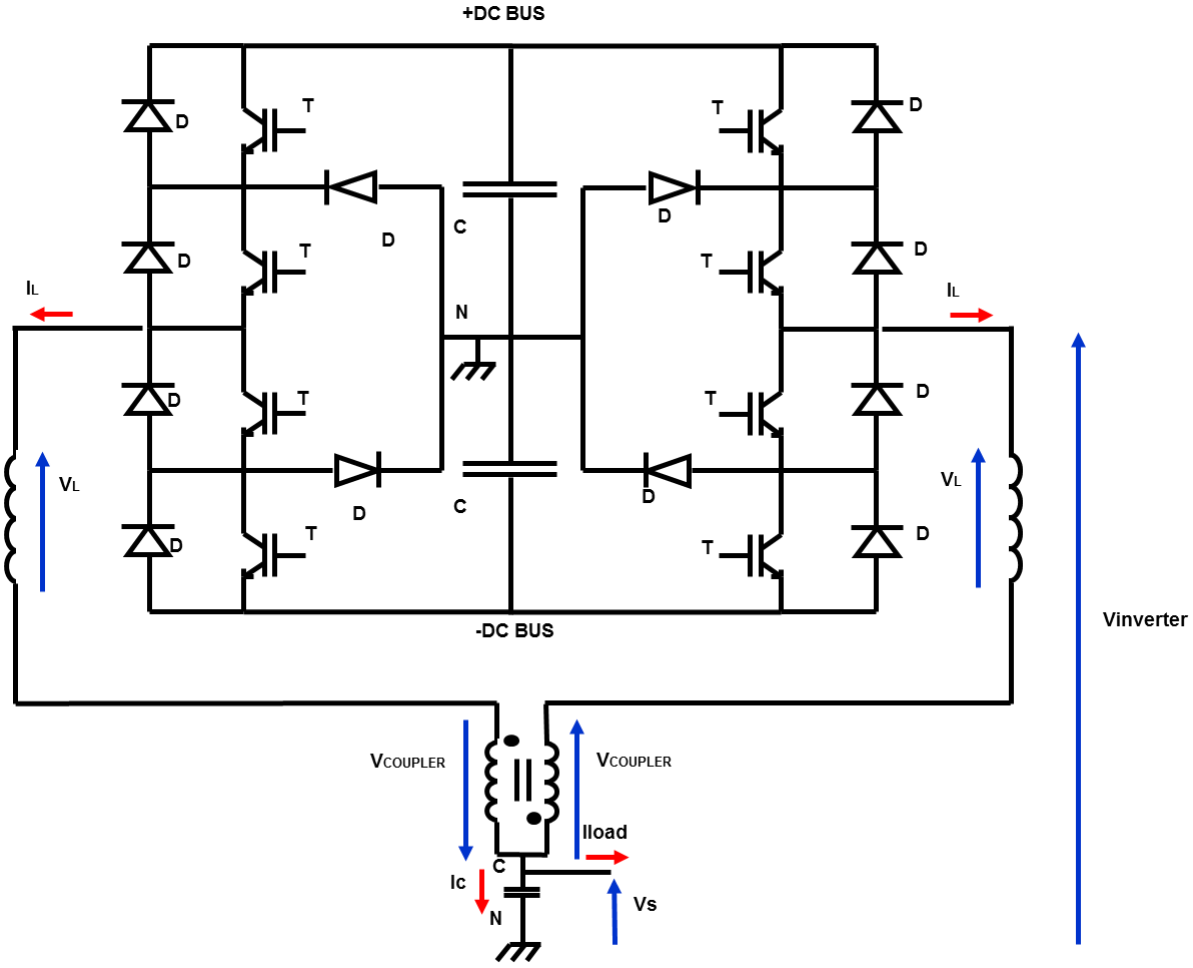

Figure 120: 3 levels NPC inverter

4.3.1.1 Interleaved solution vs coupled solution

The interleaving of legs allows the reduction of current ripple at the output (Figure 122). However the ripple is not reduced on choke themselves (Figure 121). So legs are coupled using a transformer as presented in chapter III. The coupling doubles the equivalent frequency seen by the choke and reduces the ripple on their coil (Figure 121). However a component (the coupler) is added compared to interleaved solutions and the shift is only 90° so output ripple is not drastically reduced because ripples are not in opposition as in 180° interleaving. Three optimizations are achieved; both legs are not interleaved. Then the legs are interleaved

with a 180° shift. Final optimization is done with interleaved coupled solution. The sizes are catalog ones as the materials. The objectives are the reduction of price, losses and volume. The constraints are the respect of current thresholds on the choke and the ripple to respect IGBTs maximum current, the admissible value of RMS current inside the capacitor, the THD on the load, the losses densities in coil and core and the voltage drop on legs to guarantee the capability of the inverter to deliver required sinus voltage and current. The optimizations results are presented on (Figure 123). The coupled solution is the best. A solution under Schneider Electric patent is also presented as "integrated". This pattern concerns the assembling of choke and coupler and allows significant gains on price, volume and efficiency. The capacitor is placed at the output of both connected legs. The optimal value of capacitor is slightly the same ~500µF for interleaving and ~600µF for coupling. For classic 2 chokes in parallel without interleaving the HF current is higher so capacitor need is higher for filtering ~800/900µF, (Figure 125). The THD is also dramatically reduced with interleaved and coupled solutions while with classic approach the THD always reached it higher limit of 3% for RL load (Figure 124).

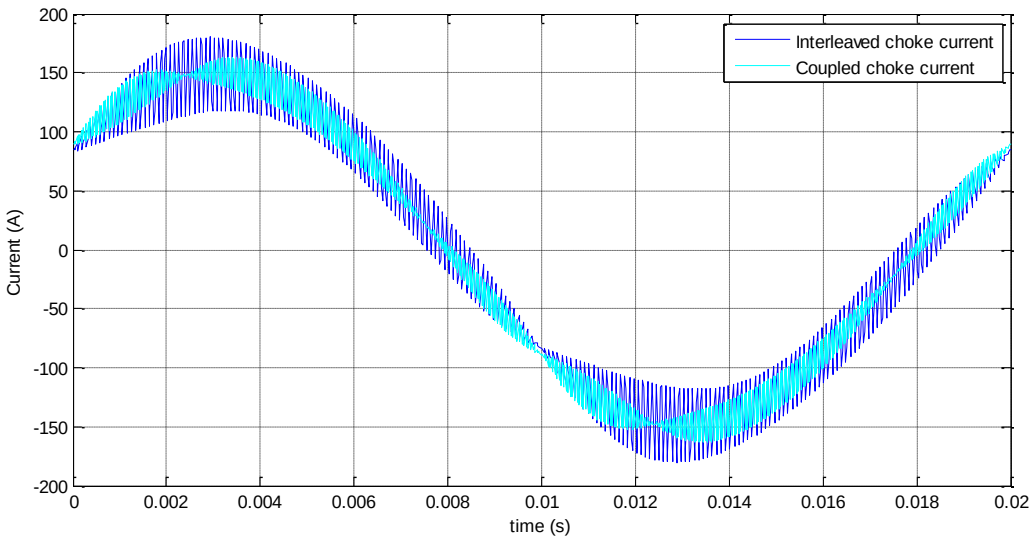

Figure 121: Current on choke for interleaved and coupled 150W solutions from optimization

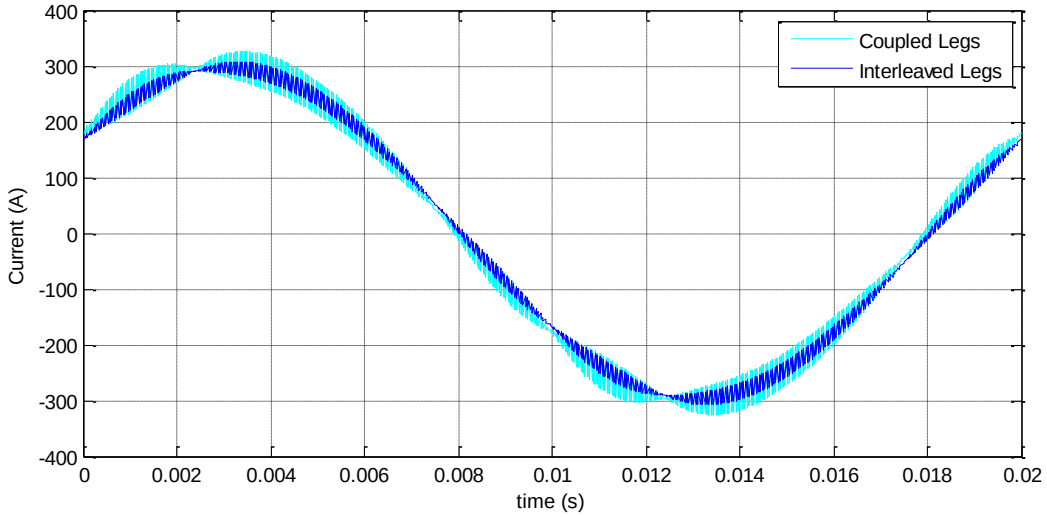

Figure 122: Legs output current for interleaved and coupled solutions

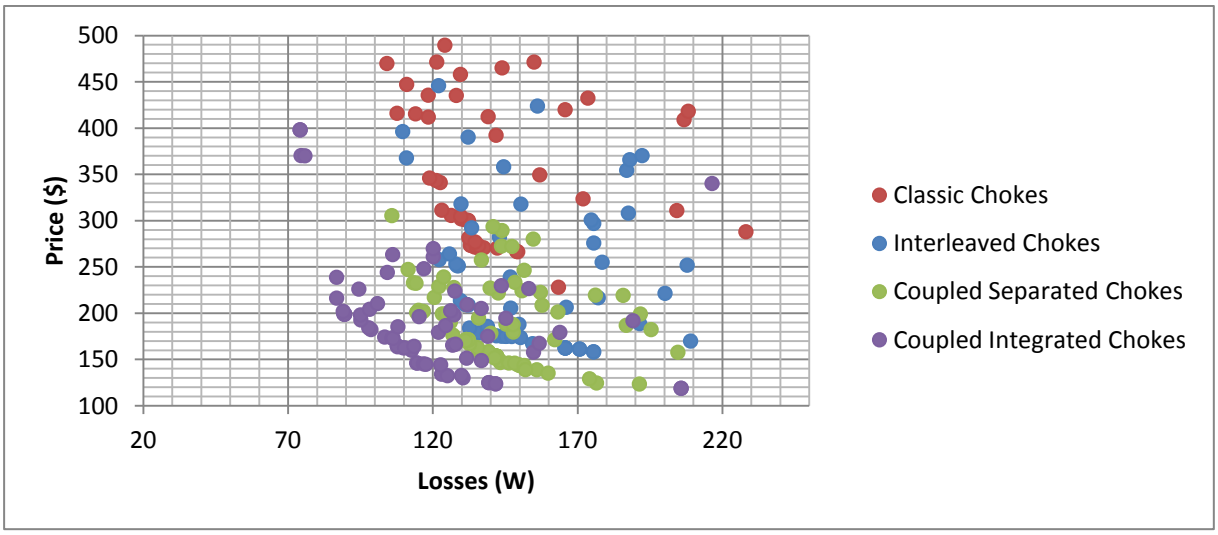

Figure 123: 3 level NPC inverter solutions for filter

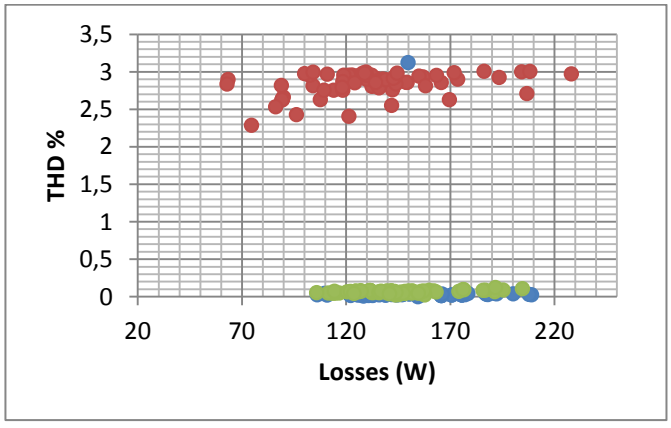

Figure 124: THD constraint for classic, interleaved and coupled solutions

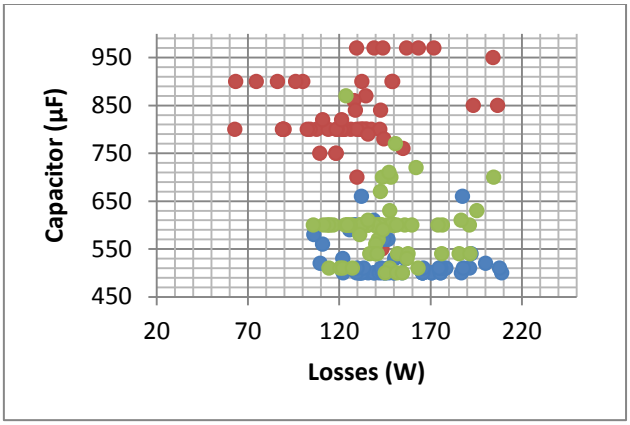

Figure 125: Capacitor value for classic, interleaved and coupled solutionsPrevious sizing vs optimization sizing

The interleaved retained solution is presented on (Figure 126). The equivalent coupled solution (chokes + coupler) are compared on (Figure 127). The gain in volume is huge. Interleaved solutions are in 5.2 inches cores while choke and coupler are 3.5 inches cores.

Figure 126: Interleaved legs filter solution

Figure 127: Interleaved chokes vs coupled solution

4.3.1 Prototype validations

The interleaved chokes have been measured under DC current condition with small square voltage pulse in order to plot the evolution of inductance regarding the current (Figure 128). Several prototypes have been supplied by different manufacturers. The simulation from model is fitting well the measurements because red curve is among the measurements curves. The variations of +/-8% of magnetic value announced by suppliers have little impact on modeling and measures.

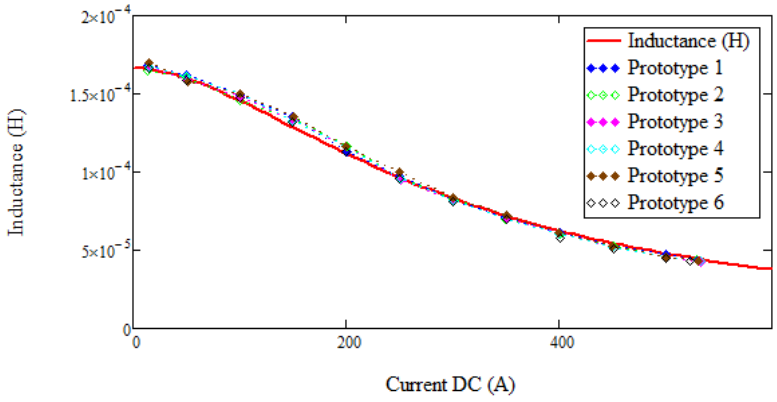

Figure 128: Evolution of inductance versus DC current

The simulation of retained solution for coupling is done using models from chapter II for components and chapter III for filter. The results are compared with measures achieved on presented prototype (Figure 127). The filter works on a RL load for full power 125kVA with power factor 0.9 and switching @10.5kHz. (Figure 129) illustrates the simulation while (Figure 130) is a scope capture. The leg voltage is in blue, the load voltage in yellow and currents on both legs are in green and magenta. The tendencies are well represented by modeling. On (Figure 131) and (Figure 132) zooms are done at peak leg current. The ripples are compared. For simulation the peak current is 139A with a ripple of 40A while measurement peak is 138A with 42A ripple. (Figure 133) and (Figure 134) illustrates the coupling effect on legs current. Note that two ripples occur for one leg voltage pulse, the frequency on chokes is well doubled.

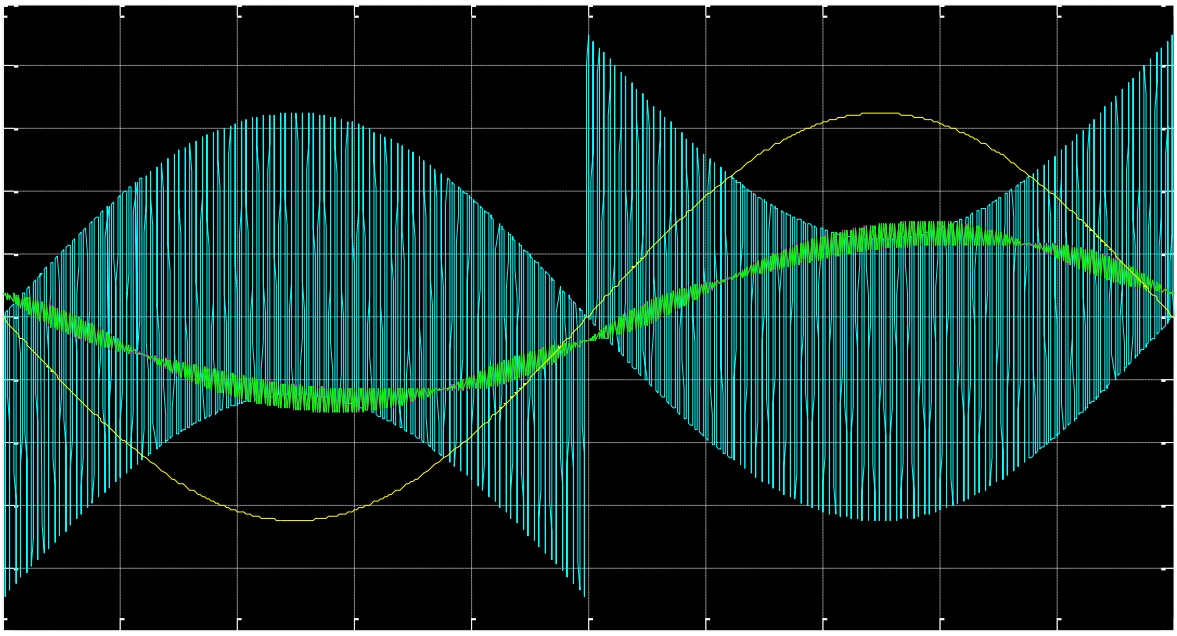

Figure 129: Coupled solution simulation using model from chapter II and III

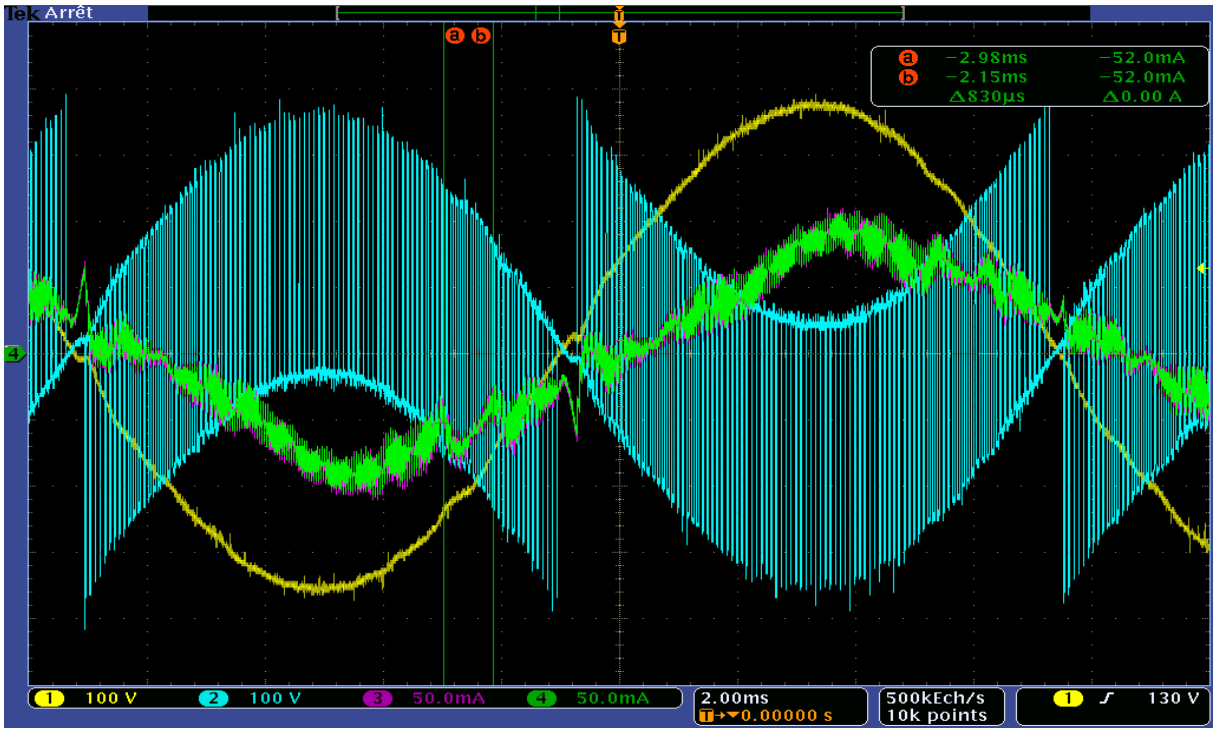

Figure 130: Measurement achieved on prototype from (Figure 127)

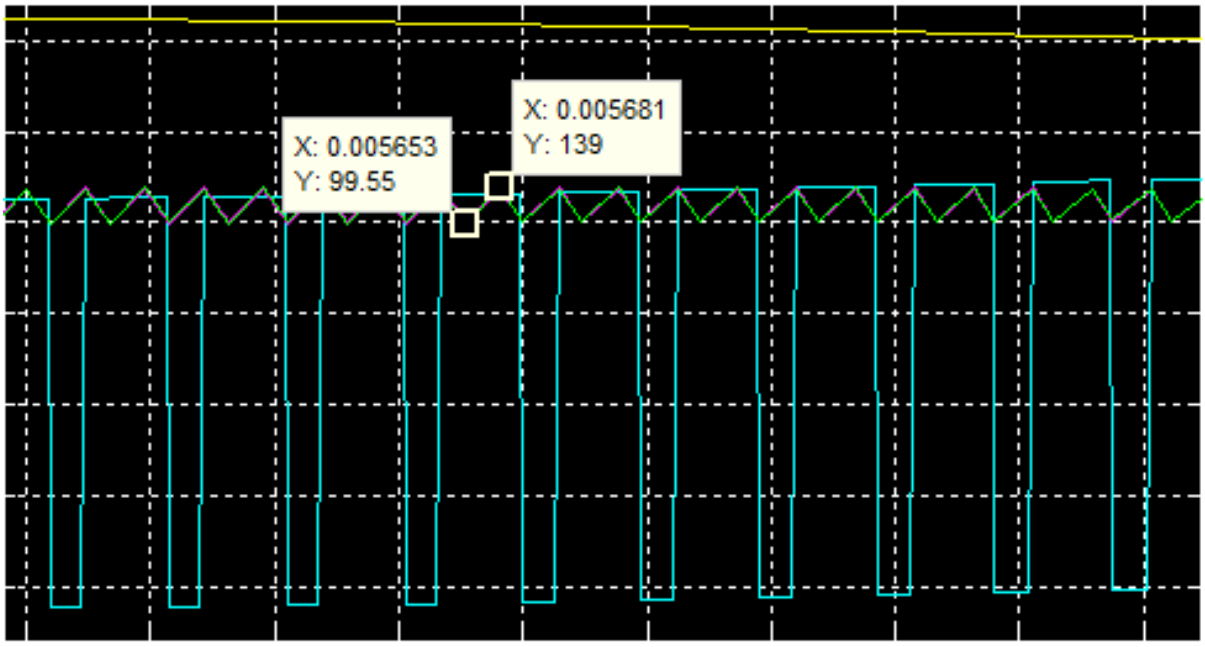

Figure 131: Simulation zoom on peak current

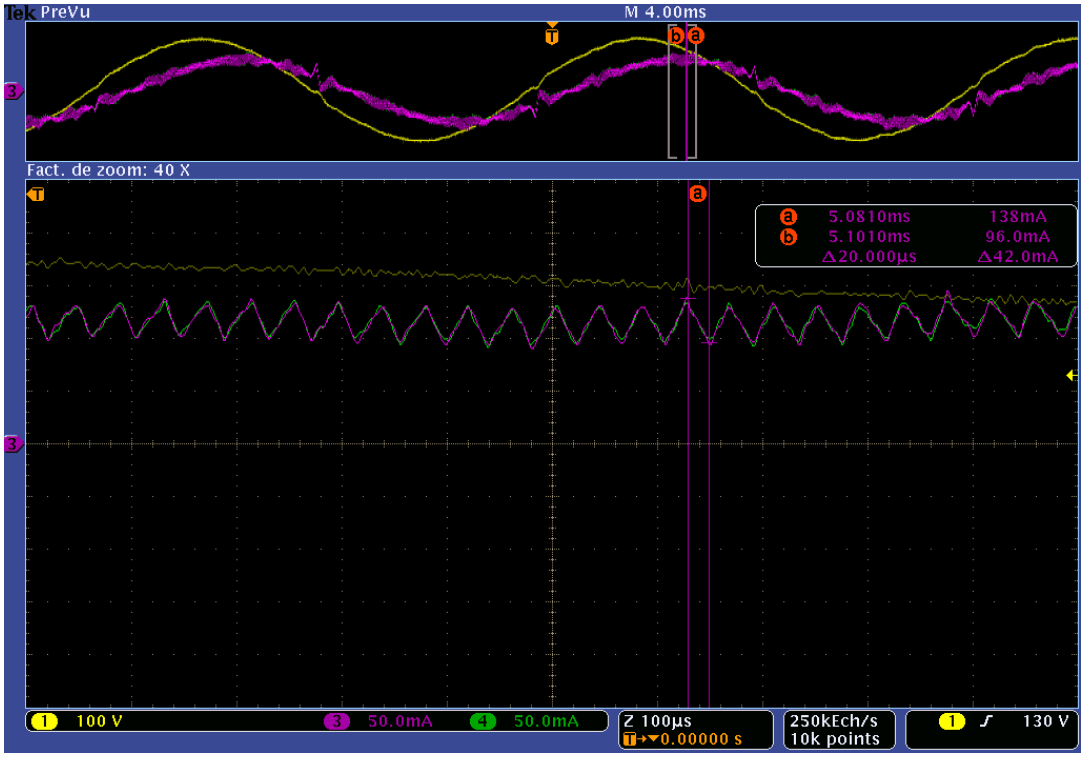

Figure 132: Measurement zoom on peak current

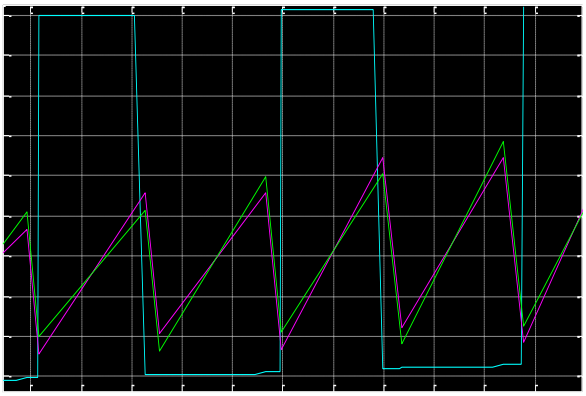

Figure 133: Simulation zoom on coupling effect

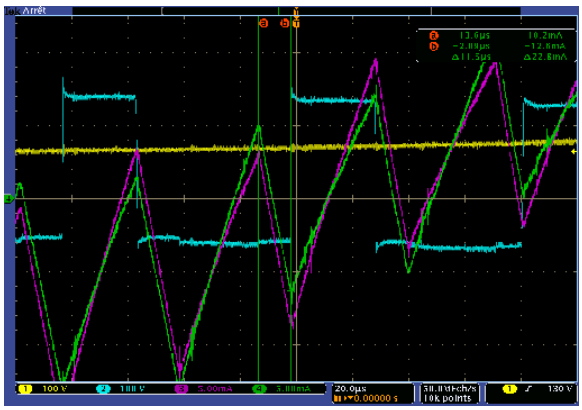

Figure 134: Measures zoom on coupling effect

4.3.2 Conclusions

A 3 level 125kVA inverter with two legs is investigated in this project. The optimization is carried out with discrete libraries of materials, wire size and core size. It allows direct prototyping from optimization results. Optimization gives Paretos for three ways to construct the output filter. Classical parallelism, interleaving and coupling are studied. Known tendencies are verified because coupled chokes are more efficient and cheaper than interleaved chokes. Classical parallelism is worst in every point without considering monitoring and regulation higher effort required in interleaving and coupling. The interleaving allows the best reduction of ripple on the output and so capacitor need and thus THD while coupling reduce dramatically the size of the chokes with doubling the frequency of choke electrical waveforms.

4.4 DC/DC COUPLED SOLUTION

4.4.1 DC/DC reversible converter

Previous project treated DC/AC or AC/DC filter. In this part three versions a 500kVA with 6 bipolar legs (450A/1200V IGBTs), a 400kVA with 4 legs and 300kVA DC/DC with 3 legs are sized using optimization. The converter is used in UPS to link batteries storage and DC capacitor bus from inverter and PFC. Component models are from chapter II and the DC/DC battery approach has been introduced in chapter III. The place allowed for the 6 legs filter is imposed, the optimization is done under geometric overall constraints. The other constraints are the limitation of RMS current ripples imposed by battery manufacturers for the four functioning mode presented in chapter III, charge and discharge with nominal modes and impacting ends of both modes. The maximum current on legs is also checked to prevent damage on IGBTs. Losses densities in coils and cores are also limited to prevent temperature rise. For cost reason the chokes/couplers must be the same for the three power UPSs. Finally the goals are the reduction of price and the increase of efficiency in charge and discharge nominal modes. Other modes being really short in time only current values leading to destruction are checked not losses.

4.4.2 Assembling investigation:

The converter is constituted of 6 independent legs we can shift or not, same for other 4 and 3 legs. A first investigation is achieved to compare possibilities of interleaving or coupling legs. But also to couple block of legs and interleaved blocks together to benefit of both coupling effect on chokes and reduction of output ripple with interleaving as seen in 4.3 results. The optimization allows the choice of the best topology (Figure 136) and assembling (Figure 135).

Figure 135: Choice of number of coupled legs vs power blocs

Figure 136: Best choice of topology

4.4.3 Best permeability:

Once the choice of assembling is done, the same approach as in 4.2.2 is used to find best materials for both choke and coupler. Coil material and parallel wires are kept the same between both choke and coupler for assembling easiness. Results of optimization are presented on (Figure 137). Losses of buck nominal mode and boost nominal mode are summed and plot with price tradeoff. (Figure 137) clearly shows that some permeabilities are better addressing zones of the Pareto. Designer choice on the tradeoff will impose the use of one material rather than another. For the coupler, the algorithm picks always the same μ5000 material. The material library is composed of 40 low permeability (μ14 to μ125) alloys and 10 medium permeability (μ200 to μ5500) amorphous and nanocrystallin.

4.4.4 Optimization results:

The previous results are presented on (Figure 138) but this time nominal boost mode and nominal buck mode are separated as they have been set as two different minimization objectives. Whereas in previous optimization global losses where set as a unique minimization objective. An interesting remark is that optimal solutions for boost mode are not the same for buck nominal mode. Indexes of solutions are labeled on the figure. The points on boost Pareto are not on the buck Pareto except for optimal solution {0,3,6,9}. Note that all solutions are not presented only 1/3 to clarify figure visibility. So the designer must done the choice between boost or buck efficiency. The buck mode being much longer than boost mode this one could be privileged during the choice. In this case the optimal solution index 0, is less than 0.2% efficiency loss so totally acceptable for the project and for the minimal price. Prototypes are currently being purchased with assembling under new Schneider Electric pattern.

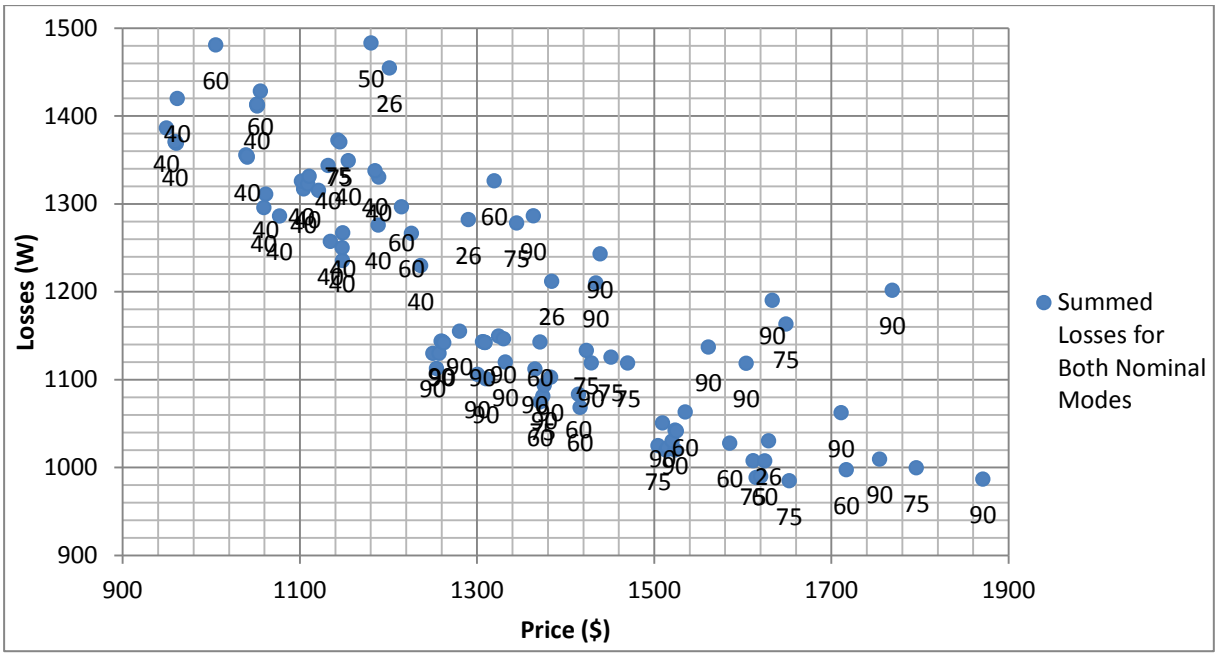

Figure 137: Best permeability for choke material, permeability as labels

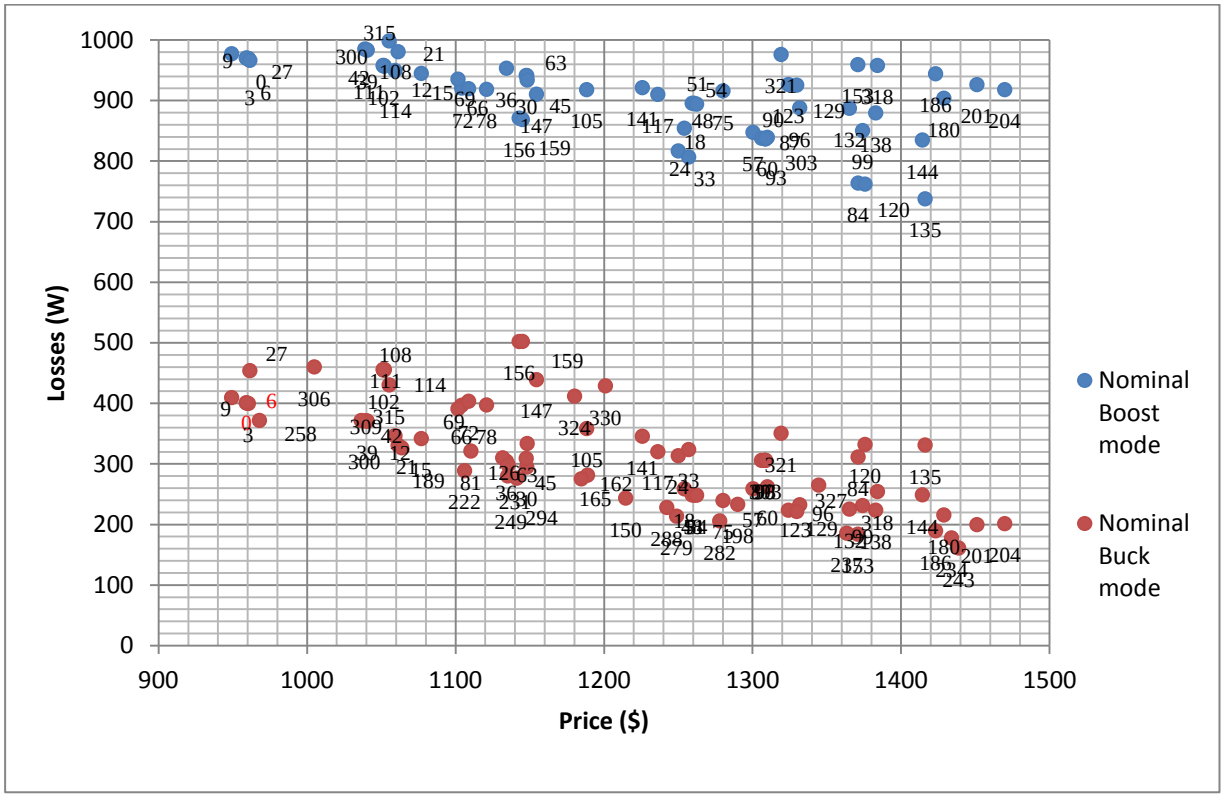

Figure 138: Paretos for nominal boost mode and nominal buck mode, results index as labels

4.4.5 Prototype validation:

Two prototypes have been done using optimization for the 6 legs DC/DC. Once is a monolithic solution with leakage flux coupling optimized using Comsol© software designed by Schneider Electric experts (Figure 139). The other is our proposition of toroid separated transformers solution (Figure 140). First conclusion is that power cabinet being small in footprint, the LEM current sensors must be close to magnetics. So leakage flux from

monolithic solution is impacting badly the acquisition and creates issues on control. Leakages being very small on toroids, the sensors are not impacted. Second conclusion is that monolithic air gaped prototype is noisy >95dB while toroid solution add only 4dB to ambient noise. Both solutions have same footprint. Temperature is tested for toroid and checked successfully at nominal power for over than 30 mins with also fault condition (Figure 141). Whereas monolithic solution saturated easily if current is not controlled equal on legs, the separated transformers solution allows great tolerance of unbalanced legs or voltage drop (Figure 143) and (Figure 145) because when saturating the transformer, all the voltage is applied to the choke part so we have still interleaved filtering. The symmetric assembling also creates an auto balance between legs preventing any issue of assembled odd components.

Figure 139: Monolithic solution

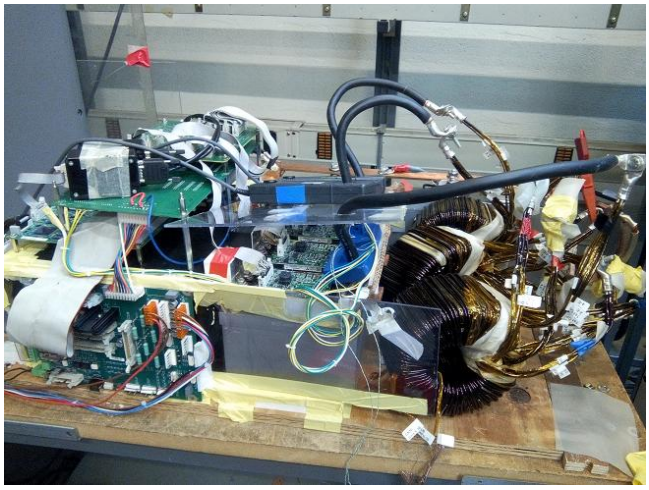

Figure 140: Toroid separated transformers solution

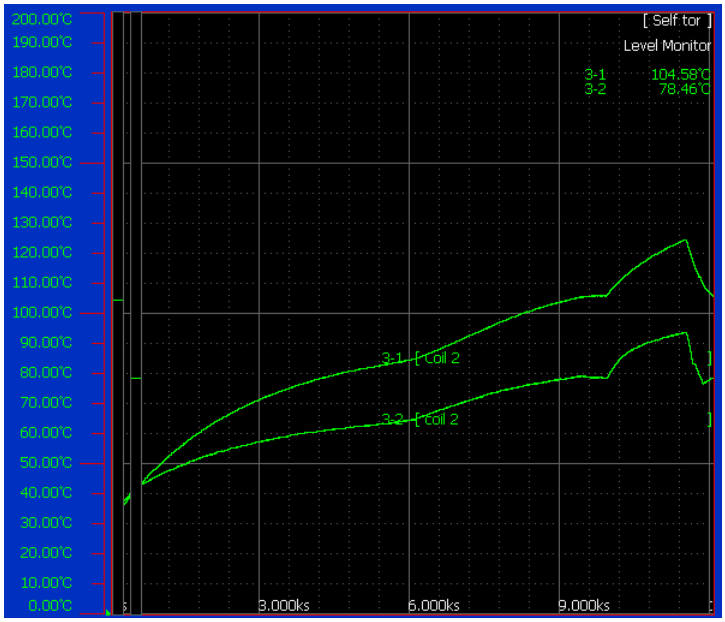

Figure 141: Temperature rise for nominal functioning with fault condition at the end, inner and outer coils temperature sensors

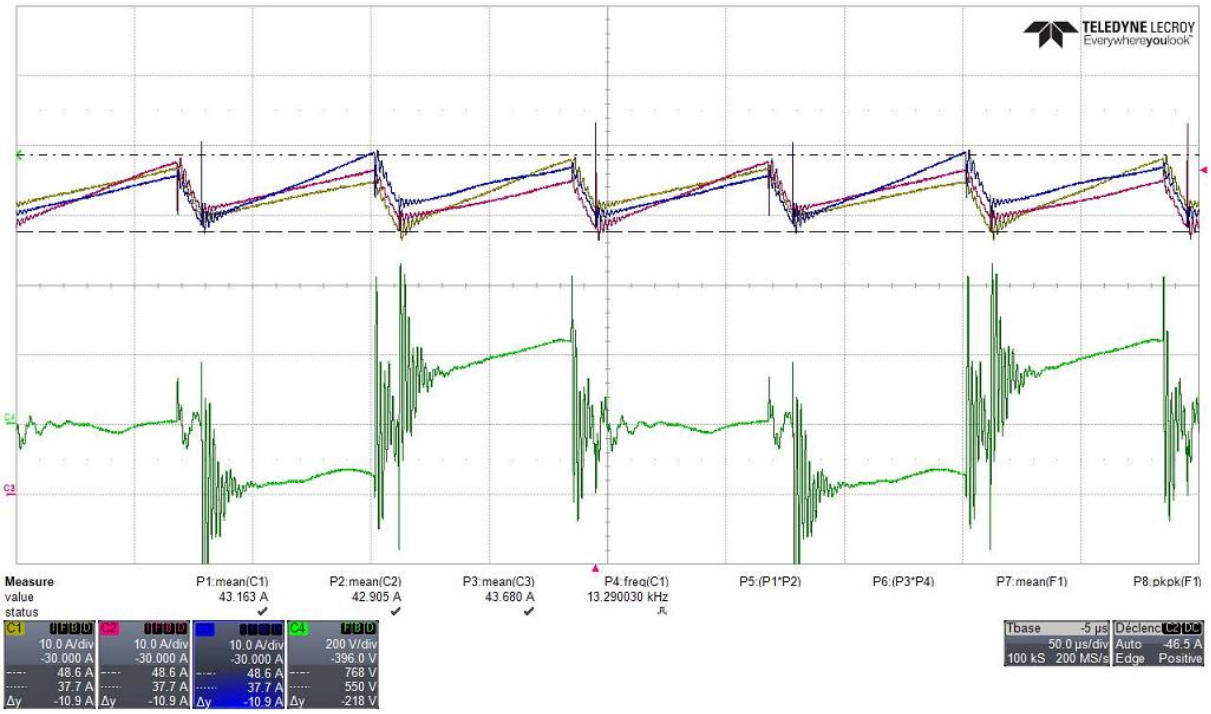

Figure 142: Normal functioning of toroid coupled legs in charging mode

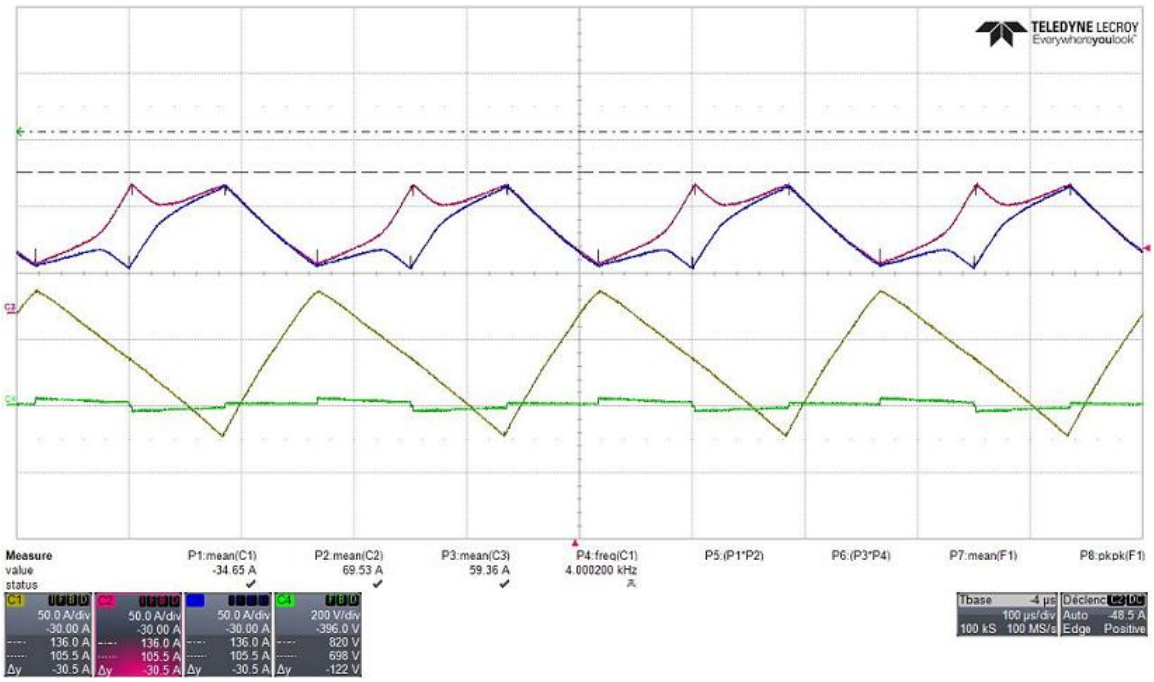

Figure 143: Fault condition with unbalanced currents on legs, the filtering is done only by choke part

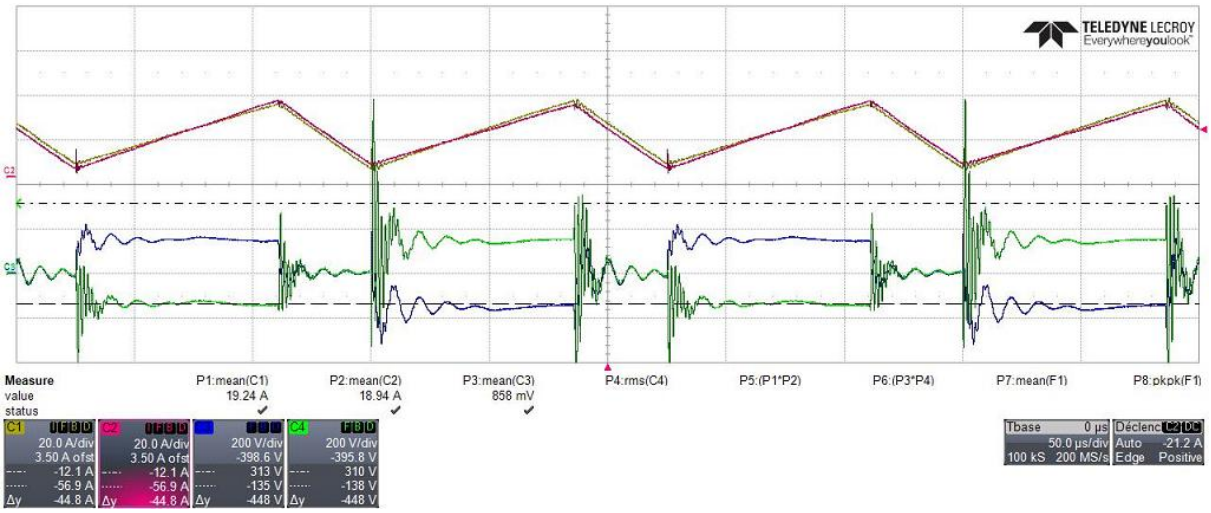

Figure 144: Normal functioning for two legs solution in charge mode

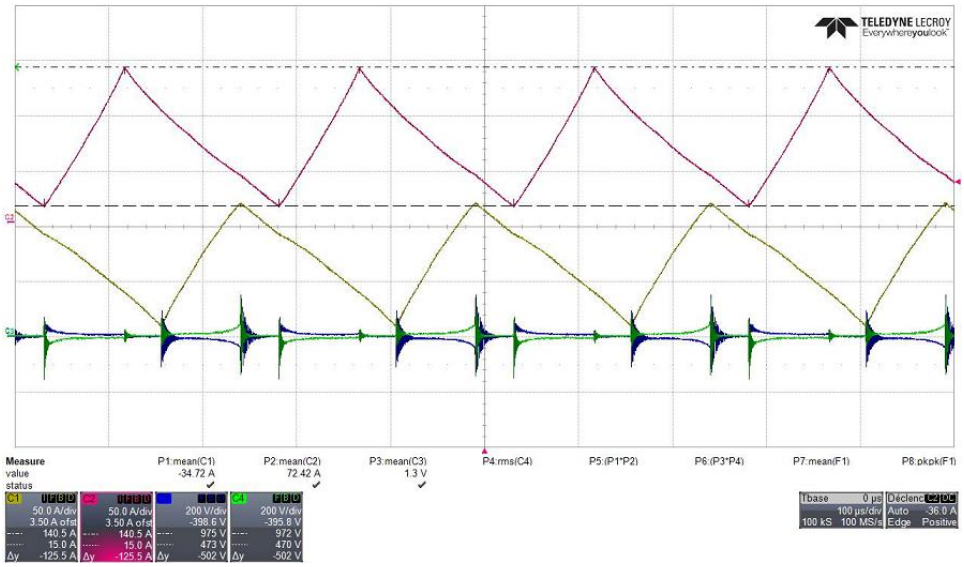

Figure 145: Fault condition, unbalanced legs currents

4.4.6 Conclusions:

A DC/DC filter is investigated for a new Schneider Electric UPS. The optimization is used to select the best assembling of the filter considering interleaving and coupling strategies. The prototypes are tested and validate all the modeling assumption and optimization results. The superiority of toroid approach is terms of efficiency, noise, easy assembling, weight and control is checked and proved over monolithic solutions.

4.5 CONCLUSIONS

The aim of the PhD was to achieve optimal sizing of passive components in UPS filter. So in this last chapter methods and models from first third chapters are implemented in optimization process. The optimization is achieved using stochastic algorithms working with discrete values for geometric and electric parameters as well as library for materials and sizes from suppliers catalogs. The goal is to get an already working solution being industrialized as optimization result. The optimizations are done with fixed topologies of converters. With this successful approach, all solutions from optimization are already the specifications for purchase.

First a 120kVA DC/AC 4 levels inverter is investigated. The replacing of an already existing solution with thermal and peak current issues is presented with successful results. The optimization is carried out under lots of geometric and electric constraints yet chained niching algorithm and GMGA are used to find optimal set of inputs for simulation models to respect all specifications. Then this topology is used as an example of several possibilities in optimal sizing approach on passive components.

The second case is a 3 levels inverter of 125kVA. Two solutions of assembling chokes in the filter are investigated, the interleaving of two legs or the coupling of the two legs. Known results are verified by optimization Paretos confirming the superiority of coupled solution. A prototype is build and measurements are done to validate model simulations. The modeling is close enough to prototype to check the effectiveness of proposed approach implemented in this PhD. Cores, conductors, capacitor and materials are catalogs.

Finally a DC/DC converter is designed using optimization process. The legs being independents the filter optimal topology is searched comparing several possibilities. The optimal electric and magnetic choice is not the optimal choice for project modularity and price gain. Indeed the second best solution is chosen because implementable in other UPS of same family but with lower power, keeping a same choke and coupler for all project reducing dramatically the total cost of the product. Like for DC/AC coupled converter, the coupled DC/DC solution is under Schneider Electric pattern and cannot be presented completely in this PhD dissertation.

The aim of the PhD is reached with successful design of industrialized filter for Schneider Electric using discrete catalogs values and accurate models. The measures done on prototypes confirm the accuracy of models and the capability of optimization to converge toward solution directly purchasable. However the optimization cannot do all the work, the designer choice and experience is still necessary.

GENERAL CONCLUSIONS

The power converter design is nowadays a complex and several years venture. In order to stay competitive i.e., reduce the time to market of UPS product and increase their efficiency, an innovating design approach is proposed in collaboration with Schneider Electric in this PhD dissertation.

The general approach of sizing using optimization algorithms is the linearization of models and inputs with the aim to implement determinist algorithms. This strategy is chosen because it can manage large number of inputs, constraints and objectives. It is also a fast method to find general tendencies of optimal size and structures of power converters. Our proposition is in addition of this approach. The tendencies and experience of power converter or topology brought by these optimizations is replaced by Schneider Electric and G2Elab experiences. Industrialized solutions work with discrete values of geometric sizes or electric parameters (e.g. number of semi-conductor, magnetic cores size, switching frequency). Then this PhD takes its place at the end of the design process when topologies and specifications are fixed. The proposition is to implement accurate models computing discrete values often from suppliers' catalogs. The aim is to provide designers with decision tools (tradeoff between several project objectives) and electrical parameters or components directly purchasable, decreasing dramatically the time to market and the need of prototyping.

In the first chapter a fast review of optimizations possibilities and algorithms is presented. The purpose is to understand the mechanisms of convergence for main types of algorithms, determinist or stochastic. This knowledge coupled with the specifications and goals of the project drove us to choose a strategy of optimization implementing stochastic evolutionary algorithms for their ability to handle discrete value and build Pareto tradeoff of objectives such as efficiency, cost reduction, footprint or volume. Conversely to determinist algorithms, niching, NSGA II or GMGA algorithms require a limited number of inputs and outputs and fast model calculation.

Then in chapter II models addressing these issues are proposed. Two guidelines are followed: modeling accurate behavior of passive component inside power converters respecting low time computation must be achieved limiting the required parameters and constraints. The difficulty is to provide enough information inside the model for optimization to converge on exact solutions without complicating the modeling. Accuracy is not necessarily synonym of complexity, and simplifications have to be proposed. Thus magnetic material behavior, conductors and capacitors are investigated to scale impact of different parameters to highlight important ones and strong interactions between components. But also to discard irrelevant modeling effort such as dynamic hysteresis models for thin hysteresis material used inside our filter. The strong impact of conductors on efficiency increase led us to focus on their behavior. To address all issues of actual models and simulate brand new coil technologies an unrivaled approach is presented and implemented in this PhD.

The second guideline is provided by aim to work with catalogs size and material. Indeed accurate and relevant models can be implemented after measurements campaigns and tests. But working from suppliers 'datasheets, it is logical to build models from those. Moreover, measures are expensive in time and cost and cannot be achieved on every new material or

semi-conductor modules proposed each year. Thus models based on datasheets are preferred and presented. A slight degradation of accuracy is acceptable if the models still provides essential information to algorithms to converge on pertinent solution. Datasheets have few lacks in available curves but suppliers could easily make additional tests and add in catalogs, based on Schneider Electric demand. Finally, some propositions are presented on component geometric definition to suppress constraints and relax the algorithm.

The optimization, although giving optimal solution to a problem if correctly implemented does not bring technology breakthroughs. Interesting researches could be done on definition of power converter for optimization to find new topology or geometry but is not part of this dissertation neither of actual known papers. Thus few investigations are proposed on promising approach for new magnetics assembling or coil geometry and winding.

Models and optimizations methods being introduced filter models for DC/AC, AC/DC and DC/DC conversions are presented respecting same considerations than passive component models. In the aim of gaining computation time and speeding up the optimization, assumptions are proposed and validated to model the filter in parts with no close control loops. Power converters, especially in UPS are subject to several working cases, different loads and perturbations free requirements. All impacting the sizing of converter parts. The UPS is supposed to deliver harmonic free power to secured loads and works with battery storage sensible to current ripples. These considerations are presented and impacts on passive components design explained. Few validations are shown on Schneider Electric UPS.

In the last chapter implementation of previous models, methods and strategies is presented on three power converters. The demonstration is made of possible analysis and gains over traditional design approach using optimization. Optimizations using catalog size and materials are run and prototypes are purchased and measured to validate the proposed method. However when talking about optimization it is awkward to consider fixed sizes and not optimal sizes. Thus a rapid survey is done on gains in efficiency, cost and volume done with free continuous parameters. The purchasing of component based on optimal solution has a cost which must be considered and once again the Paretos from optimization are a useful tool for deciders.

In works to come the discrete optimization of converters will be extended to active component also bought on catalogs. Thermal analysis will be implemented and impact on sizing analyzed. At the present time thermal is used as a check on losses density inside component but we could wonder if its implementation in optimization process could lead to prefer flat toroid rather than thin high one, or maybe other geometries. Other works have been achieved by internships on control consideration or three-phase electric power filter.

The optimization is a wonderful assistance approach for designer and industrial to create new better products with energy saving. However it is still a tool and the designer cannot be abide. Problems are various and of different natures or submitted to different requirements so no general method can be found.

The machine cannot replace entirely the man and its faculty of decision and analysis, but it can help in providing decision tools.

APPENDIX A

1st and 2nd order Algorithms

The determinist algorithms of 1st and 2nd order are often used to solve large system of linear equations written as matrix equality:

$$A.x = b$$

Where A and b are known and x is the vector of inputs we search. Some tools on matrix will be used in this annex:

$$(A.B)^T = B^T.A^T$$
$$(A.B)^{-1} = B^{-1}.A^{-1}$$
$$A \text{ positive if } x^T.A.x > 0$$
$$A \text{ orthogonal to } B \text{ if } A^T.B = 0$$

The first assumption for gradient based optimization is that the objective function f with the vector of inputs can be expended as a quadratic form:

$$f(x) = \frac{1}{2}.x^T.A.x - b^T.x + c$$

This form is chosen because the minimum of f is found for A.x=b. Indeed f described a paraboloid (Figure 146) and if A is definite positive the differentiation of the quadratic form gives:

$$f'(x) = A.x - b$$

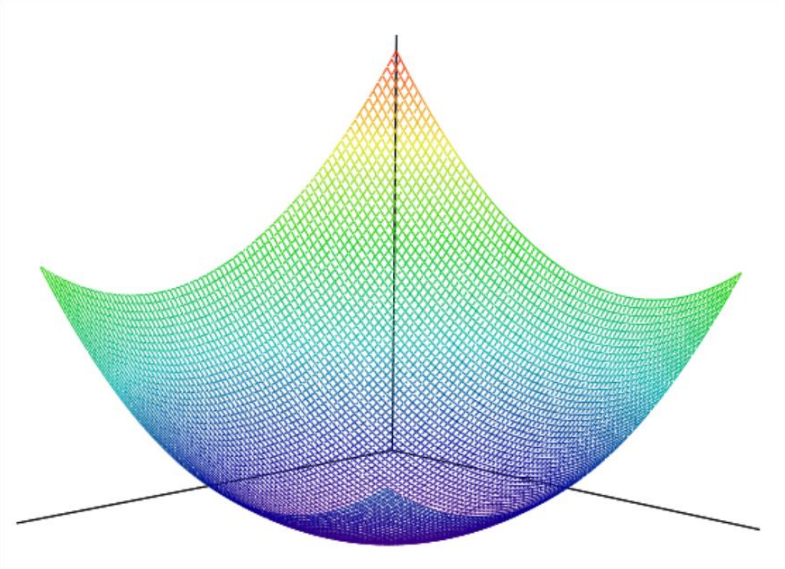

Figure 146: Paraboloid of objective function quadratic form

And when this derivative is null the solution corresponds to the linear system. So when this minimum is found for the vector x, the same vector x is solution to the system of linear equations. This approach is an easy solving pattern because the minimum of a quadratic form is unique and the form is smooth and intuitive. The other widely used approach is to find the intersection of hyperplanes defines each by an equation of the system.

The 1st and 2nd order methods are sequential meaning we start from an x_0 point and we slide from point to point towards the final solution x_n. To take a step the better way is to go in opposite direction of the gradient of *f* at the point x. Indeed the gradient expresses the greatest increase of *f*. So the next point will be:

$$x_{i+1} = x_i - \alpha \nabla_x f$$

α is a scalar setting the size of the step from x_i to x_{i+1}.

The residual indicates how far the solution with vector x_i is from b:

$$r_i = b - A.x_i$$

So with this definition and the one of the gradient of the quadratic form of *f* the step between to point is:

$$x_{i+1} = x_i + \alpha.r_i$$

The question is how to choose size of the step α? At a point x_i, the gradient defines a vertical plane. The 2D projection is a line on the paraboloid (Figure 147). So finding α is finding a value on a line, this is the Line search procedure. On the figure we see that a best value of α can be find otherwise part of the previous direction will be contain in the next direction. This is a loss of time and efficiency. Another way to formulate this is that next direction must be orthogonal to the previous direction. With matrix definition of orthogonallity we then have:

$$\begin{aligned}
&r_{i+1}^T.r_i = 0 \\
&(b - A.x_{i+1})^T.r_i = 0 \\
&(b - A.(x_i + \alpha.r_i))^T.r_i = 0 \\
&(b - A.x_i)^T.r_i - \alpha.(A.r_i)^T.r_i = 0 \\
&r_i^T.r_i - \alpha.(A.r_i)^T.r_i = 0 \\
&\alpha = \frac{r_i^T.r_i}{r_i^T.A.r_i}
\end{aligned}$$

This approach requires two matrix-vector multiplications per iteration. The computational cost of gradient method is dominated by these products. Fortunately one can be eliminated by multiplying both side of step definition by –A and adding b, we have:

$$r_{i+1} = r_i - \alpha_i.A.r_i$$

The convergence process of gradient is presented on (Figure 148).

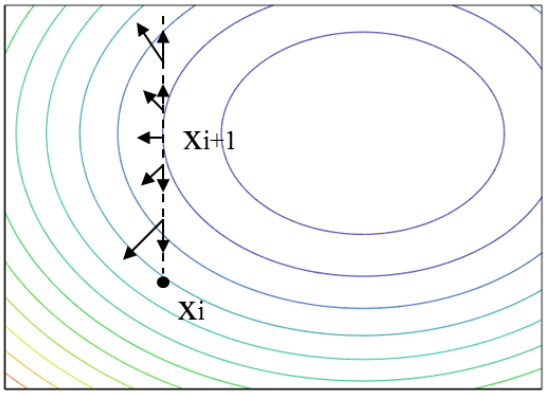

Figure 147: 2D projection of the gradient on the paraboloid surface of *f*

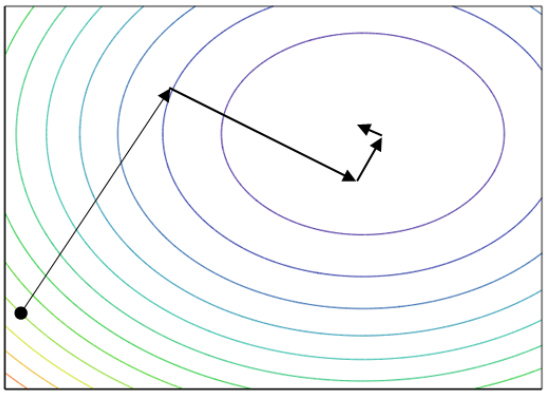

Figure 148: Gradient convergence towards minimum of quadratic form

For example, in the Bi-sphere problem:

$$f1(x_1, x_2) = (x_1 - 1)^2 + x_2^2$$

$$f2(x_1, x_2) = (x_2 - 1)^2 + x_1^2$$

The quadratic form of the objective function f to minimize f_1 and f_2 simultaneously towards o_1 and o_2 is written:

$$f(x_1, x_2) = \frac{1}{2}.(x_1 \quad x_2).\begin{pmatrix} 4 & -a \\ a & 4 \end{pmatrix}.\begin{pmatrix} x_1 \\ x_2 \end{pmatrix} - (1 \quad 1).\begin{pmatrix} x_1 \\ x_2 \end{pmatrix} + \begin{pmatrix} 1-o_1 \\ 1-o_2 \end{pmatrix}$$

The constant a is unset because whatever the value it only serve to eliminate cross product $x_1 * x_2$. So the pattern of gradient optimization for Bi-sphere will be finding $f(x_1,x_2) = 0$ by repeatedly calculating from initial vector ($x1_0$, $x2_0$) and checking after each step if x_{i+1} is satisfying minimization:

$$r_0 = b - A.x_0$$
$$r_{i+1} = r_i - \alpha_i.A.r_i$$
$$\alpha = \frac{r_i^T.r}{r_i^T.A.r_i}$$
$$x_{i+1} = x_i + \alpha.r_i$$

Now we see from (Figure 148) that this method is not the most efficient one because same search direction can be chosen several times. Indeed search direction is orthogonal to the previous one but not to all previous search direction. It will be better to choose direction orthogonal to every previous ones.

So a family of A-orthogonal search direction d_i is built. Two vectors are A-orthogonal or conjugates if $d_i^T.A.d_j = 0$ with $i > j$. Then all new d_i will be orthogonal to all previous d_j. So this time we want to express the next residual in a A-orthogonal direction search from previous residual:

$$r_{i+1} = r_i - \alpha_i.Ad_i$$

Once again we find α by expressing the orthogonality between next residual and previous A-orthogonal search direction:

$$r_{i+1}{}^T.d_i = 0$$
$$(r_i - \alpha_i.A.d_i)^T.d_i = 0$$
$$r_i^T.d_i - \alpha.(A.d_i)^T.d_i = 0$$
$$\alpha = \frac{r_i^T.d_i}{d_i^T.A.d_i}$$

The A-orthogonality is chose because each new residual r_{i+1} is just a linear combination of the previous residuals and product $A.d_i$. So, if we take the subspace $S_i = \{d_0,d_1,\ldots,d_{i-1}\}$, hence, the subspace S_{i+1} is formed from the union of S_i and the subspace $A.S_i$, thus $S_i = \{d_0,A\ d_0,\ldots,A^{i-1}\ d_0\}$, $S_i = \{r_0,A\ r_0,\ldots,A^{i-1}\ r_0\}$. This is a *Krylov subspace*, a subspace created by repeatedly applying a matrix to a vector. It has the good property that because $A.S_i$ is include in S_{i+1}, if r_{i+1} orthogonal to S_{i+1} implies r_{i+1} is A-orthogonal to S_i. So r_{i+1} is already A-orthogonal to all the previous directions except d_i. So this is not necessary to store old search vectors to ensure the A-orthogonality of the new one.

All is needed is to build a set of A-orthogonal search directions. For that we use Gram-Schmidt process. From a family of vector $\{v_0,v_1,\ldots,v_{i-1}\}$ to build the A-orthogonal family $\{d_0,d_1,\ldots,d_{i-1}\}$ the vector u_i is taken and any components that are not A-orthogonal to the previous d vectors are subtracted []. In other words the new direction vector di is built from u_i and linear combination of previous orthogonal directions:

$$d_i = u_i + \sum_{k=0}^{i-1} \beta_{ik}.d_k$$

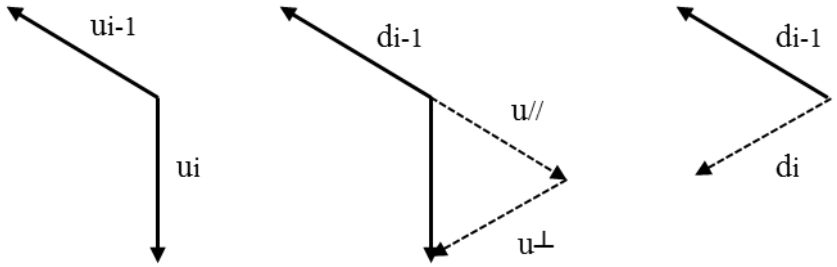

Figure 149: Gram-Schmidt conjugation of two vectors. Vector u_{i-1} and u_i are not orthogonal. d_{i-1} is set as u_{i-1}. u_i is constituted from a component u// parallel to d_{i-1} and a component $u^{\perp}$ A-orthogonal to d_{i-1}. After conjugation only the A-orthogonal part remains.

B_{ik} is defined only for k<i. To find their value we write the A-orthogonality between d_i and previous direction d_j:

$$d_i^T.A.d_j = u_i^T.A.d_j + \sum_{k=0}^{i-1} \beta_{ik}.d_k^T.A.d_j$$

$$0 = u_i^T.A.d_j + \beta_{ij}.d_j^T.A.d_j$$

$$\beta_{ij} = -\frac{u_i^T.A.d_j}{d_j^T.A.d_j}$$

Now if we take the vector family of residuals in place of u family. The new search direction d_{i+1} is built from residual r_{i+1} and $A.d_i$ which is included in r_{i+1} with Gram Schmidt coefficient β_{i+1} insuring A-orthoganility between r_i and r_{i+1}.

All together the optimization with A-orthogonality is:

$$r_0 = d_0 = b - A.x_0$$

$$\alpha = \frac{r_i^T.r_i}{d_i^T.A.d_i}$$

$$x_{i+1} = x_i + \alpha.d_i$$

$$r_{i+1} = r_i - \alpha_i.A.d_i$$

$$\beta_{i+1} = \frac{r_{i+1}^T.r_i}{r_i^T.r_i}$$

$$d_{i+1} = r_{i+1} + \beta_{i+1}.d_i$$

The gain compare to simple gradient convergence is huge because same direction will never be taken twice (Figure 150).

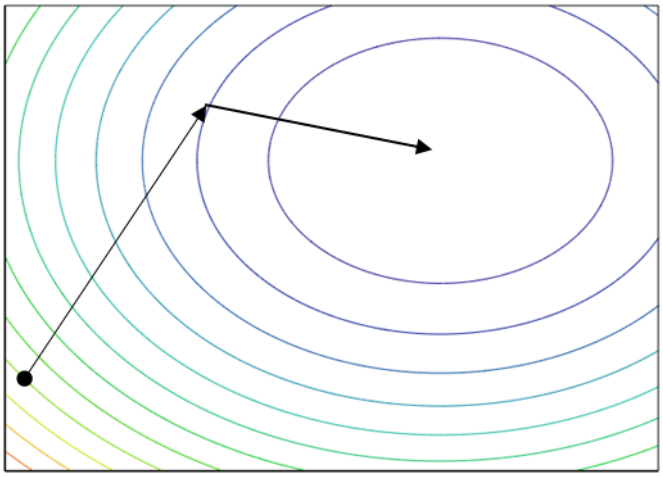

Figure 150: Convergence of gradient method with conjugate directions

APPENDIX B

Loss Surface static hysteresis

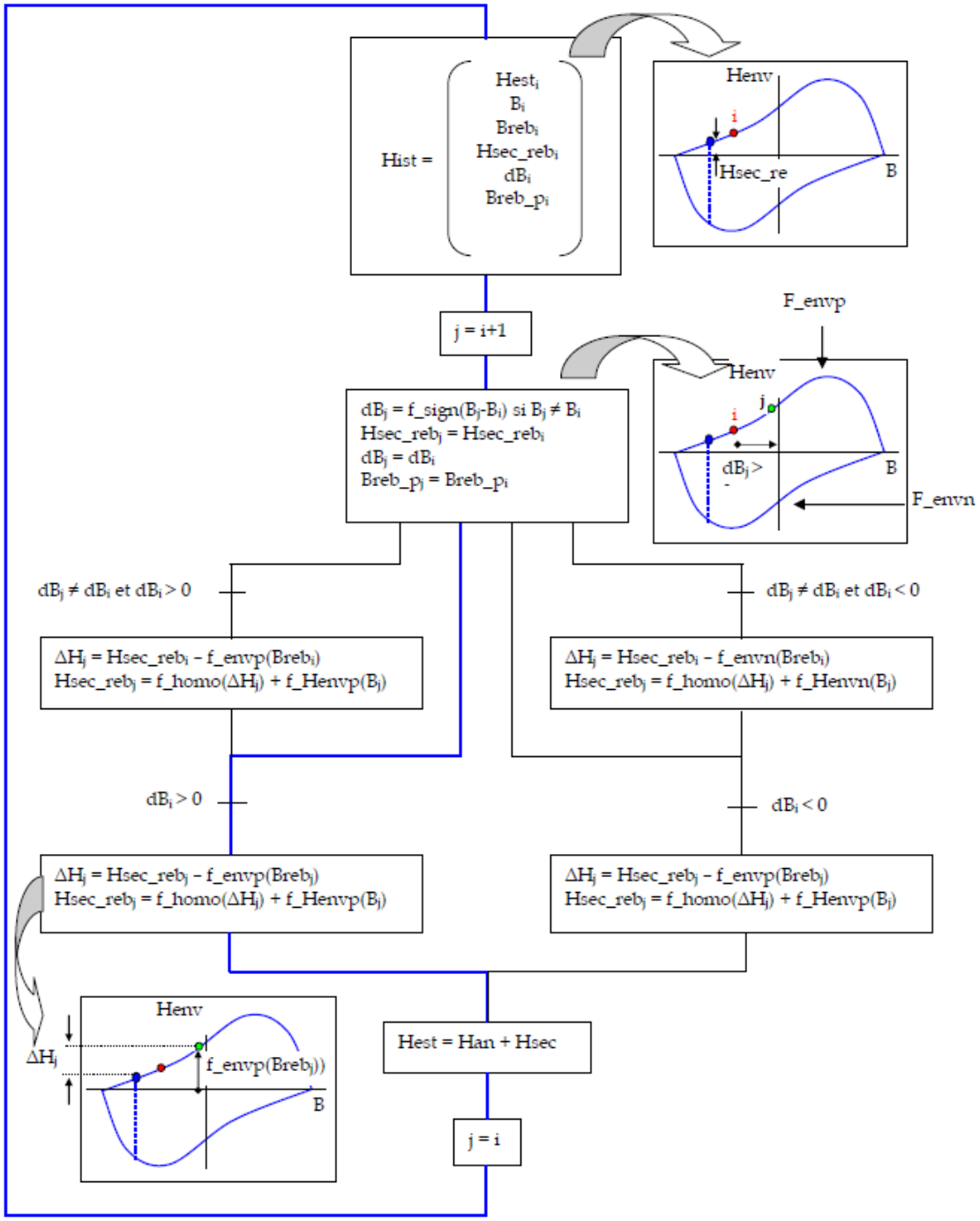

APPENDIX C

The A-model – Mathematic basics

In this appendix, some mathematics is introduced to help in A-model formulas development. The solutions are based on Bessel equation:

$$\frac{d^2}{dx^2}f + \frac{a}{x}.\left(\frac{d}{dx}f\right) + \left(b.x^p + \frac{c}{x^2}\right).f = 0$$

This equation has the general solution:

$$f = x^{\frac{1-a}{2}}.Z_v\left(\frac{2.\sqrt{b}}{p+2}.x^{\frac{p+2}{2}}\right) \quad \text{with} \quad v = \frac{\sqrt{(1-a)^2 - 4.c}}{p+2}$$

The function Z is a Bessel function defined by:

$$Z_v(z) = A.J_v(z) + B.Y_v(z)$$

J are the first kind Bessel function and Y the second kind Bessel function. The Z Bessel function has the following useful properties:

$$\frac{d}{dx}\left[Z_v(kx)\right] = k.Z_{v-1}(kx) - \frac{v}{x}.\left[Z_v(kx)\right] \quad \text{if} \quad Z = J, Y, I$$

$$\frac{d}{dx}\left[Z_v(kx)\right] = -k.Z_{v+1}(kx) + \frac{v}{x}.\left[Z_v(kx)\right] \quad \text{if} \quad Z = J, Y, K$$

$$\int_{v=0}^{u} v.J_0(v).dv = u.J_1(u)$$

$$J_{-n} = (-1)^n.J_n$$

Considering now the Helmholtz equation for magnetic potential expressed in polar coordinate:

$$\frac{d^2}{dr^2}A(r,\varphi) + \frac{1}{r}.\left(\frac{d}{dr}A(r,\varphi)\right) + \frac{1}{r^2}.\frac{d^2}{d\varphi^2}A(r,\varphi) = -\mu.J$$

We see that it is an equation that can be solved using Bessel. However the magnetic potential relies on two parameters r and φ. The separation of variables for expressing the solution can be proved:

The magnetic potential A(r,φ) is separated in two functions R(r) and Q(φ).

$$\frac{\partial A}{\partial r} = \frac{\partial R}{\partial r}.Q + \frac{\partial Q}{\partial r}.R = \frac{\partial R}{\partial r}.Q$$
$$\frac{\partial A}{\partial \varphi} = \frac{\partial R}{\partial \varphi}.Q + \frac{\partial Q}{\partial \varphi}.R = \frac{\partial Q}{\partial \varphi}.R$$

$$\frac{\partial}{\partial\varphi}\left(\frac{\partial Q}{\partial\varphi}.R\right)=\frac{\partial^2 Q}{\partial\varphi^2}.R+\frac{\partial R}{\partial\varphi}.\frac{\partial Q}{\partial\varphi}=\frac{\partial^2 Q}{\partial\varphi^2}.R$$

$$\frac{1}{r}.\frac{\partial}{\partial r}\left[r.\left(\frac{\partial R}{\partial r}.Q\right)\right]=\frac{1}{r}.\left[\left(\frac{\partial R}{\partial r}.Q\right)+r.\left(\frac{\partial^2 R}{\partial r^2}.Q+\frac{\partial R}{\partial r}.\frac{\partial Q}{\partial r}\right)\right]=\frac{1}{r}.\left[\left(\frac{\partial R}{\partial r}.Q\right)+r.\left(\frac{\partial^2 R}{\partial r^2}.Q\right)\right]$$

So all part of the polar expression of Helmholtz equation can be expressed with function R and Q independents. That why the solution using Fourier series expansion can be expressed as:

$A_z(r,\varphi)=\sum_{n=-\infty}^{+\infty}C_n(r).e^{j.n.\varphi}$ where the Cn function are all Bessel solutions.

The A-model – Reflection and transmission coefficients

The coefficient of reflection allowing sweeping from a decreasing potential to an increasing one and the transmission coefficient to sweep from increasing potential to the potential inside a solid round conductor are deduced from continuity of flux density through a surface.

The formulas of magnetic potential are reminded. In a solid round conductive area:

$$A_z(r,\varphi)=\frac{\mu_i I_i}{2\pi k r_i}\frac{J_0(kr)-J_0(kR_i)}{J_1(kR_i)}+\sum_{n=1}^{+\infty}J_n(kr)(p_n\cos(n\varphi)+q_n\sin(n\varphi))$$

In a non-conductive area:

$$A_z(r,\varphi)=-\frac{\mu_i I_i}{2\pi}\ln(\frac{r}{R_i})+\sum_{n=1}^{+\infty}r^n(a_n\cos(n\varphi)+b_n\sin(n\varphi))+\sum_{n=1}^{+\infty}r^{-n}(\alpha_n\cos(n\varphi)+\beta_n\sin(n\varphi))$$

We have using the Maxwell equation B = rot(A):

$$B_r(r,\varphi)=\frac{1}{r}.\left(\frac{dA(r,\varphi)}{d\varphi}\right)\qquad B_\varphi(r,\varphi)=-\frac{dA(r,\varphi)}{dr}$$

So inside the conductor it gives:

$$B_r(r,\varphi)=\sum_{n=1}^{+\infty}\frac{n.J_n(kr)}{r}(-p_n\sin(n\varphi)+q_n\cos(n\varphi))$$

$$B_\varphi(r,\varphi)=\frac{\mu_i I_i}{2\pi r_i}\frac{J_1(kr)}{J_1(kR_i)}-\sum_{n=1}^{+\infty}\left(k.J_{n-1}(kr)-\frac{n}{r}.J_n(kr)\right)(p_n\cos(n\varphi)+q_n\sin(n\varphi))$$

In the air:

$$B_r(r,\varphi)=\sum_{n=1}^{+\infty}n.r^{-n-1}(-\alpha_n\sin(n\varphi)+\beta_n\cos(n\varphi))+\sum_{n=1}^{+\infty}n.r^{n-1}(-a_n\sin(n\varphi)+b_n\cos(n\varphi))$$

$$B_\varphi(r,\varphi) = \frac{\mu_i I_i}{2\pi r_i} + \sum_{n=1}^{+\infty} n.r^{-n-1}(\alpha_n \cos(n\varphi) + \beta_n \sin(n\varphi)) - \sum_{n=1}^{+\infty} n.r^{n-1}(a_n \cos(n\varphi) + b_n \sin(n\varphi))$$

Expressing the continuity on the external radius R of the conductor for all n^{th} terms we have the solutions:

$$R^{-n}.a_n + R^n.\alpha_n = J_n(kR).p_n \qquad R^{-n}.a_n - R^n.\alpha_n = \left[\frac{kR}{n}.J_{n-1}(kR) - J_n(kR)\right].p_n$$

We get the ratios called reflection and transmission:

$$\mathrm{Re}_n = \frac{\alpha_n}{a_n} = \frac{\beta_n}{b_n} = R_i^{2n}\left[\frac{2n}{kR_i}\frac{J_n(kR_i)}{J_{n-1}(kR_i)} - 1\right]$$

$$Tr_n = \frac{p_n}{a_n} = \frac{q_n}{b_n} = R_i^n \frac{2n}{kR_i J_{n-1}(kR_i)}$$

The A-model – Change of coordinates system

In the A-model the change of coordinates is used to switch from one expression of the magnetic potential to another. The several possibilities used in multi-wire, magnetic core consideration or other geometries are presented bellow. To link round areas between them it is useful to switch between the both expressions of magnetic potential in non conductive areas:

$$A_{z\_increasing}(r,\varphi) = \sum_{n=1}^{+\infty} r^n(a_n \cos(n\varphi) + b_n \sin(n\varphi))$$

$$A_{z\_decreasing}(r,\varphi) = -\frac{\mu_i I_i}{2\pi}\ln(\frac{r}{R_i}) + \sum_{n=1}^{+\infty} r^{-n}(\alpha_n \cos(n\varphi) + \beta_n \sin(n\varphi))$$

The first possibility is to express the decreasing part of the magnetic potential as an increasing formula in another coordinate system presented in chapter II. The others are presented in this appendix.

From increasing to increasing

This change of formulation is use in the case of a potential inside a ring (e.g. a conductor inside a tore).

The formula is expressed in a general Cartesian coordinate system:

$$r^n(a_n \cos(n\varphi) + b_n \sin(n\varphi)) = a_n \,\mathrm{Re}\left[(re^{i\varphi})^n\right] + b_n \,\mathrm{Im}\left[(re^{i\varphi})^n\right] =_n \mathrm{Re}\left[(x+iy)^n\right] + b_n \,\mathrm{Im}\left[(x+iy)^n\right]$$

Using the Newton binomial development and noting that real terms are the pairs and imaginary terms are impair sums we deduced:

$$r^n(a_n\cos(n\varphi)+b_n\sin(n\varphi))=a_n\sum_{k=0}^{n/2}\left[\frac{(-1)^k n!}{(2k)!(n-2k)!}x^{n-2k}y^{2k}\right]+b_n\sum_{k=0}^{n/2}\left[\frac{(-1)^k n!}{(2k+1)!(n-2k-1)!}x^{n-2k-1}y^{2k+1}\right]$$

Now if we use Maclaurin expansion or the Taylor expansion of an expression A(x,y) at a point of coordinate (X,Y), we get:

$$A(x+X,y+Y)=A(X,Y)+\sum_{n=1}^{+\infty}\left[\frac{1}{n!}\frac{d^n}{dx^n}A\sum_{k=0}^{n/2}\left[\frac{(-1)^k n!}{(2k)!(n-2k)!}x^{n-2k}y^{2k}\right]+\frac{1}{n!}\frac{d^{n-1}}{dx^{n-1}}\frac{d}{dy}A\sum_{k=0}^{n/2}\left[\frac{(-1)^k n!}{(2k+1)!(n-2k-1)!}x^{n-2k-1}y^{2k+1}\right]\right]$$

A magnetic potential increasing with the radius is expressed in Cartesian coordinate:

$$A_{increasing}(x,y)=\sum_{n=1}^{+\infty}\left[a_n\sum_{k=0}^{n/2}\left[\frac{(-1)^k n!}{(2k)!(n-2k)!}x^{n-2k}y^{2k}\right]+b_n\sum_{k=0}^{n/2}\left[\frac{(-1)^k n!}{(2k+1)!(n-2k-1)!}x^{n-2k-1}y^{2k+1}\right]\right]$$

By analogy between the two previous equations we get:

$$a_n=\frac{1}{n!}.\frac{d^n}{dx^n}A(x,y)\qquad b_n=\frac{1}{n!}.\frac{d^{n-1}}{dx^{n-1}}.\frac{d}{dy}A(x,y)$$

Now if we want to express the increasing coefficients a_i and b_i in another polar system *j* as an increasing magnetic potential:

$$a_{j,n}=\frac{1}{n!}.\frac{d^n}{dx^n}A_{i,increasing}(x,y)$$
$$=\frac{1}{n!}.\frac{d^n}{dx^n}\left[\sum_{m=1}^{+\infty}\left[a_{i,m}\sum_{k=0}^{m/2}\left[\frac{(-1)^k m!}{(2k)!(m-2k)!}x^{m-2k}y^{2k}\right]+b_{i,m}\sum_{k=0}^{m/2}\left[\frac{(-1)^k m!}{(2k+1)!(m-2k-1)!}x^{m-2k-1}y^{2k+1}\right]\right]\right]$$

The derivative of a converging sum is the sum of the derivatives so we must differentiate:

$\frac{d^n}{dx^n}x^{m-2k}$ this differentiation is non-null only if $m\text{-}2k\geq n$ i.e. $k\leq\frac{m-n}{2}$ and also m≥n for the sum to be true. Finally we have:

$$\frac{d^n}{dx^n}x^{m-2k}=\frac{(m-2k)!}{(m-n-2k)!}x^{m-n-2k}$$

$$a_{j,n}=\frac{1}{n!}.\sum_{m=n}^{+\infty}\left[a_{i,m}\sum_{k=0}^{(m-n)/2}\left[\frac{(-1)^k m!}{(2k)!(m-n-2k)!}x^{m-n-2k}y^{2k}\right]+b_{i,m}\sum_{k=0}^{(m-n)/2}\left[\frac{(-1)^k m!}{(2k+1)!(m-n-2k-1)!}x^{m-n-2k-1}y^{2k+1}\right]\right]$$

So if we express this coefficient in another coordinate system with Rij the length between two coordinate centers and Φij the angle between both, using the binome of Newton to swhitch between polar and Cartesian we have:

$$aj_n = \sum_{m=n}^{+\infty} \frac{m!}{(m-n)!\,n!} . R_{ij}^{m-n} \left[a_{i\,n} \cos((m-n)\Phi_{ij}) + b_{i\,n} \sin((m-n)\Phi_{ij}) \right]$$

$$bj_n = \sum_{m=n}^{+\infty} \frac{m!}{(m-n)!\,n!} . R_{ij}^{m-n} \left[b_{i\,n} \cos((m-n)\Phi_{ij}) - a_{i\,n} \sin((m-n)\Phi_{ij}) \right]$$

From decreasing to decreasing

The decreasing formula is in two parts, first the logarithm and then the sum. The expansion of the logarithm is presented in:

H.B.Ngoc, "Modelisation µPEEC: representation des materiaux magnetiques par des courants de surface. Application aux noyaux ferrites 2D", PhD dissertation Grenoble University, defended on 03 may 2012 in Grenoble, France.

The logarithm in the new *j* coordinate system with distance R_{ij} from the old *i* coordinate and angle Φ_{ij} is developed as:

$$Log_{\,j}(r,\varphi) = -\frac{\mu_i I_i}{2\pi} \ln(r) + \sum_{n=1}^{+\infty} \frac{r^{-n}}{n} . R_{ij}^{n} \left[\cos(n.\varphi).\cos(n.\Phi_{ij}) + \sin(n.\varphi).\sin(n.\Phi_{ij}) \right]$$

For the sum the same process as before is used:

$$A_{decreasing,m} = r^{-m} (\alpha_m \cos(m\varphi) + \beta_m \sin(m\varphi)) = \alpha_m \,\mathrm{Re}\left[(x-iy)^{-m} \right] + \beta_m \,\mathrm{Im}\left[(x-iy)^{-m} \right]$$

Express in another point of coordinate (X, Y) it becomes:

$$A_{decreasing,m} = \alpha_m \,\mathrm{Re}\left[(x-iy+X-iY)^{-m} \right] + \beta_m \,\mathrm{Im}\left[(x-iy+X-iY)^{-m} \right]$$

The Newton binomial for negative power gives:

$$A_{decreasing,m} = \alpha_m \,\mathrm{Re}\left[\sum_{k=0}^{\infty} \left[\frac{(m+k-1)!}{(m-1)!\,k!} . (-1)^k . (X-iY)^{-(m+k)} . (x-iy)^k \right] \right]$$
$$+ \beta_m \,\mathrm{Im}\left[\sum_{k=0}^{\infty} \left[\frac{(m+k-1)!}{(m-1)!\,k!} . (-1)^k . (X-iY)^{-(m+k)} . (x-iy)^k \right] \right]$$

With the change of variable k = n-m:

$$A_{decreasing,m} = \alpha_m \,\mathrm{Re}\left[\sum_{n=m}^{\infty} \left[\frac{(n-1)!}{(m-1)!(n-m)!} . (-1)^{n-m} . (X-iY)^{n-m} . (x-iy)^{-n} \right] \right]$$
$$+ \beta_m \,\mathrm{Im}\left[\sum_{n=m}^{\infty} \left[\frac{(n-1)!}{(m-1)!(n-m)!} . (-1)^{n-m} . (X-iY)^{n-m} . (x-iy)^{-n} \right] \right]$$

By analogy with the development of an decreasing portential we have:

$$\alpha j_n = \sum_{m=1}^{n}\left[\frac{(n-1)!}{(m-1)!(n-m)!}.(-1)^{n-m}.\left[\alpha_{i,m}.\mathrm{Re}(X-x-i(Y-y))^{n-m}+\beta_{i,m}.\mathrm{Im}(X-x-i(Y-y))^{n-m}\right]\right]$$

$$\beta j_n = \sum_{m=1}^{n}\left[\frac{(n-1)!}{(m-1)!(n-m)!}.(-1)^{n-m}.\left[\alpha_{i,m}.\mathrm{Im}(X-x-i(Y-y))^{n-m}-\beta_{i,m}.\mathrm{Re}(X-x-i(Y-y))^{n-m}\right]\right]$$

The A-model – Bi-metal or hollow conductor solution

The solution for solid round conductor is presented in the manuscript. The applications for bi-metal conductor or hollow conductor are introduced in this appendix. The same development can be used for multi-layers conductors.

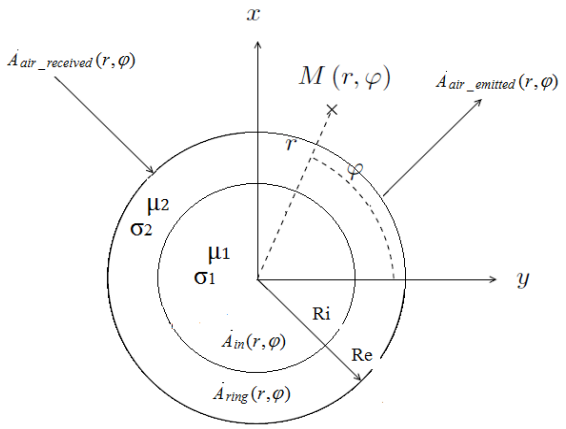

Figure 151: Hollow/Clad conductor notation of magnetic potential's parts

Solution of Laplace and Helmholtz equations

The mathematic solutions of the Laplace and Helmholtz equations are found in the manuscript. However, the solution differs from solid round shape for new technologies. Thus, the solutions in polar coordinates are expressed using classical Fourier expansion and notation from (Figure 151) Two domains are considered. First the ring part [Ri;Re] where solutions are:

for hollow wire

$$A_{hollow\_ring}(r,\varphi) = \frac{\mu_0 I\left[Y_1(kRi)(J_0(kr)-J_0(k\,\mathrm{Re}))-J_1(kRi)(Y_0(kr)-Y_0(k\,\mathrm{Re}))\right]}{2\pi k\,\mathrm{Re}(J_1(k\,\mathrm{Re})Y_1(kRi)-J_1(kRi)Y_1(k\,\mathrm{Re}))}+\frac{\mu_0}{2\pi}\sum_{n=1}^{N}J_n(kr)(p_n\cos(n\varphi)+q_n\sin(n\varphi))+Y_n(kr)(\kappa_n\cos(n\varphi)+\lambda_n\sin(n\varphi))$$

for bi-material wire

$$A_{hollow\_in}(r,\varphi)=\frac{\mu_0 I\left[Y_1(kRi)(J_0(kRi)-J_0(k\,\mathrm{Re}))-J_1(kRi)(Y_0(kRi)-Y_0(k\,\mathrm{Re}))\right]}{2\pi k\,\mathrm{Re}(J_1(k\,\mathrm{Re})Y_1(kRi)-J_1(kRi)Y_1(k\,\mathrm{Re}))}+\frac{\mu_0}{2\pi}\sum_{n=1}^{N}r^n(cr_n\cos(n\varphi)+dr_n\sin(n\varphi))$$

In the second part [0;Ri], the solutions are given by

for hollow

$$A_{clad\_ring}(r,\varphi)=$$
$$\frac{\mu_0 I\left[(J_0(k_2r)-J_0(k_2\,\mathrm{Re}))+C(Y_0(k_2r)-Y_0(k_2\,\mathrm{Re}))\right]}{2\pi k_2\,\mathrm{Re}(J_1(k_2\,\mathrm{Re})+CY_1(k_2\,\mathrm{Re}))}+\frac{\mu_0\mu_2}{2\pi}\sum_{n=1}^{N}J_n(k_2r)(p_n\cos(n\varphi)+q_n\sin(n\varphi))$$
$$+Y_n(k_2r)(\kappa_n\cos(n\varphi)+\lambda_n\sin(n\varphi))$$

for bi-material:

$$A_{clad\_in}(r,\varphi)=\frac{\mu_0 I\left[(J_0(k_2Ri)J_0(k_1r)-J_0(k_2\,\mathrm{Re})J_0(k_1Ri))\right]}{2\pi k_2\,\mathrm{Re}\,J_0(k_1Ri)(J_1(k_2\,\mathrm{Re})+CY_1(k_2\,\mathrm{Re}))}$$
$$+\mu_0 I\frac{\left[C(Y_0(k_2Ri)J_0(k_1r)-Y_0(k_2\,\mathrm{Re})J_0(k_1Ri))\right]}{2\pi k_2\,\mathrm{Re}\,J_0(k_1Ri)(J_1(k_2\,\mathrm{Re})+CY_1(k_2\,\mathrm{Re}))}+\frac{\mu_0\mu_1}{2\pi}\sum_{n=1}^{N}J_n(k_1r)(cr_n\cos(n\varphi)+dr_n\sin(n\varphi))$$

The C coefficient is described by:

$$C=\frac{k_1J_1(k_1Ri)J_0(k_2Ri)-k_2J_0(k_1Ri)J_1(k_2Ri)}{k_2J_0(k_1Ri)Y_1(k_2Ri)-k_1J_1(k_1Ri)Y_0(k_2Ri)}$$

The solution in the air being unchanged, the process to switch from an emitted potential to a received potential is also the same as for solid round conductors. However, magnetic potential in conductors being changed, the reflection and transmission coefficients are replaced and introduced in next section.

Transmission and Reflexion

Study concerns bi-area geometry, both the reflection and transmission are still considered on outer radius Re of the conductor, but in this case second transmission is expressed on the inner radius Ri.

For hollow wire on Re:

$$\mathrm{Re}_n=\frac{\alpha_n}{a_n}=\frac{\beta_n}{b_n}=\mathrm{Re}^{2n}\left[\frac{2n}{k\,\mathrm{Re}}\frac{(J_n(k\,\mathrm{Re})+CrY_n(k\,\mathrm{Re}))}{(J_{n-1}(k\,\mathrm{Re})+CrY_{n-1}(k\,\mathrm{Re}))}-1\right]$$

$$Tr_n=\frac{p_n}{a_n}=\frac{q_n}{b_n}=\mathrm{Re}^n\frac{2n}{k\,\mathrm{Re}(J_{n-1}(k\,\mathrm{Re})+CrY_{n-1}(k\,\mathrm{Re}))}$$

On Ri:

$$Tr2_n=\frac{cr_n}{p_n}=\frac{dr_n}{q_n}=\frac{J_n(kRi)+CrY_n(kRi)}{Ri^n}$$

The coefficient Cr is defined by:

$$Cr_n = \frac{\kappa_n}{p_n} = \frac{\lambda_n}{q_n} = \frac{-(\frac{kRi}{n} J_{n-1}(kRi) - 2J_n(kRi))}{\frac{kRi}{n} Y_{n-1}(kRi) - 2Y_n(kRi)}$$

In the case of bi-material conductors, the inner part is conductive so the formulas are defined differently:

On Re:

$$\mathrm{Re}_n = \frac{\alpha_n}{a_n} = \frac{\beta_n}{b_n} = \mathrm{Re}^{2n}\left[\frac{2n}{k_2 \mathrm{Re}} \frac{(J_n(k_2 \mathrm{Re}) + CrY_n(k_2 \mathrm{Re}))}{(J_{n-1}(k_2 \mathrm{Re}) + CrY_{n-1}(k_2 \mathrm{Re}))} - 1\right] \quad Tr_n = \frac{p_n}{a_n} = \frac{q_n}{b_n} = \mathrm{Re}^n \frac{2n}{\mu_2 k_2 \mathrm{Re}(J_{n-1}(k_2 \mathrm{Re}) + CrY_{n-1}(k_2 \mathrm{Re}))}$$

On Ri:

$$Tr2_n = \frac{cr_n}{p_n} = \frac{dr_n}{q_n} = \frac{\mu_2}{\mu_1} \frac{J_n(k_2 Ri) + CrY_n(k_2 Ri)}{J_n(k_1 Ri)}$$

The coefficient Cr is defined by:

$$Cr_n = \frac{\kappa_n}{p_n} = \frac{\lambda_n}{q_n} = \frac{k_1 J_n(k_2 Ri) J_{n-1}(k_1 Ri) - k_2 J_n(k_1 Ri) J_{n-1}(k_2 Ri)}{k_2 J_n(k_1 Ri) Y_{n-1}(k_2 Ri) - k_1 J_{n-1}(k_1 Ri) Y_n(k_2 Ri)}$$

Mathematic description that differs from solid round conductor is introduced. The solution to find harmonic coefficients is exactly the same as presented in chapter II. Thus, magnetic potential A can be solved in the 2D space for mix of round conductor, hollow conductor and bi-metal conductor.

Current density in hollow conductor:

$$J_{hollow\_ring}(r,\varphi) = \frac{-kI}{2\pi \mathrm{Re}} \frac{\left[Y_1(kRi) J_0(kr) - J_1(kRi) Y_0(kr)\right]}{\left[J_1(k \mathrm{Re}) Y_1(kRi) - J_1(kRi) Y_1(k \mathrm{Re})\right]} - \frac{k^2}{2\pi} \sum_{n=1}^{N} J_n(kr)(p_n \cos(n\varphi) + q_n \sin(n\varphi)) + Y_n(kr)(\kappa_n \cos(n\varphi) + \lambda_n \sin(n\varphi))$$

Current density in bi-metal conductor:

In the ring:

$$J_{clad\_ring}(r,\varphi) = \frac{-k_2 I}{2\pi \mathrm{Re}} \frac{\left[J_0(k_2 r) + CY_0(k_2 r)\right]}{J_1(k_2 \mathrm{Re}) + CY_1(k_2 \mathrm{Re})} - \frac{k_2}{2\pi} \sum_{n=1}^{N} J_n(k_2 r)(p_n \cos(n\varphi) + q_n \sin(n\varphi)) + Y_n(k_2 r)(\kappa_n \cos(n\varphi) + \lambda_n \sin(n\varphi))$$

In the inner part:

$$J_{clad\_in}(r,\varphi) = \frac{-k_2 I}{2\pi \mathrm{Re}} \frac{\left[(J_0(k_2 Ri) J_0(k_1 r) + CY_0(k_2 Ri) J_0(k_1 r)\right]}{J_0(k_1 Ri)(J_1(k_2 \mathrm{Re}) + CY_1(k_2 \mathrm{Re}))} - \frac{k_2}{2\pi} \sum_{n=1}^{N} J_n(k_1 r)(cr_n \cos(n\varphi) + dr_n \sin(n\varphi))$$

The C coefficient is the same as in magnetic potential expressions.

RESUME

L'innovation dans sa définition la plus générale est un moyen pour les industriels de préserver et créer de la valeur par rapport aux concurrents. Principalement technologique, l'innovation est également présente dans l'usage. Une nouvelle façon d'utiliser un produit ou un service pour répondre aux besoins du marché. Cette thèse est une innovation dans le domaine du design assisté par ordinateur des composants passifs pour l'électronique de puissance.

Le domaine de l'électronique de puissance est sujet aux mêmes objectifs que toutes les recherches actuelles, c.à.d. augmenter l'efficacité énergétique des systèmes en réduisant leurs coûts et leurs temps de développement. Parmi les multitudes de solutions proposées ces dernières années, les structures multi-niveaux et multi-bras, les composants grands gaps SiC ou GaN ou les stratégies de régulation, le choix est cornélien pour le designer. Le besoin d'assistance au choix est donc clairement formulé dans le milieu industriel.

Pour répondre à cette problématique, ces travaux proposent la mise en œuvre de dimensionnement par optimisation des composants passifs simulés par des modèles précis et discrets basés sur la réalité industrielle. C'est-à-dire un dimensionnement s'appuyant sur les catalogues de fournisseurs pour les dimensions et les matériaux, mais également un dimensionnement contraint par la faisabilité industrielle des solutions trouvées.

Dans un premier temps le manuscrit de thèse introduit les principaux algorithmes d'optimisation ainsi que les stratégies associées. L'expérience du G2Elab ainsi que celle de Schneider Electric nous ont conduit au choix d'une stratégie adaptée au besoin défini par un cahier des charges. Les avantages et inconvénients de cette stratégie mais également des autres choix possibles sont présentés sur des exemples simples.

Dans un second temps des modèles de composants passifs répondant aux besoins des algorithmes stochastiques choisis sont développés. Un important effort est fait sur la modélisation des inductances car leur dimensionnement est prépondérant comparé à celui des condensateurs. Ces efforts sont faits sur la modélisation des pertes et du comportement magnétique des matériaux poudreux et amorphes principalement utilisés chez Schneider Electric. L'expérience montre également qu'avec ces matériaux à faible densité de pertes, l'efficacité des inductances se gagne sur les conducteurs. Les modèles existant d'homogénéisation ne répondent pas au besoin de précision et de modélisation de nouveaux concepts. C'est pourquoi un nouveau modèle semi-analytique est proposé afin de rivaliser avec les méthodes de types intégrales ou éléments finis en termes de précision tout en les surpassant en termes de rapidité de calcul.

Les modèles de composants présentés, le manuscrit se focalise ensuite sur la modélisation des filtres dans les structures de conversion AC/DC, DC/AC et DC/DC utilisées dans les Alimentations Sans Interruptions. Cette modélisation doit tenir compte de tous les modes de

fonctionnement des ASI qui impactent fortement le comportement des filtres. Enfin les filtres utilisant des inductances couplées sont étudiés.

Finalement des exemples d'applications développées pour Schneider Electric sont présentés. La mise en œuvre des méthodes d'optimisation discrète utilisant les modèles choisis sont employées pour fournir des outils d'aide à la décision lors du dimensionnement des convertisseurs. Les résultats sont validés par des mesures faites sur les prototypes issus des optimisations

ABSTRACT

Innovation in its whole definition is a way for industrial groups to preserve and create value over competitors on the market. Mainly technologic, innovation is also of use, a new way of using a product or service to answer market or user requirements. This work is an innovation for component design in power electronic systems, both in tools and user customs.

Power electronic is subject to same research goals as any modern system, i.e. cost and time to market reduction, efficiency increase in the global energy save world concern and modularity of solution to answer maximum customer needs. Among the multitude of proposed solutions during the last decade, multi-legs and multi-levels converters, new SiC and GaN semiconductors or new control strategies, the choice is cornelian for the designer. The need of tool to help designers in their choices is clearly identified in industry.

To answer this problem, this work proposes the implementation of passive component sizing using discrete optimization methods. The choice of accuracy and industrial constraints is done to get already purchasable solution from optimization results to suppliers.

In the first part of the PhD dissertation the main optimization algorithms are introduced with the optimization strategies. G2Elab experience and Schneider electric one lead to privileged discrete optimization using stochastic algorithms and libraries of components and materials.

In the second part the models for passive components are developed to match stochastic algorithms requirements. Focus is done on magnetics because their sizing is dominant compare to capacitor. The effort is done on losses computation and magnetic behavior of powder alloy and amorphous materials widely used in Schneider Electric applications. With these low loss density materials, the gain on efficiency is achieved on conductors. Thus a new semi-analytic model is developed to overcome standard models issues and to compete with integral or finite element method in terms of accuracy and overcoming them in terms of calculation speed.

In the third part, filter modeling approach is introduced for AC/DC, DC/AC and DC/DC converters. This modeling takes into account all working cases of UPS impacting passive components design. Interleaved and coupled solutions are investigated.

Finally some examples of developed applications for Schneider Electric are presented. The sizing of passive component using discrete optimization methods are implemented with success. Measures are achieved on prototypes to validate our approach.